Comparison of 294 nm and 355 nm excitation wavelengths in UVLIF standoff detection of biological aerosols released in a semi-closed chamber

Øystein Farsund, Gunnar Rustad and Gunnar Skogan

Norwegian Defence Research Establishment (FFI)

7 February 2012

FFI-rapport 2012/00211

1116

P: ISBN 978-82-464-2093-6
E: ISBN 978-82-464-2094-3

Keywords

Avstandsdeteksjon

Ultrafiolett laserindusert fluorescens

Biologiske stridsmidler

Lidar

Approved by

Hans Christian Gran	Project Manager
Jan Ivar Botnan	Director

English summary

FFI has previously developed a lidar for standoff detection of biological aerosols based on ultraviolet laser induced fluorescence, using an excitation wavelength at 355 nm. A 294 nm laser source has been developed and installed in the lidar. The FFI standoff test range, featuring a semi-closed chamber for the release of biological aerosols, allows for 210 m standoff distance. This report describes the standoff detection experiment carried out in 2011 using the semi-closed chamber, which has air curtains in both ends to confine the aerosols within the chamber. Seven different simulants for biological warfare agents were disseminated. Lidar data using both excitation wavelengths, 294 nm and 355 nm, were acquired. The measured spectra are presented and the results for the two excitation wavelengths are compared in the report. The fluorescence relative to excitation laser pulse energy is in general and in particular for the anthrax simulants higher at 294 nm excitation. However, most importantly, the mutual agent spectra differ significantly when exciting with 294 nm light compared to those at the longer excitation wavelength. Previous work using the 355 nm laser has shown that we are able to discriminate agents based on their fluorescence spectra. Even though classification is not subject to this report, it seems obvious that an excitation wavelength in the 280-290 nm spectral range will improve instrument performance in terms of lower false alarm rates. However, the increase in performance has to be traded off against increased system complexity following the use of a non-commercial laser source.

Sammendrag

FFI har tidligere utviklet en lidar for avstandsdeteksjon av biologiske aerosoler ved bruk av ultrafiolett laserindusert fluorescens med 355 nm eksitasjonsbølgelengde. I et annet prosjekt er en 294 nm kilde utviklet og integrert i lidaren. FFI har også opparbeidet en testbane for avstandsdeteksjon med 210 m mellom standplass og utslippskammeret, som har luftgardiner i åpningene i hver ende av kammeret for å holde aerosolene innenfor. Rapporten beskriver utslippseksperimentene gjennomført høsten 2011, hvor syv ulike simulanter for biologiske agens ble spredt som aerosoler. Det ble gjort opptak både med 355 nm og 294 nm eksitasjonsbølgelengde. Målte spektre presenteres, og resultat fra de to eksitasjonsbølgelengdene sammenliknes. Fluorescensnivået relativt til energien i eksitasjonspulsen er generelt, og spesielt for miltbrannsimulantene, høyere ved bruk av 294 nm eksitasjon. Likevel er det viktigste resultatet at spektrene for alle simulantene er innbyrdes betydelig mer forskjellig ved 294 nm eksitasjon enn ved 355 nm. Prosjektet har utviklet algoritmer som klarer å klassifisere ulike agens basert på målte fluorescensspektre med 355 nm eksitasjonsbølgelengde, og det fremstår som åpenbart at en eksitasjonsbølgelengde rundt 290 nm vil bedre instrumentets ytelse i form av lavere falsk-alarm-rate, selv om det ikke er gjort klassifikasjonsforsøk på data tatt opp i dette eksperimentet. Likevel må en eventuelt forbedret ytelse i form av bruk av en ikke-kommersiell laserkilde avveies mot økt systemkompleksitet.

Contents

1 Introduction

Most standoff instruments for the detection of aerosolized biological agents based on ultraviolet laser induced fluorescence (UVLIF) technology use either the third or fourth harmonic of a Q-switched Nd:YAG 1064 nm laser as excitation source. The laser and harmonic stages are commercially available and deliver pulses of appropriate duration and sufficient energy for detection up to several hundred meters standoff distance. On the other side, the most important fluorophores, tryptophan and NADH, absorb most efficiently at wavelengths shorter than 355 nm, and at 266 nm light absorption by atmospheric ozone close to the ground can dramatically reduce standoff distance. More specifically, the 280 nm region has been held to be up to four times more efficient in terms of excitation for fluorescence than 355 nm [1]. As a consequence, such a laser source was designed and built under FFI projects P1052 and P1179 to be tested with the FFI lidar developed under P1001 and P1116.

In this report, we describe the implementation of the source in the lidar instrument, and the experiments carried out under P1116 using 355 nm and 294 nm excitation of seven different biological agents. The experiments were carried out at the "Dompa" test range at FFI. The agents were released in the semi-closed chamber and the lidar was located approximately 210 m from the release container.

This report gives a brief theoretically based motivation for choosing a more difficult accessible excitation wavelength, followed by a description of the lidar instrument and the experimental setup. The measurement results are presented in Chapter 4, and discussed in Chapter 5. The experiences and results of the experiment are summed up in the conclusion, whereas recommendations regarding possible instrument improvements based on all our experiences gained in the standoff projects are given in the final remarks.

2 Theory

The FFI biological lidar (hereafter *biolidar*) uses ultraviolet laser induced fluorescence to detect biological aerosols at a distance. Here, the fact that some parts of the biological material emit fluorescence when exposed to ultraviolet light is utilized [2], and we have previously seen that the fluorescence following 355 nm illumination from different substances exhibit sufficient difference that the different substances can be classified [3, 4].

The main reason for using 355 nm laser light is that it is easily available through third harmonic generation of the 1064 nm Nd:YAG laser light. The main substance that fluoresces after 355 nm excitation is the molecule NADH. This is the reduced form of nicotinamide adenine dinucleotide (NAD^+), and is important in cell respiration and hence metabolism. NADH is therefore present in bacteria and other living cells, but to a lesser degree in spores or viruses. The perhaps most important fluorophore, tryptophan, is not excited in this approach because tryptophan requires excitation at wavelengths below ~310 nm, see Figure 2.1. As tryptophan is an amino acid and therefore present in all biological material, this is an important limitation with the current

excitation scheme. Tryptophan can be excited with 266 nm, which is the fourth harmonic of the Nd:YAG laser, and this has been used in some instruments [5]. However, presence of ozone close to the ground will absorb this wavelength. For example, at 100 ppb O_3 concentration, which can occur in urban areas in the summer [6], 266 nm light experience ~90% loss per km. For comparison, at 280 nm and 290 nm, the corresponding loss is ~60% and ~30%, respectively (see Figure 2.2). As the absorption cross section for tryptophan is significantly larger for 280 nm than 266 nm, it has been of interest to examine wavelengths in the 280-290 nm range for their suitability in standoff detection of biological aerosols. This has been the topic of this work.

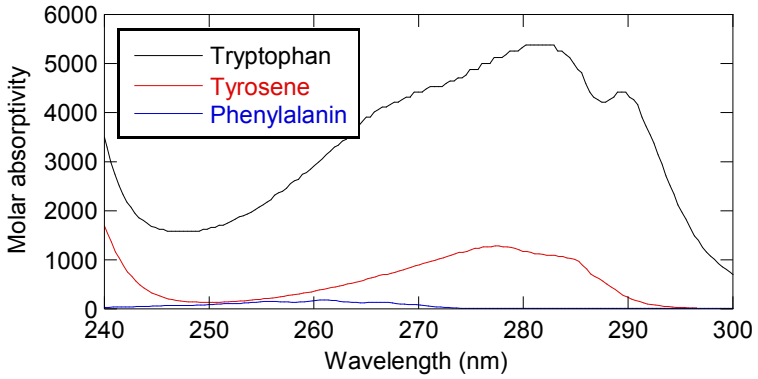

Figure 2.1 Absorption spectra for the most important fluorescing amino acids; tryptophan, tyrosine and phenylalanine (spectra taken from [7])

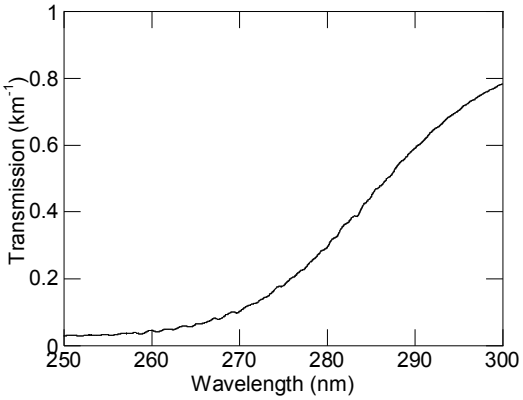

Figure 2.2 Calculated transmission through 1 km of USTD atmosphere with 100 ppb O_3 [8]

3 Experiment

3.1 Lidar

The FFI biolidar is described in [2]. For the experiments discussed herein, the lidar was modified for the ability to excite at 294 nm in addition to the previously used and more common wavelength at 355 nm. We use an optical parametric oscillator pumped by the laser fundamental wavelength to generate 1700 nm radiation, with which 294 nm is generated by sum frequency

mixing with 355 nm using a nonlinear crystal (BBO), see [9]. In the lidar, both the 294 nm beam and the 355 nm beam could be used as excitation source. Both beams were aligned parallel to the optical axis of the collecting optics and the excitation wavelength was chosen by flipping a mirror in a kinetic mount, while blocking or unblocking the IR beam from the OPO, see Figure 3.1. It proved difficult to remove all 355 nm light from the 294 nm light; hence remnants of scattering of 355 nm light can be seen even in measurements with 294 nm excitation.

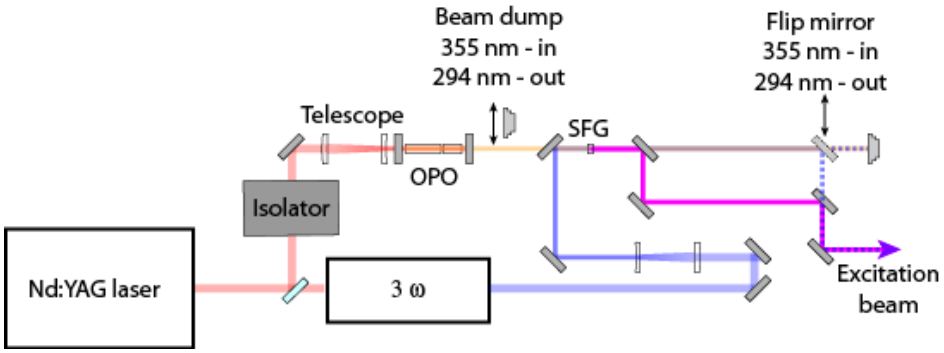

Figure 3.1 Excitation laser of the lidar. A 294 nm beam is generated by sum frequency mixing the 1.7 µm OPO signal with the third harmonic (355 nm) of the laser. 294 nm or 355 nm excitation wavelength was selected by adjusting the flip mirror and beam dump, as is explained in the figure

The collecting optics path was not modified from the lidar described in [2]. However, the PMT channel measuring time of flight of the elastic backscatter to estimate the distance to the aerosol cloud, was not employed in these experiments as the gating was constant and determined by the distance between the instrument and release chamber. To recapture the principle of operation, the pulse repetition rate of the laser is 10 Hz; however, in order to correct for ambient (sun) light, the camera is operated at 20 frames per second, and the most recent background spectrum is subtracted from the spectrum obtained with laser illumination. Moreover, the lidar is a point sensor in the sense that the total fluorescence within the volume determined by the field of view and gating, is measured, thus it has no transversal spatial resolution. The camera detector is therefore operated in full vertical binning mode. The horizontal binning is adapted to the spectral resolution determined by the spectrograph and slit width, or fiber diameter in our case. In these experiments the spectral resolution corresponded to seven pixels, and the horizontal binning was set to five pixel columns.

The average laser power was measured immediately prior to, and sometimes subsequent to, dissemination of the agent. During 294 nm operation, the output pulse energy was 3-5 mJ, whereas approximately 30 mJ was used during 355 nm operation. These levels were used to allow for stable operation. We have demonstrated 15-20 mJ operation of the 294 nm light source in a fine-tuned experiment in the lab, but unstable operation of the 355 nm source with changing ambient temperature affects the stability of the 294 nm energy severely. When operating at 3-5 mJ output levels, the 294 nm remained fairly stable over a 5-10 minutes measurement. The

Shamrock 163i spectrograph was employed with either one of two different gratings during the experiment, both with 300 lines/mm ruling, however blazed (i.e. having peak reflectance) at 500 nm and 300 nm. Color glass filters were used to reduce elastic backscatter levels to avoid saturation of the ICCD camera. WG 305 and CVI LP385 were used for 294 nm and 355 nm excitation, respectively. The relative spectral efficiencies for the components used in the experiment are presented in Figure 3.2.

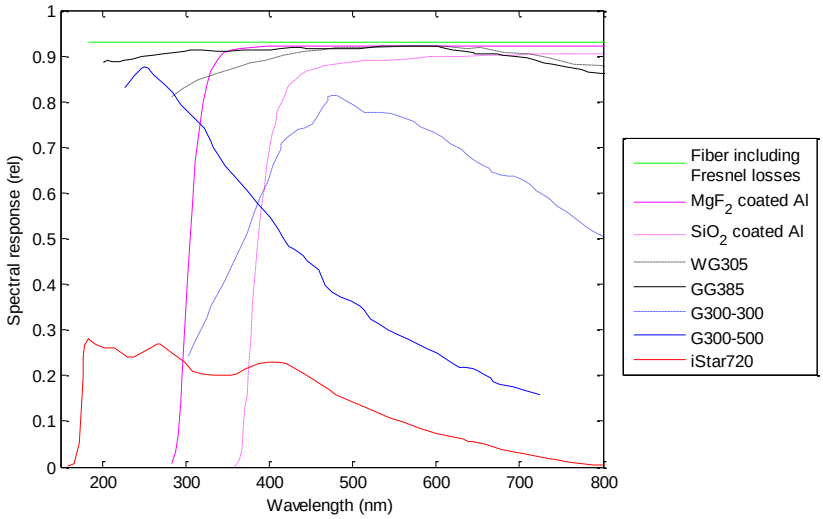

Figure 3.2 Spectral response for the components used in the experimental lidar: transmission of 2 m of BFH22 fiber [10] including Fresnel losses resulting from coupling light between fiber and air; reflectance for MgF_2 coated aluminum mirrors used in Shamrock 163i spectrometer, [11]; reflectance for SiO_2-coated aluminum (assumed coating used in telescope mirrors, [12]; transmission of color glass filters used for 294 nm (WG305) and 355 nm (GG385), [13, 14], excitation; relative grating efficiencies for the two gratings used in the experiment; and quantum efficiency for the Andor ICCD camera without gain (no voltage across micro channel plates) , [15]

Putting all components of the optical path together yields the overall calculated spectral response of the instrument:

- Two telescope mirrors
- Color glass filter
- Fiber including Fresnel-losses (normal incidence, air - fused-silica interface)
- Collimating and focusing mirror of spectrometer
- Grating efficiency (the relative efficiency has been used for the calculations, as the absolute efficiency is not available from the supplier). Measurements at one wavelength indicate that the reflection into first order is significantly lower than the relative efficiency.

- ICCD quantum efficiency, meaning the ratio of photoelectrons to incident photons of the photocathode. During operation of a gen II ICCD, high voltage across the micro channel plate provides high gain (1-500 for the model we used) to overcome the read noise of the CCD.

Two different gratings were used, and the color glass filter was selected with respect to excitation wavelength. A total of four different configurations were used during the experiments:

1. WG305 filter (for 294 nm excitation) and grating blazed at 300 nm
2. WG305 filter (for 294 nm excitation) and grating blazed at 500 nm
3. GG385 filter (for 355 nm excitation) and grating blazed at 300 nm
4. GG385 filter (for 355 nm excitation) and grating blazed at 500 nm

The calculated total instrument spectral responses for all four different configurations (including mirrors, optical fiber and camera) are given in Figure 3.3. These curves are used later in this report to compare spectra acquired with different instrument configurations.

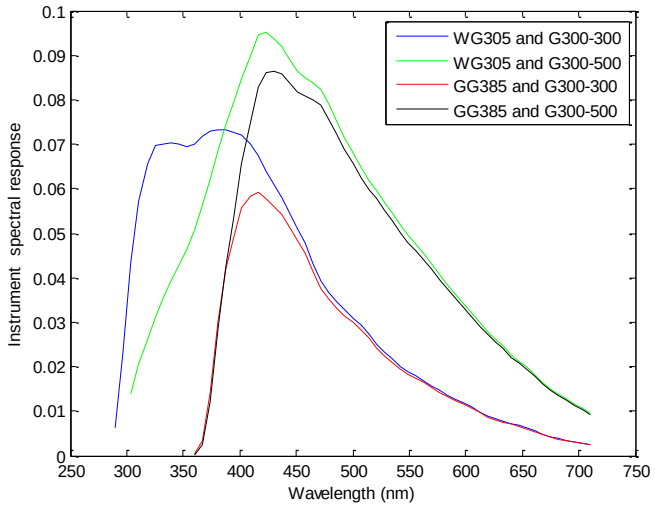

Figure 3.3 Calculated instrument spectral responses for the four different combinations of color glass filter and grating; other components used in all configurations are included in the calculations (without ICCD camera gain)

3.2 Semi-closed release chamber

The semi-closed container systems was designed and manufactured by Combitech AB (Östersund, Sweden) with support from FOI and FFI. The system consists of two 20 feet containers where one is the semi-closed release chamber and the other is a service container containing pumps, valves, filters and control electronics. The containers were installed at the "Dompa" test range as shown in Figure 3.4.

for about 2 m/s wind speed perpendicular to the openings without failure of the curtains. At higher wind speed the leakage of particles through the curtains becomes noticeable.

Figure 3.4 FFI semi-closed chamber release system with release container placed on top of service container

3.3 Agent dissemination and referencing

As the diameter of the laser beam inside the test chamber 210 m behind the lidar was only ~10 cm, it was advantageous to modify the release container slightly to obtain higher concentration levels more rapidly. This was done using a 500 mm diameter and 3 m long ventilation duct which was fixed between the air curtains of the container. The aerosol generator and a fan were placed at the far end of the pipe; whereas the inlet of an Aerodynamic Particle Sizer (APS) was located half way down the duct, see Figure 3.5.

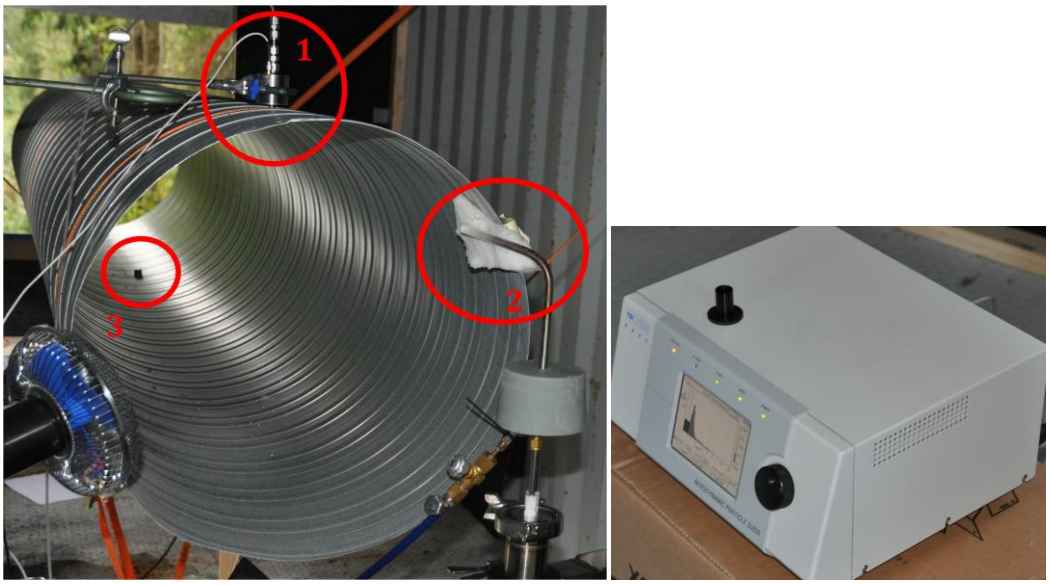

Figure 3.5 Left: Ø500 mm pipe through which the lidar was directed, and into which the bioaerosols were released either wet (1) using the Sonotek or dry (2) using the FOI release mechanism. The APS (right) measured the aerosol size distribution, and was located with its inlet protruding into the pipe (3)

Agents dissolved in water solution were disseminated using an ultrasonic spray nozzle (from Sono-Tek). Dry agents were released using custom built gear which was borrowed from FOI-Umeå. The lidar was located 210 meters away from the release container in a 10 feet container, see Figure 3.6-3.7.

Figure 3.6 The instrument container as seen through the release container, 210 m behind. The size of the laser beam inside the test chamber is slightly smaller than the cross section of the instrument container as viewed in the picture

Figure 3.7 Lidar located in 10 feet instrument container

3.4 Biological agents released in the experiments

Seven different agents were released during the experiments. BG is spores of *Bacillus atrophaeus* (previously designated *Bacillus globigii* or *Bacillus subtilis var. niger*). The spores originate from *Dugway Proving Ground*, batch #026, lot #19076-03268. The spores were suspended in deionized water at a concentration of 8 mg/ml. BG is a simulant for *bacillus anthracis*, or anthrax spores.

BT is spores of *Bacillus thuringiensis* (we used a commercial preparation called Turex, normally used as a biological insecticide). BT is another simulant for anthrax spores.

EH is *Pantoea agglomerans* (previously *Erwinia herbicola)*, originating from the *American Type Culture Collection* (ATCC 33243). The culture was cultivated overnight at 30^{o}C in nutrient broth from Merck (5.0 g/l peptone from meat and 3.0 g/l meat extract). EH was used as a simulant for pathogenic gram-negative bacteria, like *Francisella tularemia* (rabbit fever) and *Yersinia pestis* (plague).

E.coli is the gram negative bacterium *Escherichia coli*, from *Deutsche Sammlung von Mikroorganismen und Zellkulturen* (DSM 4230). This culture was also grown at 30^{o}C overnight in nutrient broth. *E.coli* can be used as a simulant for pathogenic gram-negative bacteria.

MS2 is a bacteriophage, i.e. a virus infecting bacteria. MS2 was inoculated with *E.coli* (DSM 5695) and grown overnight at 37^{o}C in LB medium (10 g/l tryptone, 5 g/l yeast extract and 10 g/l NaCl). After cultivation, bacteria were removed by centrifuging at 2000 min^{-1} for ten minutes, followed by filtration using 0.2 µm filter. MS2 is used as a simulant for pathogenic viruses, e.g. smallpox or ebola.

OA is short for ovalbumin, which is albumin from egg white. We used OA named Sigma-Aldrich A5253. Fumed silica, Sigma-Aldrich S5505, was added in a concentration of 1 % to make the OA more "volatile". Ovalbumin is used as a simulant for toxins, e.g. ricin.

SM is *Serratia marcescens* originating from *Collection de Institut Pasteur* (CIP 53.90). The culture was grown overnight at 30^{o}C in nutrient broth. SM was used as a simulant for pathogenic gram-negative bacteria.

The agents were released either in an aqueous solution (deionized water) or dry (powder), see Table 3.1. The table also addresses which biological threat the agent simulates.

Agent	Wet or dry release	Simulant for
BG	Wet	Anthrax (*Bacillus Anthracis* spores)
BT	Dry	Anthrax (*Bacillus Anthracis* spores)
EH	Wet	Gram-negative bacteria (e.g. *Francisella tularensis, Yersinia pestis*)
E.Coli	Wet	Gram-negative bacteria
MS2	Wet	Virus
OA	Dry	Toxin
SM	Wet	Gram-negative bacteria

Table 3.1 List of the biological agents released during the field trial, whether they were released dry or in an aqueous solution and which biological threat they are similar to

The laser beam was pointed to shine through the duct, and the camera was gated to capture the return signal ranging a few meters in front to a few meters behind the release container, not measuring the fluorescence from the ground vegetation about 10 m behind the container. The camera measured the total fluorescence of the particles in the beam (a cylindrical volume with diameter approximately 10 cm and 3 m length). The APS measured the total particle content in a fixed air volume withdrawn from a hole half way down the duct (about 2.5 m from the release). The particle concentration homogeneity within the conduit was not measured; hence the setup does not allow instrument sensitivity calculations with acceptable accuracy. The particle concentration was measured every 10 seconds, whereas the lidar captured background corrected spectra at 10 Hz.

4 Results

The aim of the experiments was to compare the fluorescence spectra in terms of responsivity and shape, or spectral features, as function of the laser excitation wavelength and pulse energy. In the first section of this chapter, the way from raw data to a comparable, instrument corrected spectrum is shown for an arbitrary release. The same method was used for other selected data representing the seven different agents. In 4.2, the spectra corrected for instrument spectral response are shown. The agent spectra are compared for the two laser excitation wavelengths in 4.3. A complete set of data and Matlab files for reading and simple viewing of the data are appended electronically, see Appendix A. All releases, regardless of data quality, are shown in comparable format (fluorescence, APS-data and measured spectrum) in Appendix B.

4.1 Method for data selection

The lidar acquired background corrected spectra at 10 Hz pulse rate. The spectrum between 280 nm and 630 nm was measured with the camera. As this could potentially lead to problems with overlapping of the second order of the high frequency part of the spectrum with the first order of the low frequency part, we chose to only regard the 280-560 nm spectral range when exciting the agent with 294 nm. For 355 nm excitation we used data up to 610 nm. Previous measurements with 355 nm excitation showed that the spectral range above ~600 nm does not contain useful information [2]. The raw data consisted of 205 channels at 10 Hz sample rate. The signal between 280 nm and 630 nm consists of ~170 channels. An example of the raw data acquired during the release of OA is shown in Figure 4.1.

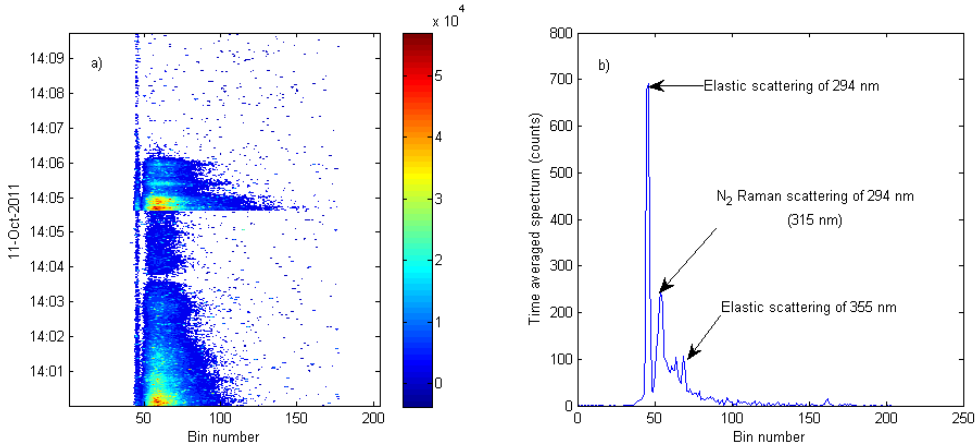

Figure 4.1 a) Example of raw data during measurement with 294 nm excitation and dissemination of OA. Color coding indicates signal strength, and a bin corresponds to a spectral channel. b) Time average of the spectra measured between 14:07 and 14:09

The time-averaged spectrum in Figure 4.1b shows several distinct lines. The most pronounced is elastic scattering at the excitation wavelength (294 nm), but also remnants of 355 nm laser light (see Section 3.1), as well as Raman-scattering by atmospheric nitrogen (and more weakly, water and oxygen) can be recognized. The locations of these lines were used to calibrate the wavelength axis. The time intervals of higher signal levels appear during the dissemination of the biological agent. This signal is caused by the fluorescence. Raw data are not suitable for extracting spectral features of the agent in consideration directly; therefore, our strategy was to isolate time intervals of considerable measured fluorescence signal caused by the presence of the agent, disregarding intervals with little or no fluorescence. Figure 4.2 shows the total fluorescence as function of time from the raw data shown in Figure 4.1a.

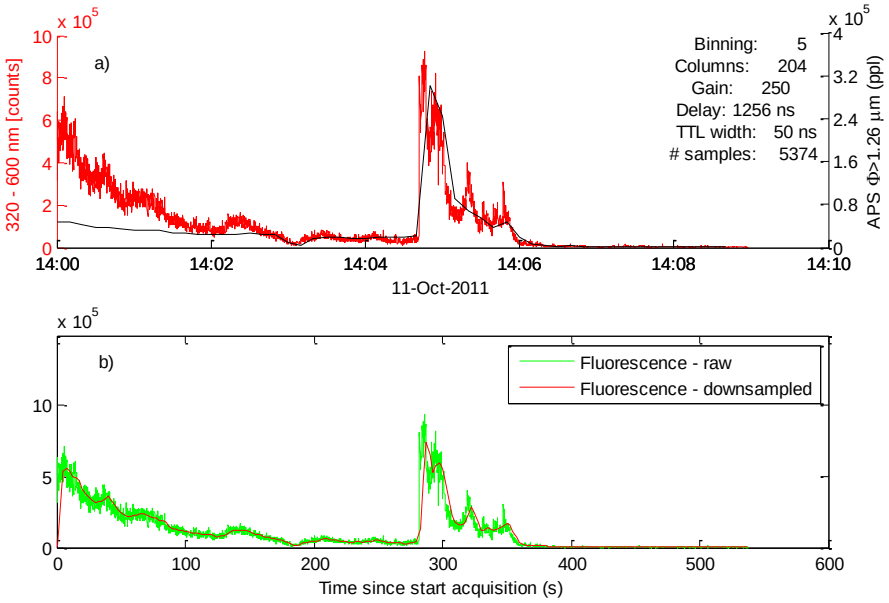

Figure 4.2 a) Total measured fluorescence (red) and APS data (black). b) Fluorescence data at sampling rate, 10 Hz (green), and after filtering with a 50 samples moving average filter (red)

The total fluorescence is expressed as the integral of the signal in the spectral range from above the N_2 Raman-scattering line to the long wavelength end of the signal. The fluorescence is plotted together with parts of the APS signal. Background measurements with the APS suggest that a vast majority of background particles have diameters less than 1 µm. Hence, we have chosen to only regard the integral of all particles with aerodynamic diameter above 1.26 µm from the APS in the measurements. Moreover, a moving average filter using the 50 last samples was applied to smooth the fluorescence curve. This corresponds to a 5 second moving average. By comparing the smoothed fluorescence signal with the APS measurement, the time interval of significant fluorescence signal (high signal to noise ratio) can be estimated, in this case around 280 s after acquisition startup. The fluorescence signal is significantly stronger than the APS-measurement during the first two minutes of the release (see Figure 4.2a). The discrepancy is most likely caused by large particles, many of which never reached the APS-inlet, as they fell out and were deposited on their way down the tube. Moreover, a large particle has a higher fluorescence cross section than a small one, while it gives rise to only one count in the APS (if it reaches this far down the tube). This particular release was among the first dry releases and turned out to be a heavy release in terms of amount of agent.

The fluorescence signal is important to take into consideration because a substantial fluorescence signal corresponding well with the APS measurement implies that the instrument is properly aligned and measures the disseminated aerosols, and that the highest possible S/N is used to determine the best possible fluorescence spectrum. The average of all spectra within the proposed time interval is therefore taken as an estimate of the measured fluorescence spectrum for the agent in consideration, see Figure 4.3.

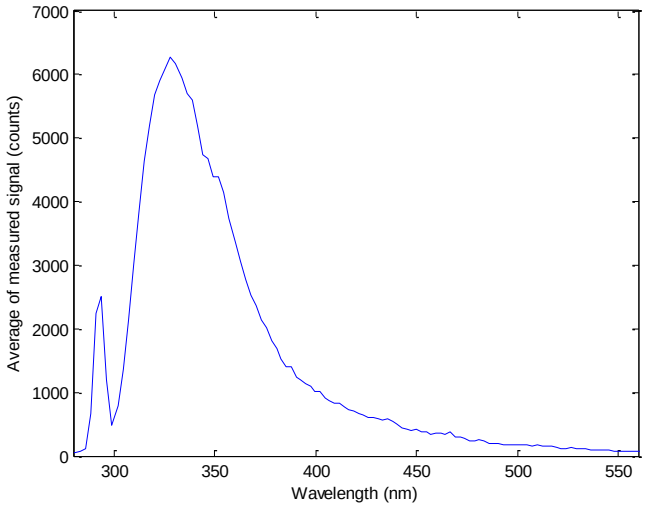

Figure 4.3 *Spectral average of the measurements in the time interval from 190 to 300 s of the release in consideration (noting that this is a vigorous release). The 294 nm elastic scattering appears clearly despite of the WG305 filter employed to reduce the elastic backscatter which is several orders of magnitude larger than the fluorescence*

This argumentation rests on the assumption that the features, or shape, of the fluorescence spectrum are the same for different aerosol concentrations. In Figure 4.4 the average spectra during four intervals (see Figure 4.2b for time reference) of different agent concentrations are plotted. The similar spectral shapes indicate our assumption be appropriate.

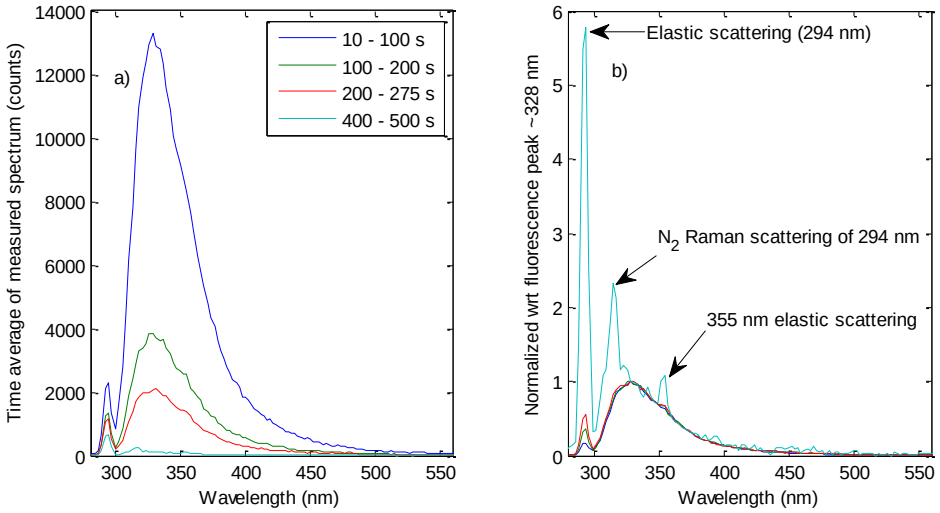

Figure 4.4 *a) Spectral average of measurements in the time intervals as given; different agent concentration levels impose different signal levels. b) Spectra normalized with respect to the fluorescence peak coincide at different agent concentrations until the signal approaches background level, where other effects become prominent (same color coding as in a)*

Using the signal preconditioning as described above, spectra obtained for different biological agents may be compared, keeping in mind which grating and excitation wavelength were used. Thus, by correcting for the instrument spectral response (depending on filter and grating configuration, see Figure 3.3), the different measurement series are comparable. Figure 4.5 presents the spectrum when corrected for instrument spectral response.

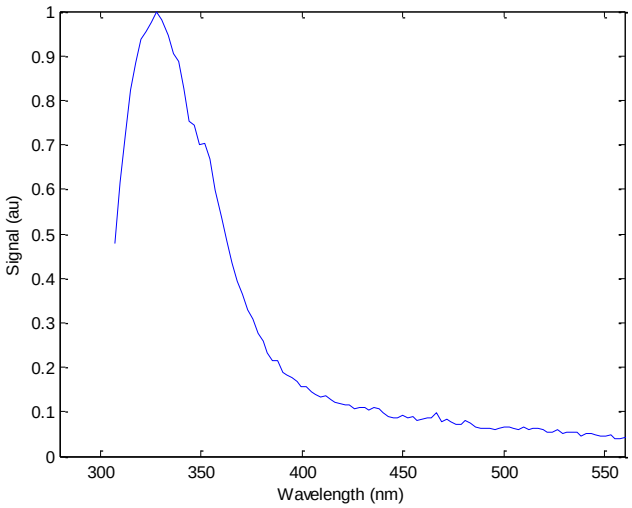

Figure 4.5 Spectrum corresponding to Figure 4.3 when correcting for instrument spectral responce

As discussed above, the spectrum above 560 nm is disregarded because of potential problems with overlapping orders in the spectrograph, and we have also omitted wavelengths below 305 nm because the instrument has virtually no response here.

In the following subsections the instrument corrected spectra as a result of 294 nm and 355 nm excitation wavelengths for all agents in consideration are given. The camera gain has not been taken into account in the spectrum correction, and it should be noted that high gain levels have been used throughout the experiment. The spectra are also corrected for laser energy and for APS-measured particle concentration. For the signals with 355 nm excitation, there is no overlapping problem so we chose to present these spectra out to ~610 nm.

4.2 Agent spectra

4.2.1 BG

BG, which is a simulant for anthrax, fluoresces significantly stronger when excited by 294 nm than 355 nm, see Figure 4.6. When exciting the aerosolized agent by a given pulse energy, the fluorescence is 6-8 times more intense at 294 nm than 355 nm laser wavelength. The strong 355 nm signal in the 294 nm excitation curve stems from backscattered 355 nm light that was not sufficiently removed from the 294 nm light. This was improved later in the experiments. We notice that the fluorescence peak seems to be close to the N_2 Raman-scatter peak. This is

unwanted, and would be an argument to move to a shorter excitation wavelength (since the frequency shift of Raman-scattering is fixed).

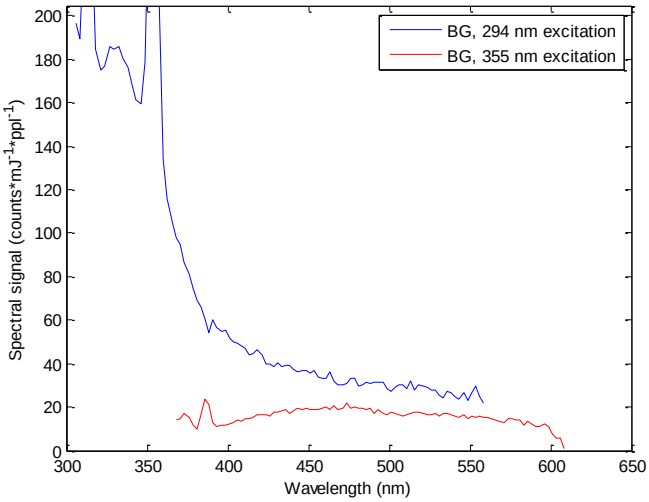

Figure 4.6 Fluorescence from BG excited by 294 nm (blue) and 355 nm (red) pulses

4.2.2 BT

The fluorescence from BT is presented in Figure 4.7. BT is another simulant for anthrax, and fluoresces 6-8 times stronger when excited by 294 nm than 355 nm pulses of similar pulse energy. We notice that the location of the fluorescence is very different from BG.

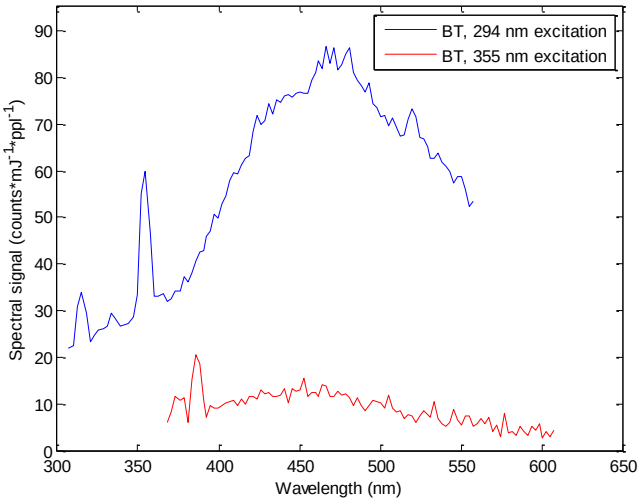

Figure 4.7 Fluorescence from BT excited by 294 nm (blue) and 355 nm (red) pulses

4.2.3 *E.coli*

Figure 4.8 shows the *E.coli* fluorescence, which is slightly higher at 355 nm excitation than the shorter wavelength. This probably indicates a significant content of NADH in the cells.

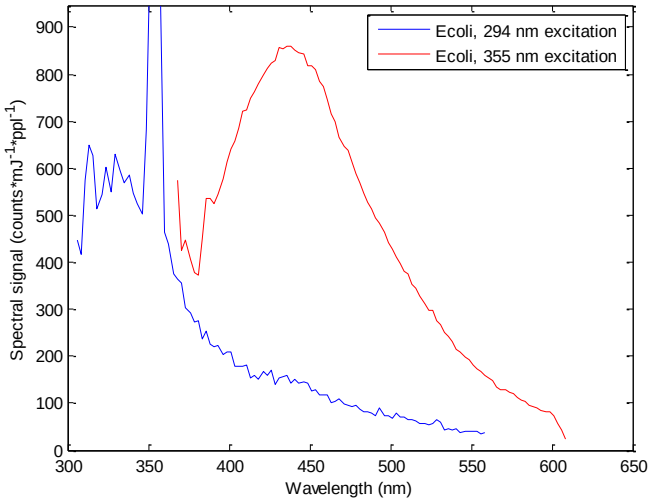

Figure 4.8 The fluorescence spectra from E.coli *excited by 294 nm (blue) and 355 nm (red) pulses*

4.2.4 EH

The fluorescence from an aerosol containing EH has approximately the same magnitude for both excitation wavelengths, see Figure 4.9. Like for *E.coli*, it also seems clear that there is significant NADH content in the cells.

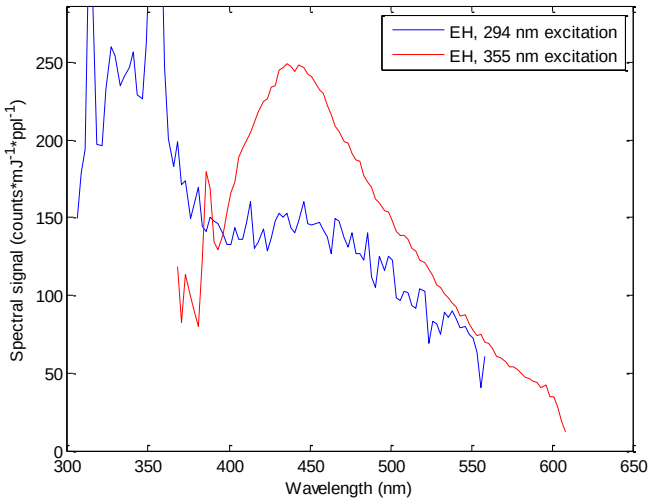

Figure 4.9 Fluorescence from EH excited by 294 nm (blue) and 355 nm (red) pulses

4.2.5 MS2

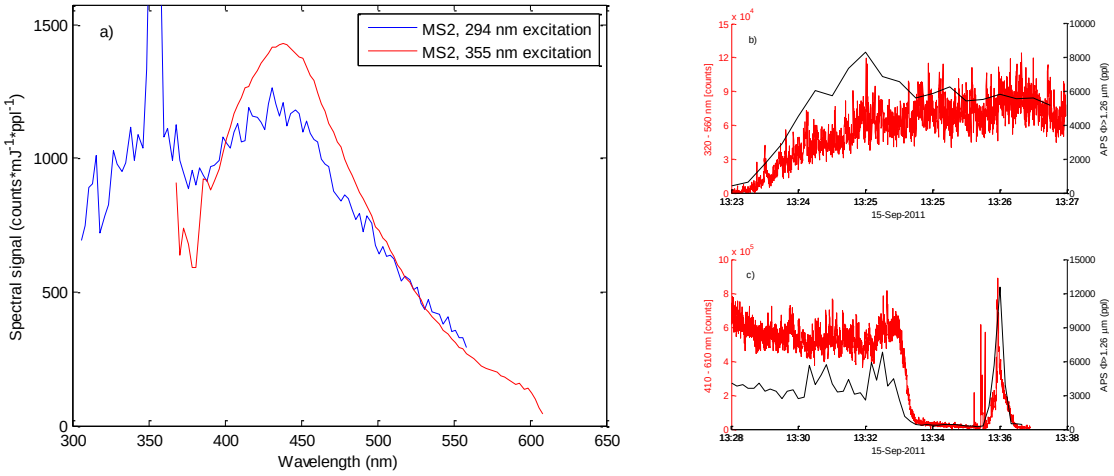

Figure 4.10 a) Fluorescence from MS2 excited by 294 nm (blue) and 355 nm (red) pulses. APS-signal and total fluorescence during 294 nm excitation (b) and 355 nm excitation (c)

MS2 is a simulant for BWA in the form of virus. The magnitudes of the spectra are similar for the two excitation wavelengths, see Figure 4.10a. The bacteriophage MS2 is a virus that infects *E.coli*. The solution was filtrated using a 0.2 µm filter before it was released in order to remove the *E.coli* bacteria. Even though the MS2 viruses pass the filter, and are thus less than 0.2 µm, they may cluster to form aggregates of different sizes in the release mechanism. This was not investigated. Considering that the background as measured by the APS instrument mainly consists of particles with aerodynamic diameters less than 1 µm, it may be difficult to estimate the particle concentration based on APS measurements. However, fluorescence and APS measurement for particles with aerodynamic diameter greater than 1.26 µm seem to correspond well, as seen in Figure 4.10b-c. The fluorescence at 355 nm (see Figure 4.10a) excitation indicates presence of NADH, related to metabolism which does not take place in virus. On the other side, the bacteria, and thus NADH, should have been significantly reduced by centrifuging and filtration. However, NADH from damaged *E.coli* cells may be dissolved and pass filtration.

4.2.6 OA

Approximately 60 % of the protein of egg white is ovalbumin. OA is a simulant for toxins, and contains 1-2 % tryptophan, an important fluorophore at excitation below 300 nm. We expected significantly stronger fluorescence at 294 nm than at 355 nm. Indeed it is stronger, however only a factor two, see Figure 4.11.

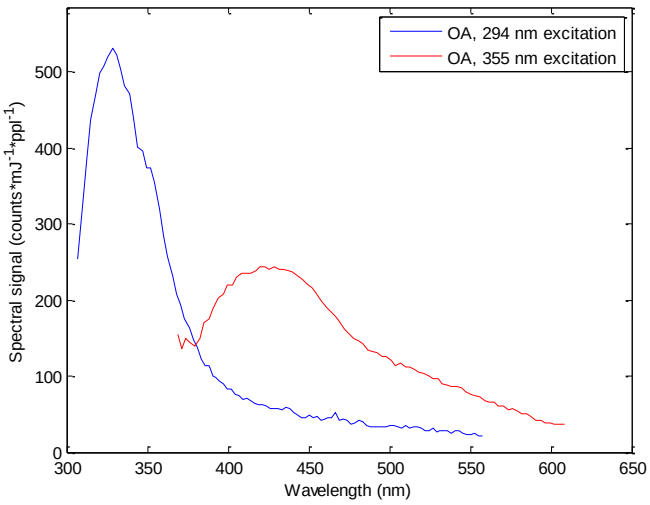

Figure 4.11 Fluorescence from OA excited by 294 nm (blue) and 355 nm (red) pulses

4.2.7 SM

Figure 4.12 shows that 294 nm excited SM fluoresces about twice as strongly as if excited at 355 nm.

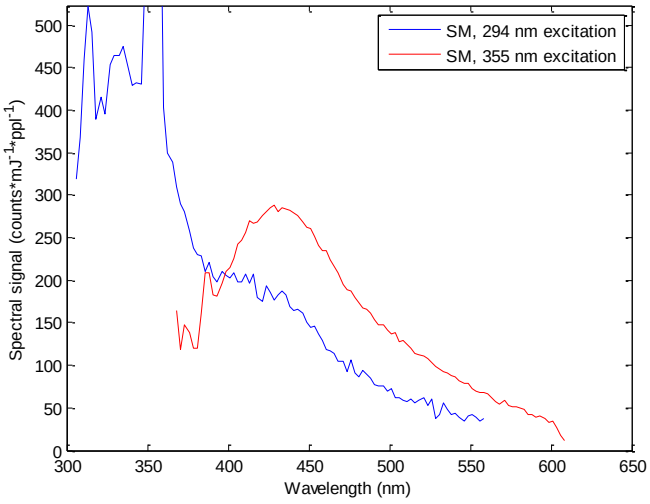

Figure 4.12 Fluorescence from SM excited by 294 nm (blue) and 355 nm (red) pulses

4.3 Comparison of spectra for different excitation wavelengths

In general, the following should be noted; spikes in the spectra are not characteristics of the agent fluorescence. Elastic scattering at the laser wavelength is seen even though the color glass filter attenuates the radiation at excitation wavelength by several orders of magnitude. Moreover, Raman-scattering of atmospheric constituents, in particular for N_2 shifting the wavenumber by 2330 cm^{-1} (to approximately 387 nm and 315 nm for 355 nm and 294 nm excitation, respectively), are inevitable, but may be attenuated by narrow bandstop filters if camera saturation becomes a problem. 355 nm elastic scattering also appears when operating the lidar at

294 nm, because our source uses 355 nm to generate the 294 nm radiation. The emitted 355 nm radiation is on the order of one in thousand of the 294 nm radiation due to optical leakage through dichroic optical components, thus the fluorescence due to excitation by the longer wavelength may be neglected. On the other hand, the elastic scattering is several orders of magnitude stronger than the fluorescence; hence the return signal is significant compared to the fluorescence. In an improved version of the lidar, the 355 nm leakage should be further reduced.

Another important parameter is the fluorescence cross section as function of the excitation wavelength. For the anthrax simulants BG and BT as well as the toxin simulant OA the 294 nm fluorescence appear to be a factor 6-8 and 2 larger than the 355 nm excited fluorescence, respectively, whereas 355 nm excitation appears to be as good as or better for the other agents. Also important are the fluorescence spectral features for the purpose of agent classification. The spectra for the different agents and excitation wavelengths are presented in Figure 4.13-4.14.

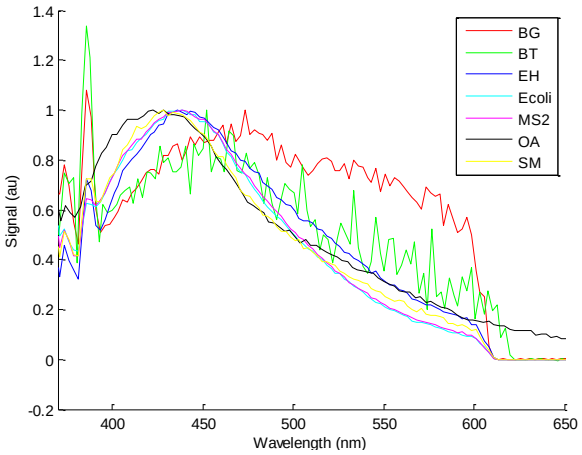

Figure 4.13 Fluorescence spectra when corrected for instrument spectral response for the seven different agents when excited by 355 nm radiation

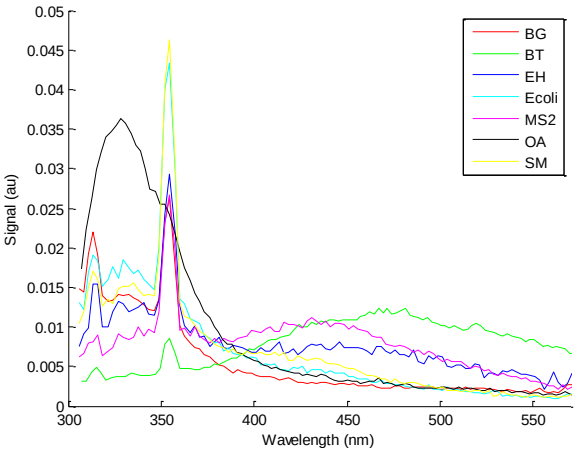

Figure 4.14 Fluorescence spectra when corrected for instrument spectral response for the seven different agents when excited by 294 nm radiation

By visual comparison, an excitation wavelength at 294 nm seems to generate more distinct fluorescence spectra than 355 nm excitation does. Previous work has shown that we are able to classify with low false alarm rate based on 355 nm excitation [4]. The significantly larger variation in spectra with 294 nm excitation implies that we should expect even lower false alarm rates and detection thresholds when classifying them. However, such classification has not been a topic of this work.

5 Discussion

In order to avoid problems with Raman scattering of atmospheric constituents appearing within the fluorescence spectrum, the excitation wavelength should ideally be shorter than the 294 nm used in these experiments. The fluorescence cross section of tryptophan has a peak at 280 nm (see Figure 2.1), but shorter wavelengths can also experience reduced transmission in air caused by ozone pollution (Figure 2.2). Therefore, an optimal excitation wavelength is probably in the 280-290 nm range.

Using the shorter excitation wavelength has to be traded off against the cost of generating it. The ~290 nm pulse energy will probably be less than 40 % of that at 355 nm. In addition, system complexity is added. On the other hand, the shorter wavelength fluorescence absorption cross section is larger for the important simulants, and, maybe more importantly, the spectra are apparently more distinct. In order to avoid problems with elastic backscatter of leaked 355 nm with the 294 nm excitation laser; this could be generated via an alternative approach where a 640 nm pulse is mixed with a 532 nm pulse [16]. Even this laser geometry is being studied in project 1179 [17].

6 Conclusion

The experiment verified our hypothesis that UVLIF featuring excitation by a laser with wavelength 294 nm is more efficient than one at 355 nm for standoff detection of biological aerosols that are BWA simulants. In particular, the anthrax simulants BG and BT had almost an order of magnitude stronger fluorescence, whereas the toxin simulant OA fluoresced approximately twice as strong at the shorter excitation wavelength. For the virus simulant MS2, and the *E.Coli* and SM cultures of bacteria, the fluorescence responses were approximately the same in terms of magnitude for the different excitation wavelengths. Stronger fluorescence means higher sensitivity for a given excitation pulse energy. This is crucial for standoff distance and detectable concentration levels. More importantly, however, was the prominent differences between the agent spectra at the shorter excitation wavelength. More distinguishable spectra allow for better classification thus lower false alarm rates, which turns out to be the major challenge of standoff detection.

Our test range worked well, and the trial proved the FFI-range has the capacities needed for standoff instrument semi-closed chamber testing. With little effort, we were able to use in-house

dissemination equipment developed for releasing lower number of particles than necessary if the whole release chamber were to be filled to proper concentration levels. Two persons were sufficient to run the experiment; one to operate the release chamber and reference equipment, and the other to operate the standoff instrument.

7 Final remarks

At the end of the project, some general considerations regarding possible instrument improvements were made. Lowering the optical loss is of major concern, as the standoff capability is limited by the fluorescence signal strength.

- Laser source: the pulse energy emitted within the instrument field of view is what counts. The highest possible output has to be traded off against complexity and increased fluorescence cross section when selecting wavelength. Moreover, the wavelength should be placed such that Raman-scattering misses the most important spectral regions of fluorescence.
- The losses in the collecting optics and optical path should be minimized by appropriate coatings and low number of optical elements.
- The instrument spectral resolution should be as low as possible, for the benefit of increased signal to noise level in each spectral channel. Moreover, prisms as dispersive elements should be considered as an alternative to reflective gratings, which has significant optical losses.

When the excitation wavelength, and thus the spectral interval of the fluorescence, has been determined, an appropriate reflective coating, e.g. UV-enhanced aluminum, should be used for all mirrors. The refractive elements, and fiber ends if applicable, should be broadband AR-coated for the fluorescence spectral range, and proper angles of incidence. In particular, a refractive dispersive element should be considered once the spectral resolution has been specified, due to significant loss of reflective gratings. A prism may also render a color glass filter for the removal of elastic backscattering at the excitation wavelength superfluous, by orienting the prism such that the focus of the elastic scattering falls outside the detector/ focal plane array. Our investigations point to 10-20 spectral channels in order to be able to discriminate a handful of agents [18]. Spectral response must be traded off against cost and complexity in the choice of detector, which could be either an ICCD camera or a PMT-array.

In terms of signal conditioning and classification, previously developed methods for classification and false alarm rates should be applied to 294 nm excitation data for a qualitative comparison to results achieved with results using a 355 nm laser.

Acknowledgement

We would like to thank Torbjörn Tjärnhage, FOI Umeå, for lending us equipment necessary to carry out some of the experiments, and instructing us on how to use them.

References

[1] M Sletmoen (2008). *Vekselvirkning mellom lys og biologisk materiale*. FFI-notat 2008-00828 (In Norwegian), FFI, Kjeller. www.ffi.no

[2] G Rustad and Ø Farsund (2008). *Standoff detection of biological aerosols by UV-laser induced fluorescence*. FFI-rapport 2008/02025, FFI, Kjeller. www.ffi.no

[3] Ø Farsund and G Rustad (2008). *Standoff detection of biologic aerosols by means of UV-laser induced fluorescence - results from Umeå trial*. FFI-rapport 2008/01990, FFI, Kjeller. www.ffi.no

[4] R Nyhavn, H J F Moen, Ø Farsund, and G Rustad. *Optimal classification of standoff bioaerosol measurements using evolutionary algorithms*. Proc. SPIE vol. 8018 (2011) 801806. doi: 10.1117/12.883919

[5] K Baxter, M Castle, S Barrington, P Withers, V Foot, A Pickering, and N Felton. *UK small scale UVLIF lidar for standoff BW detection*. Proc. SPIE vol. 6739 (2007) Z7390-Z7390. doi: 10.1117/12.737730

[6] S Solberg, NILU, Kjeller. Personal communication. 2005

[7] D B Wetlaufer. *Ultraviolet Spectra of Proteins and Amino Acids*. Adv. Prot. Chem. vol. 17 (1962) 303-390.

[8] *MODTRAN*, v 4. Air Force Research Labs, Hanscom AFB, MA. www.kirtland.af.mil/library/factsheets/factsheet.asp?id=7915

[9] O Farsund and G Rustad. *Sum-Frequency Generation of High-Energy and High-Beam-Quality Ultraviolet Pulses*. Int. J. Opt. vol. 2011 (2011) doi: 10.1155/2011/737684

[10] (2011). *Thorlabs Catalog.* http://www.thorlabs.de/Thorcat/12200/12239-S01.pdf

[11] (2011). *Shamrock 163 specifications.* http://www.andor.com/spectrographs/czerny-turner_spectrographs/shamrock_163/specifications/

[12] (2011). *Edmund Optics, optics and optical instruments catalog.* http://www.edmundoptics.com/images/articles/curve.gif

[13] (2011). *Schott GG385 Glass Transmission Filter Data*. http://www.optical-filters.com/gg385.html

[14] (2011). *Schott WG305 Glass Transmission Filter Data.* http://www.optical-filters.com/wg305.html

[15] (2011). *Andor iStar 720 Intensified CCD Camera Series Specification.* http://www.andor.com/scientific_cameras/istar_iccd_camera/720-intensified-detector/

[16] G Rustad and Ø Farsund (2008). *Evaluation of methods and materials for optical generation of high pulse energies at 290 nm*. FFI-rapport 2008/02107, FFI, Kjeller. www.ffi.no

[17] G Rustad and O Farsund. *High pulse energy and symmetrical far field from an optical parametric oscillator in the red spectral range*. JEOS:RP vol. 6 (2011) 11058. doi: 10.2971/jeos.2011.11058

[18] Ø Farsund, G Rustad, I Kåsen, and T V Haavardsholm. *Required Spectral Resolution for Bioaerosol Detection Algorithms Using Standoff Laser-Induced Fluorescence Measurements*. IEEE Sens. J. vol. 10 (2010) 655-661. doi: 10.1109/2009.2037794

List of acronyms

APS	Aerodynamical Particle Sizer	Instrument measuring the number and aerodynamic diameter of particles
AR	Anti Reflection	
ATCC	*American Type Culture Collection*	
BBO	Beta-barium borate	Nonlinear optical crystal
BG	*Bacillus atrophaeus*	Simulant for Anthrax
Biolidar		Lidar measuring biological aerosols
BT	*Bacillus thuringiensis*	Simulant for Anthrax
BWA	Biological warfare agent	
CCD	Charge coupled device	Si-based focal plane array common in visible imaging cameras
CIP	*Collection de Institut Pasteur*	
DSM	*Deutsche Sammlung von Mikroorganismen und Zellkulturen*	
E.coli	*Escherichia coli*	
EH	*Pantoea Agglomerans*	Simulant for *tularemia*
FOI	Totalförsvarets forskningsinstitut	
ICCD	Intensified CCD	Camera with light amplification
IR	Infrared	
KTA	Potassium Titanyl Arsenate	Nonlinear optical crystal
Lidar	Light detection and ranging	
LIF	Laser Induced Fluorescence	
MS2		Bacteriophage (virus that infects *E.coli*)
NADH	Nicotinamide adenine dinucleotide	
nm	nanometer, 10^{-9} m	
O_3	Ozone	
OA	Ovalbumin	Simulant for toxins
OPO	Optical parametric oscillator	Optical resonator for generating two frequencies of lower frequencies of the input light by means of a nonlinear optical crystal
PMT	Photo Multiplier Tube	
SM	*Serratia Marcescens*	
USTD	US Standard	
UV	Ultraviolet	
µm	Micrometer, 10^{-6} m	

Appendix A Data

The acquired data sets are included in the appended DVD. Each data set is found in a separate folder named with the agent released and start-time of acquisition. The folders contain data files in *.mat*- (Matlab) and *.bin*-formats (binary format written by the acquisition program). The *.bin* files contain raw data, for which a dedicated Matlab script must be used to read the data. APS-data are found in the folder with the same name, containing different versions of files from the APS-instrument in addition to the *APSData.mat* file, see Table A.1 below.

File name	Format	Description
CalibrationData.mat	Matlab matrix named *CalibrationData*	Wavelength calibration data. Column 1: wavelength [nm] Column 2: pixel number (as if no binning were used)
IStar_kalibrert	Matlab struct named *TSdata*	Fields of *TSdata*: *ts*: timeseries of spectra: *signal – reference* (acquired without laser illumination) data values *lambda*: wavelength associated with spectra in *ts* *Laserout*: NA in this experiment *LaserDump*: NA in this experiment *Header*: Camera and calibration parameters *grating*: 'l/mm - blaze wavelength' *laserenergy*: pulse energy [mJ] measured before acquisition *excwl*: excitation wavelength [nm]
TSnew	Matlab struct named *TSnew*	Same as TSdata, but with additional fields: *Spectrum*: time average of spectra during significant fluorescence due to disseminated agent *StartSpec* and *EndSpec*: time [s after start of acquisition] defining the interval from which *Spectrum* is obtained *corrSpectrum*: spectrum corrected for instrument spectral response *lamcorrSpec*: wavelength axis of *corrSpectrum*
iStar_Data.bin	Binary file containing raw data from ICCD camera	
PMT_Data.bin	Binary file containing raw data from PMT-measurement	Not applicable in this experiment as the PMT-channel was not used.
APSData	Matlab struct named APSdata	Fields of *APSdata*: *counts*: APS instrument samples [particles/ml] divided in 52 aerodynamic diameter intervals *APSDate*: date of samples *APSTime*: time of samples *AeroDiam*: the 52 diameter intervals

Table A.1 Data files and their content

A set of Matlab-files is also included. The different files are explained in Table A.2 below. The paths found in the Matlab scripts need to be adjusted.

File name	Format	Description
MakeTSdata.m	Matlab script	Read raw data and puts data into the struct *TSdata*
ISTARDataReader.m	Matlab script	Function used by *MakeTSdata.m* to read raw data
PlotAlleUtslipp.m	Matlab script	Plots all releases in the format shown in Appendix B
Sammenlikne_Spektra_v5.m	Matlab Script	Plots the selected release data of the different agents for 294 nm and 355 nm excitation
Spektralrespons_Biolidar.m	Matlab script	Plots the spectral responses of the components constituting the biolidar, component by component and for the different instrument configurations
gitterdata.mat	Matlab data	Spectral response data for the different lidar components
Tab_kronologisk.mat	Matlab data	Names of data folders for all release data of the field trial ordered chronologically
TabDompaData2011.mat	Matlab data	Names of folders containing release data ordered in different ways. Most importantly *UV* and *UV355*, where releases representing all agents have been selected for 294 nm and 355 nm excitation respectively (the spectra presented in this report)

Table A.2 Matlab files appended and brief description of contents; for reading data to and simple plotting in Matlab

Appendix B Total fluorescence, APS data and integrated spectrum

In this appendix, the total fluorescence as function of time, APS-data and spectrum for all acquisitions of the experiment, regardless of other parameters such as saturation, software failure or other problems, are presented. Each acquisition is presented on a separate page, however in the same format:

- Uppermost graph: Total fluorescence (red) and APS measurement (black), referring to left and right axes, respectively. The left axis also states the spectral range over which the data have been integrated (320 – 560 nm for 294 nm excitation, 420 – 610 nm otherwise). The APS-data have been integrated for aerodynamic diameters exceeding 1.26 µm. The x-axis is computer time (the two computers were not perfectly synchronized). The text in the upper right hand corner states camera parameters, and the duration of the recording in terms of number of samples at approximately 10 Hz (*# samples*).
- Lowermost graph: Time average of all measured spectra, of which maximum value of the total fluorescence exceeds 10 % of the corresponding maximum value of the entire data set (assuming that this simple restriction extracts the spectra caused by fluorescence). The title of the lowermost figure is simply the folder name of the data. This name is self explanatory in the sense that the agent (if one was released during the recording) and start time of acquisition appear in it.

The data are appended to this report electronically as well, see Appendix A.

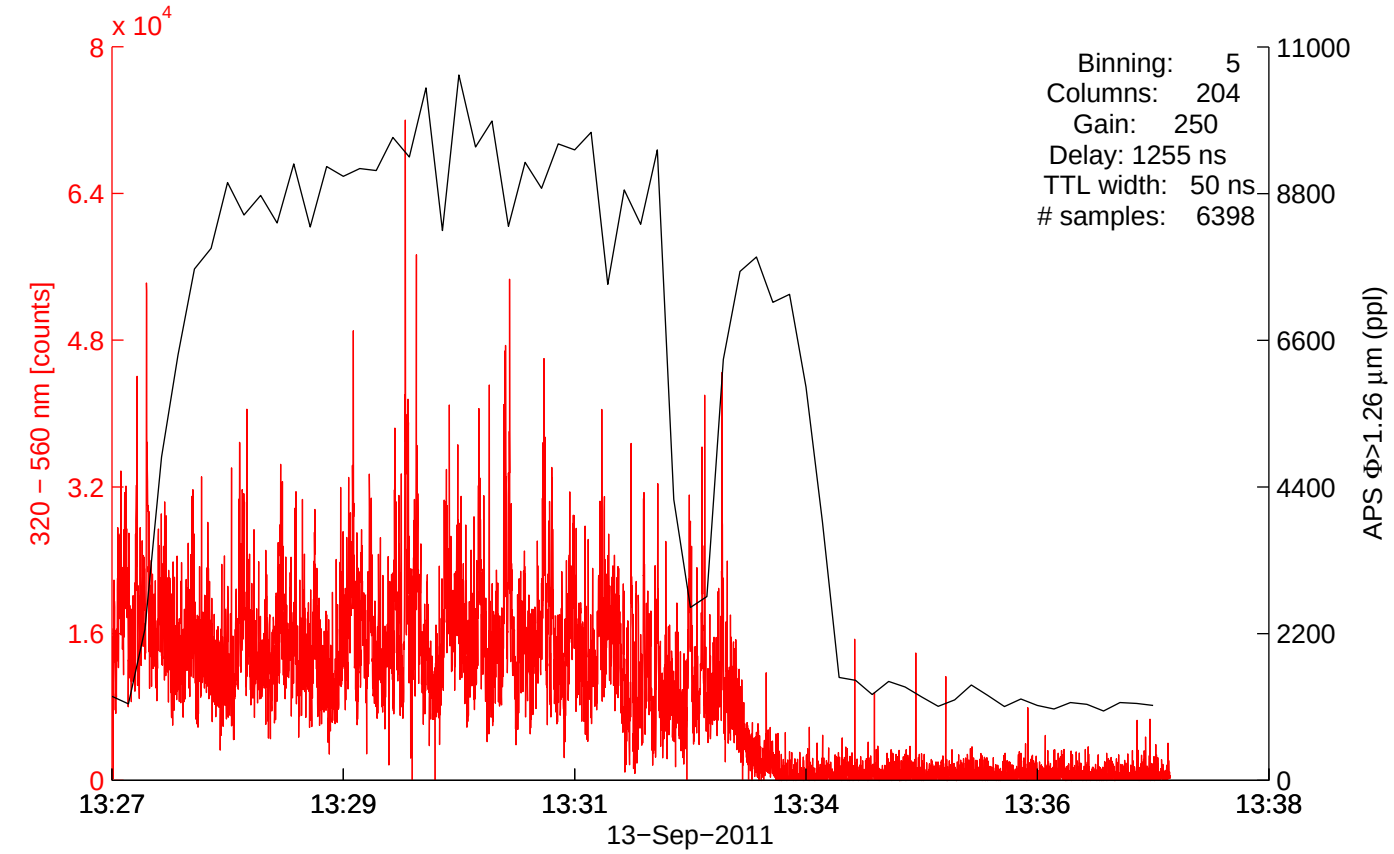
x 10^4
8
6.4
4.8
3.2
1.6
0
320 – 560 nm [counts]
11000
8800
6600
4400
2200
0
APS Φ>1.26 µm (ppl)
Binning: 5
Columns: 204
Gain: 250
Delay: 1255 ns
TTL width: 50 ns
samples: 6398
13:27
13:29
13:31
13:34
13:36
13:38
13−Sep−2011

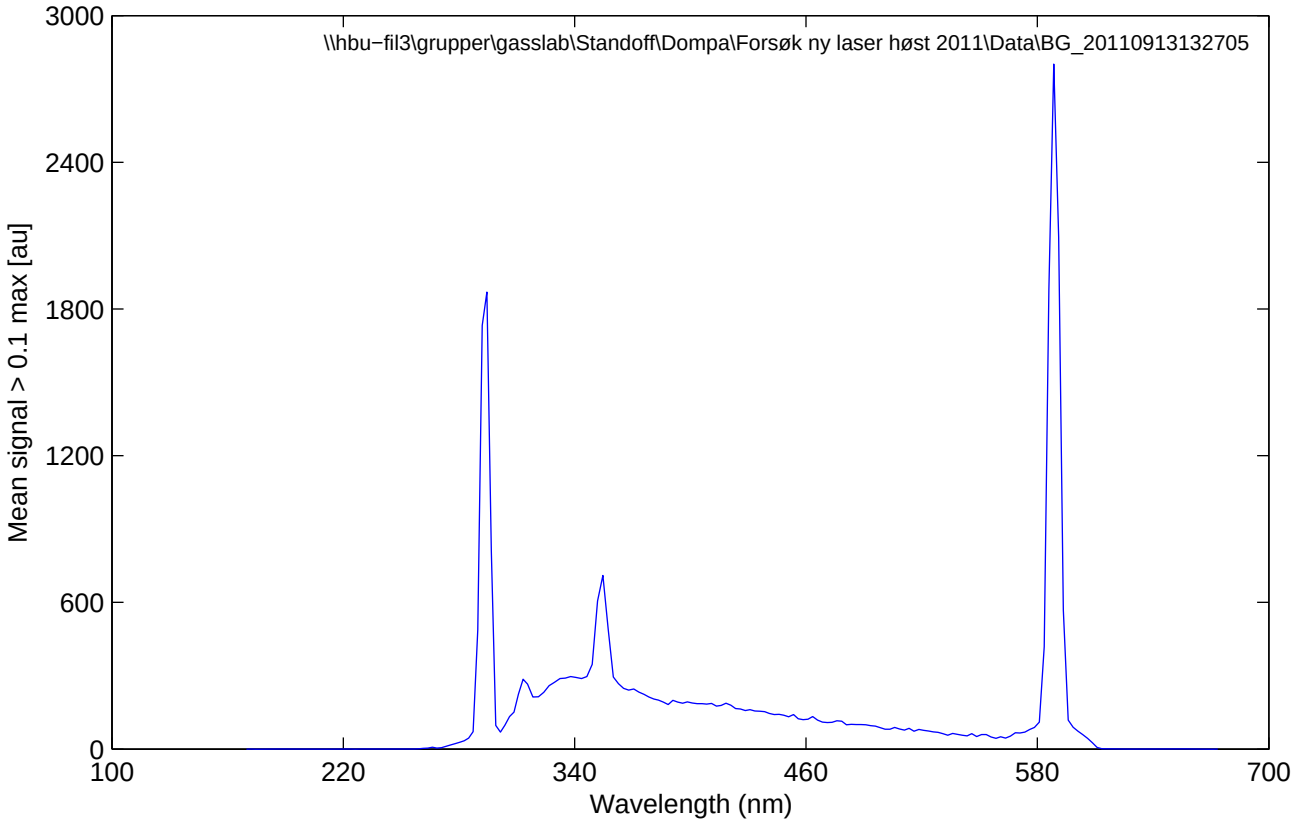
\\hbu−fil3\grupper\gasslab\Standoff\Dompa\Forsøk ny laser høst 2011\Data\BG_20110913132705
3000
2400
1800
1200
600
0
Mean signal > 0.1 max [au]
100
220
340
460
580
700
Wavelength (nm)

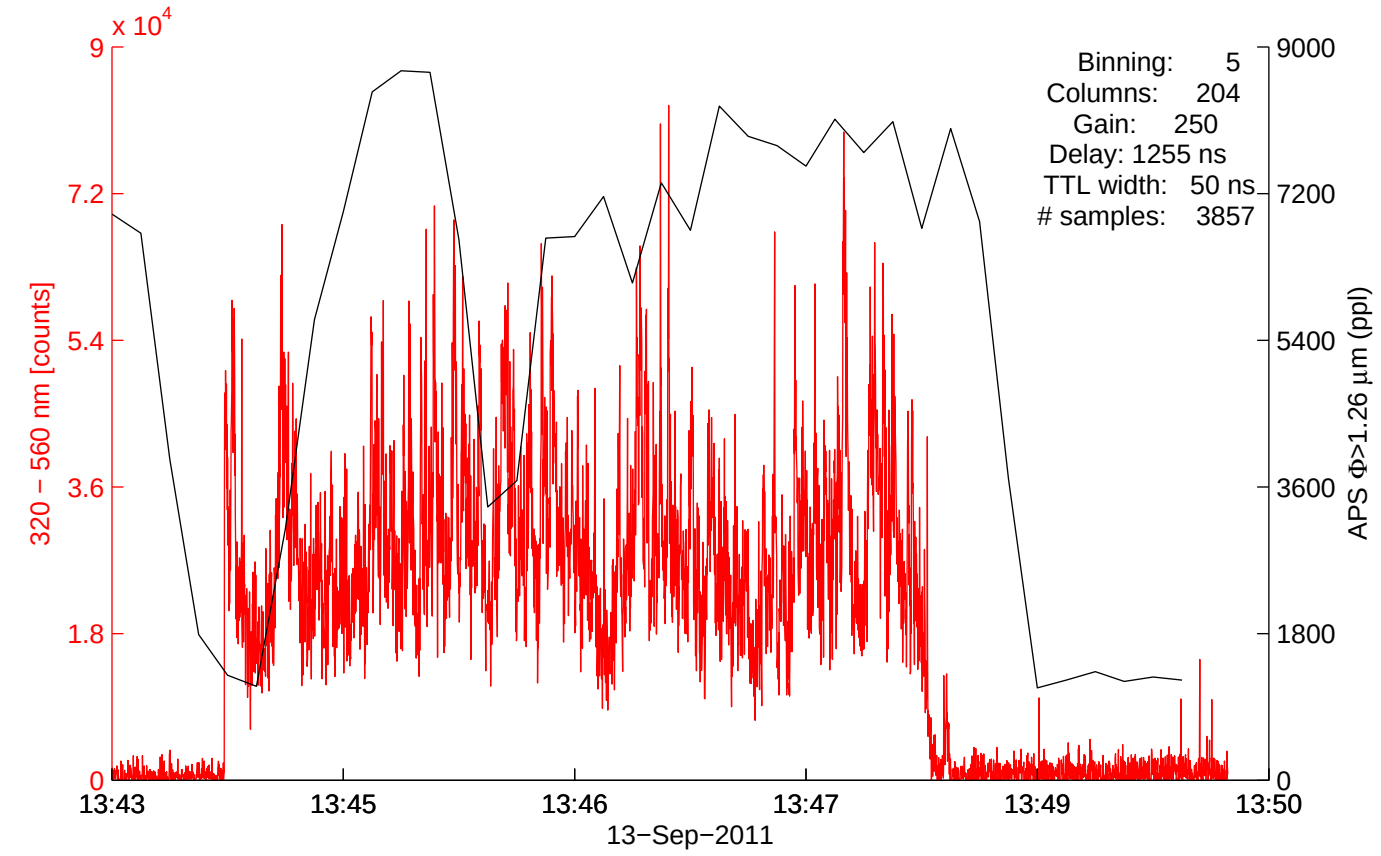
x 10^4
9
7.2
5.4
3.6
1.8
0
320 – 560 nm [counts]
9000
7200
5400
3600
1800
0
APS Φ>1.26 µm (ppl)
Binning: 5
Columns: 204
Gain: 250
Delay: 1255 ns
TTL width: 50 ns
samples: 3857
13:43
13:45
13:46
13:47
13:49
13:50
13−Sep−2011

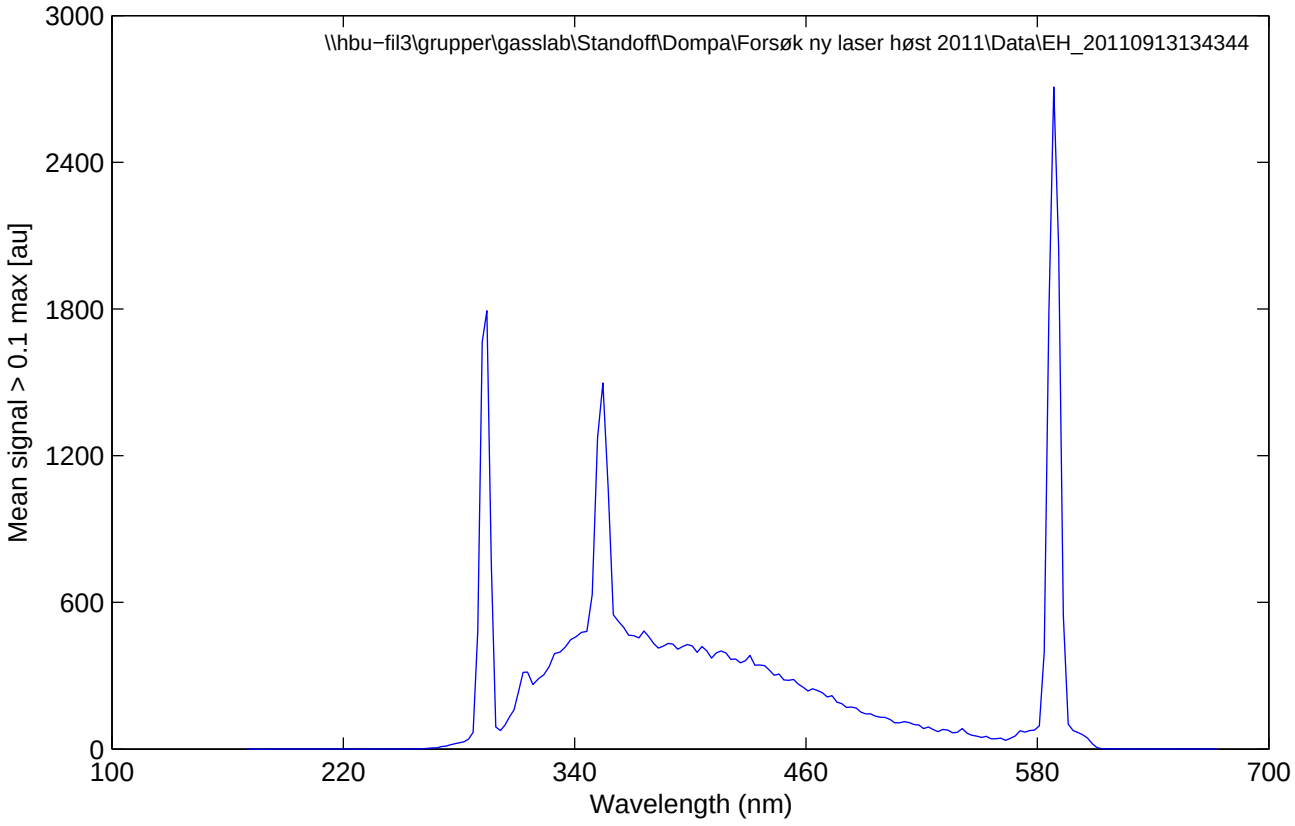
\\hbu−fil3\grupper\gasslab\Standoff\Dompa\Forsøk ny laser høst 2011\Data\EH_20110913134344
3000
2400
1800
1200
600
0
Mean signal > 0.1 max [au]
100
220
340
460
580
700
Wavelength (nm)

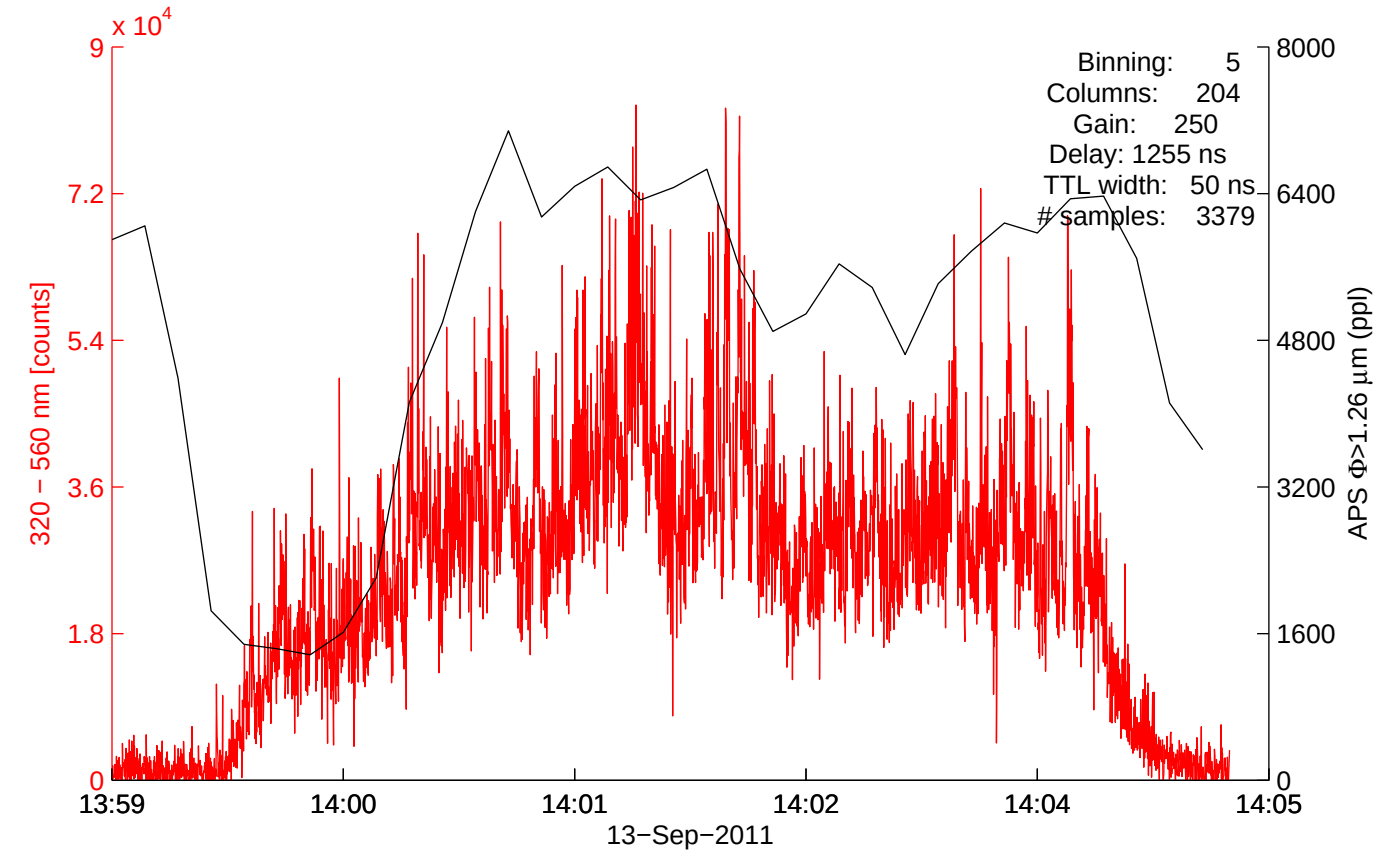
x 10^4
9
7.2
5.4
3.6
1.8
0
320 – 560 nm [counts]
8000
6400
4800
3200
1600
0
APS Φ>1.26 µm (ppl)
Binning: 5
Columns: 204
Gain: 250
Delay: 1255 ns
TTL width: 50 ns
samples: 3379
13:59
14:00
14:01
14:02
14:04
14:05
13−Sep−2011

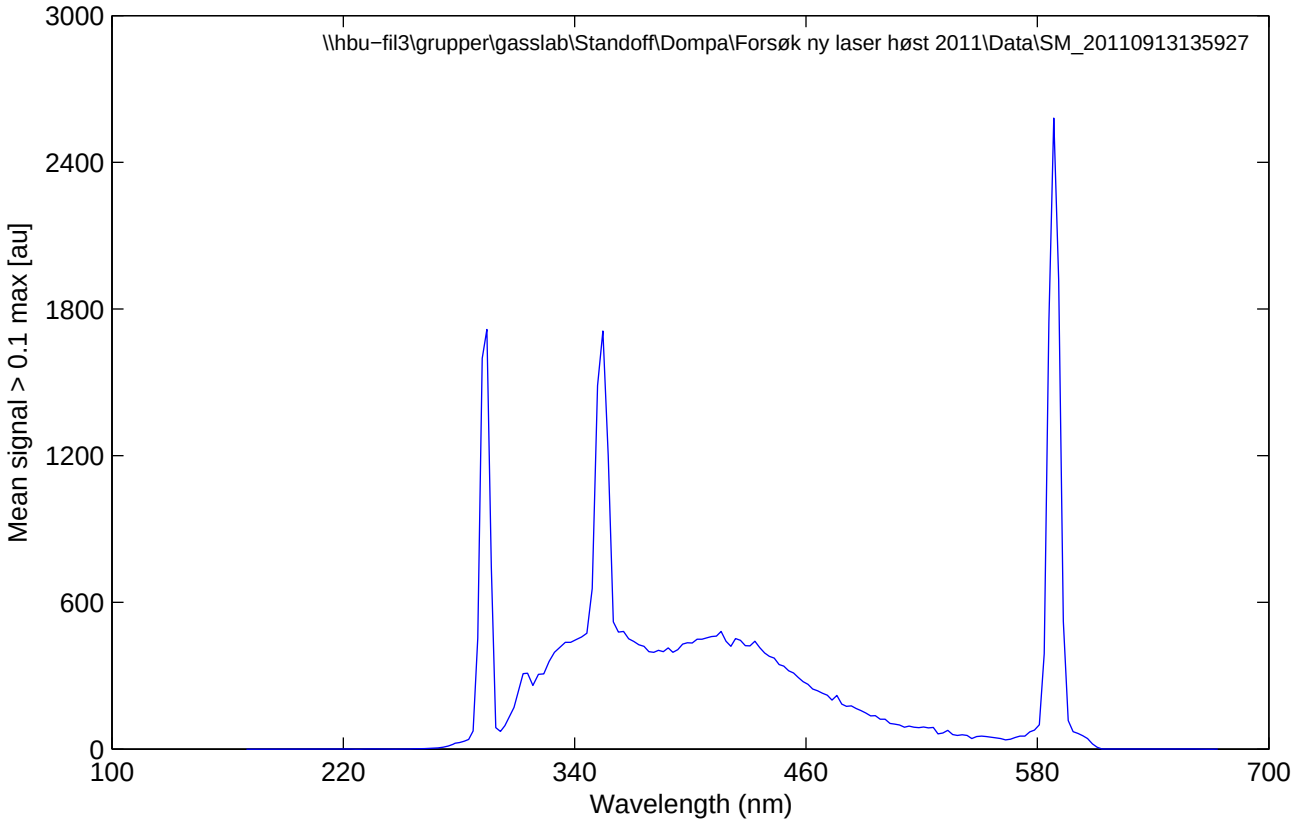
\\hbu−fil3\grupper\gasslab\Standoff\Dompa\Forsøk ny laser høst 2011\Data\SM_20110913135927
3000
2400
1800
1200
600
0
Mean signal > 0.1 max [au]
100
220
340
460
580
700
Wavelength (nm)

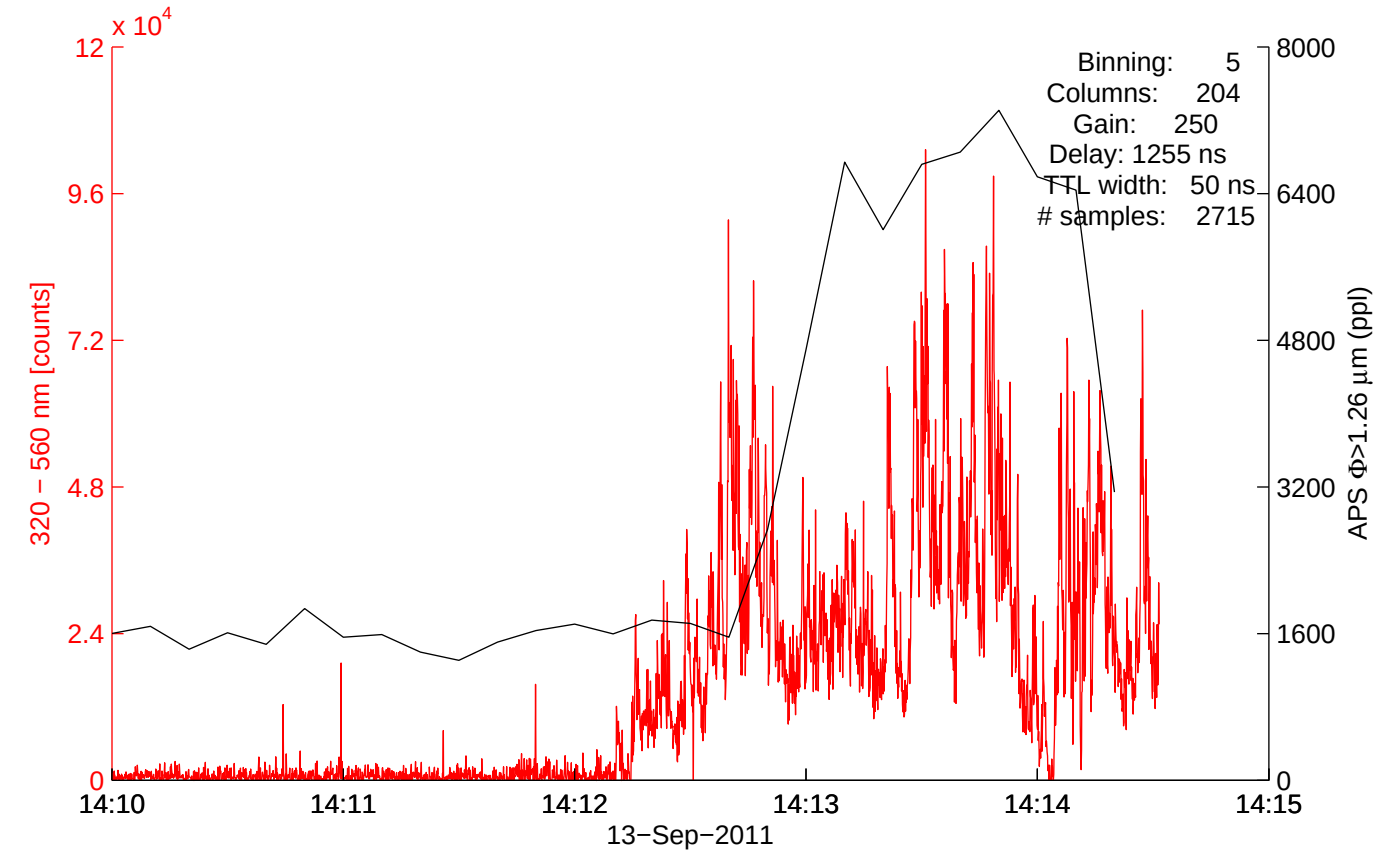
x 10^4
12
9.6
7.2
4.8
2.4
0
320 – 560 nm [counts]
8000
6400
4800
3200
1600
0
APS Φ>1.26 µm (ppl)
Binning: 5
Columns: 204
Gain: 250
Delay: 1255 ns
TTL width: 50 ns
samples: 2715
14:10
14:11
14:12
14:13
14:14
14:15
13−Sep−2011

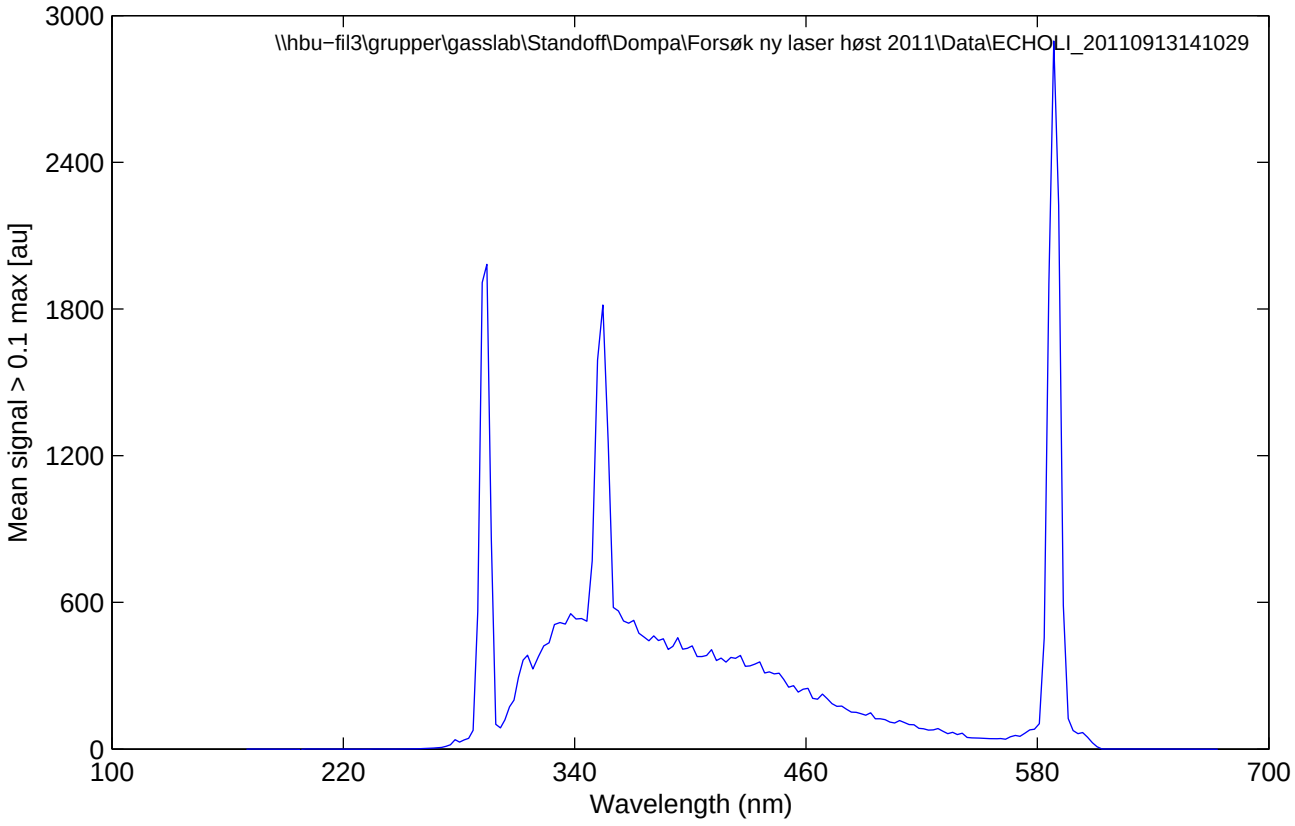
\\hbu−fil3\grupper\gasslab\Standoff\Dompa\Forsøk ny laser høst 2011\Data\ECHOLI_20110913141029
3000
2400
1800
1200
600
0
Mean signal > 0.1 max [au]
100
220
340
460
580
700
Wavelength (nm)

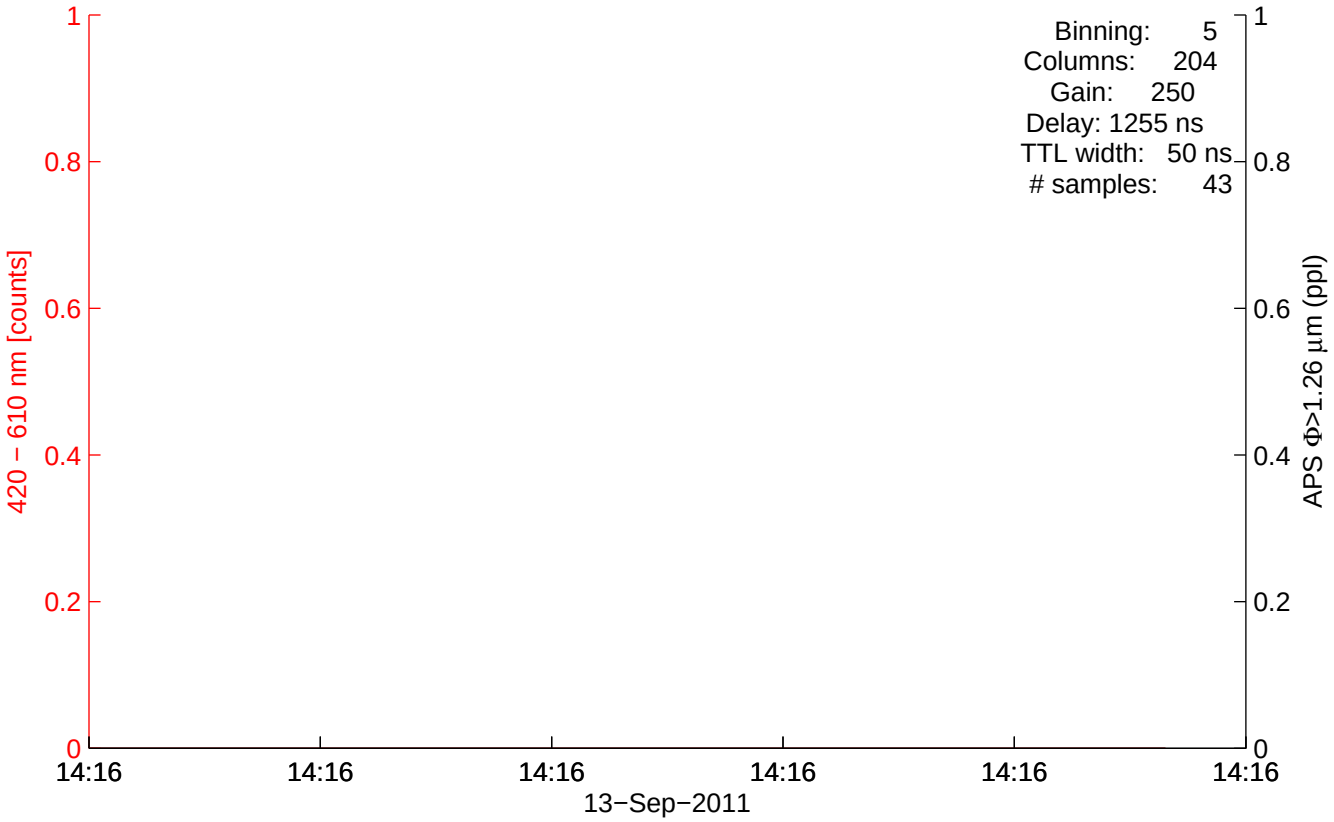
Binning: 5
Columns: 204
Gain: 250
Delay: 1255 ns
TTL width: 50 ns
samples: 43
420 – 610 nm [counts]
APS Φ>1.26 µm (ppl)
0
0.2
0.4
0.6
0.8
1
14:16
13−Sep−2011

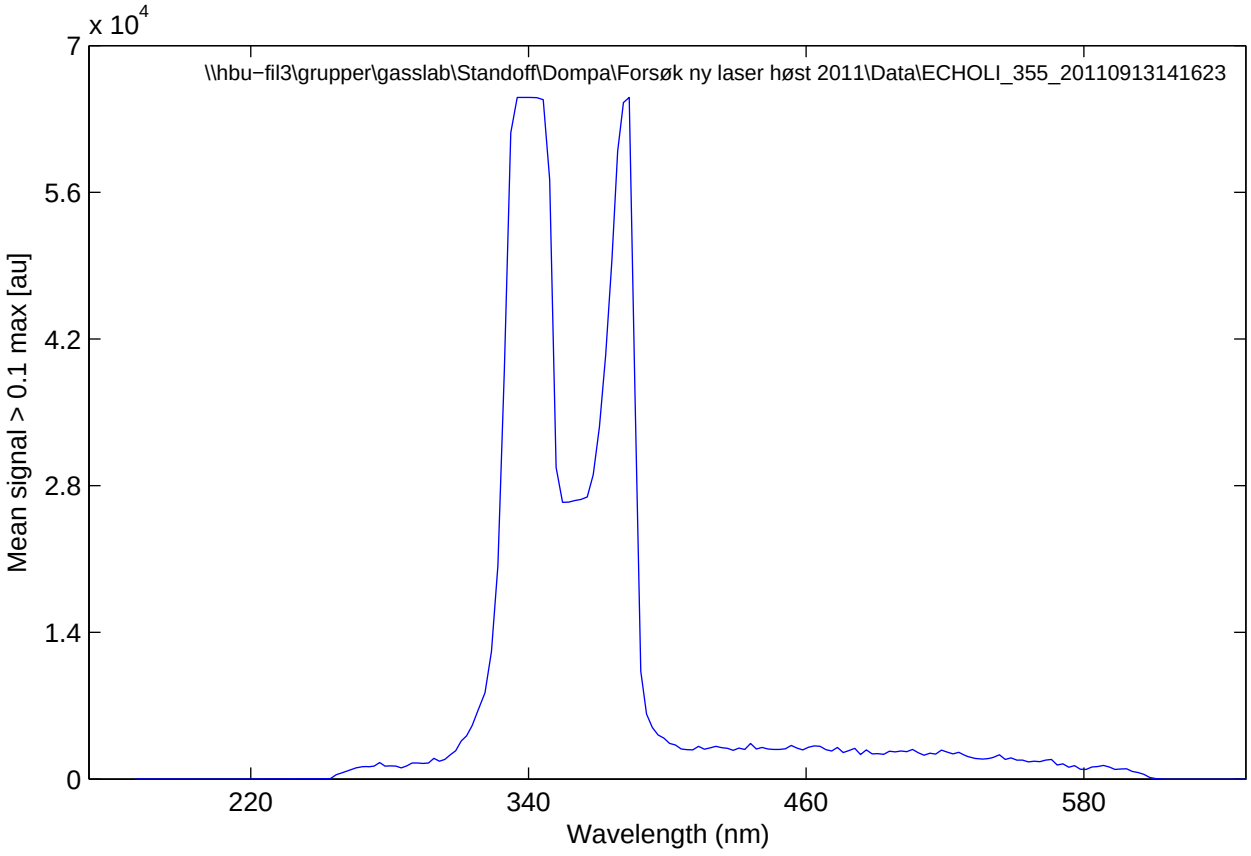
x 10^4
\\hbu−fil3\grupper\gasslab\Standoff\Dompa\Forsøk ny laser høst 2011\Data\ECHOLI_355_20110913141623
Mean signal > 0.1 max [au]
0
1.4
2.8
4.2
5.6
7
220
340
460
580
Wavelength (nm)

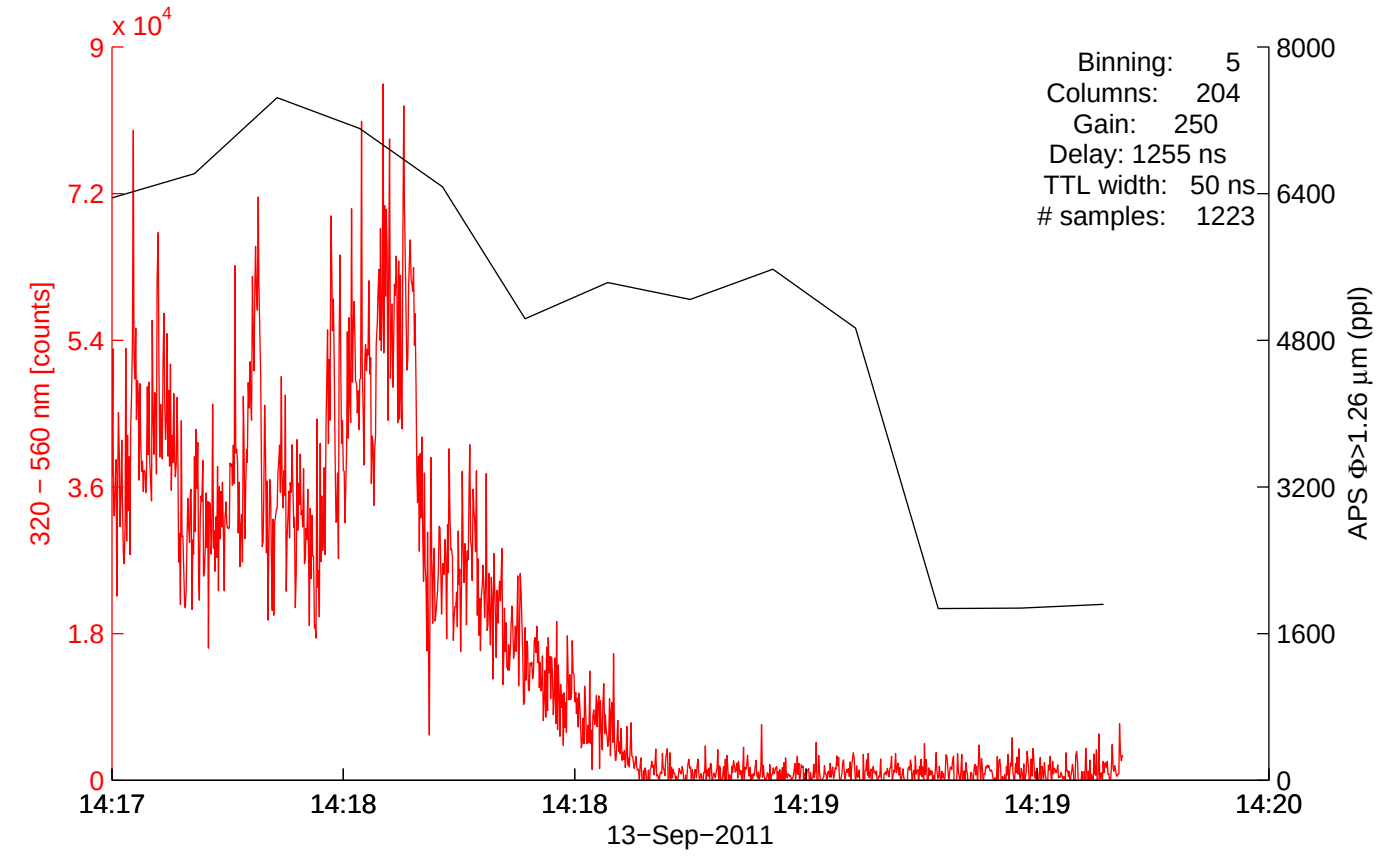
x 10^4
9
7.2
5.4
3.6
1.8
0
320 – 560 nm [counts]
8000
6400
4800
3200
1600
0
APS Φ>1.26 µm (ppl)
Binning: 5
Columns: 204
Gain: 250
Delay: 1255 ns
TTL width: 50 ns
samples: 1223
14:17
14:18
14:18
14:19
14:19
14:20
13−Sep−2011

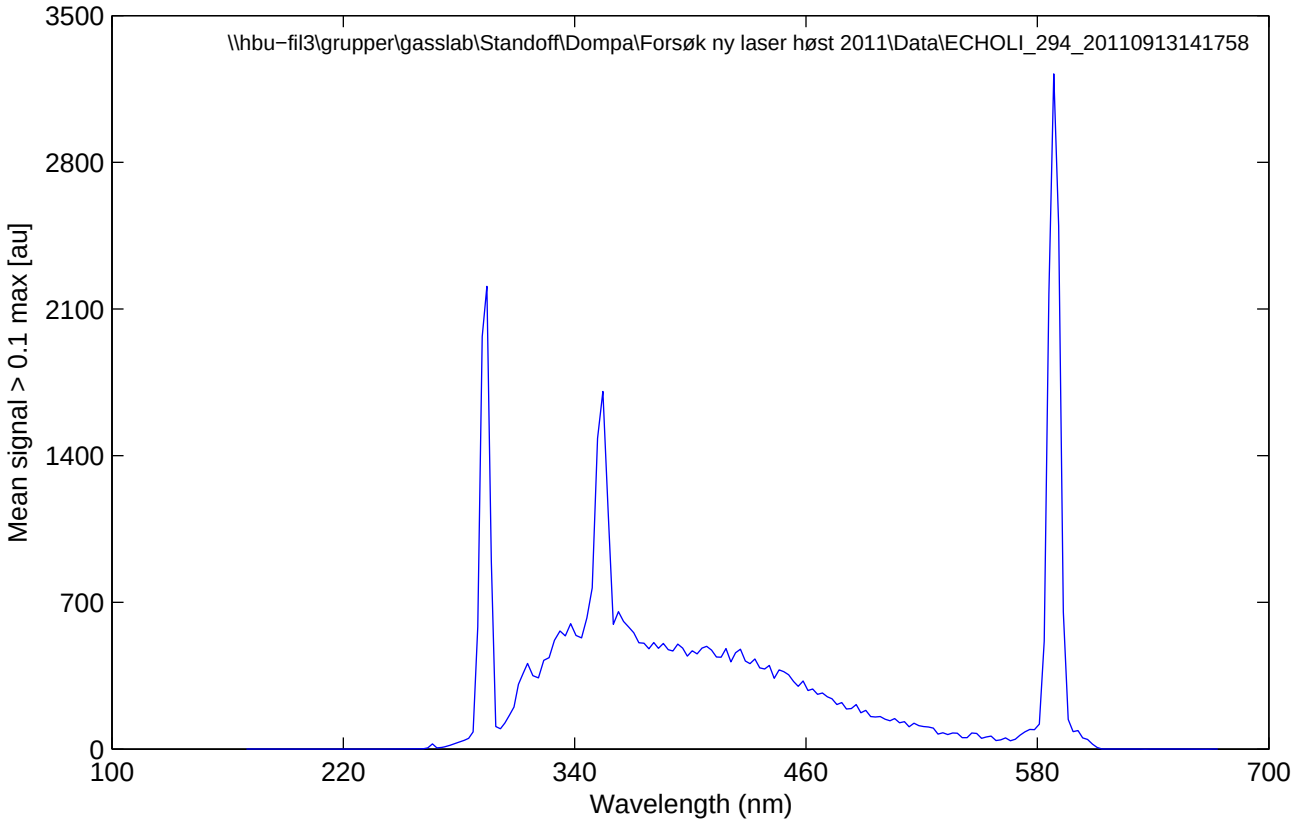
\\hbu−fil3\grupper\gasslab\Standoff\Dompa\Forsøk ny laser høst 2011\Data\ECHOLI_294_20110913141758
3500
2800
2100
1400
700
0
Mean signal > 0.1 max [au]
100
220
340
460
580
700
Wavelength (nm)

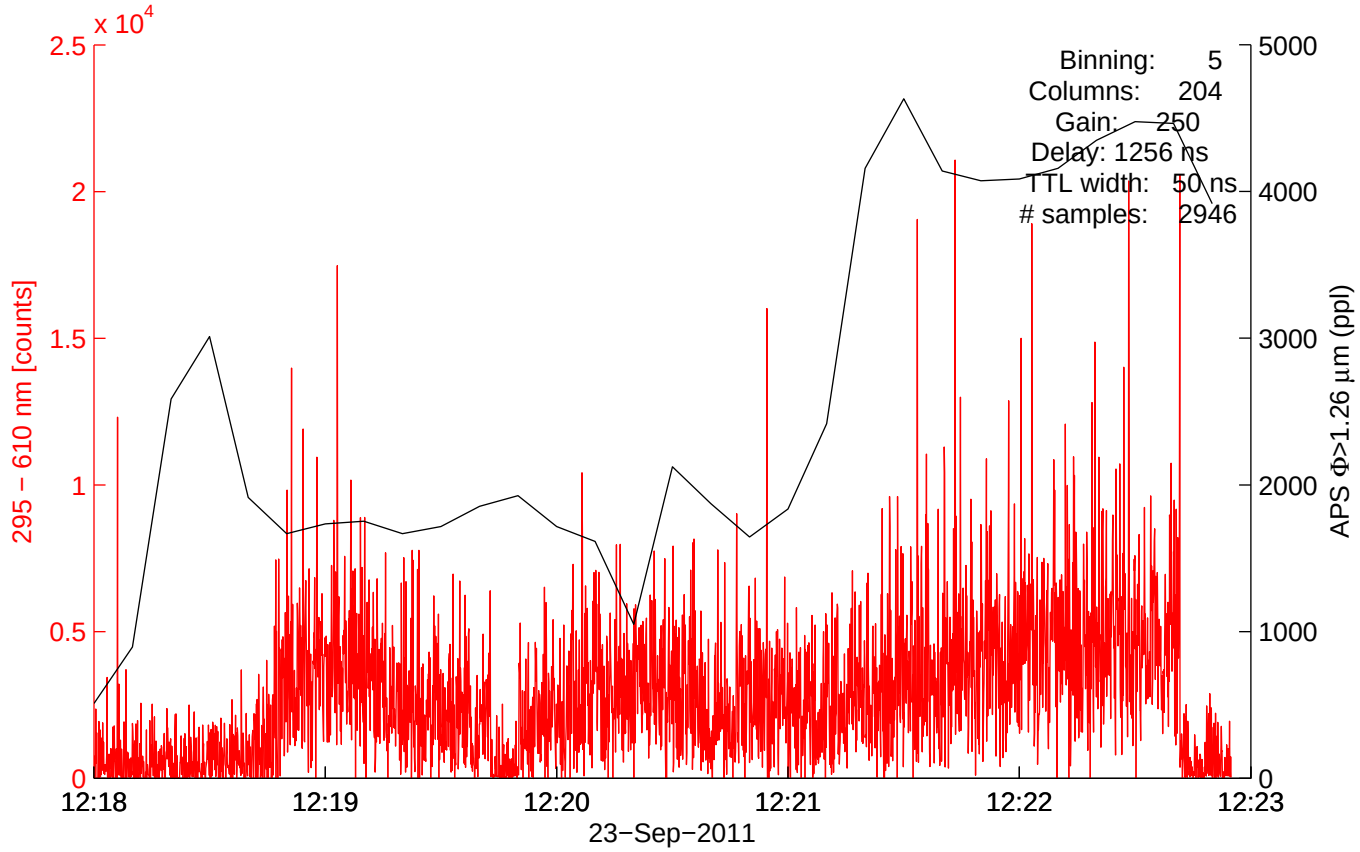
x 10^4
2.5
2
1.5
1
0.5
0
295 – 610 nm [counts]
5000
4000
3000
2000
1000
0
APS Φ>1.26 µm (ppl)
Binning: 5
Columns: 204
Gain: 250
Delay: 1256 ns
TTL width: 50 ns
samples: 2946
12:18
12:19
12:20
12:21
12:22
12:23
23−Sep−2011

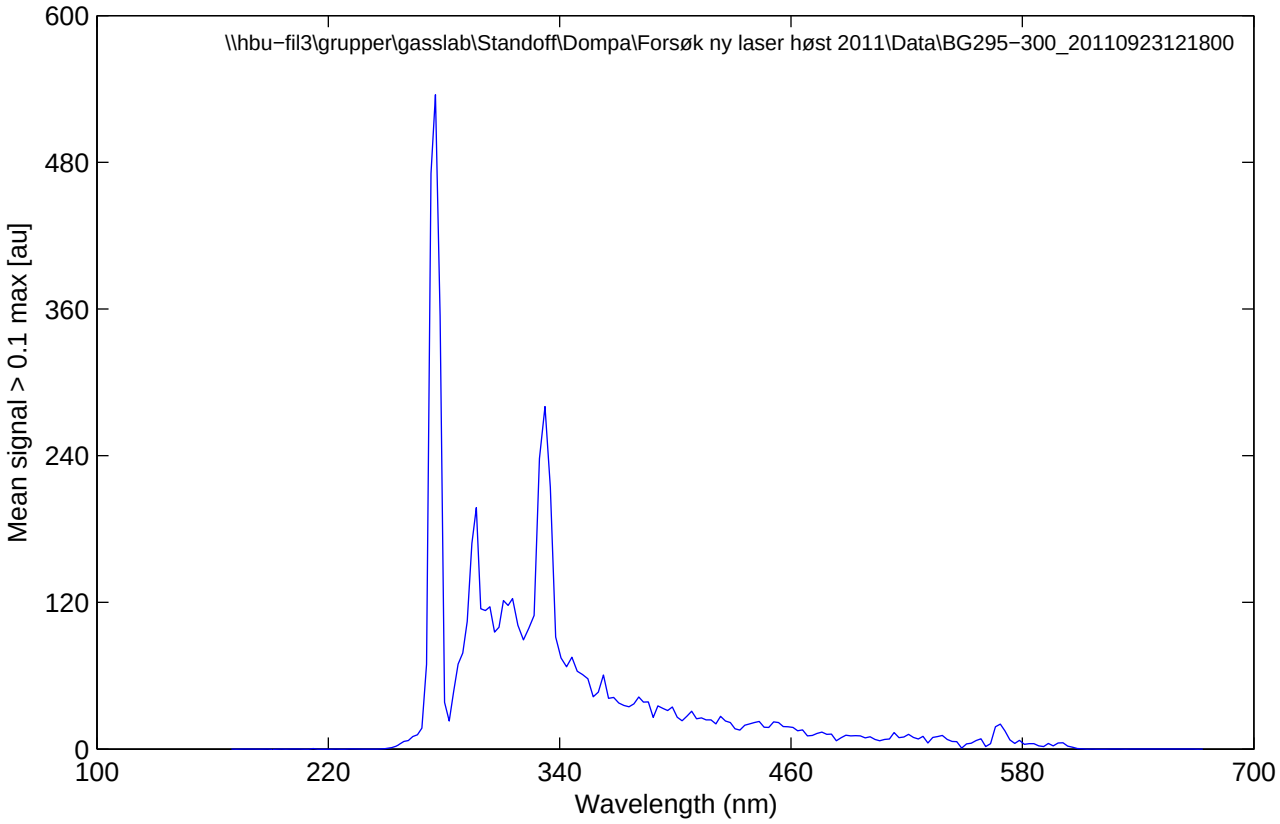
\\hbu−fil3\grupper\gasslab\Standoff\Dompa\Forsøk ny laser høst 2011\Data\BG295−300_20110923121800
600
480
360
240
120
0
Mean signal > 0.1 max [au]
100
220
340
460
580
700
Wavelength (nm)

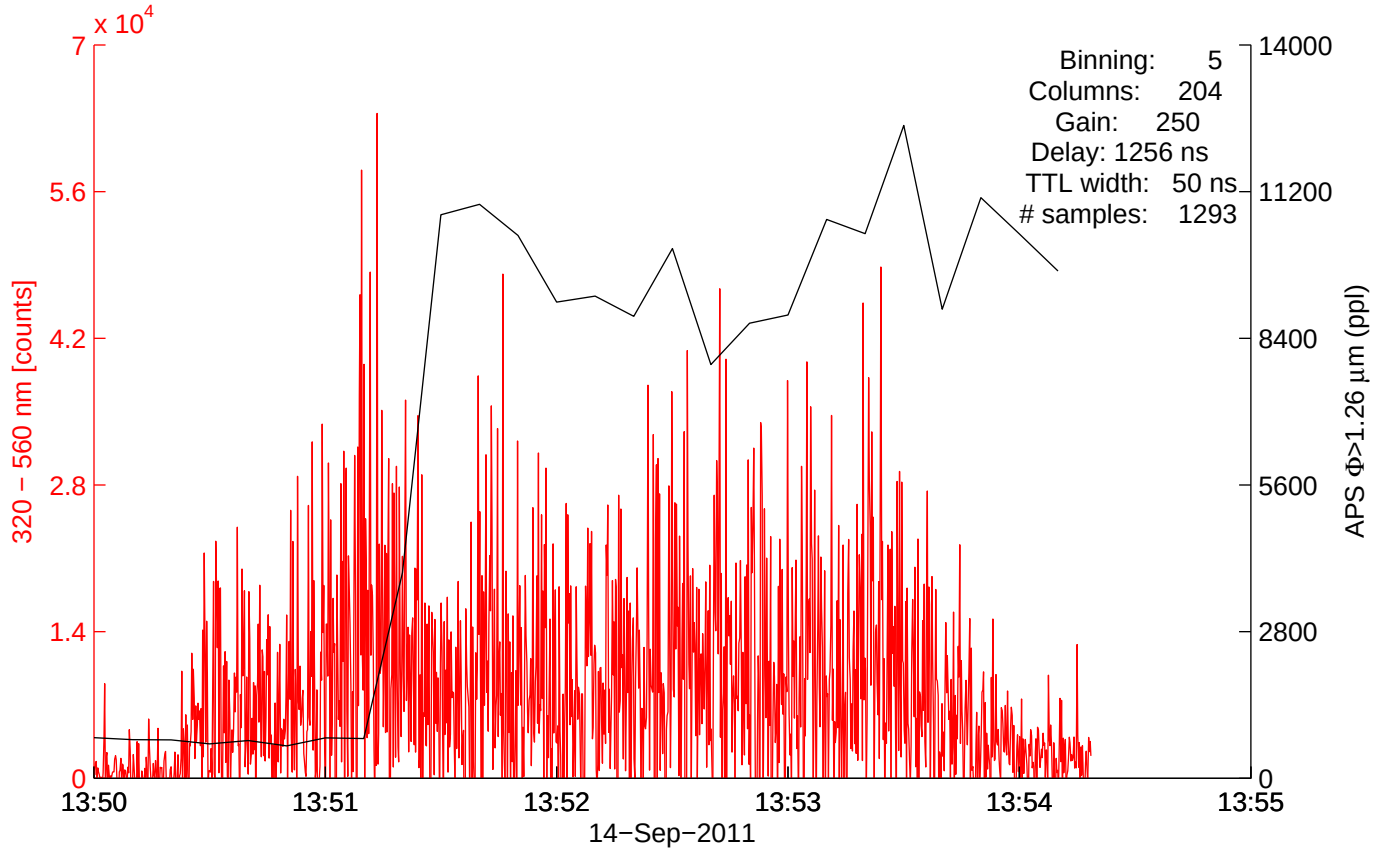
x 10^4
7
5.6
4.2
2.8
1.4
0
320 – 560 nm [counts]
14000
11200
8400
5600
2800
0
APS Φ>1.26 µm (ppl)
Binning: 5
Columns: 204
Gain: 250
Delay: 1256 ns
TTL width: 50 ns
samples: 1293
13:50
13:51
13:52
13:53
13:54
13:55
14−Sep−2011

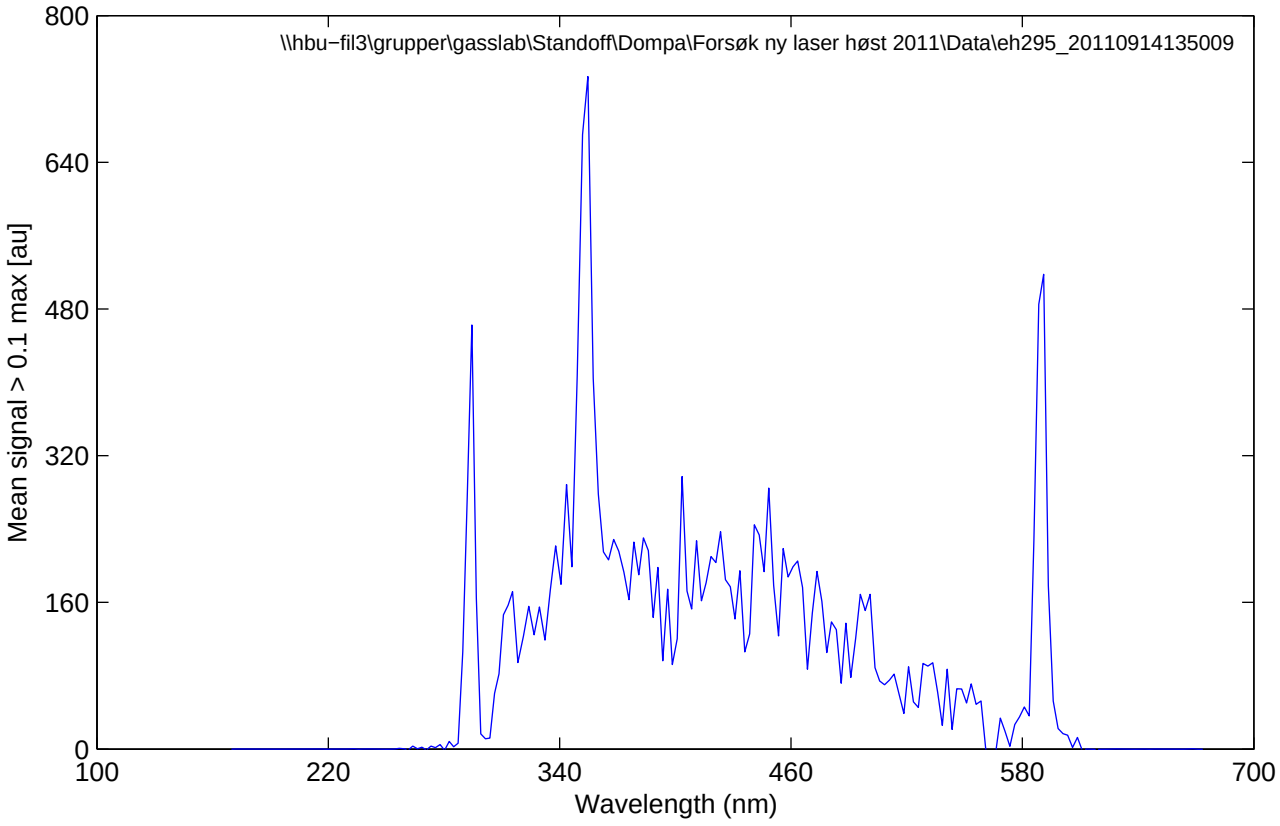
\\hbu−fil3\grupper\gasslab\Standoff\Dompa\Forsøk ny laser høst 2011\Data\eh295_20110914135009
800
640
480
320
160
0
Mean signal > 0.1 max [au]
100
220
340
460
580
700
Wavelength (nm)

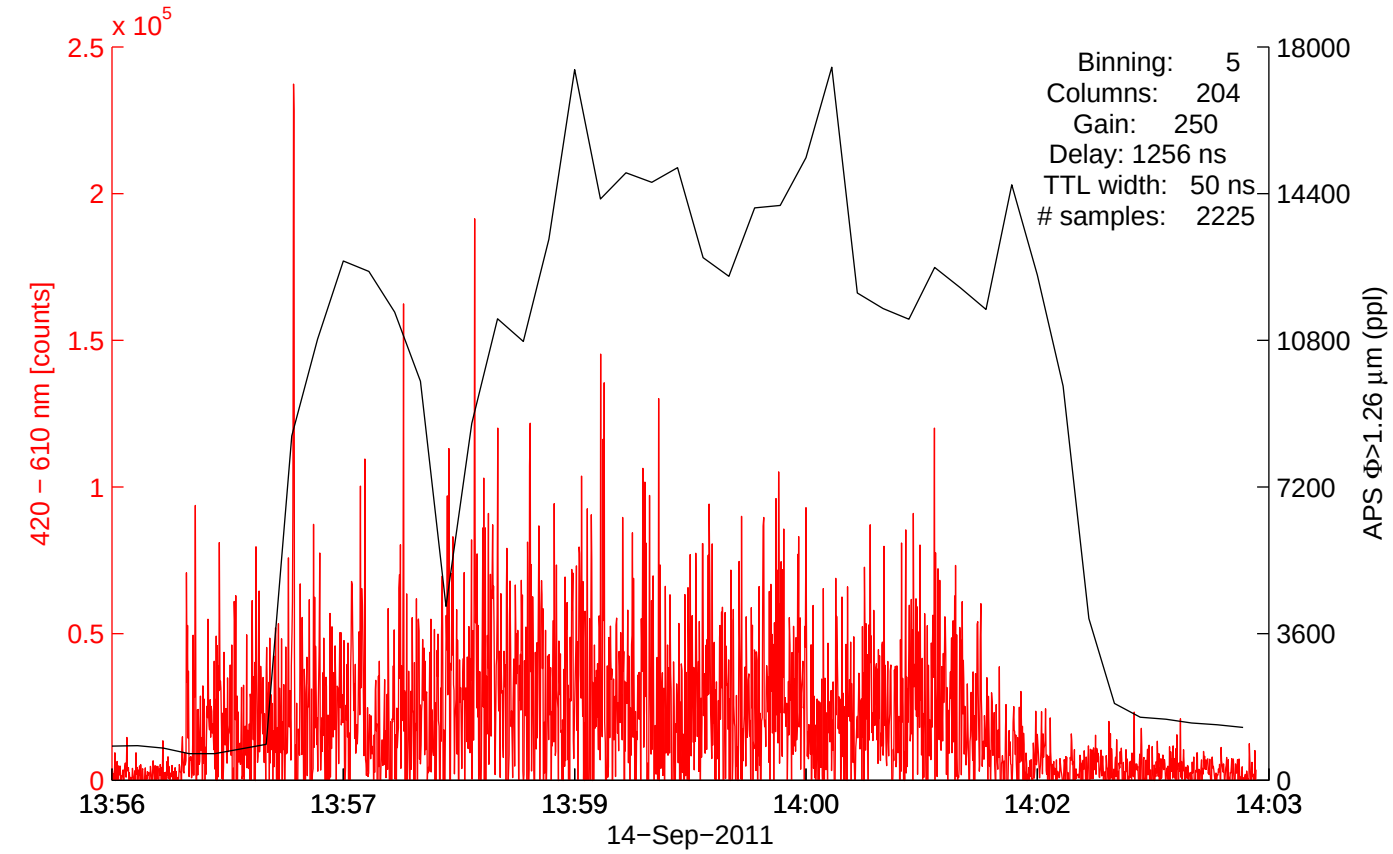
x 10^5
2.5
2
1.5
1
0.5
0
420 – 610 nm [counts]
18000
14400
10800
7200
3600
0
APS Φ>1.26 µm (ppl)
Binning: 5
Columns: 204
Gain: 250
Delay: 1256 ns
TTL width: 50 ns
samples: 2225
13:56
13:57
13:59
14:00
14:02
14:03
14−Sep−2011

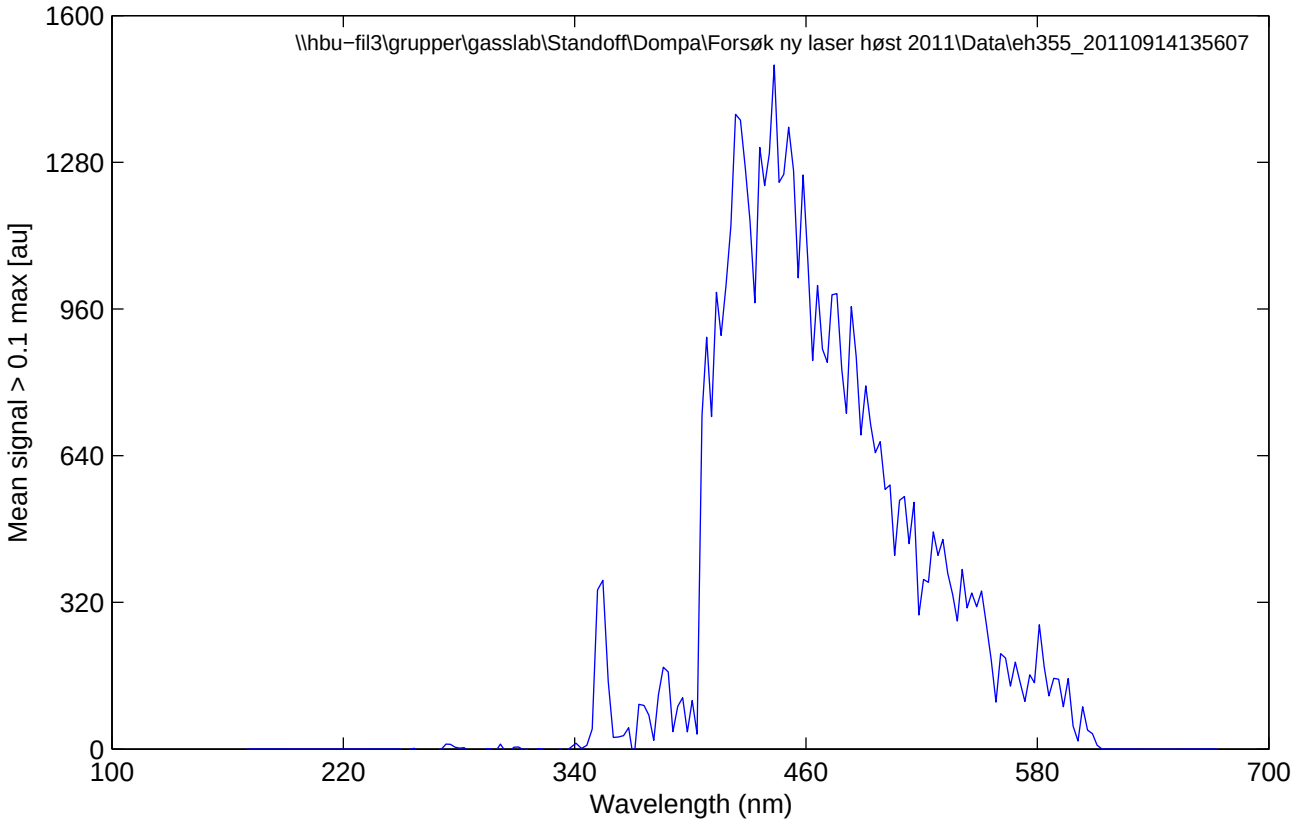
\\hbu−fil3\grupper\gasslab\Standoff\Dompa\Forsøk ny laser høst 2011\Data\eh355_20110914135607
1600
1280
960
640
320
0
Mean signal > 0.1 max [au]
100
220
340
460
580
700
Wavelength (nm)

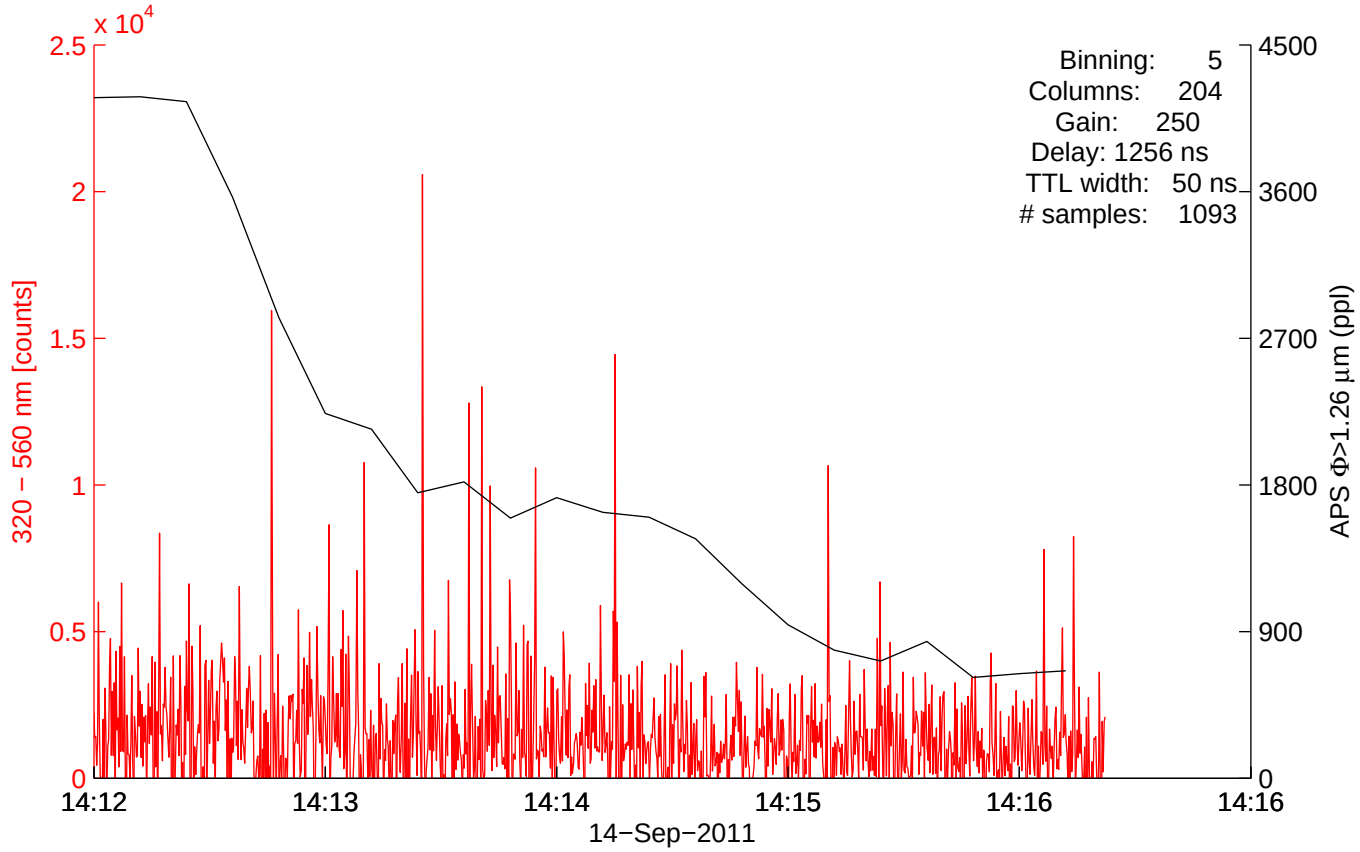
x 10^4
2.5
2
1.5
1
0.5
0
320 – 560 nm [counts]
4500
3600
2700
1800
900
0
APS Φ>1.26 µm (ppl)
Binning: 5
Columns: 204
Gain: 250
Delay: 1256 ns
TTL width: 50 ns
samples: 1093
14:12
14:13
14:14
14:15
14:16
14:16
14−Sep−2011

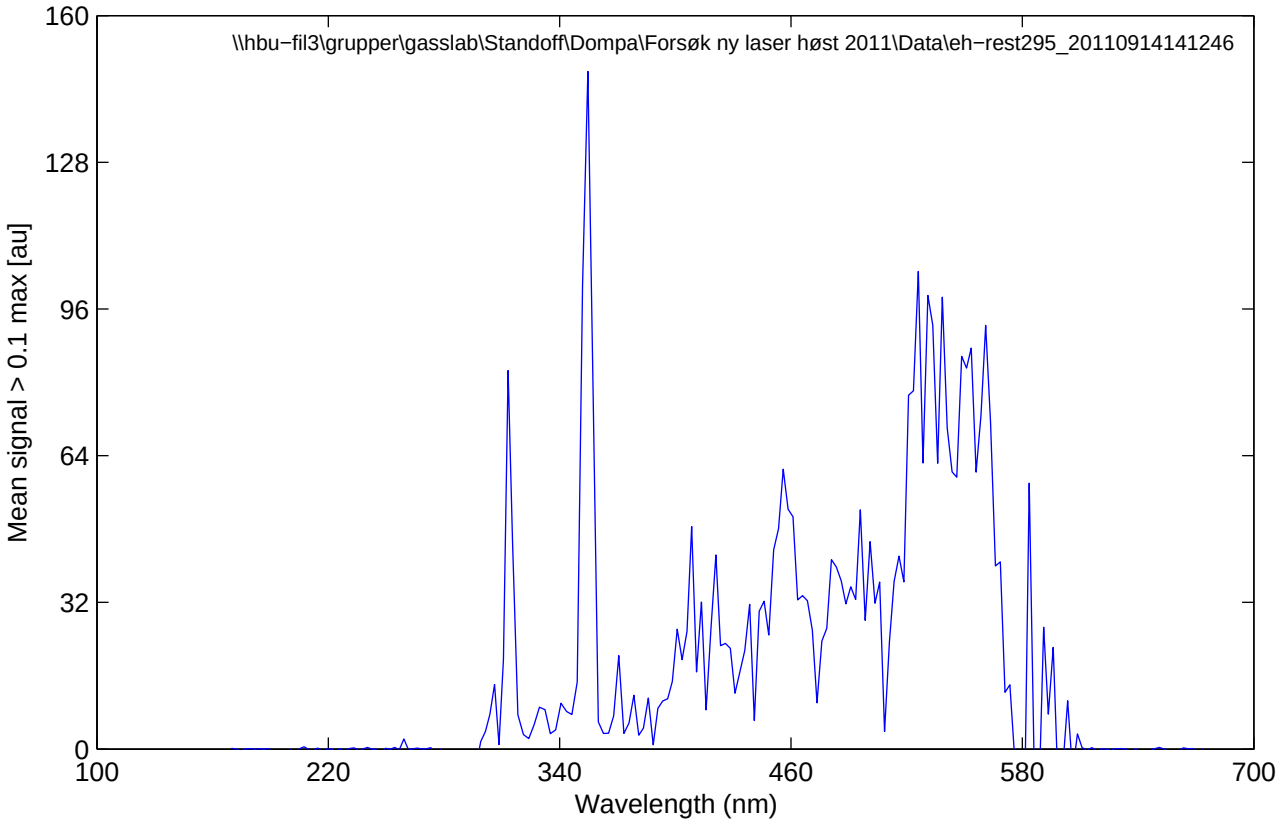
\\hbu−fil3\grupper\gasslab\Standoff\Dompa\Forsøk ny laser høst 2011\Data\eh−rest295_20110914141246
160
128
96
64
32
0
Mean signal > 0.1 max [au]
100
220
340
460
580
700
Wavelength (nm)

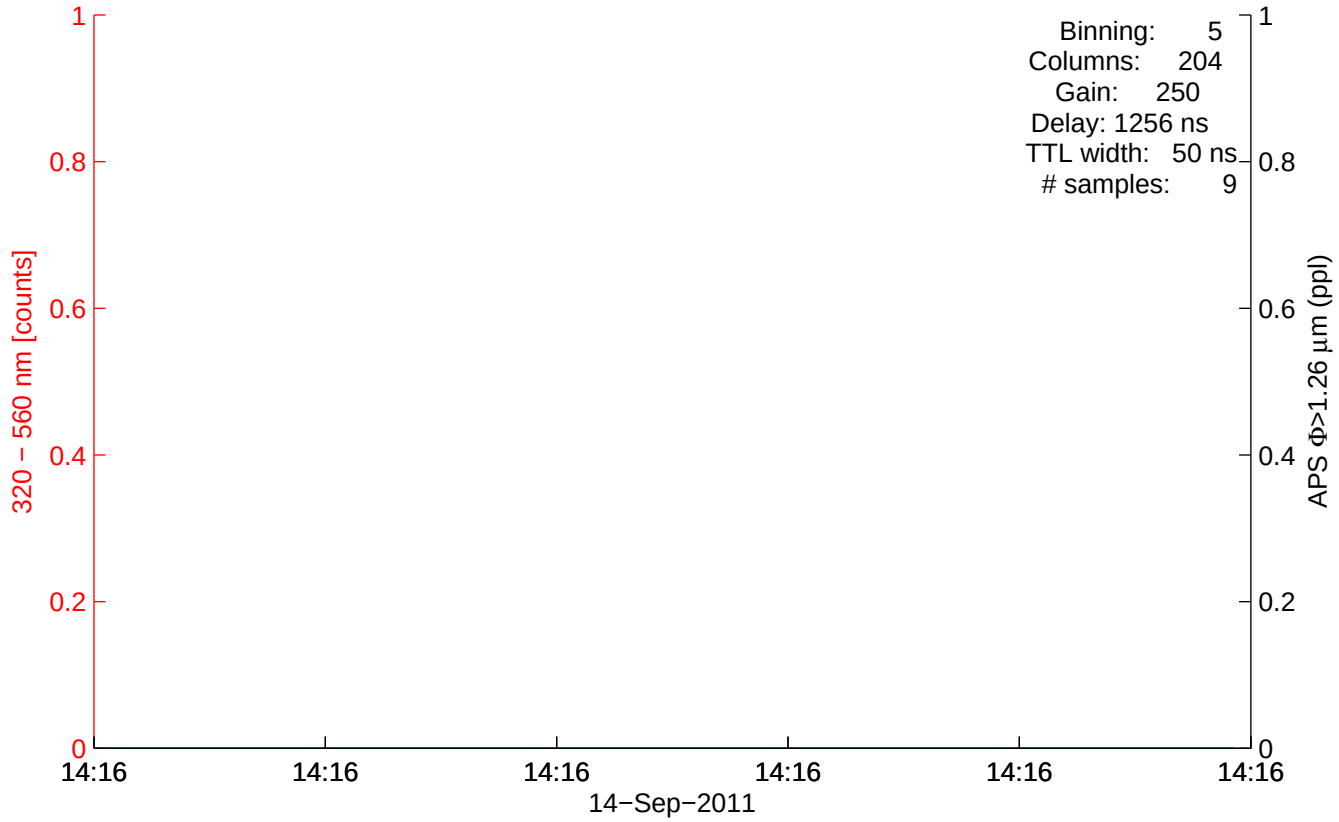
Binning: 5
Columns: 204
Gain: 250
Delay: 1256 ns
TTL width: 50 ns
samples: 9
320 – 560 nm [counts]
APS Φ>1.26 µm (ppl)
0
0.2
0.4
0.6
0.8
1
14:16
14:16
14:16
14:16
14:16
14:16
14−Sep−2011

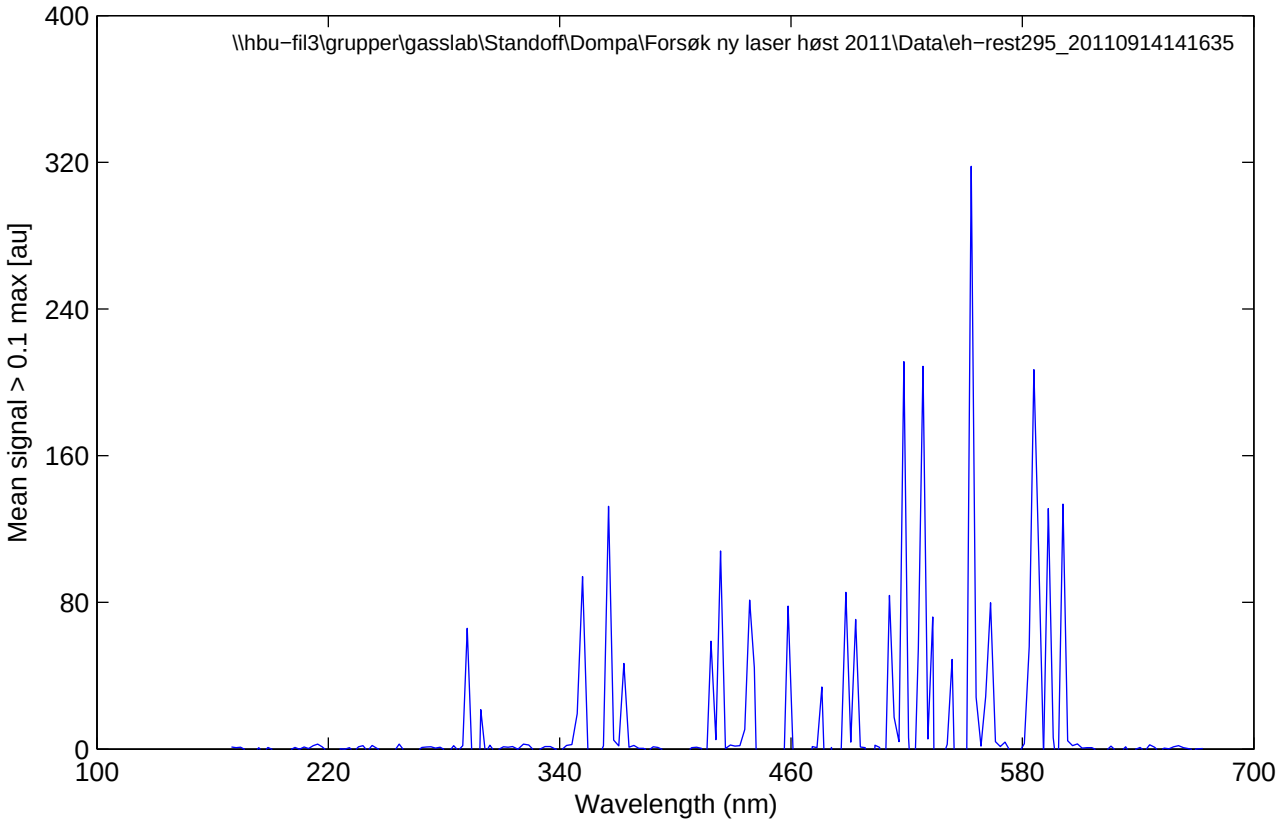
\\hbu−fil3\grupper\gasslab\Standoff\Dompa\Forsøk ny laser høst 2011\Data\eh−rest295_20110914141635
Mean signal > 0.1 max [au]
0
80
160
240
320
400
100
220
340
460
580
700
Wavelength (nm)

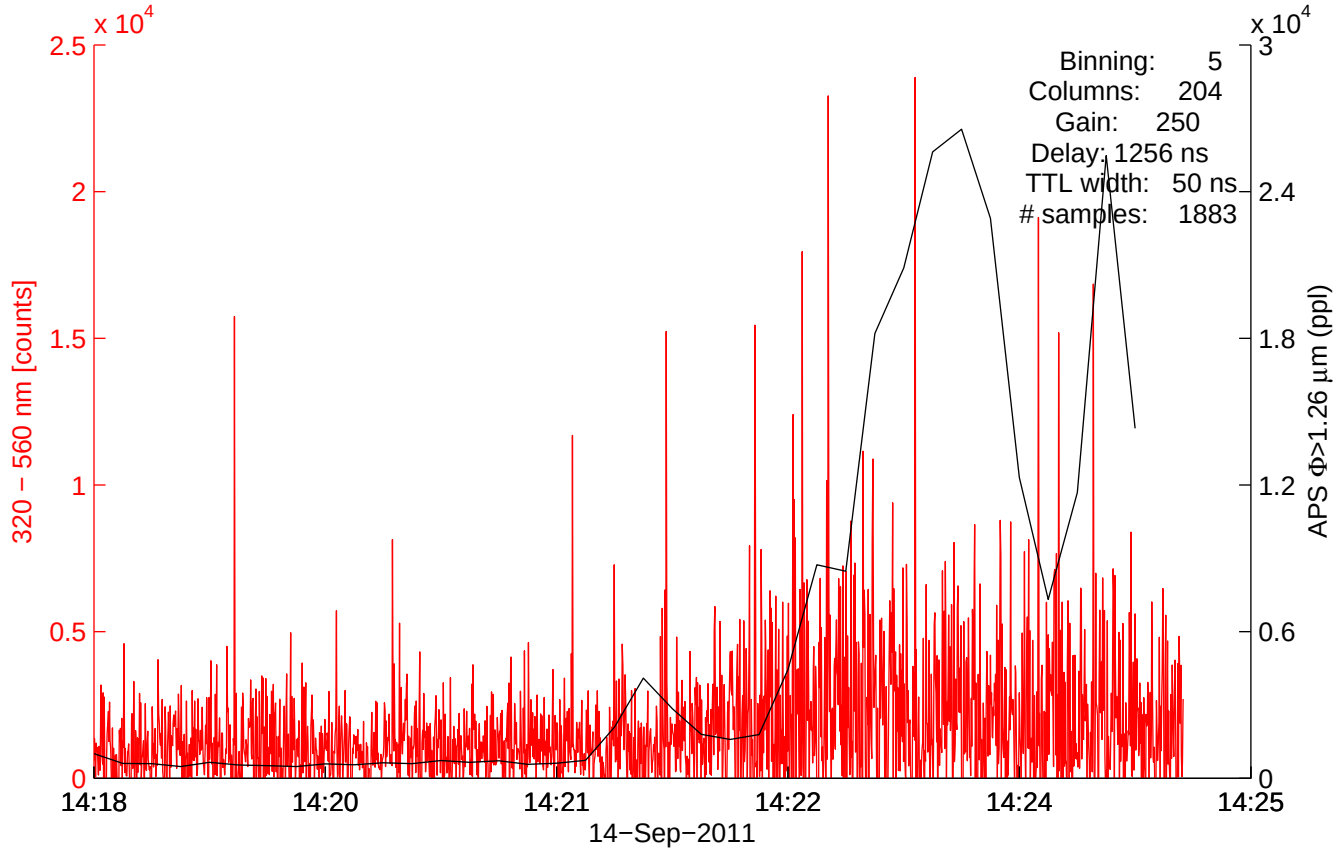
x 10^4
2.5
2
1.5
1
0.5
0
320 – 560 nm [counts]
x 10^4
3
2.4
1.8
1.2
0.6
0
APS Φ>1.26 µm (ppl)
Binning: 5
Columns: 204
Gain: 250
Delay: 1256 ns
TTL width: 50 ns
samples: 1883
14:18
14:20
14:21
14:22
14:24
14:25
14−Sep−2011

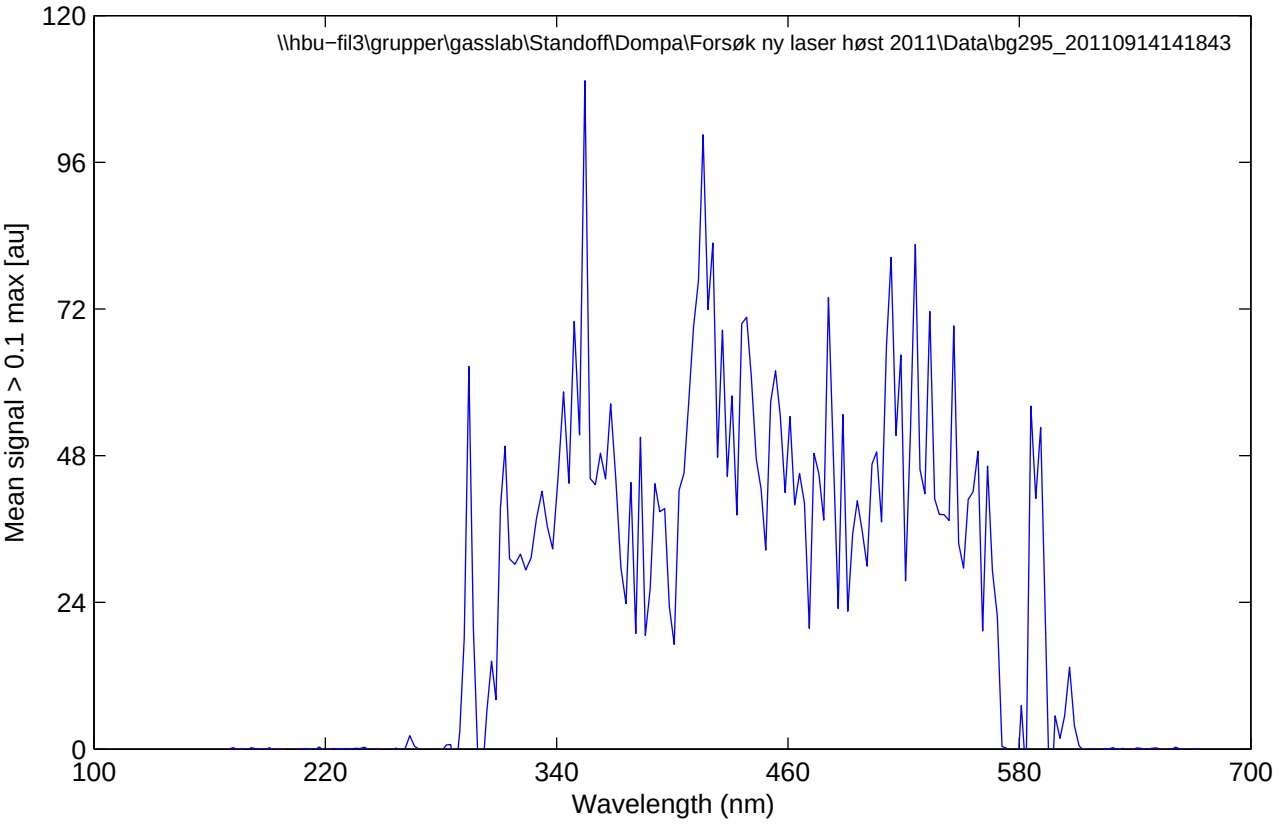
\\hbu−fil3\grupper\gasslab\Standoff\Dompa\Forsøk ny laser høst 2011\Data\bg295_20110914141843
120
96
72
48
24
0
Mean signal > 0.1 max [au]
100
220
340
460
580
700
Wavelength (nm)

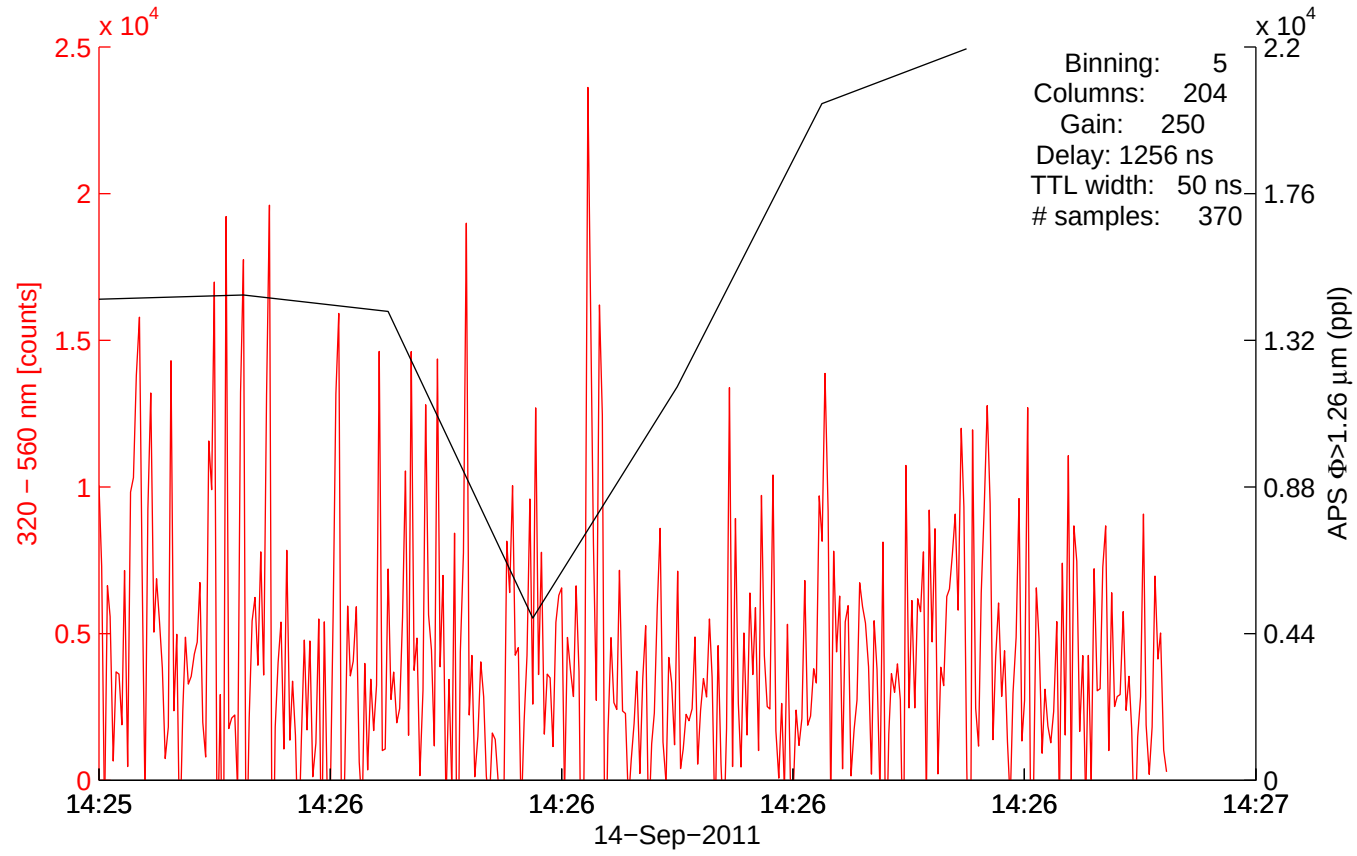
x 10^4
2.5
2
1.5
1
0.5
0
320 – 560 nm [counts]
x 10^4
2.2
1.76
1.32
0.88
0.44
0
APS Φ>1.26 µm (ppl)
Binning: 5
Columns: 204
Gain: 250
Delay: 1256 ns
TTL width: 50 ns
samples: 370
14:25
14:26
14:26
14:26
14:26
14:27
14−Sep−2011

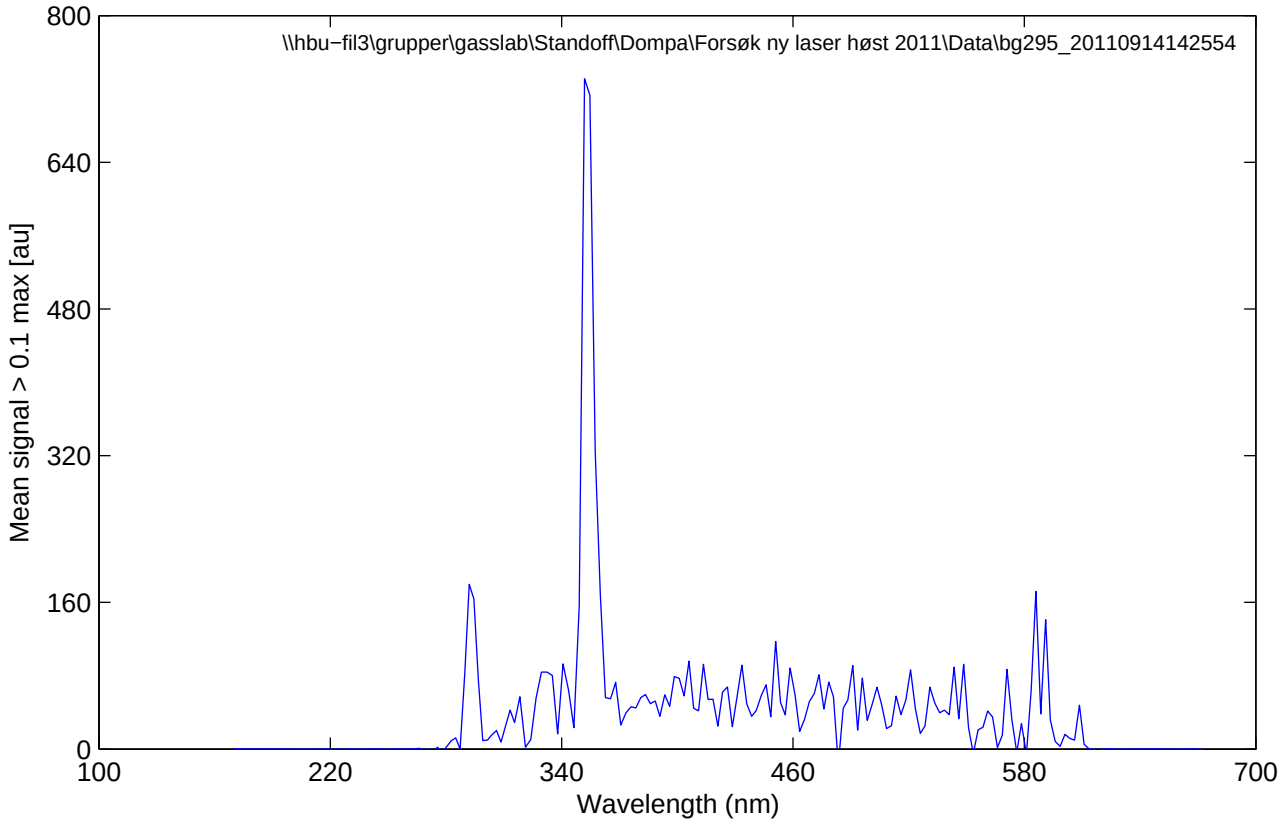
\\hbu−fil3\grupper\gasslab\Standoff\Dompa\Forsøk ny laser høst 2011\Data\bg295_20110914142554
800
640
480
320
160
0
Mean signal > 0.1 max [au]
100
220
340
460
580
700
Wavelength (nm)

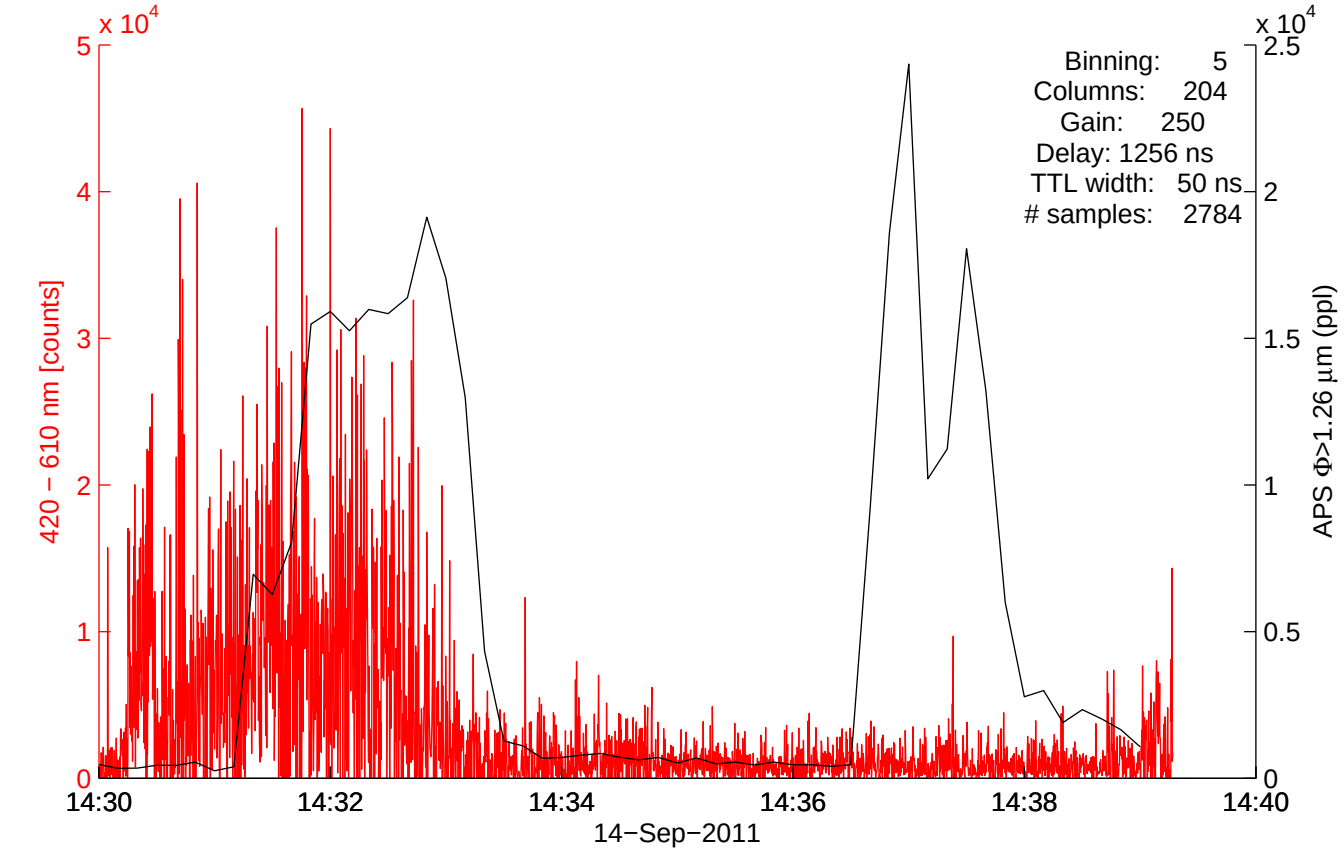
x 10^4
5
4
3
2
1
0
420 – 610 nm [counts]
x 10^4
2.5
2
1.5
1
0.5
0
APS Φ>1.26 µm (ppl)
Binning: 5
Columns: 204
Gain: 250
Delay: 1256 ns
TTL width: 50 ns
samples: 2784
14:30
14:32
14:34
14:36
14:38
14:40
14−Sep−2011

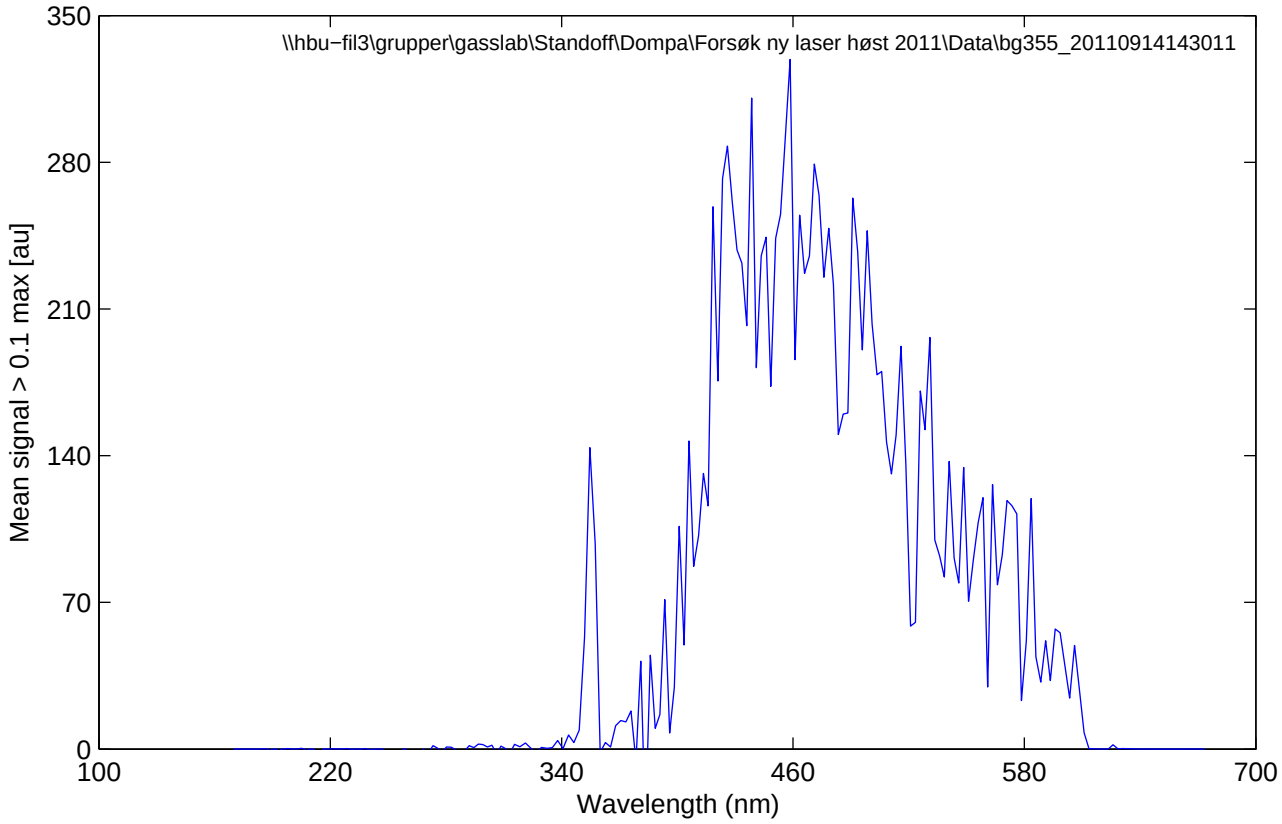
\\hbu−fil3\grupper\gasslab\Standoff\Dompa\Forsøk ny laser høst 2011\Data\bg355_20110914143011
350
280
210
140
70
0
Mean signal > 0.1 max [au]
100
220
340
460
580
700
Wavelength (nm)

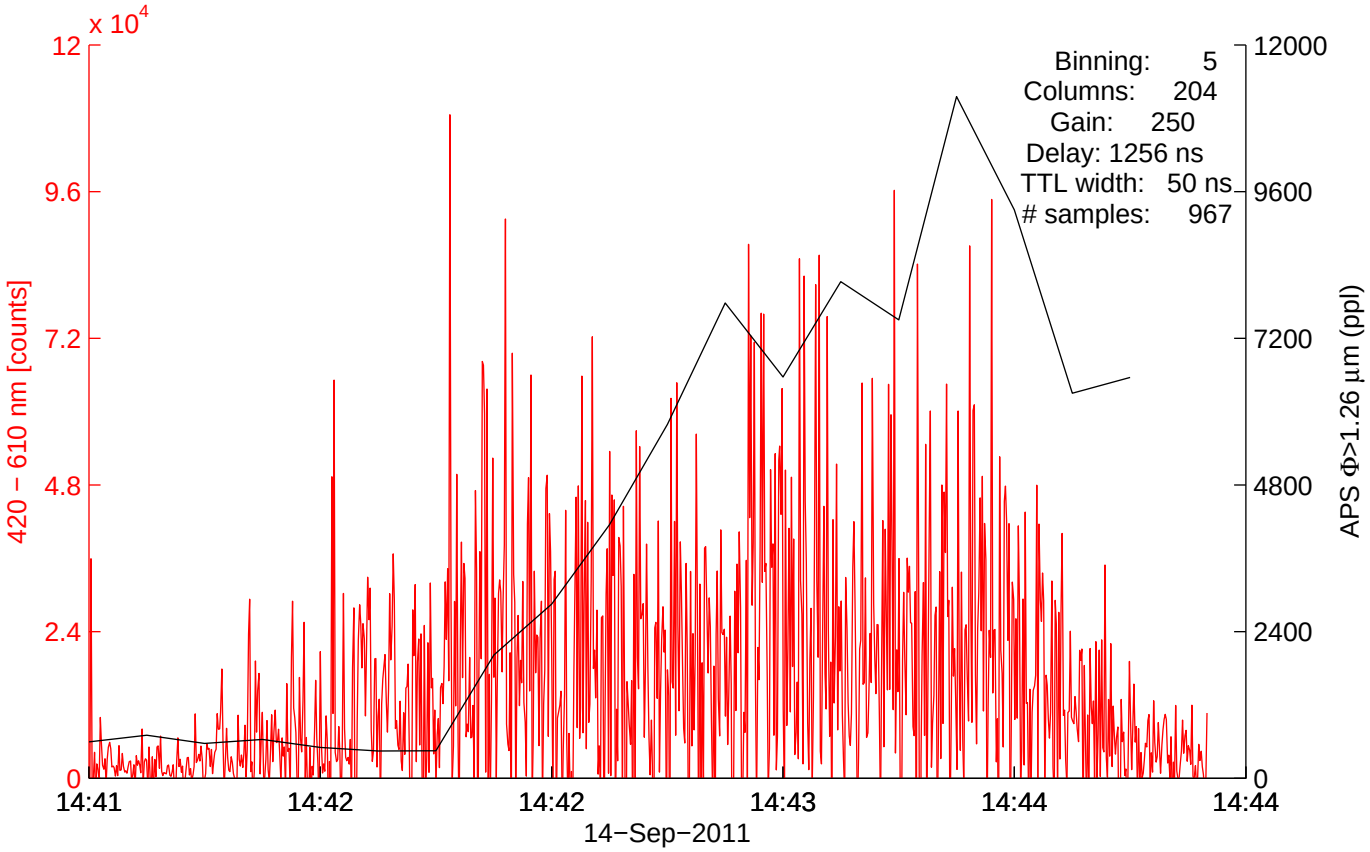
x 10^4
12
9.6
7.2
4.8
2.4
0
420 – 610 nm [counts]
12000
9600
7200
4800
2400
0
APS Φ>1.26 µm (ppl)
Binning: 5
Columns: 204
Gain: 250
Delay: 1256 ns
TTL width: 50 ns
samples: 967
14:41
14:42
14:42
14:43
14:44
14:44
14−Sep−2011

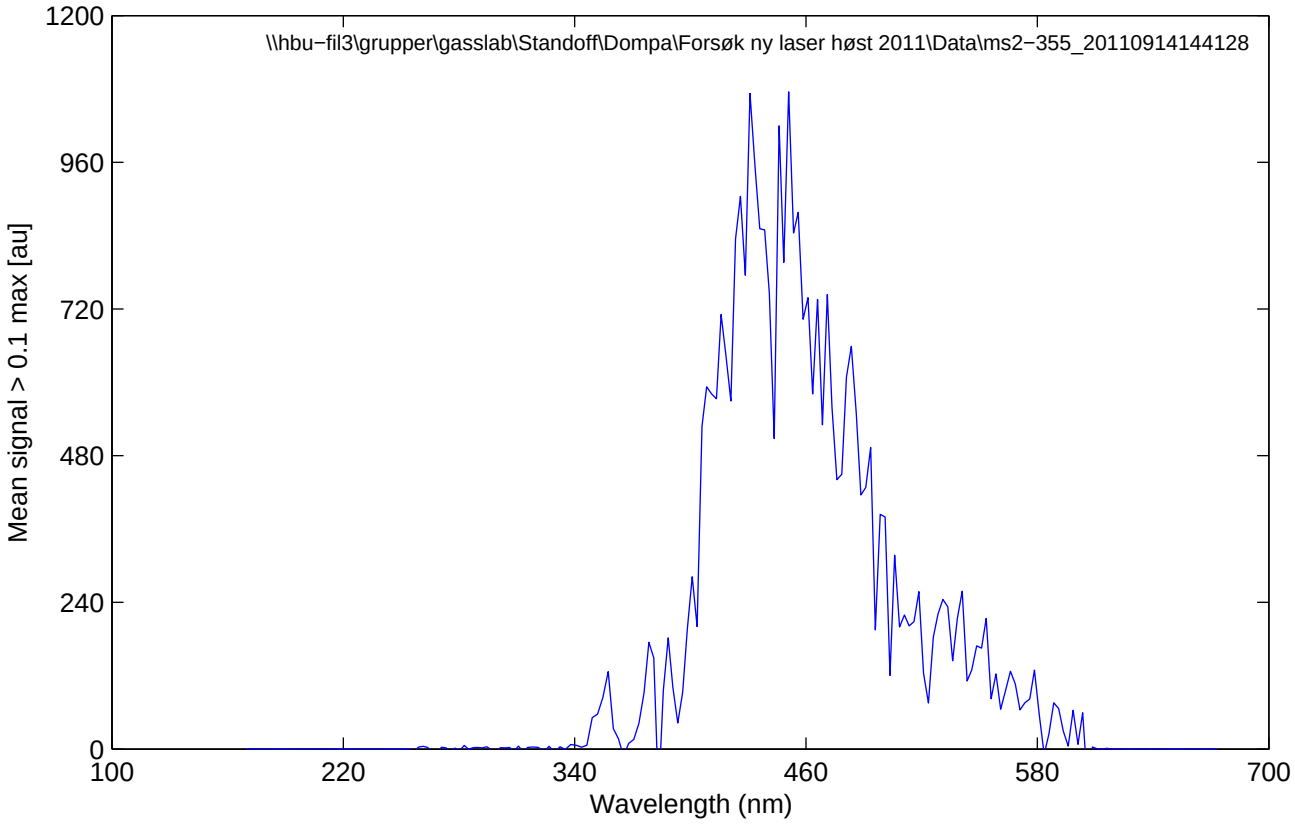
\\hbu−fil3\grupper\gasslab\Standoff\Dompa\Forsøk ny laser høst 2011\Data\ms2−355_20110914144128
1200
960
720
480
240
0
Mean signal > 0.1 max [au]
100
220
340
460
580
700
Wavelength (nm)

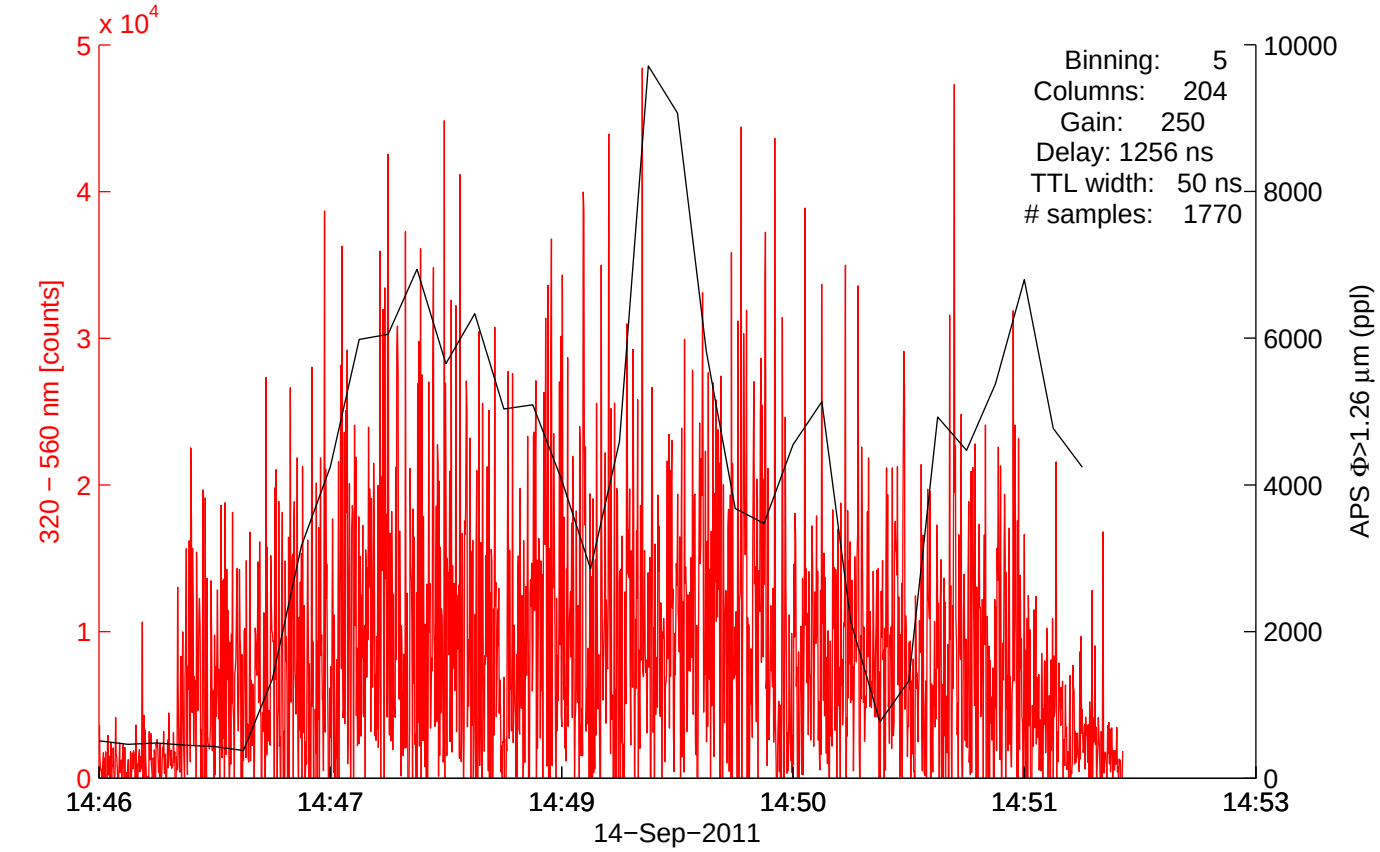
x 10^4
320 – 560 nm [counts]
APS Φ>1.26 µm (ppl)
Binning: 5
Columns: 204
Gain: 250
Delay: 1256 ns
TTL width: 50 ns
samples: 1770
14:46
14:47
14:49
14:50
14:51
14:53
14−Sep−2011

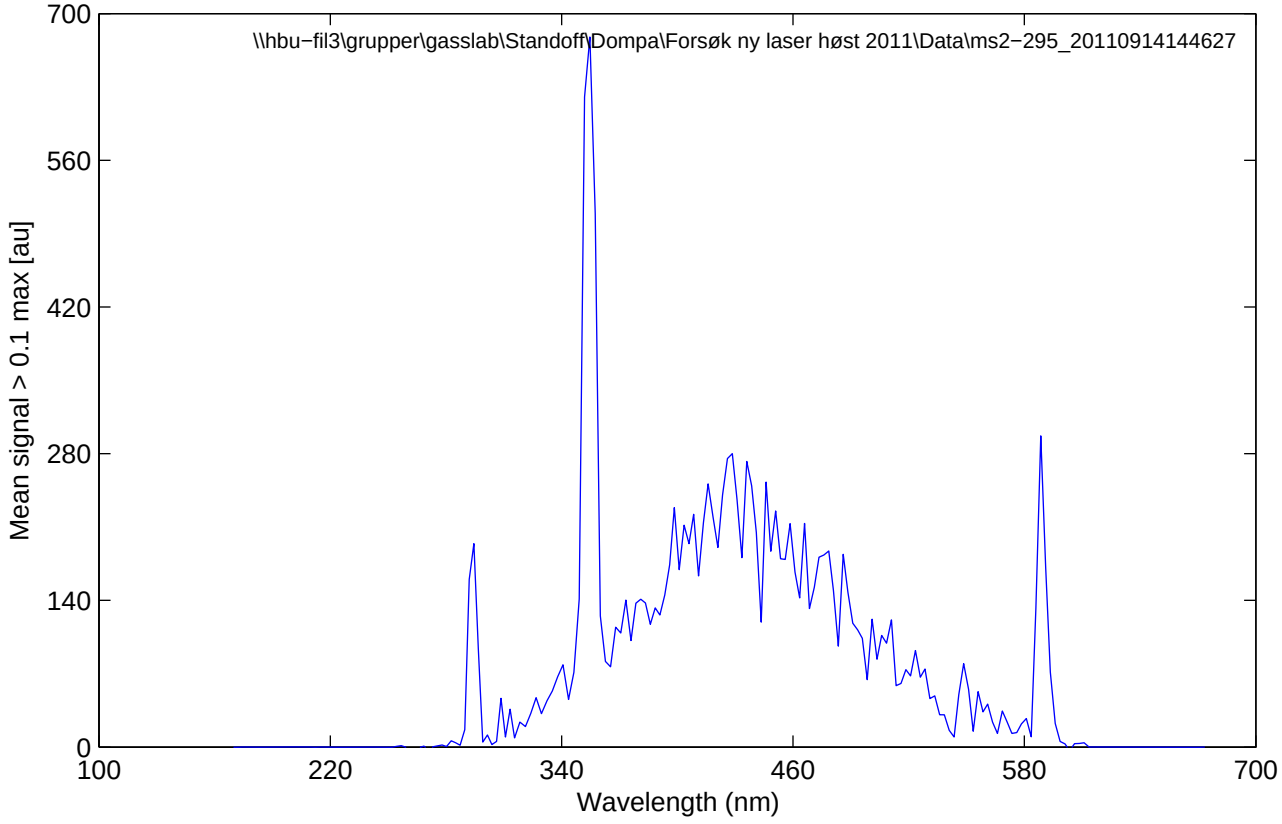
\\hbu−fil3\grupper\gasslab\Standoff\Dompa\Forsøk ny laser høst 2011\Data\ms2−295_20110914144627
Mean signal > 0.1 max [au]
Wavelength (nm)

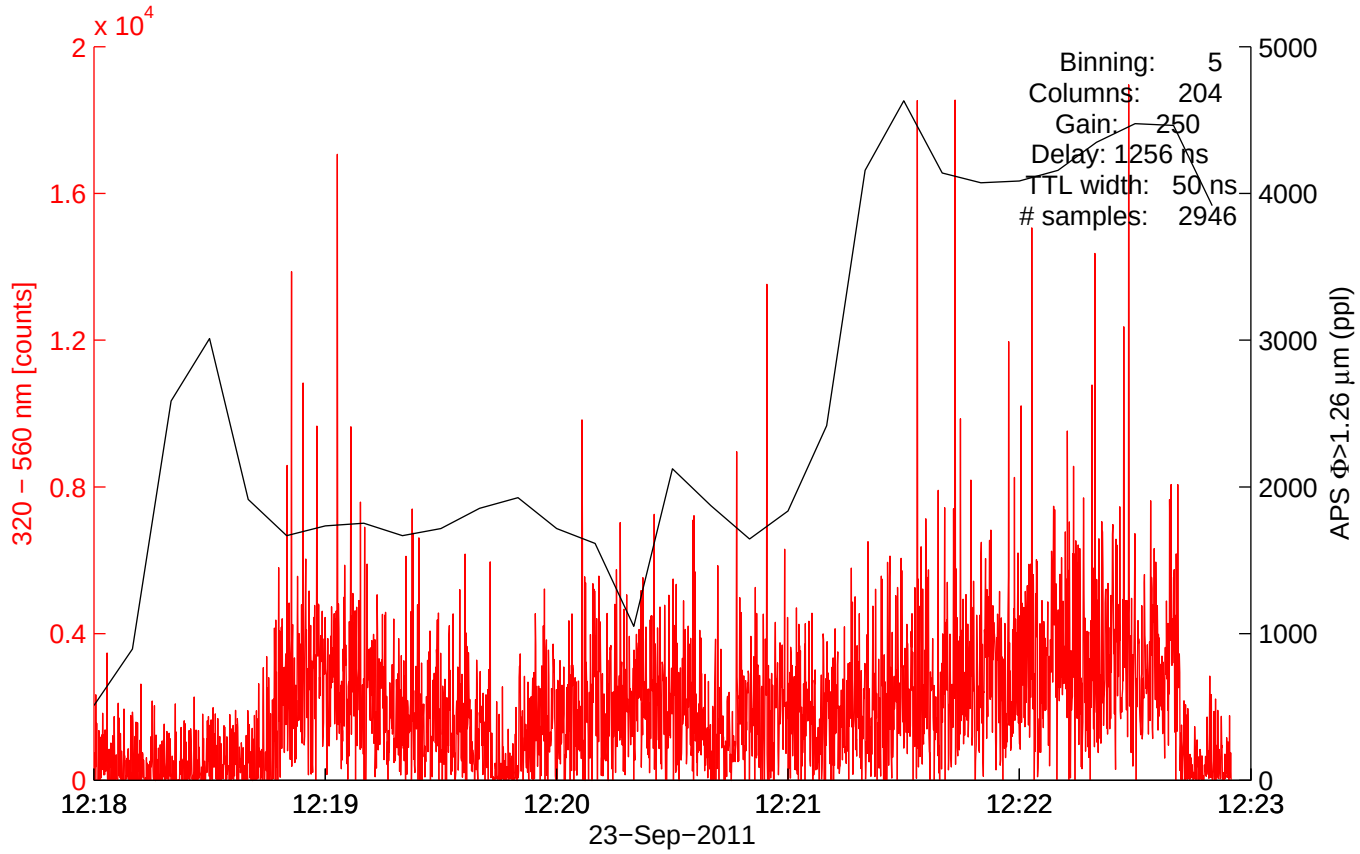
x 10^4
2
1.6
1.2
0.8
0.4
0
320 – 560 nm [counts]
5000
4000
3000
2000
1000
0
APS Φ>1.26 µm (ppl)
Binning: 5
Columns: 204
Gain: 250
Delay: 1256 ns
TTL width: 50 ns
samples: 2946
12:18
12:19
12:20
12:21
12:22
12:23
23−Sep−2011

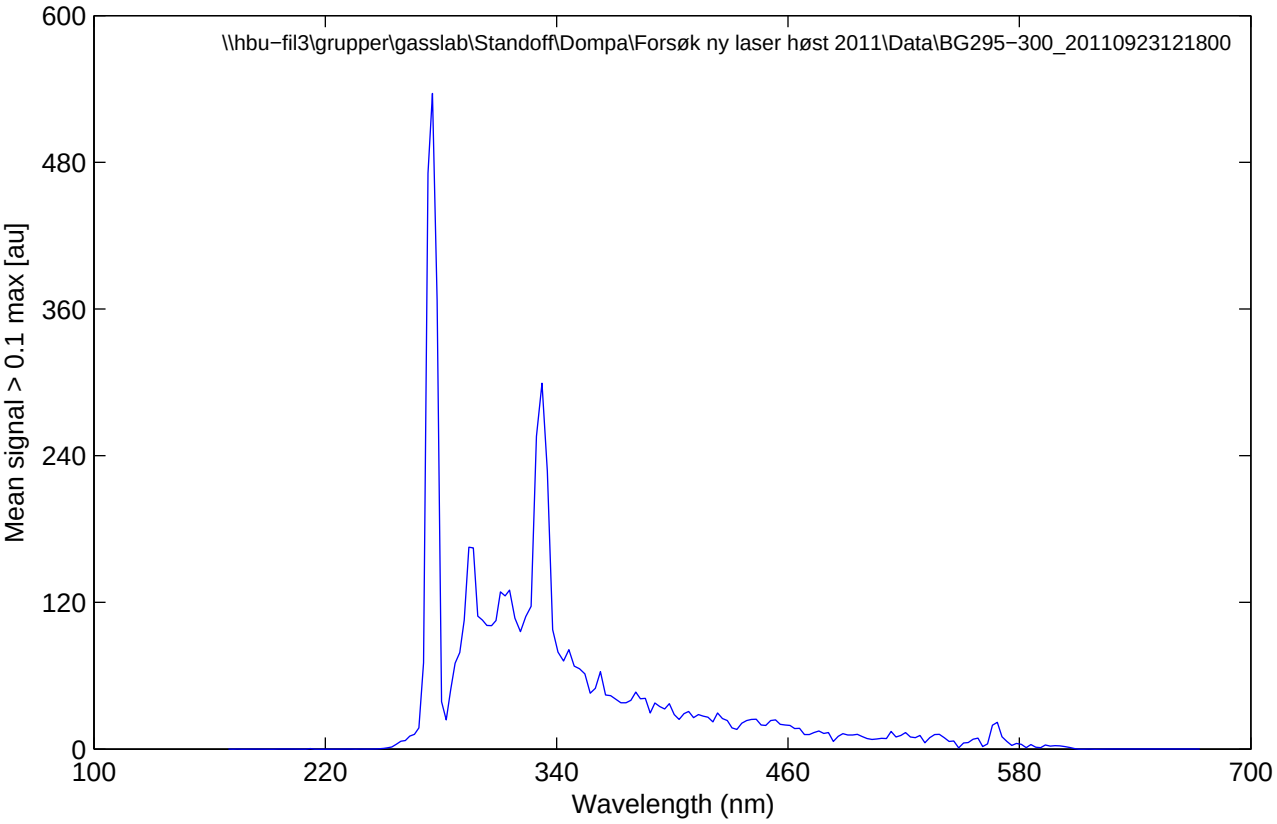
\\hbu−fil3\grupper\gasslab\Standoff\Dompa\Forsøk ny laser høst 2011\Data\BG295−300_20110923121800
600
480
360
240
120
0
Mean signal > 0.1 max [au]
100
220
340
460
580
700
Wavelength (nm)

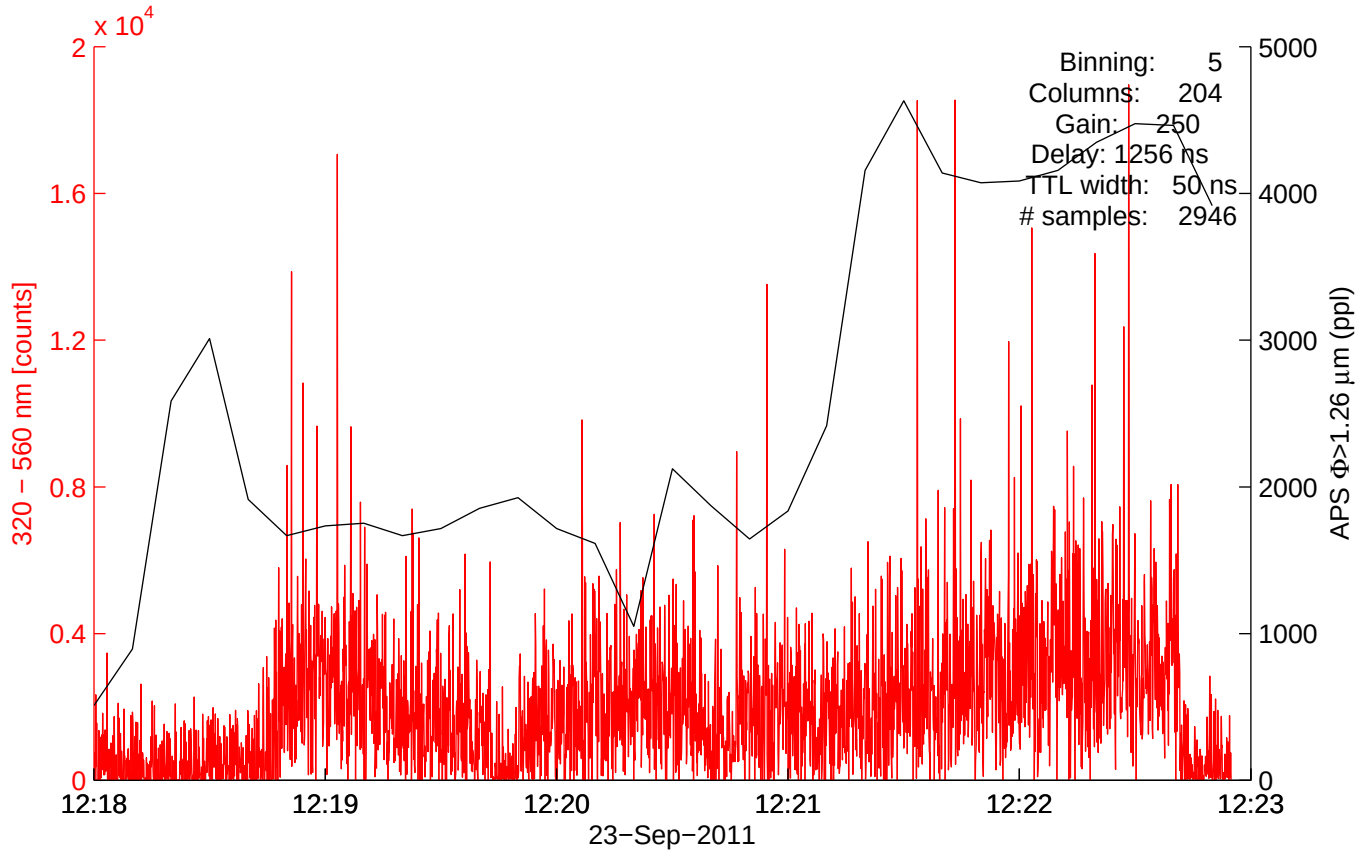
x 10^4
2
1.6
1.2
0.8
0.4
0
320 – 560 nm [counts]
5000
4000
3000
2000
1000
0
APS Φ>1.26 µm (ppl)
Binning: 5
Columns: 204
Gain: 250
Delay: 1256 ns
TTL width: 50 ns
samples: 2946
12:18
12:19
12:20
12:21
12:22
12:23
23−Sep−2011

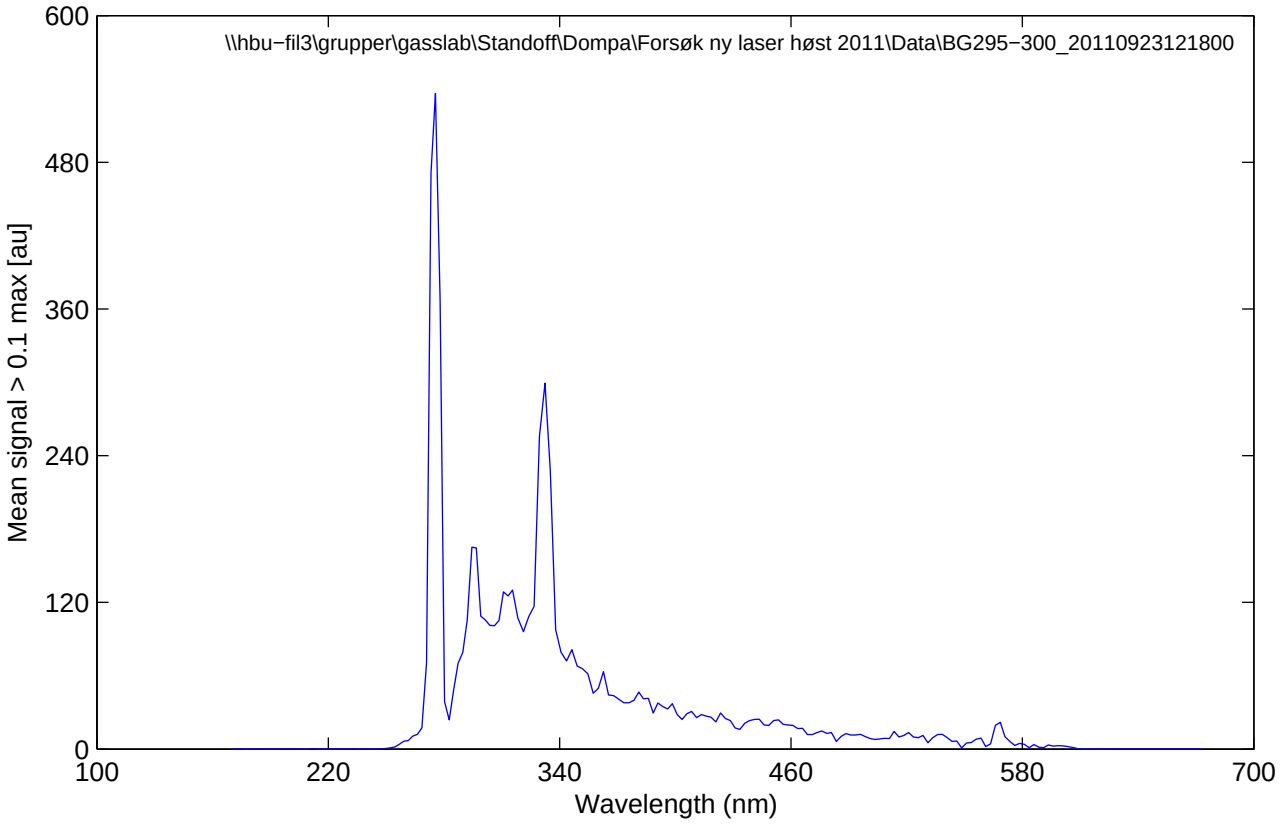
\\hbu−fil3\grupper\gasslab\Standoff\Dompa\Forsøk ny laser høst 2011\Data\BG295−300_20110923121800
600
480
360
240
120
0
Mean signal > 0.1 max [au]
100
220
340
460
580
700
Wavelength (nm)

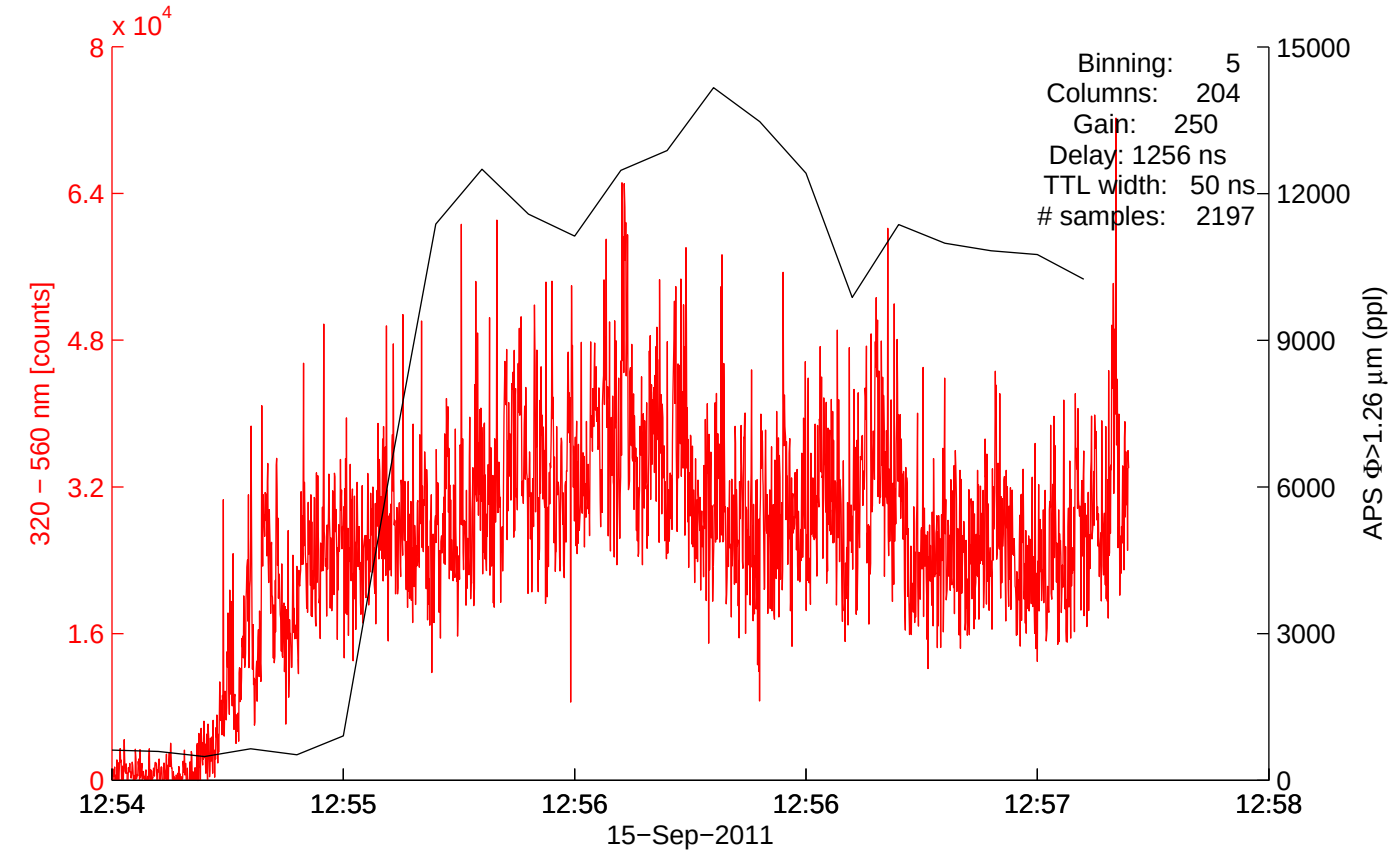
x 10^4
8
6.4
4.8
3.2
1.6
0
320 – 560 nm [counts]
15000
12000
9000
6000
3000
0
APS Φ>1.26 µm (ppl)
Binning: 5
Columns: 204
Gain: 250
Delay: 1256 ns
TTL width: 50 ns
samples: 2197
12:54
12:55
12:56
12:56
12:57
12:58
15−Sep−2011

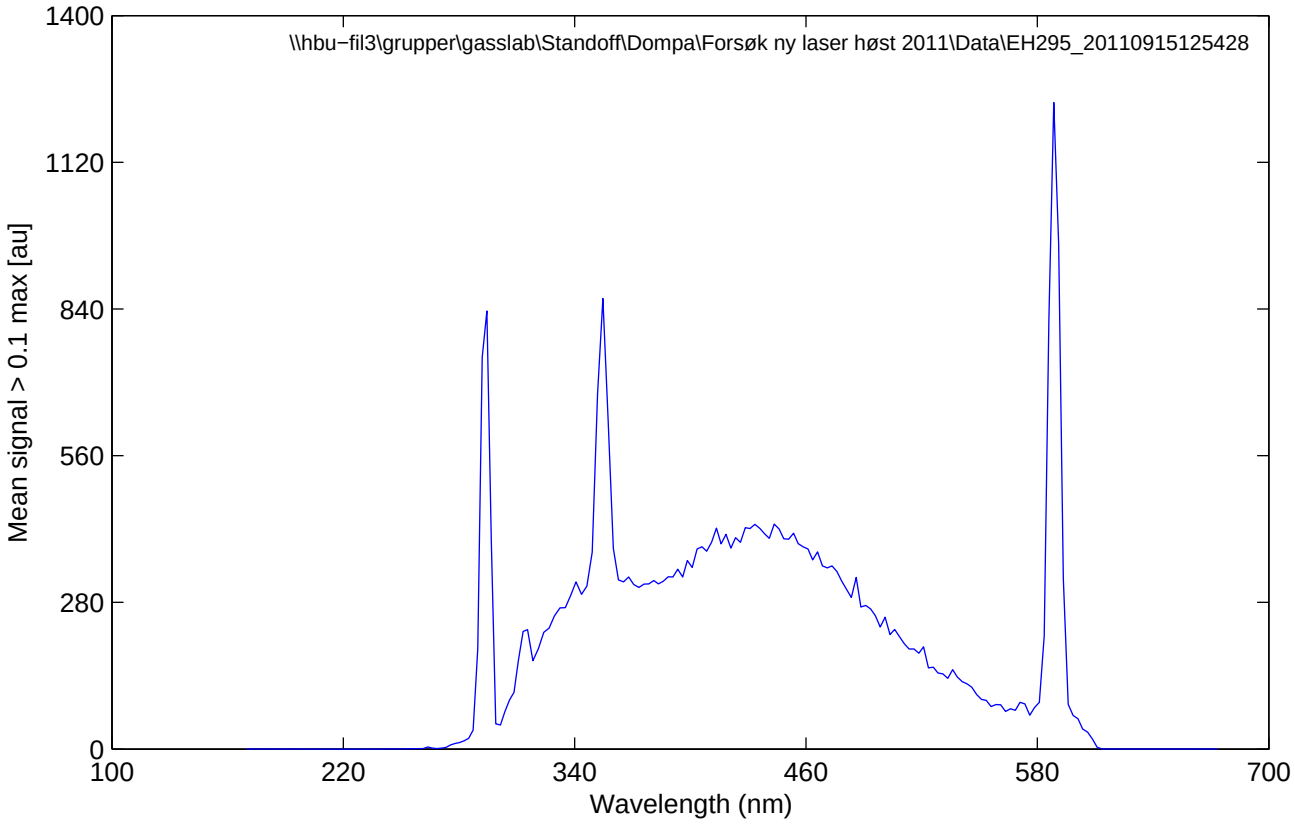
\\hbu−fil3\grupper\gasslab\Standoff\Dompa\Forsøk ny laser høst 2011\Data\EH295_20110915125428
1400
1120
840
560
280
0
Mean signal > 0.1 max [au]
100
220
340
460
580
700
Wavelength (nm)

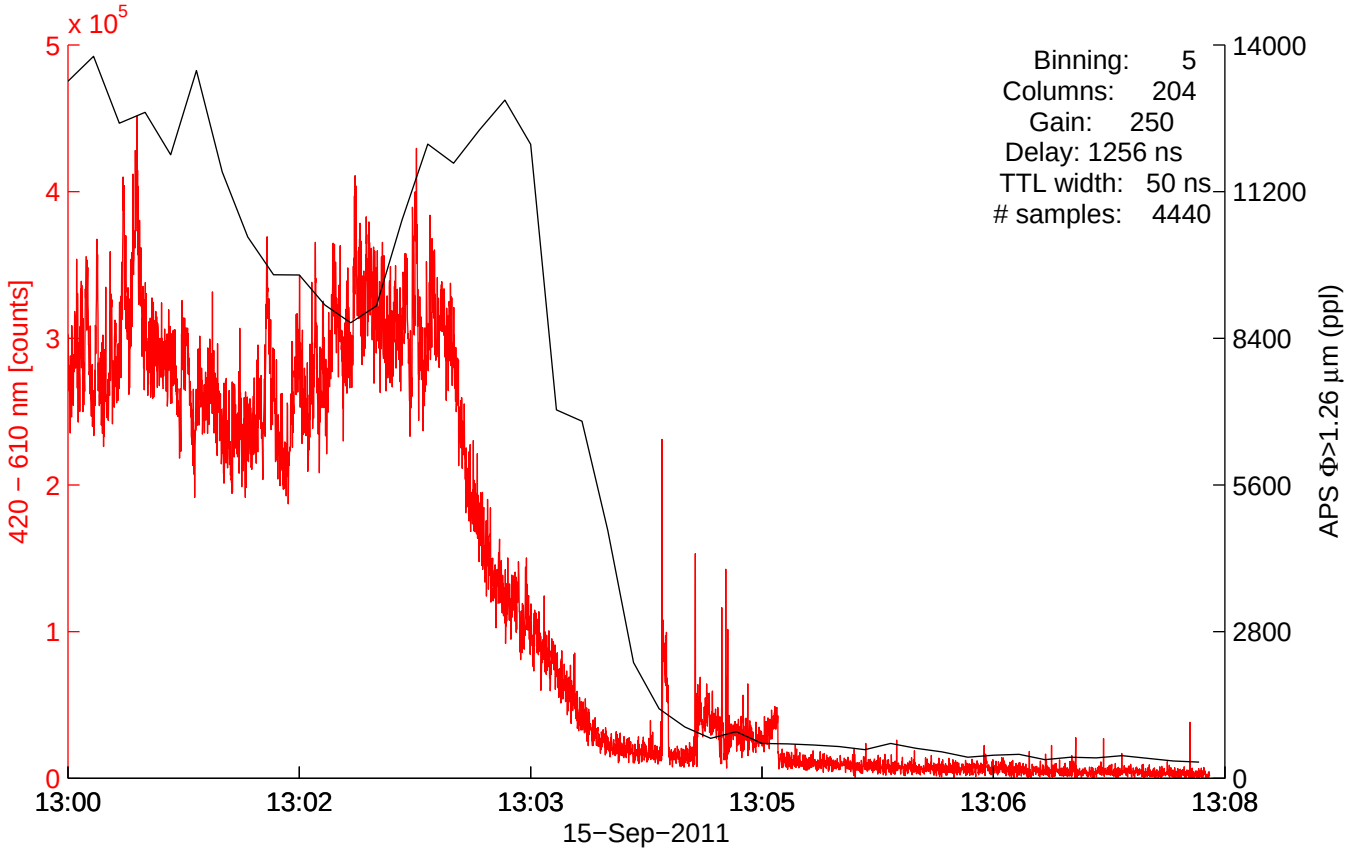
x 10^5
5
4
3
2
1
0
420 – 610 nm [counts]
14000
11200
8400
5600
2800
0
APS Φ>1.26 µm (ppl)
Binning: 5
Columns: 204
Gain: 250
Delay: 1256 ns
TTL width: 50 ns
samples: 4440
13:00
13:02
13:03
13:05
13:06
13:08
15−Sep−2011

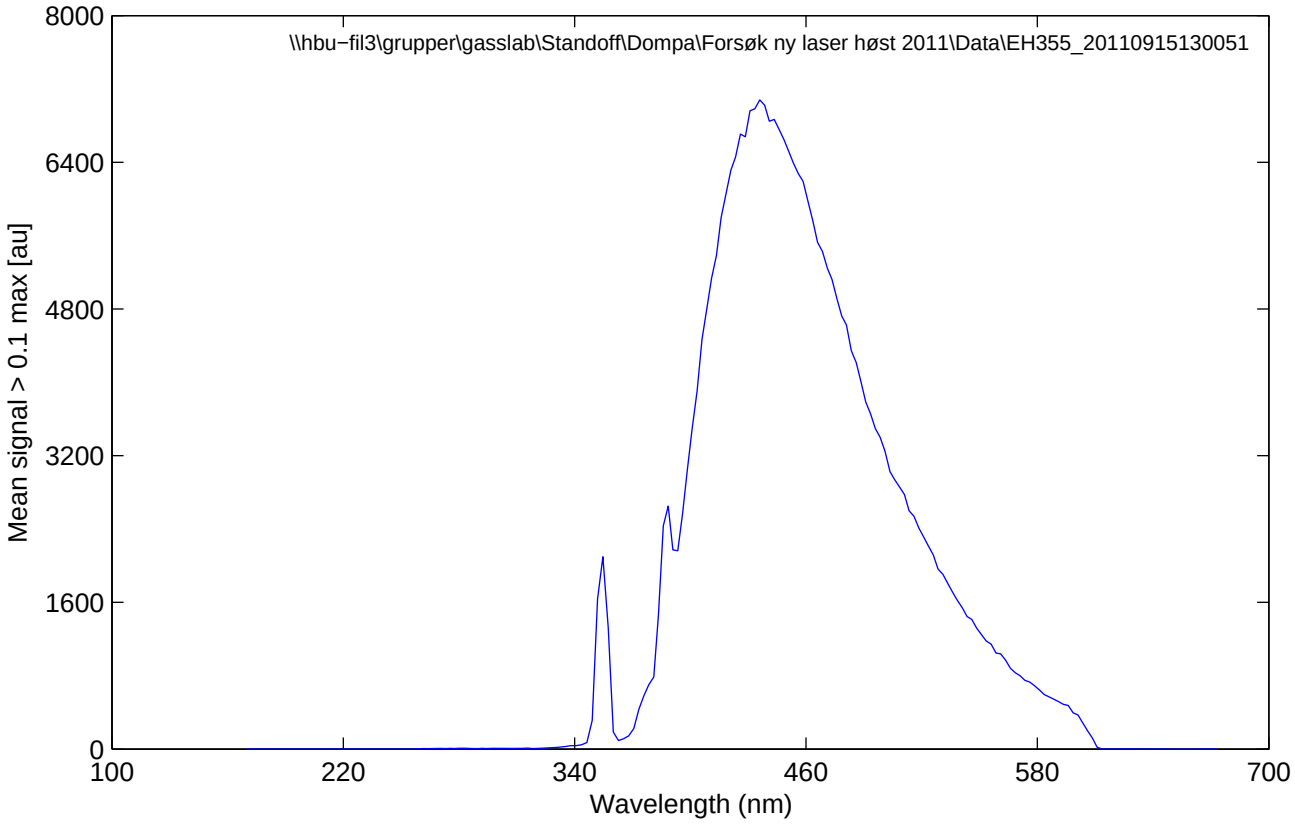
\\hbu−fil3\grupper\gasslab\Standoff\Dompa\Forsøk ny laser høst 2011\Data\EH355_20110915130051
8000
6400
4800
3200
1600
0
Mean signal > 0.1 max [au]
100
220
340
460
580
700
Wavelength (nm)

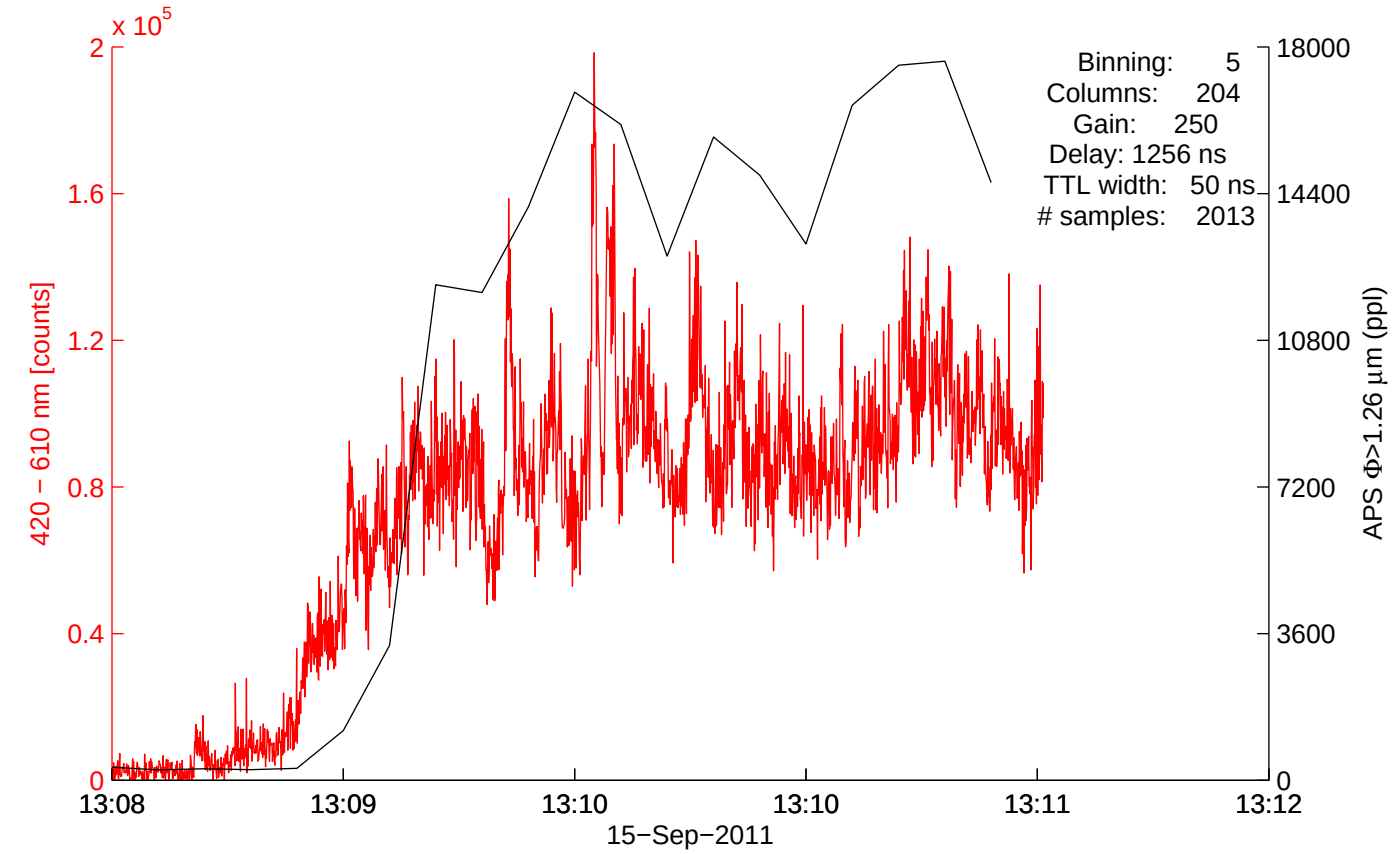
x 10^5
2
1.6
1.2
0.8
0.4
0
420 – 610 nm [counts]
18000
14400
10800
7200
3600
0
APS Φ>1.26 µm (ppl)
Binning: 5
Columns: 204
Gain: 250
Delay: 1256 ns
TTL width: 50 ns
samples: 2013
13:08
13:09
13:10
13:10
13:11
13:12
15−Sep−2011

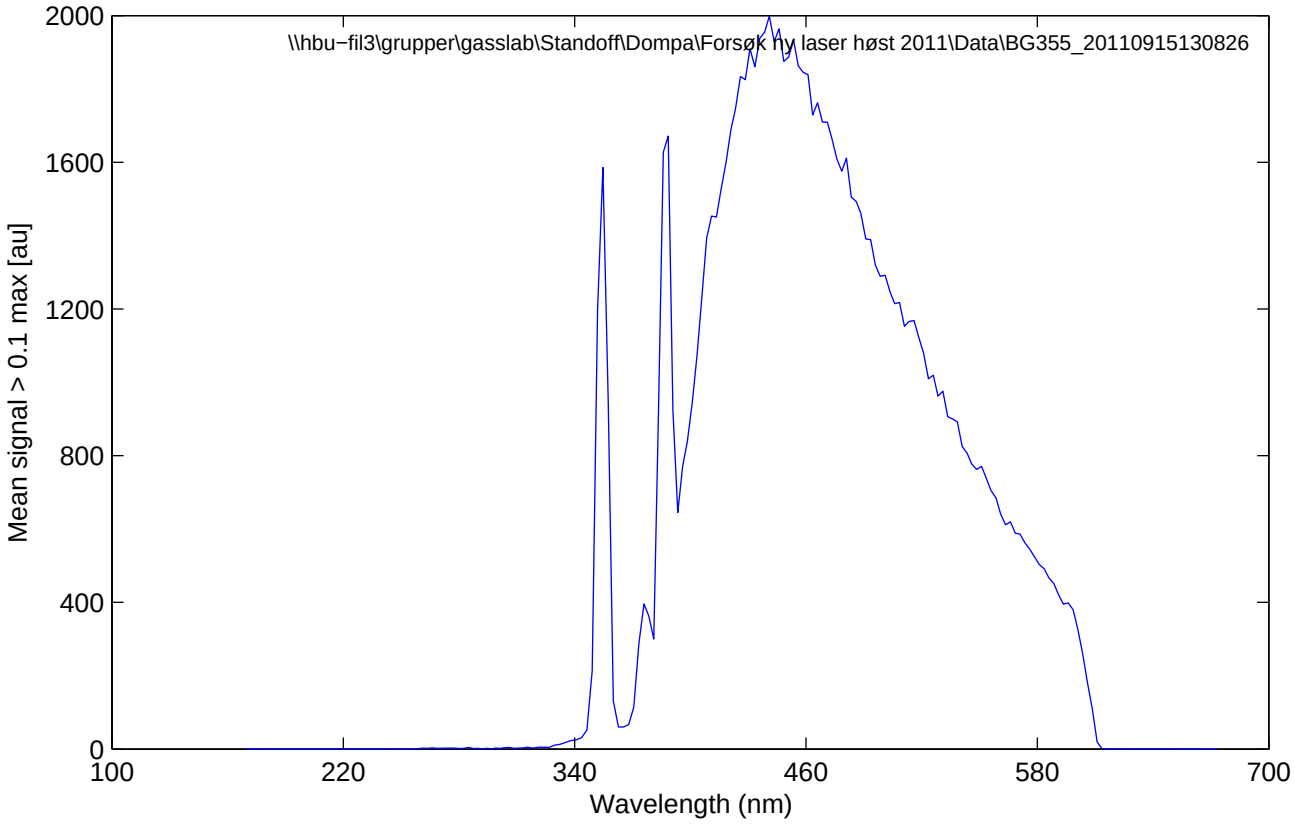
\\hbu−fil3\grupper\gasslab\Standoff\Dompa\Forsøk ny laser høst 2011\Data\BG355_20110915130826
2000
1600
1200
800
400
0
Mean signal > 0.1 max [au]
100
220
340
460
580
700
Wavelength (nm)

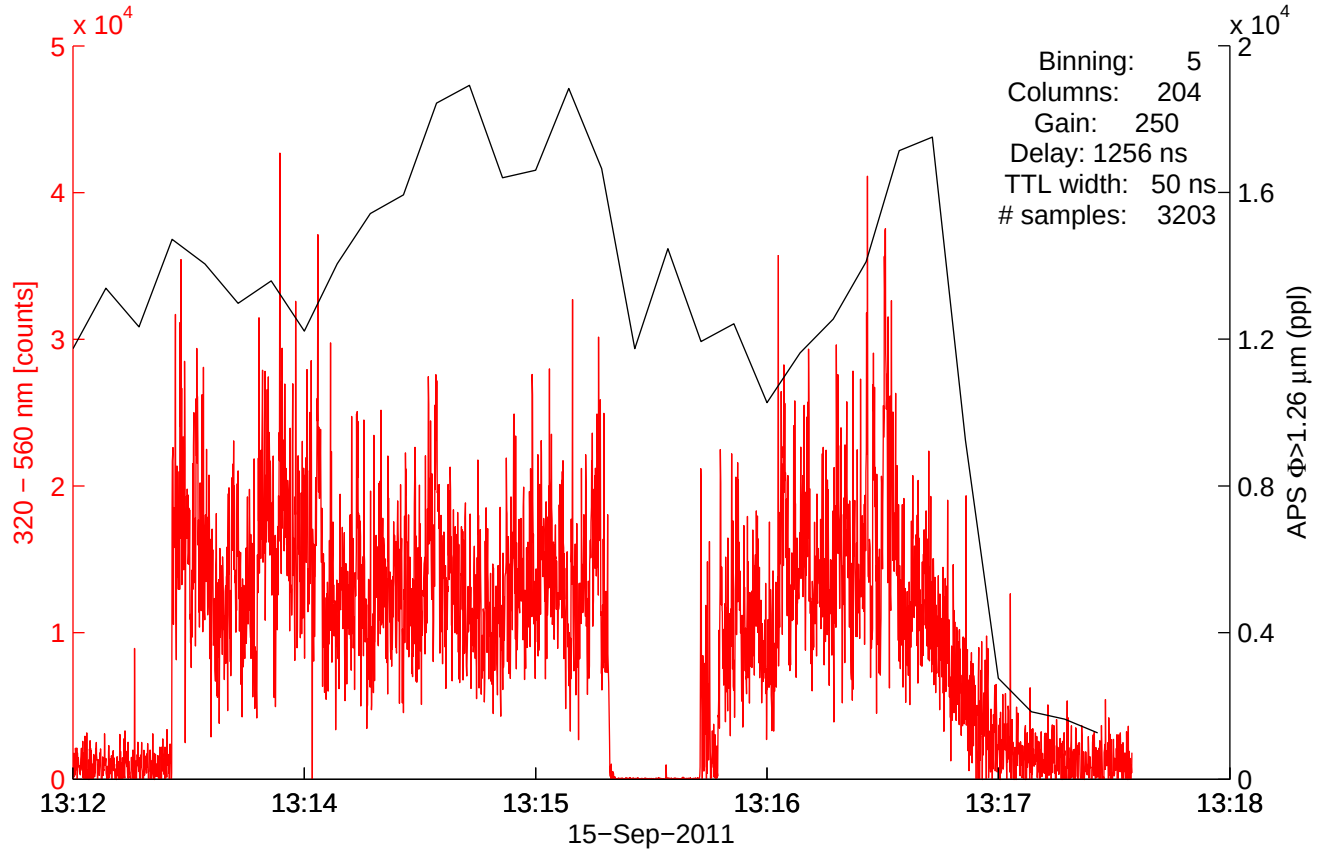
x 10^4
5
4
3
2
1
0
320 – 560 nm [counts]
x 10^4
2
1.6
1.2
0.8
0.4
0
APS Φ>1.26 µm (ppl)
Binning: 5
Columns: 204
Gain: 250
Delay: 1256 ns
TTL width: 50 ns
samples: 3203
13:12
13:14
13:15
13:16
13:17
13:18
15−Sep−2011

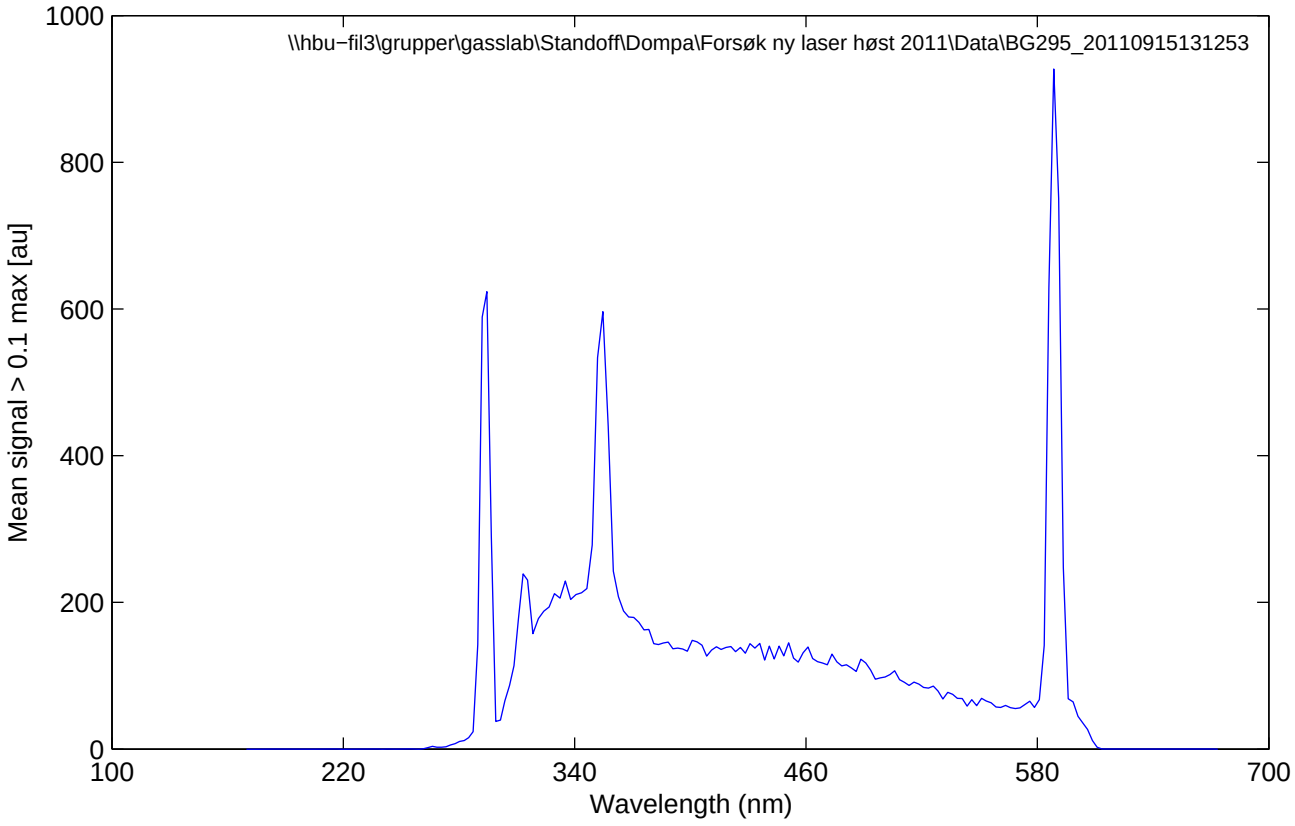
\\hbu−fil3\grupper\gasslab\Standoff\Dompa\Forsøk ny laser høst 2011\Data\BG295_20110915131253
1000
800
600
400
200
0
Mean signal > 0.1 max [au]
100
220
340
460
580
700
Wavelength (nm)

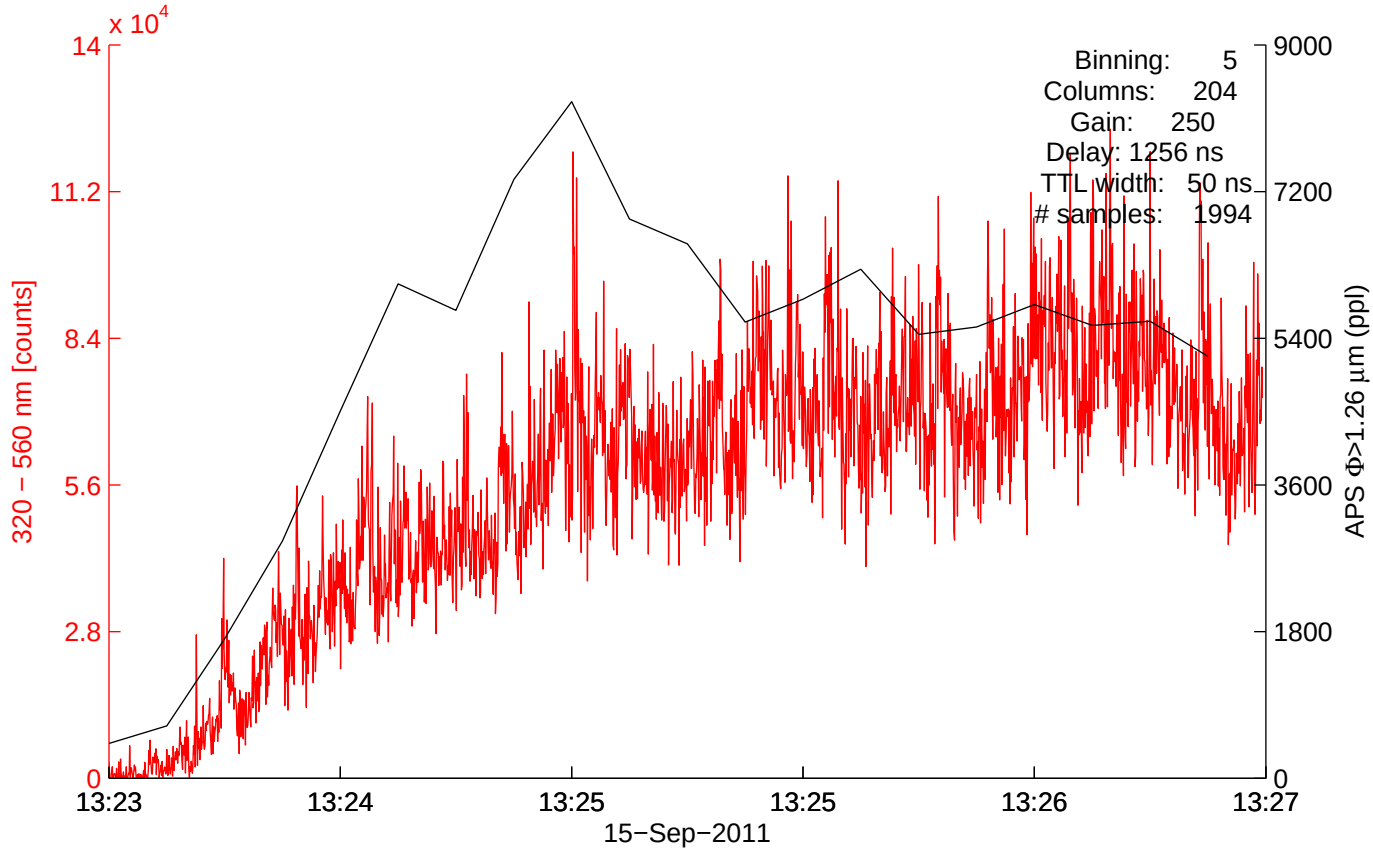
x 10^4
14
11.2
8.4
5.6
2.8
0
320 – 560 nm [counts]
9000
7200
5400
3600
1800
0
APS Φ>1.26 µm (ppl)
Binning: 5
Columns: 204
Gain: 250
Delay: 1256 ns
TTL width: 50 ns
samples: 1994
13:23
13:24
13:25
13:25
13:26
13:27
15−Sep−2011

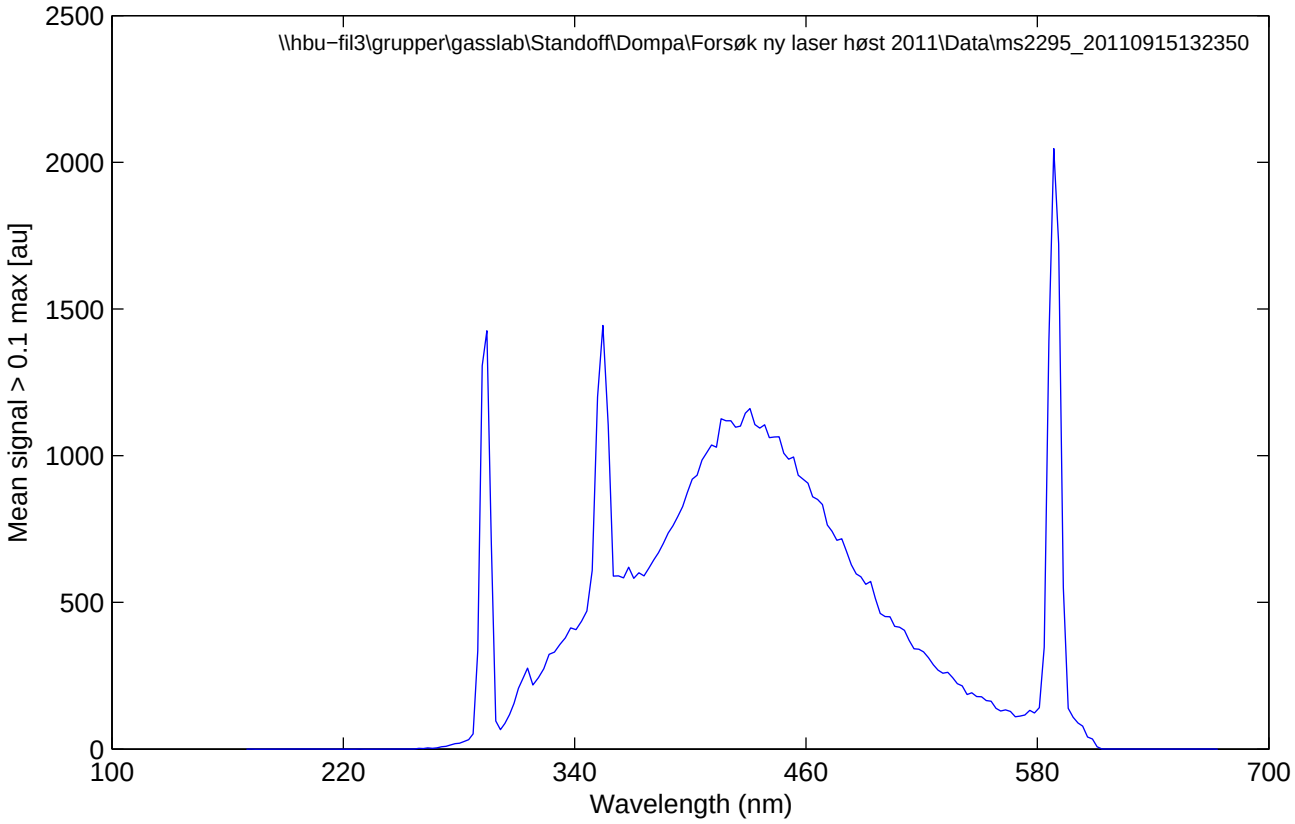
\\hbu−fil3\grupper\gasslab\Standoff\Dompa\Forsøk ny laser høst 2011\Data\ms2295_20110915132350
2500
2000
1500
1000
500
0
Mean signal > 0.1 max [au]
100
220
340
460
580
700
Wavelength (nm)

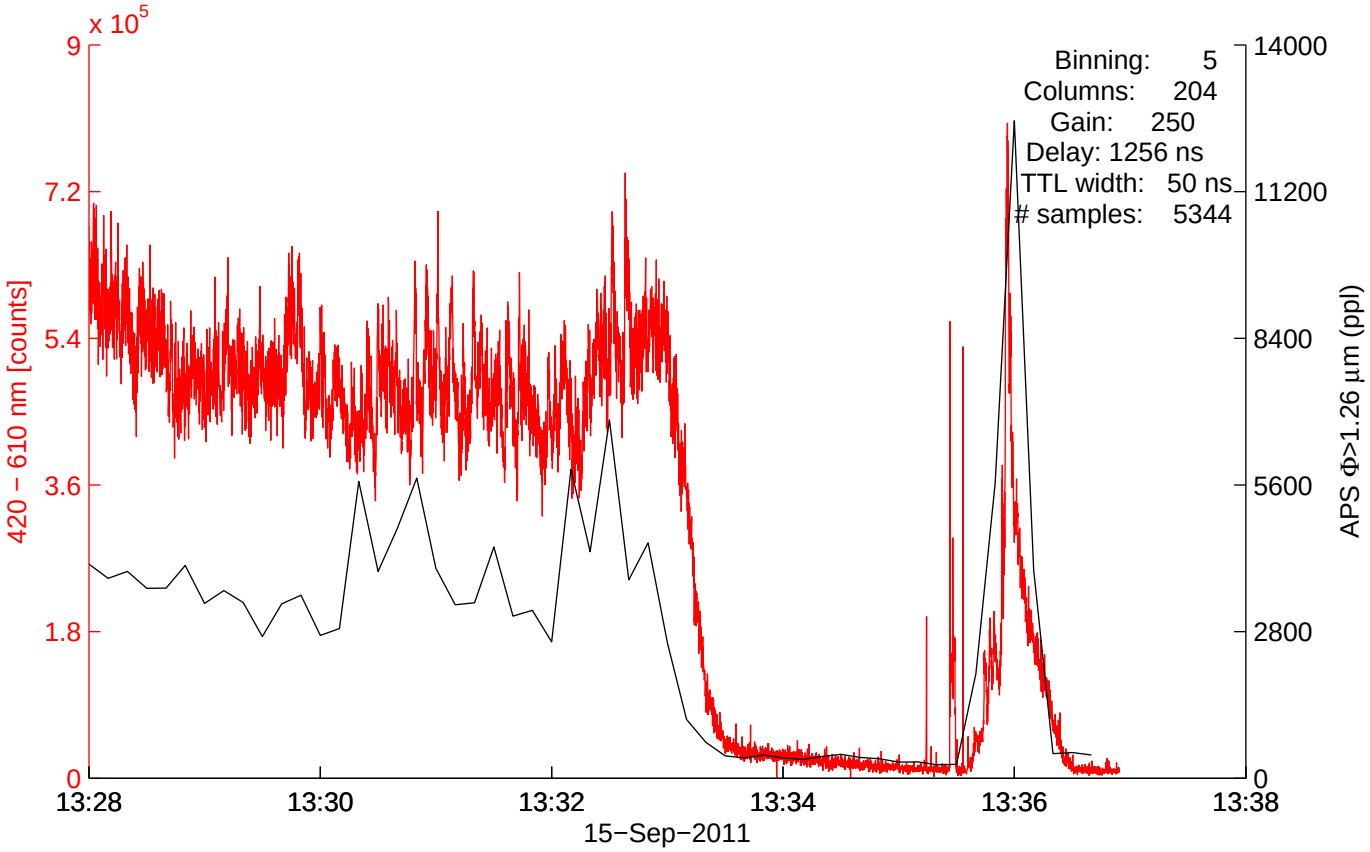
x 10^5
9
7.2
5.4
3.6
1.8
0
420 – 610 nm [counts]
14000
11200
8400
5600
2800
0
APS Φ>1.26 µm (ppl)
Binning: 5
Columns: 204
Gain: 250
Delay: 1256 ns
TTL width: 50 ns
samples: 5344
13:28
13:30
13:32
13:34
13:36
13:38
15−Sep−2011

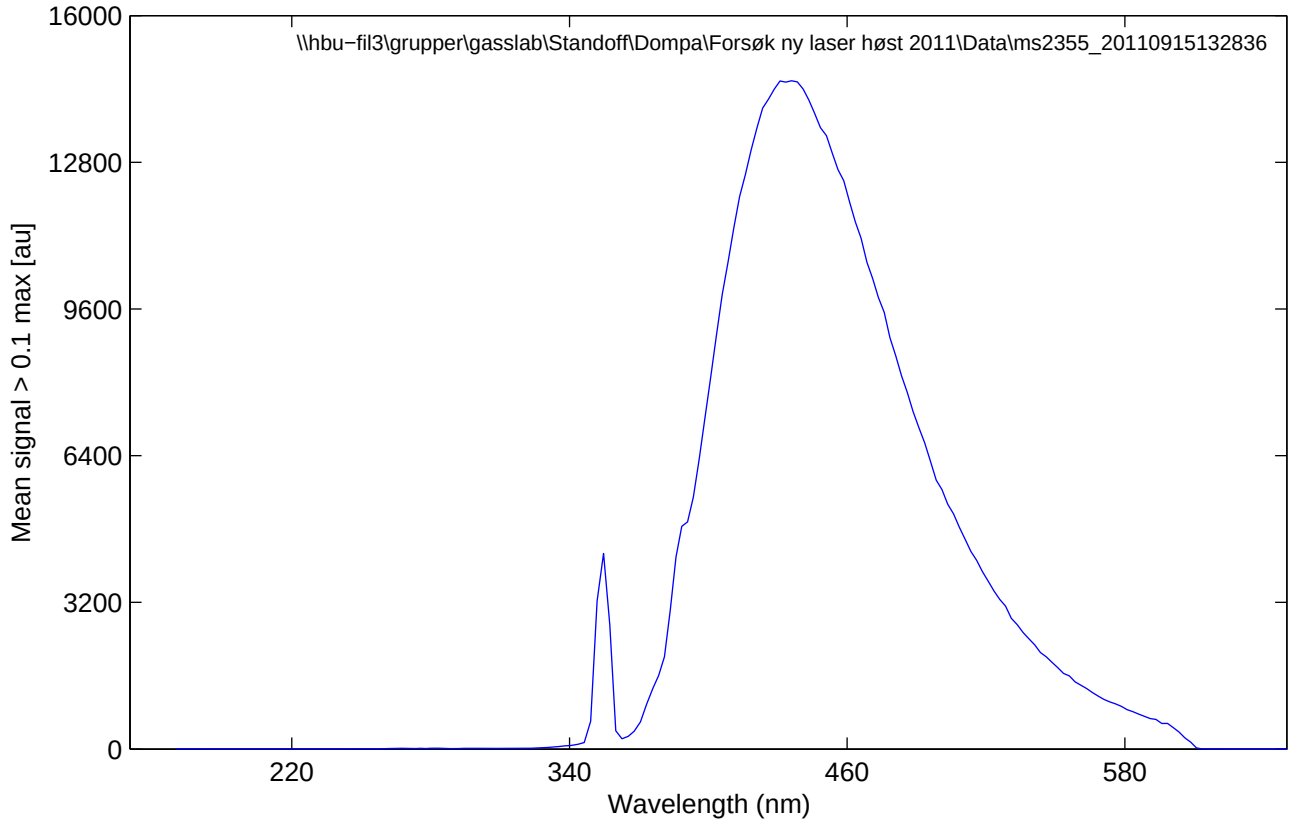
\\hbu−fil3\grupper\gasslab\Standoff\Dompa\Forsøk ny laser høst 2011\Data\ms2355_20110915132836
16000
12800
9600
6400
3200
0
Mean signal > 0.1 max [au]
220
340
460
580
Wavelength (nm)

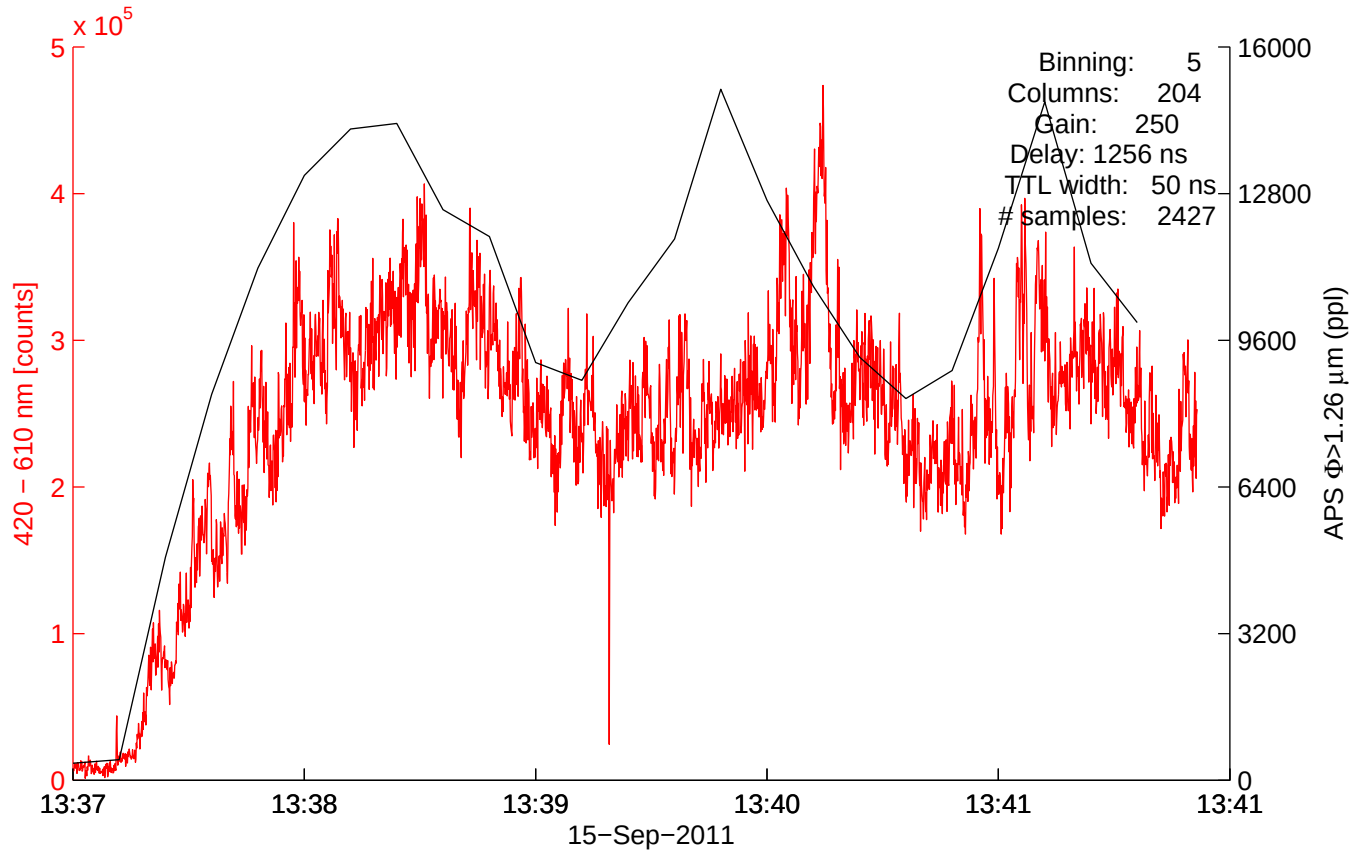
x 10^5
5
4
3
2
1
0
420 – 610 nm [counts]
16000
12800
9600
6400
3200
0
APS Φ>1.26 µm (ppl)
Binning: 5
Columns: 204
Gain: 250
Delay: 1256 ns
TTL width: 50 ns
samples: 2427
13:37
13:38
13:39
13:40
13:41
13:41
15−Sep−2011

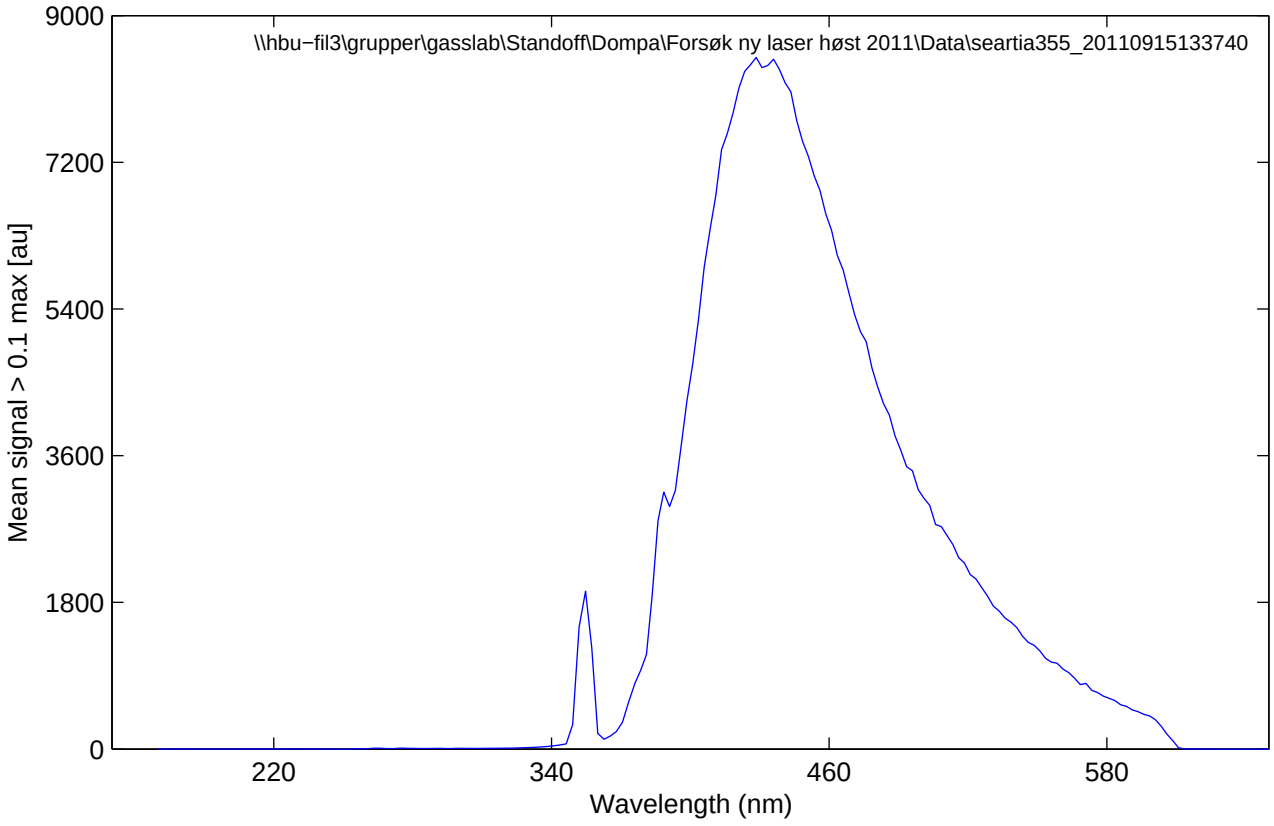
\\hbu−fil3\grupper\gasslab\Standoff\Dompa\Forsøk ny laser høst 2011\Data\seartia355_20110915133740
9000
7200
5400
3600
1800
0
Mean signal > 0.1 max [au]
220
340
460
580
Wavelength (nm)

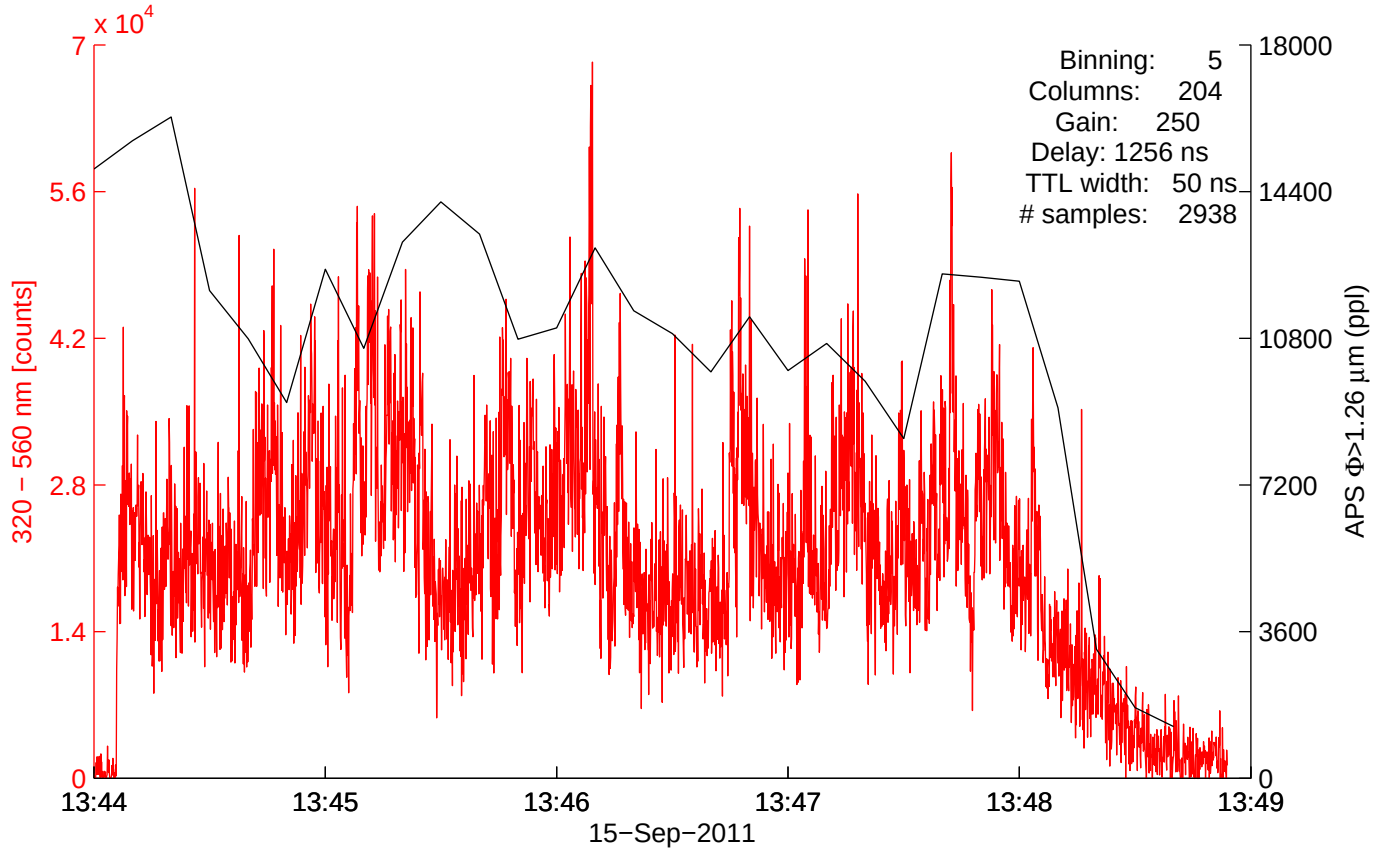
x 10^4
7
5.6
4.2
2.8
1.4
0
320 – 560 nm [counts]
18000
14400
10800
7200
3600
0
APS Φ>1.26 µm (ppl)
Binning: 5
Columns: 204
Gain: 250
Delay: 1256 ns
TTL width: 50 ns
samples: 2938
13:44
13:45
13:46
13:47
13:48
13:49
15−Sep−2011

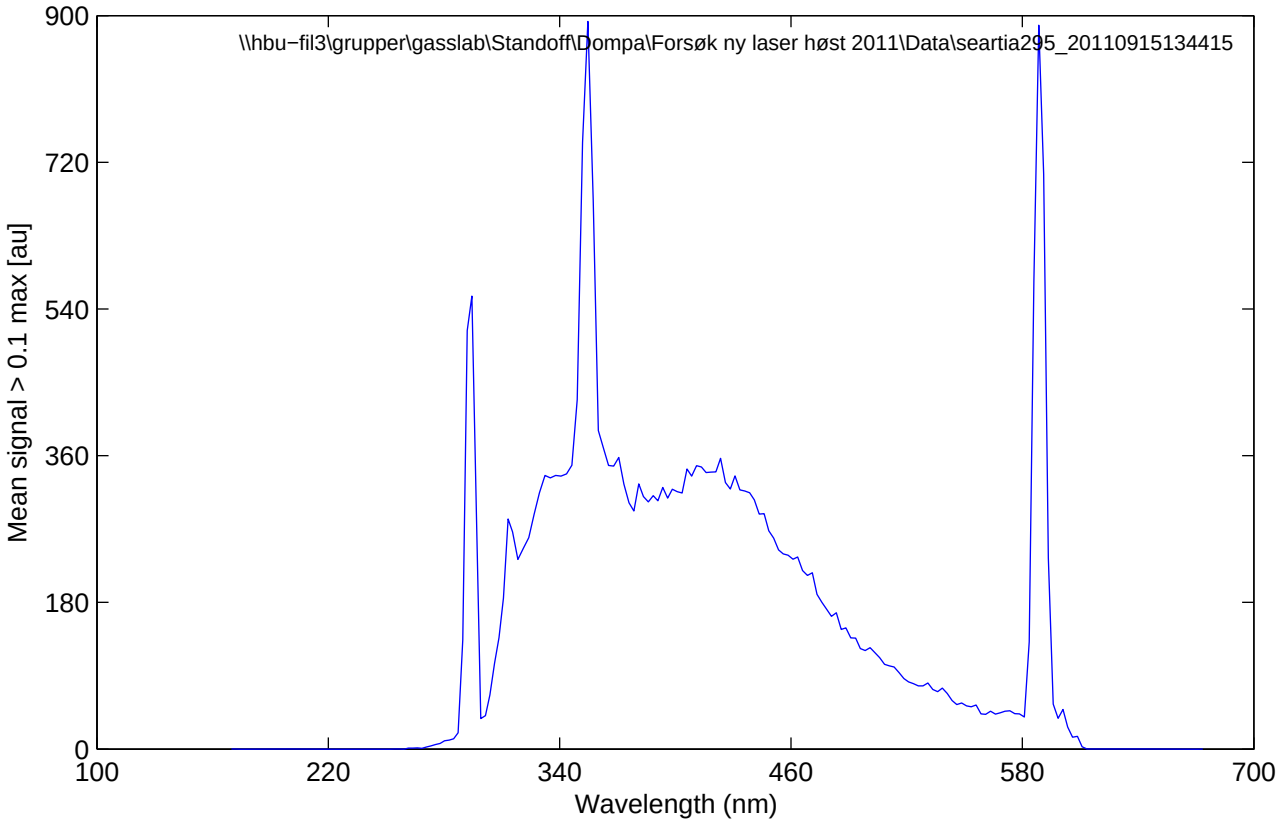
\\hbu−fil3\grupper\gasslab\Standoff\Dompa\Forsøk ny laser høst 2011\Data\seartia295_20110915134415
900
720
540
360
180
0
Mean signal > 0.1 max [au]
100
220
340
460
580
700
Wavelength (nm)

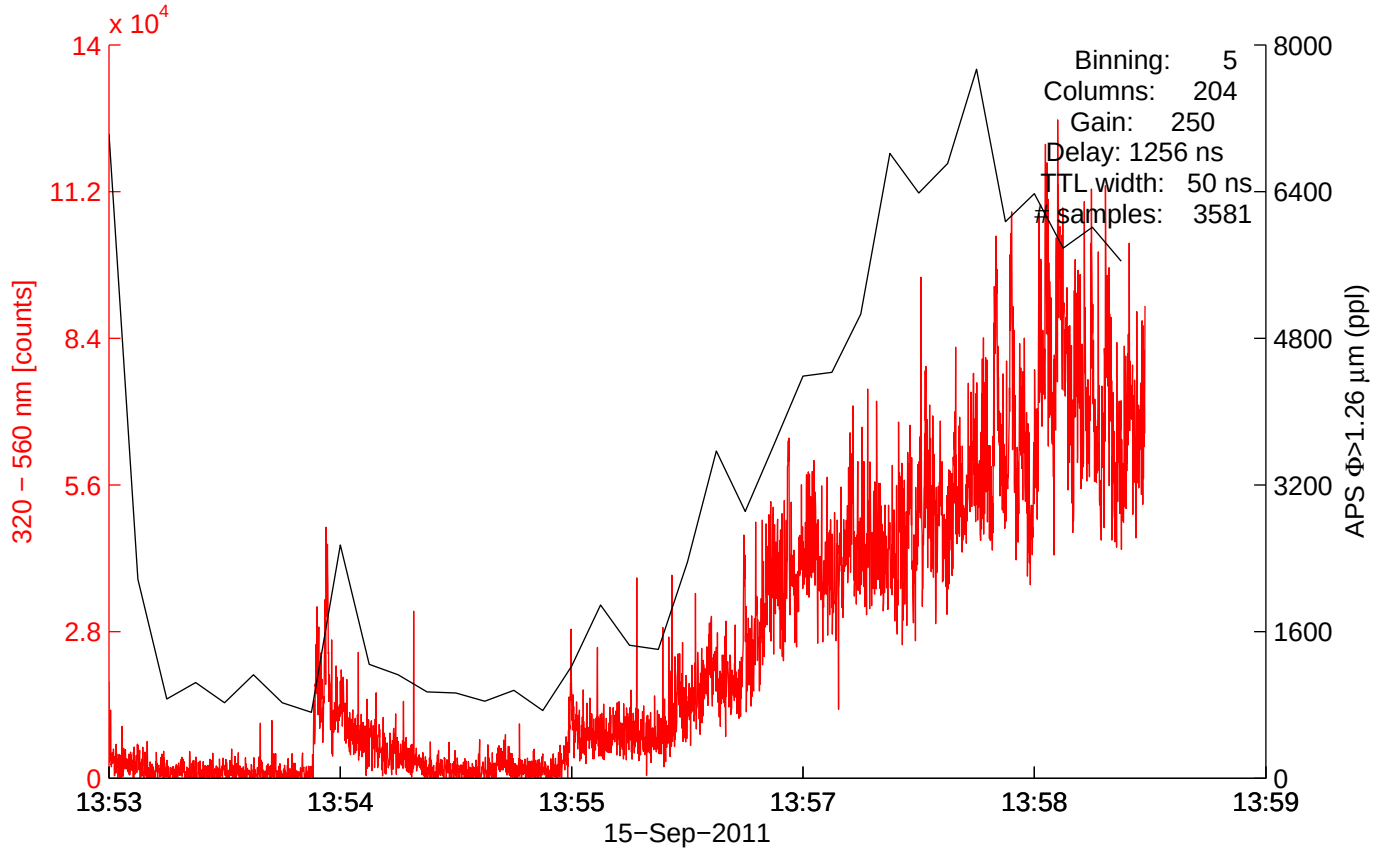
x 10^4
14
11.2
8.4
5.6
2.8
0
320 – 560 nm [counts]
8000
6400
4800
3200
1600
0
APS Φ>1.26 µm (ppl)
Binning: 5
Columns: 204
Gain: 250
Delay: 1256 ns
TTL width: 50 ns
samples: 3581
13:53
13:54
13:55
13:57
13:58
13:59
15−Sep−2011

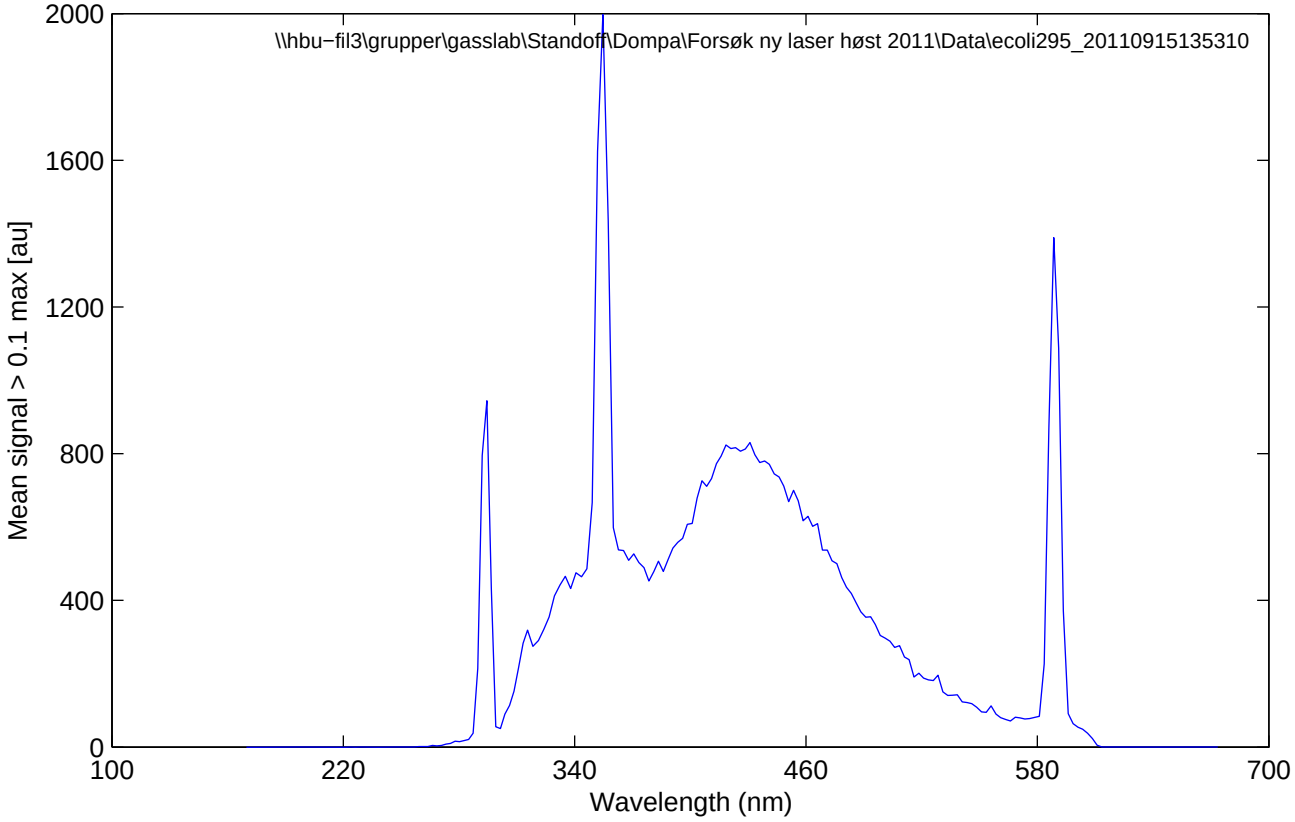
\\hbu−fil3\grupper\gasslab\Standoff\Dompa\Forsøk ny laser høst 2011\Data\ecoli295_20110915135310
2000
1600
1200
800
400
0
Mean signal > 0.1 max [au]
100
220
340
460
580
700
Wavelength (nm)

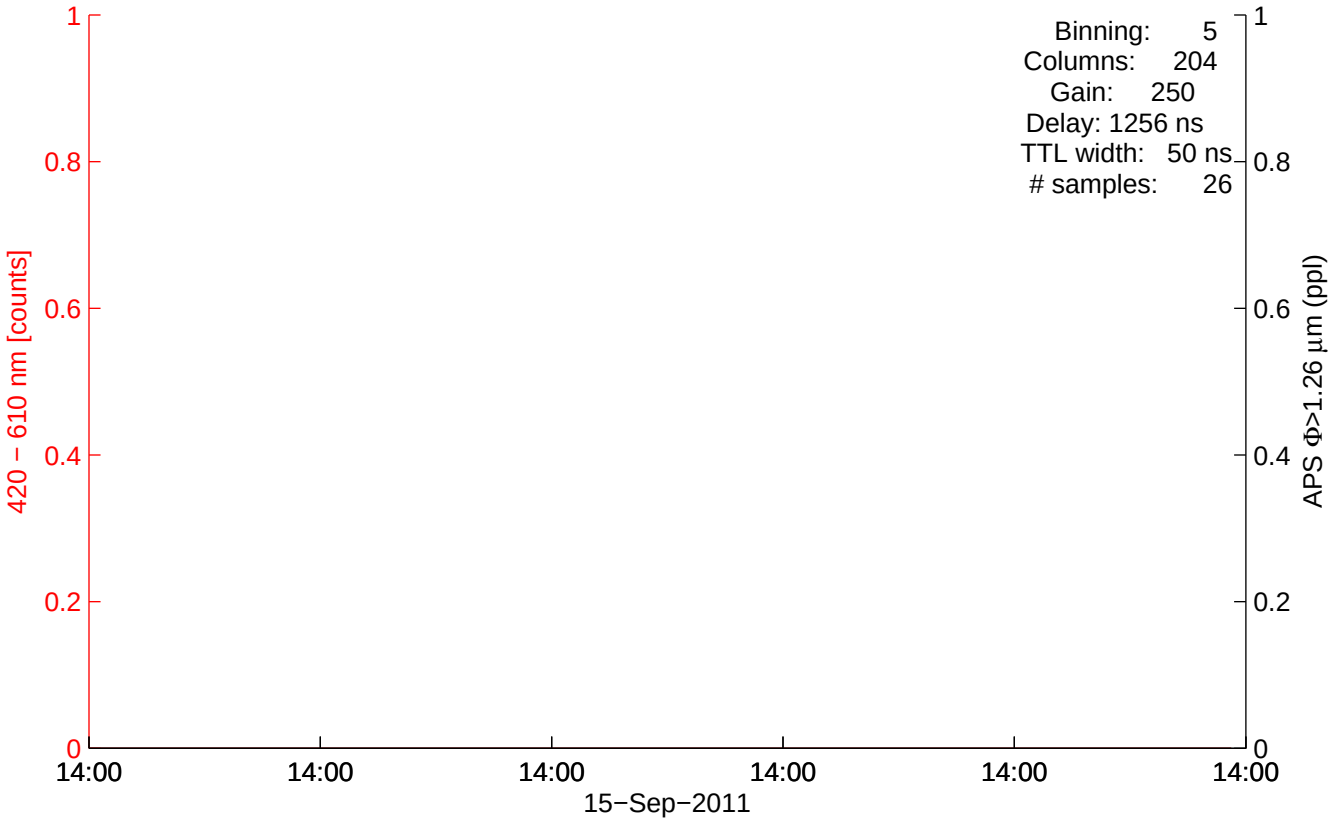
Binning: 5
Columns: 204
Gain: 250
Delay: 1256 ns
TTL width: 50 ns
samples: 26
420 – 610 nm [counts]
APS Φ>1.26 µm (ppl)
0
0.2
0.4
0.6
0.8
1
14:00
15−Sep−2011

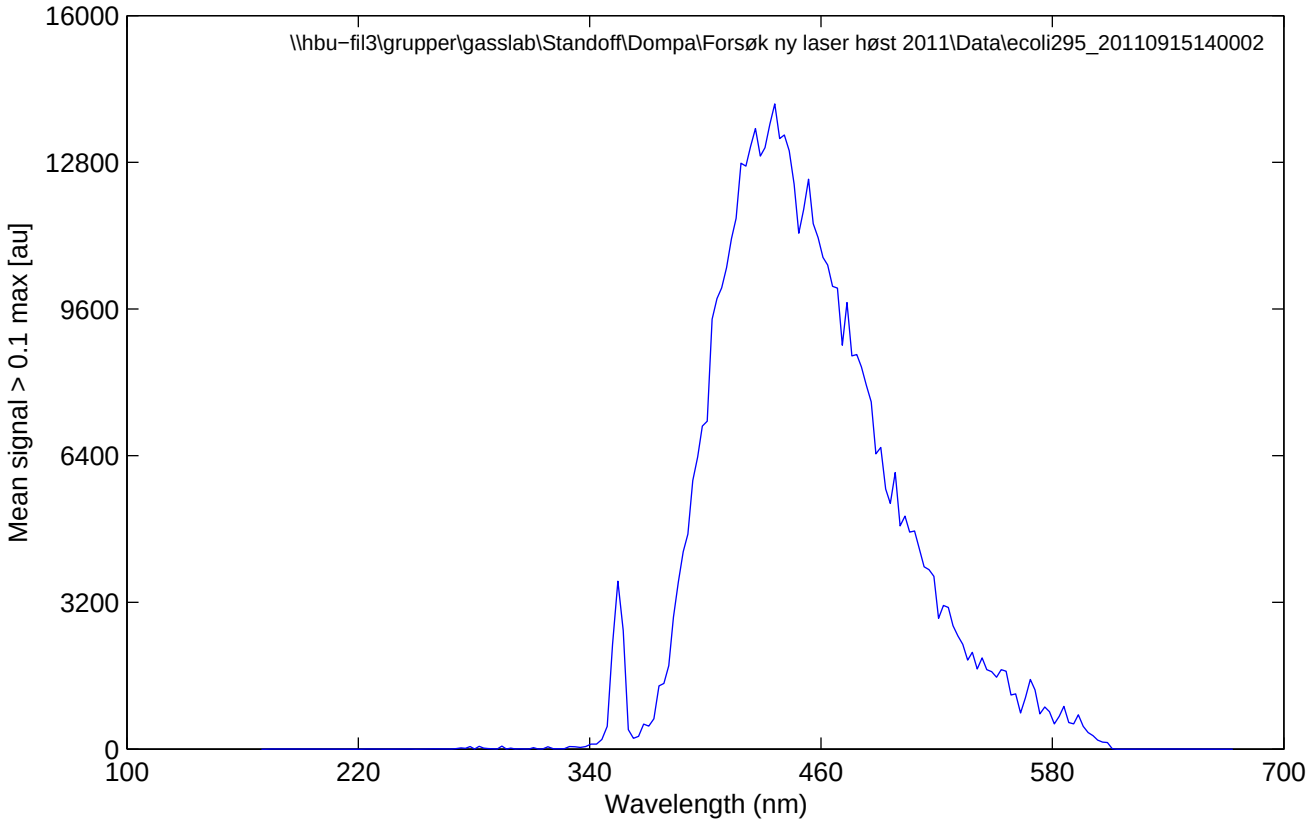
\\hbu−fil3\grupper\gasslab\Standoff\Dompa\Forsøk ny laser høst 2011\Data\ecoli295_20110915140002
Mean signal > 0.1 max [au]
0
3200
6400
9600
12800
16000
100
220
340
460
580
700
Wavelength (nm)

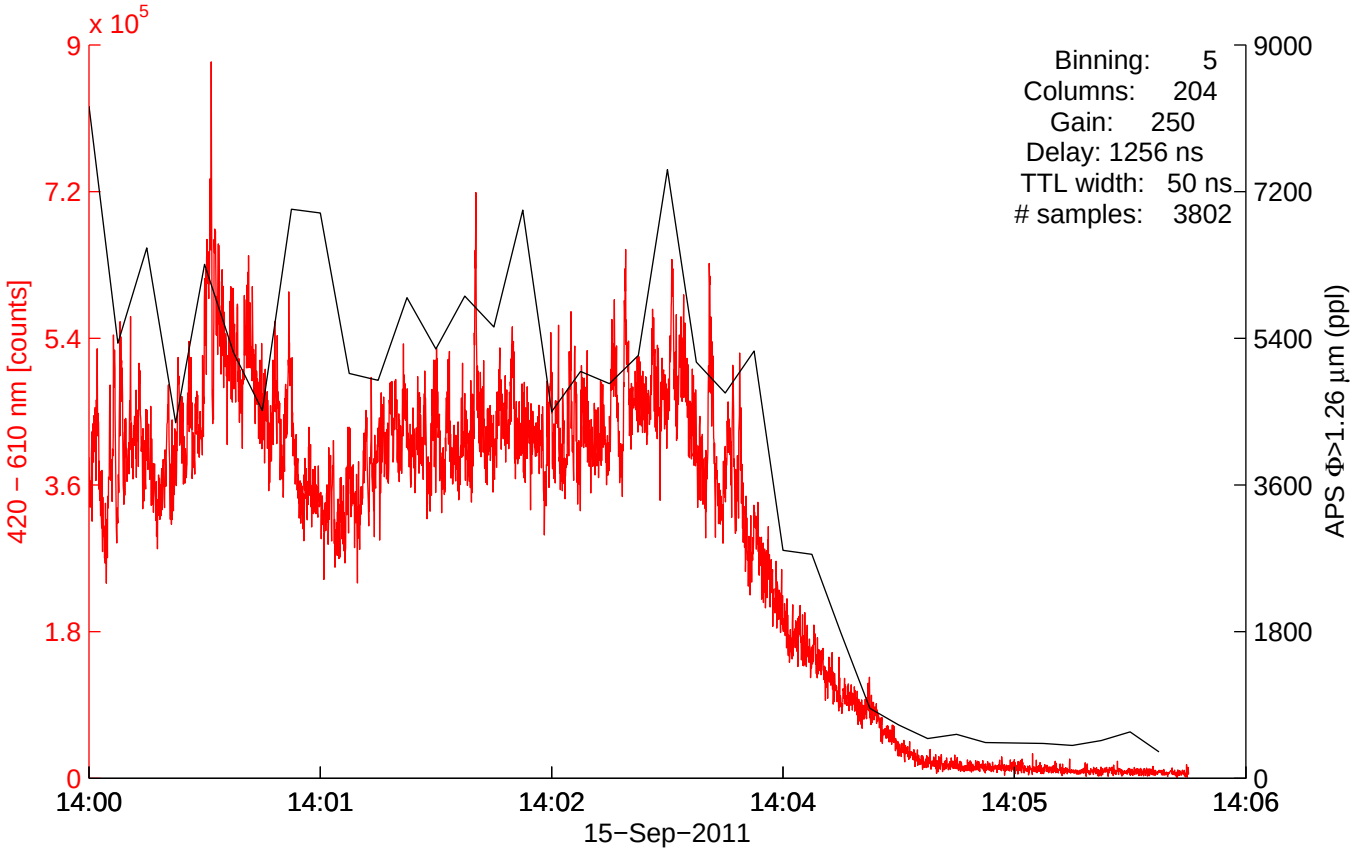
x 10^5
9
7.2
5.4
3.6
1.8
0
420 – 610 nm [counts]
9000
7200
5400
3600
1800
0
APS Φ>1.26 µm (ppl)
Binning: 5
Columns: 204
Gain: 250
Delay: 1256 ns
TTL width: 50 ns
samples: 3802
14:00
14:01
14:02
14:04
14:05
14:06
15−Sep−2011

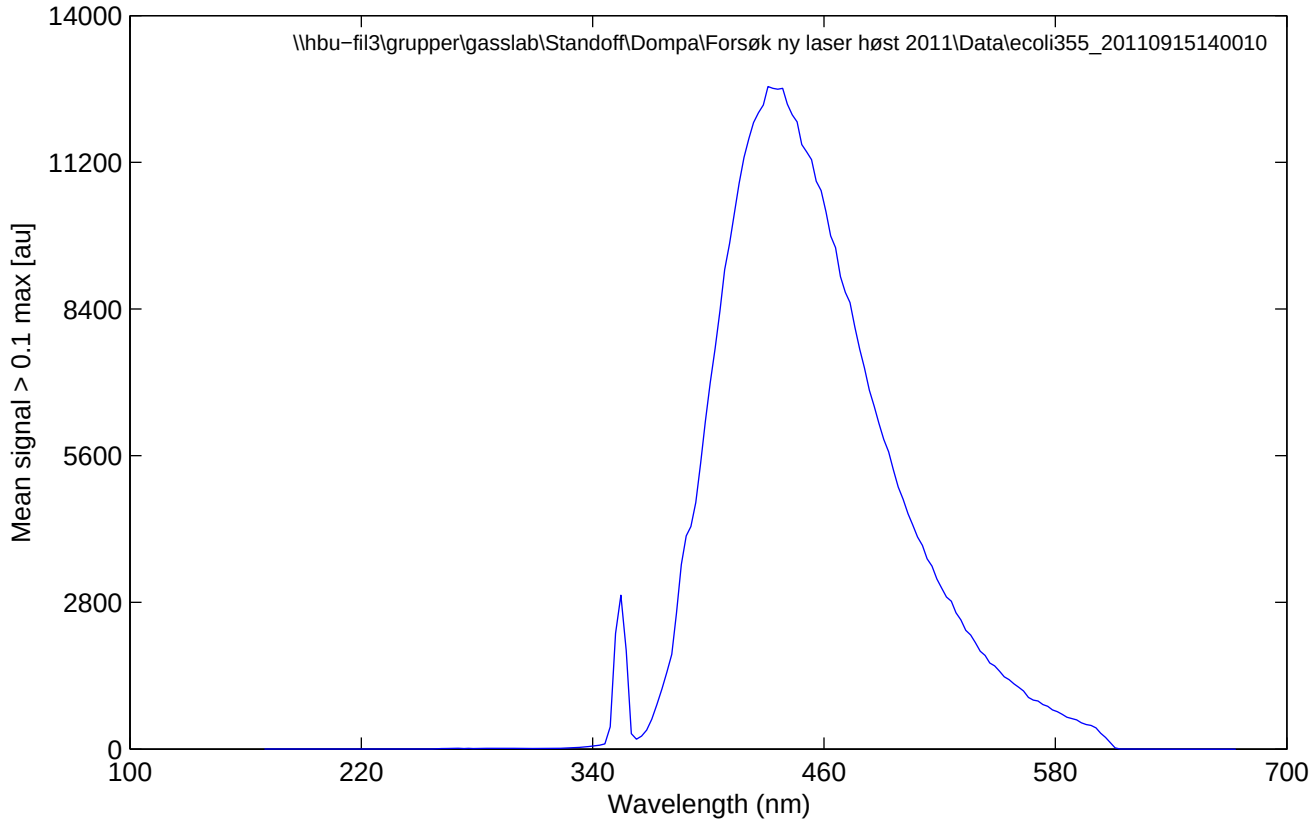
\\hbu−fil3\grupper\gasslab\Standoff\Dompa\Forsøk ny laser høst 2011\Data\ecoli355_20110915140010
14000
11200
8400
5600
2800
0
Mean signal > 0.1 max [au]
100
220
340
460
580
700
Wavelength (nm)

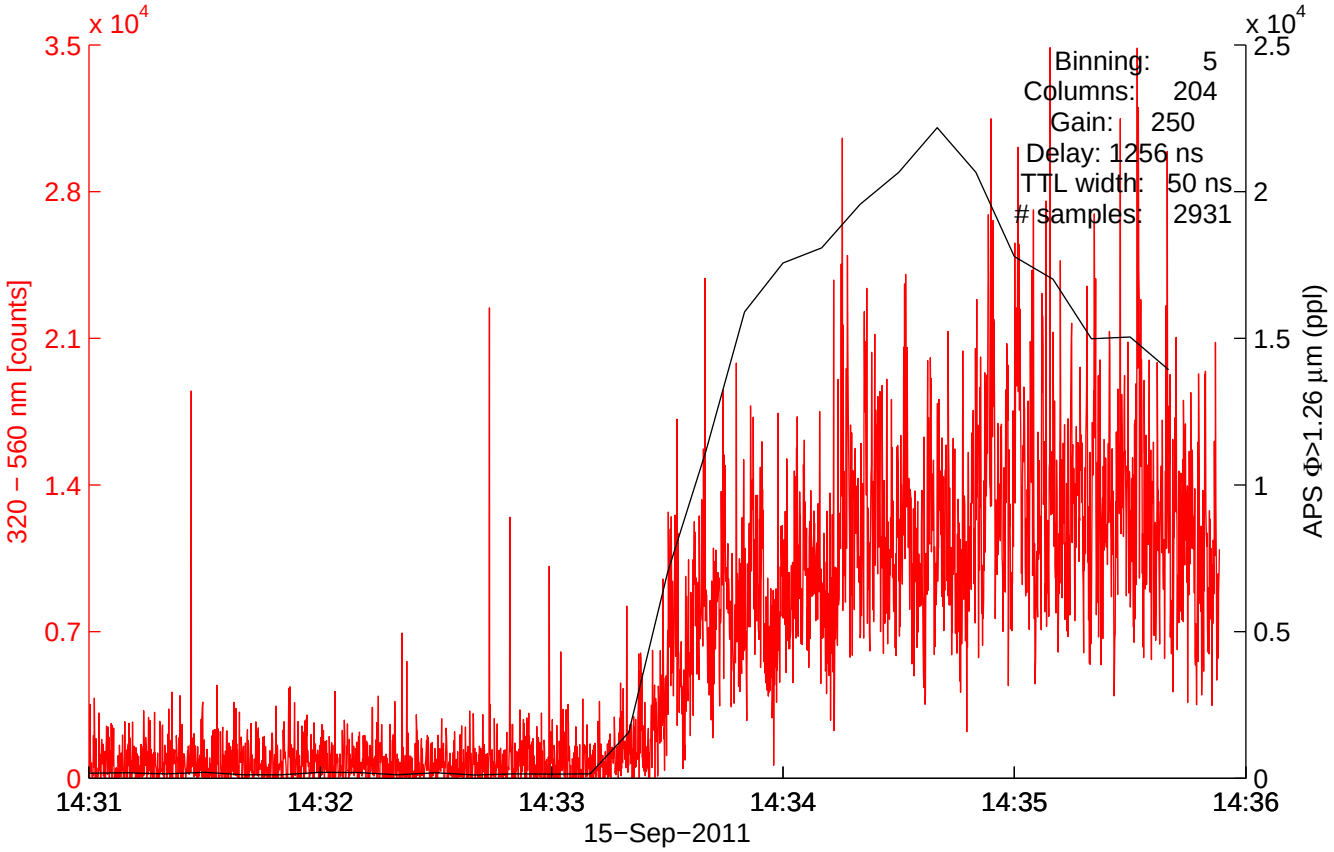
x 10^4
3.5
2.8
2.1
1.4
0.7
0
320 – 560 nm [counts]
x 10^4
2.5
2
1.5
1
0.5
0
APS Φ>1.26 µm (ppl)
Binning: 5
Columns: 204
Gain: 250
Delay: 1256 ns
TTL width: 50 ns
samples: 2931
14:31
14:32
14:33
14:34
14:35
14:36
15−Sep−2011

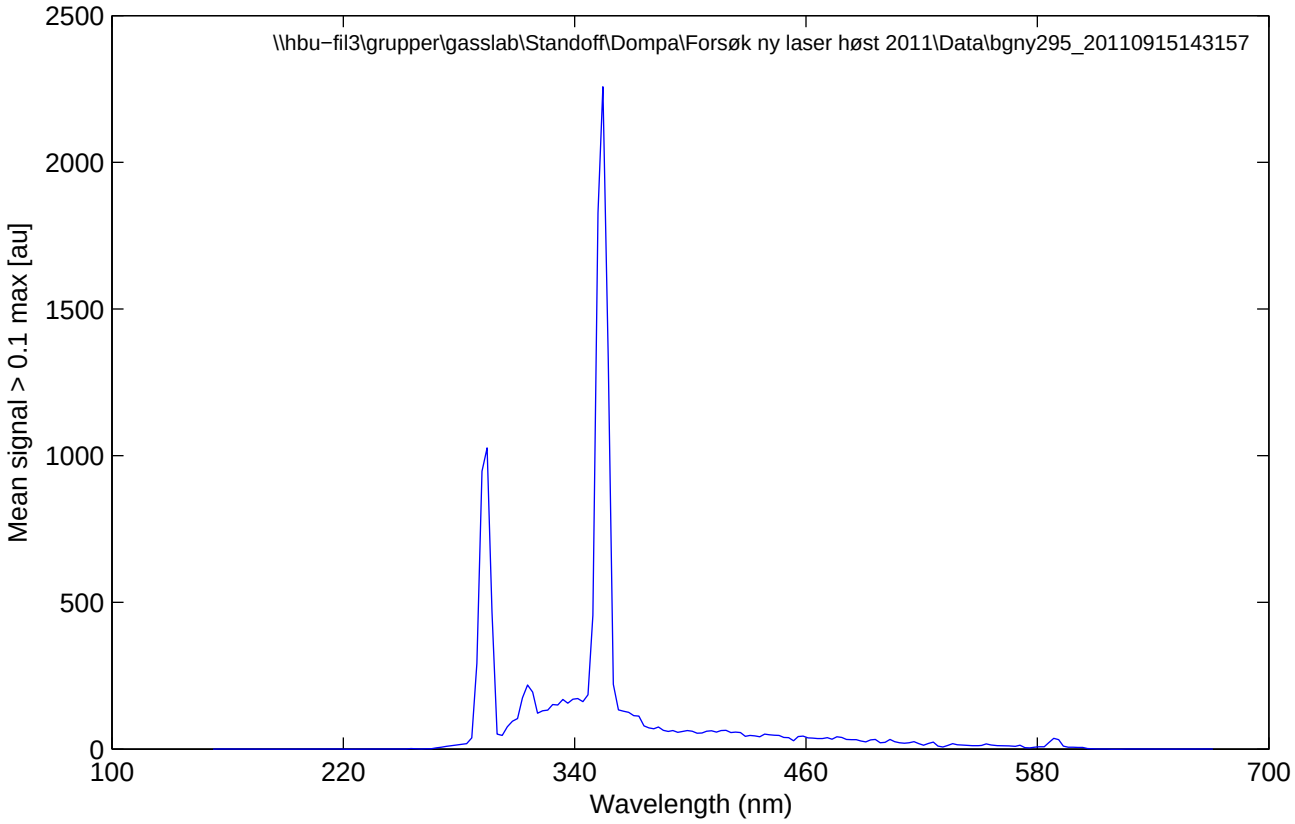
\\hbu−fil3\grupper\gasslab\Standoff\Dompa\Forsøk ny laser høst 2011\Data\bgny295_20110915143157
2500
2000
1500
1000
500
0
Mean signal > 0.1 max [au]
100
220
340
460
580
700
Wavelength (nm)

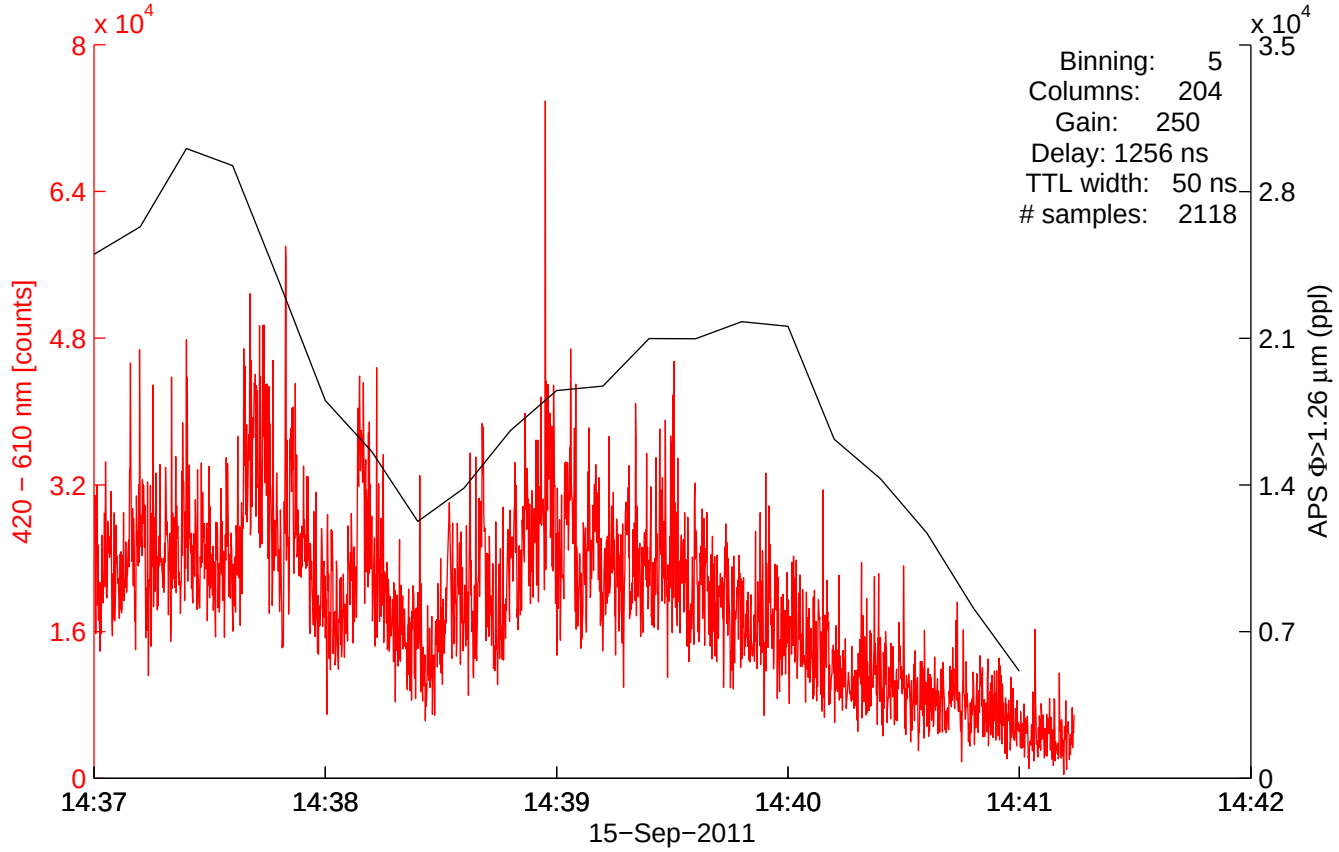
x 10^4
8
6.4
4.8
3.2
1.6
0
420 – 610 nm [counts]
x 10^4
3.5
2.8
2.1
1.4
0.7
0
APS Φ>1.26 µm (ppl)
Binning: 5
Columns: 204
Gain: 250
Delay: 1256 ns
TTL width: 50 ns
samples: 2118
14:37
14:38
14:39
14:40
14:41
14:42
15−Sep−2011

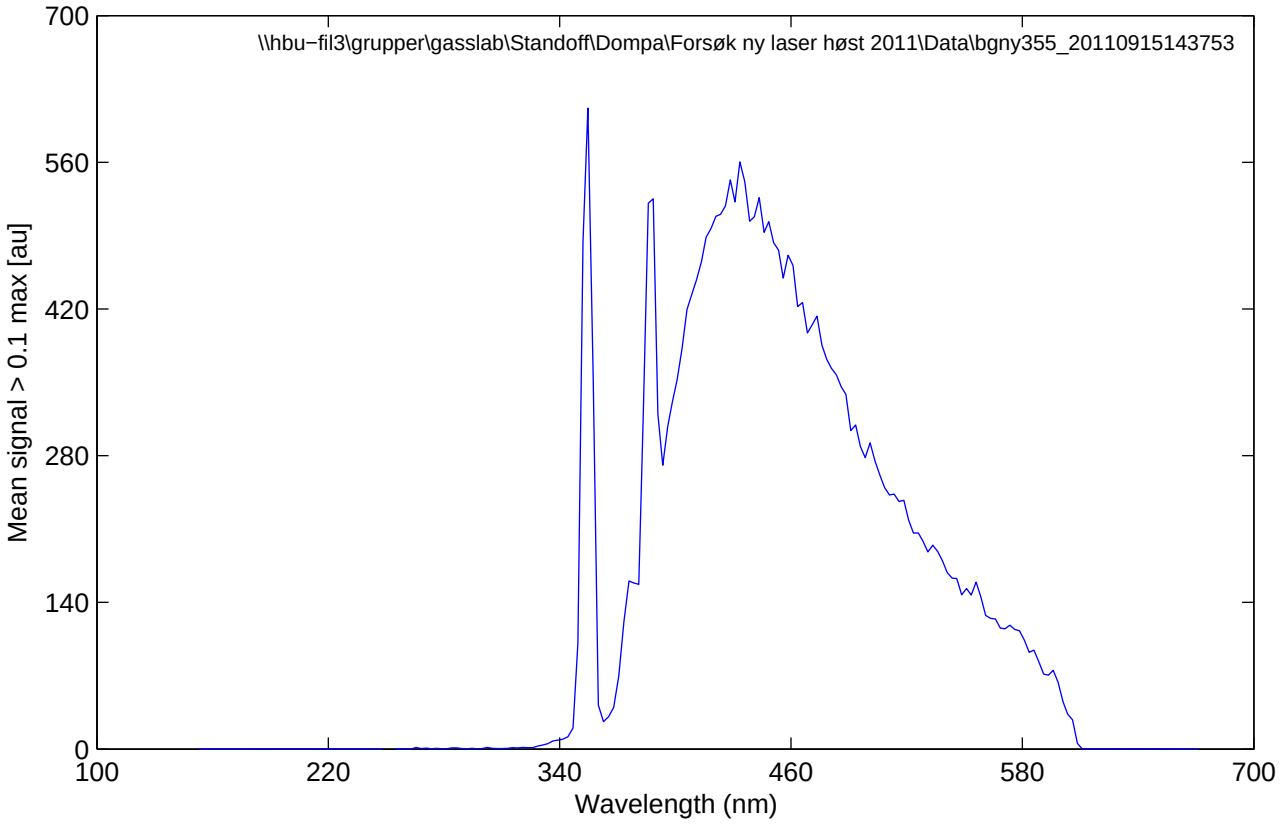
\\hbu−fil3\grupper\gasslab\Standoff\Dompa\Forsøk ny laser høst 2011\Data\bgny355_20110915143753
700
560
420
280
140
0
Mean signal > 0.1 max [au]
100
220
340
460
580
700
Wavelength (nm)

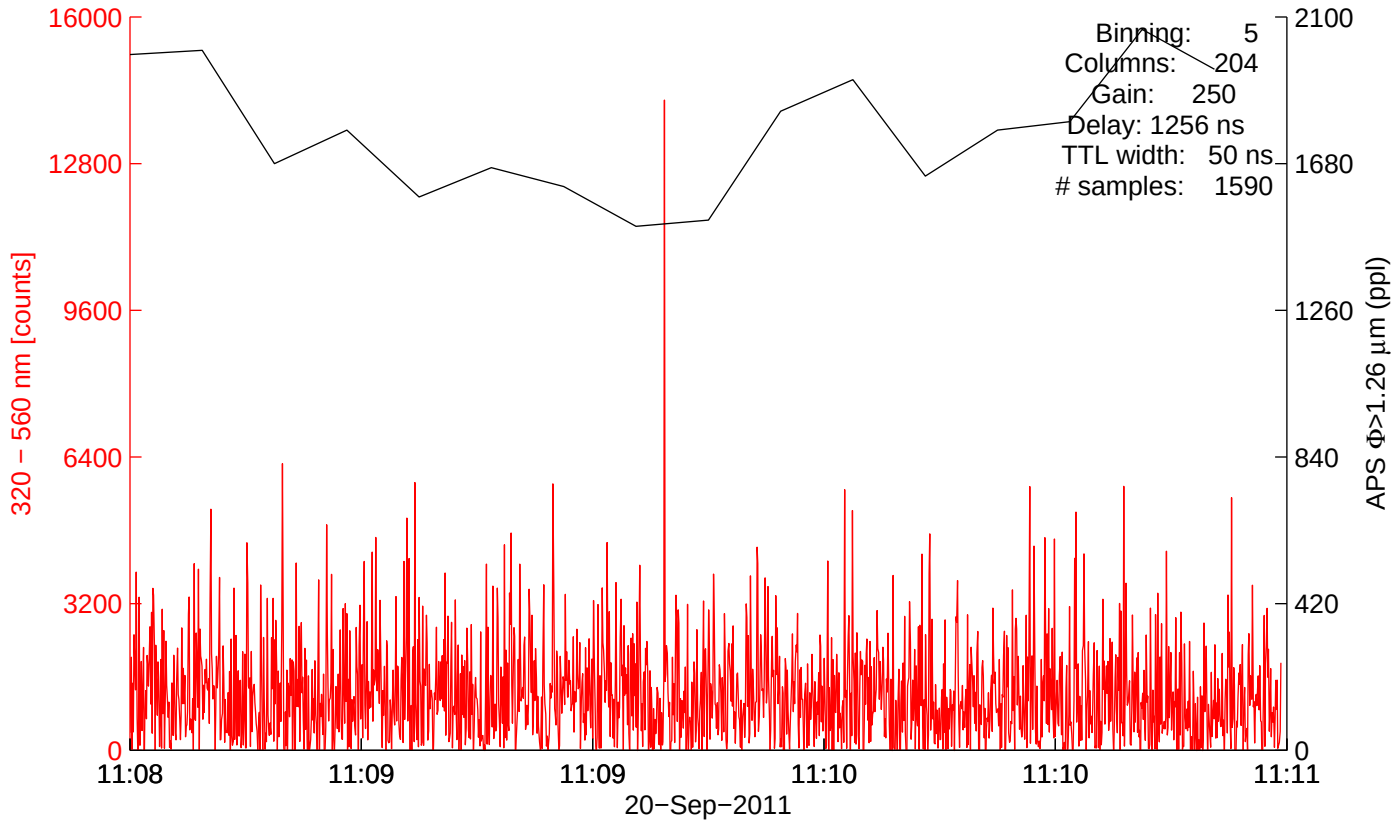
Binning: 5
Columns: 204
Gain: 250
Delay: 1256 ns
TTL width: 50 ns
samples: 1590
320 − 560 nm [counts]
APS Φ>1.26 µm (ppl)
16000
12800
9600
6400
3200
0
2100
1680
1260
840
420
0
11:08
11:09
11:09
11:10
11:10
11:11
20−Sep−2011

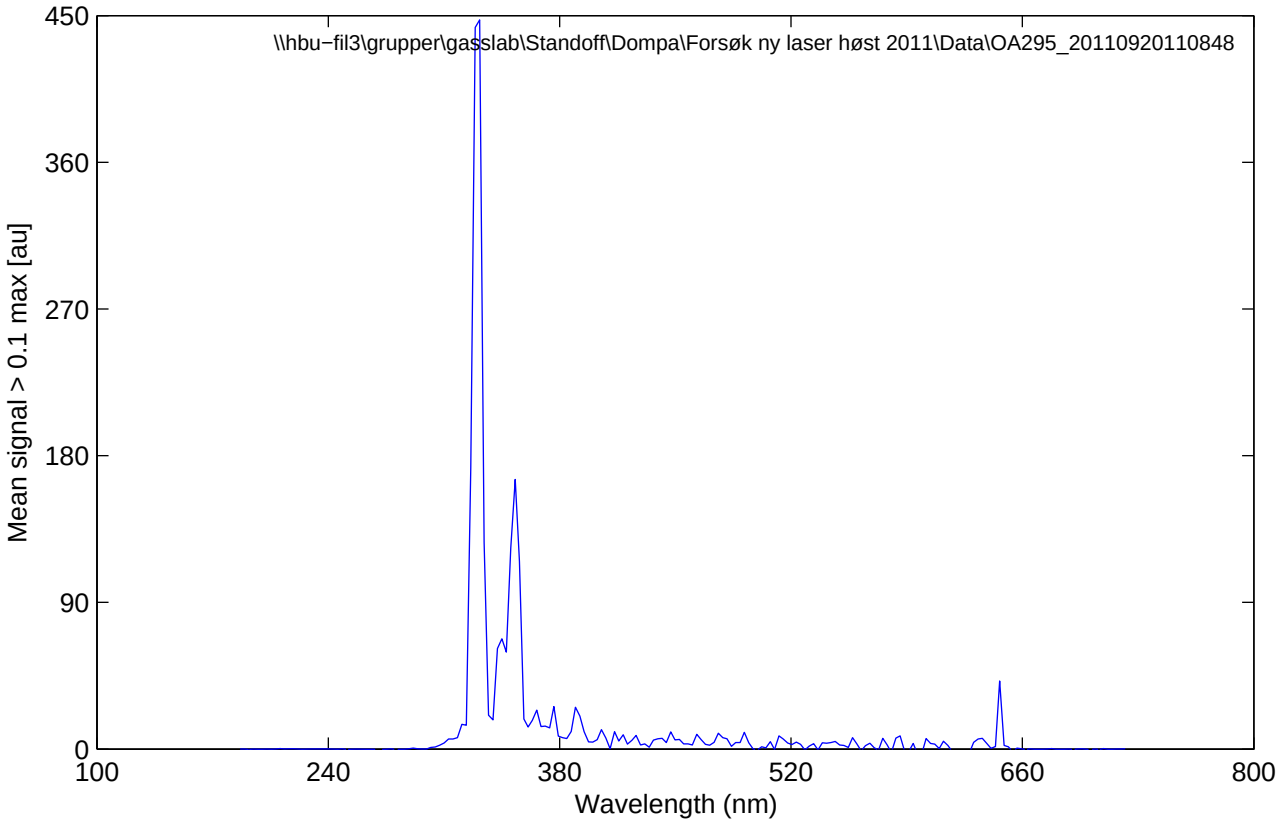
\\hbu−fil3\grupper\gasslab\Standoff\Dompa\Forsøk ny laser høst 2011\Data\OA295_20110920110848
Mean signal > 0.1 max [au]
450
360
270
180
90
0
100
240
380
520
660
800
Wavelength (nm)

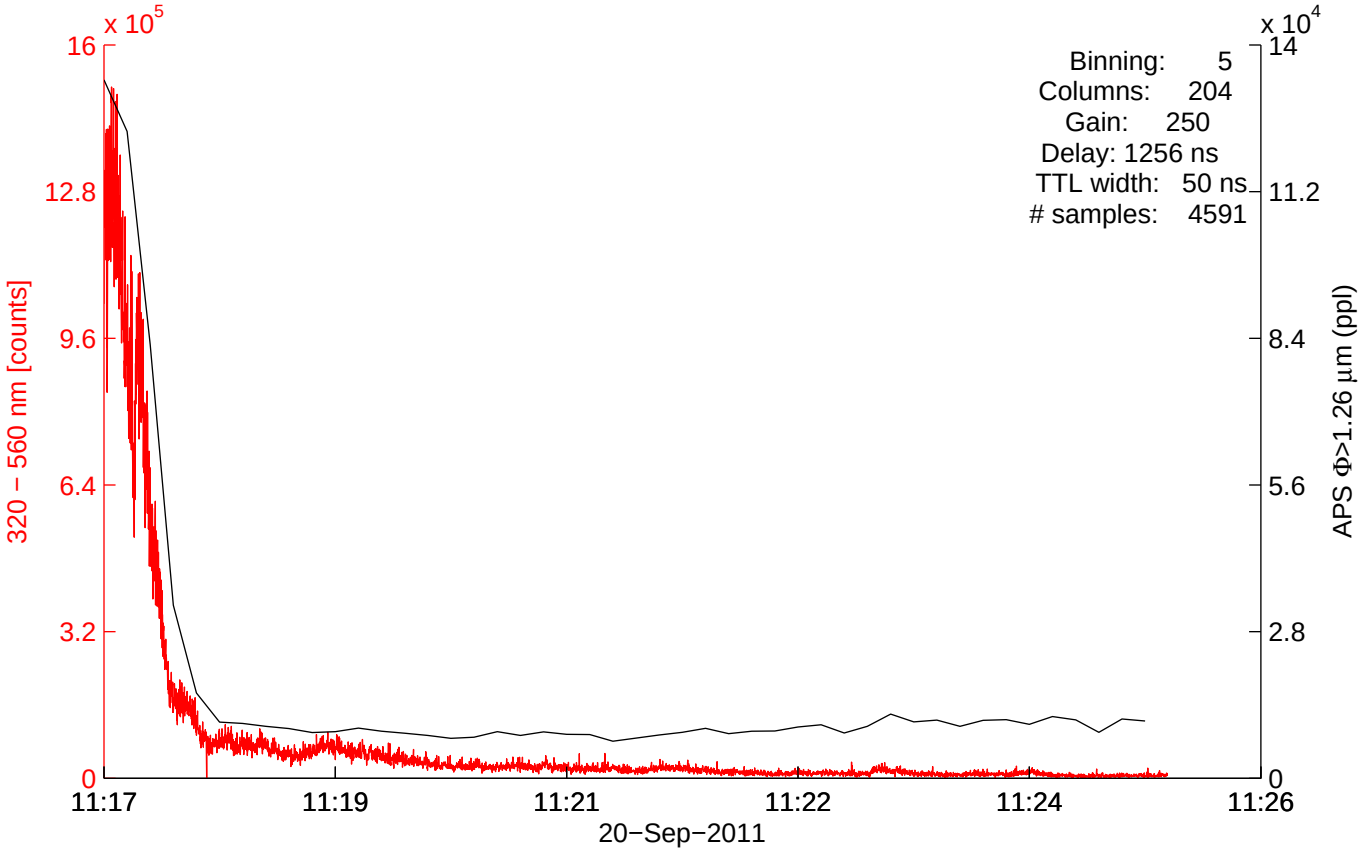
x 10^5
16
12.8
9.6
6.4
3.2
0
320 – 560 nm [counts]
x 10^4
14
11.2
8.4
5.6
2.8
0
APS Φ>1.26 µm (ppl)
Binning: 5
Columns: 204
Gain: 250
Delay: 1256 ns
TTL width: 50 ns
samples: 4591
11:17
11:19
11:21
11:22
11:24
11:26
20−Sep−2011

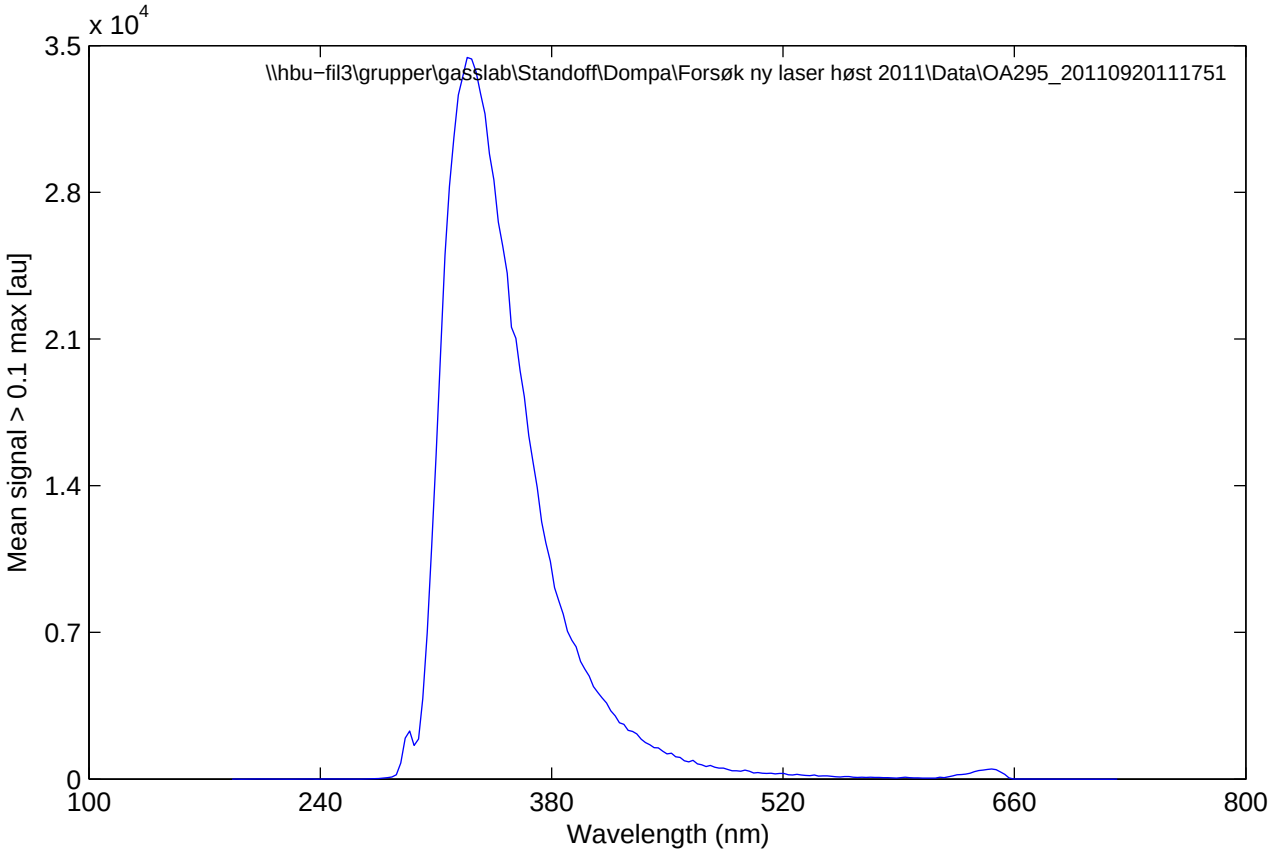
x 10^4
3.5
2.8
2.1
1.4
0.7
0
Mean signal > 0.1 max [au]
\\hbu−fil3\grupper\gasslab\Standoff\Dompa\Forsøk ny laser høst 2011\Data\OA295_20110920111751
100
240
380
520
660
800
Wavelength (nm)

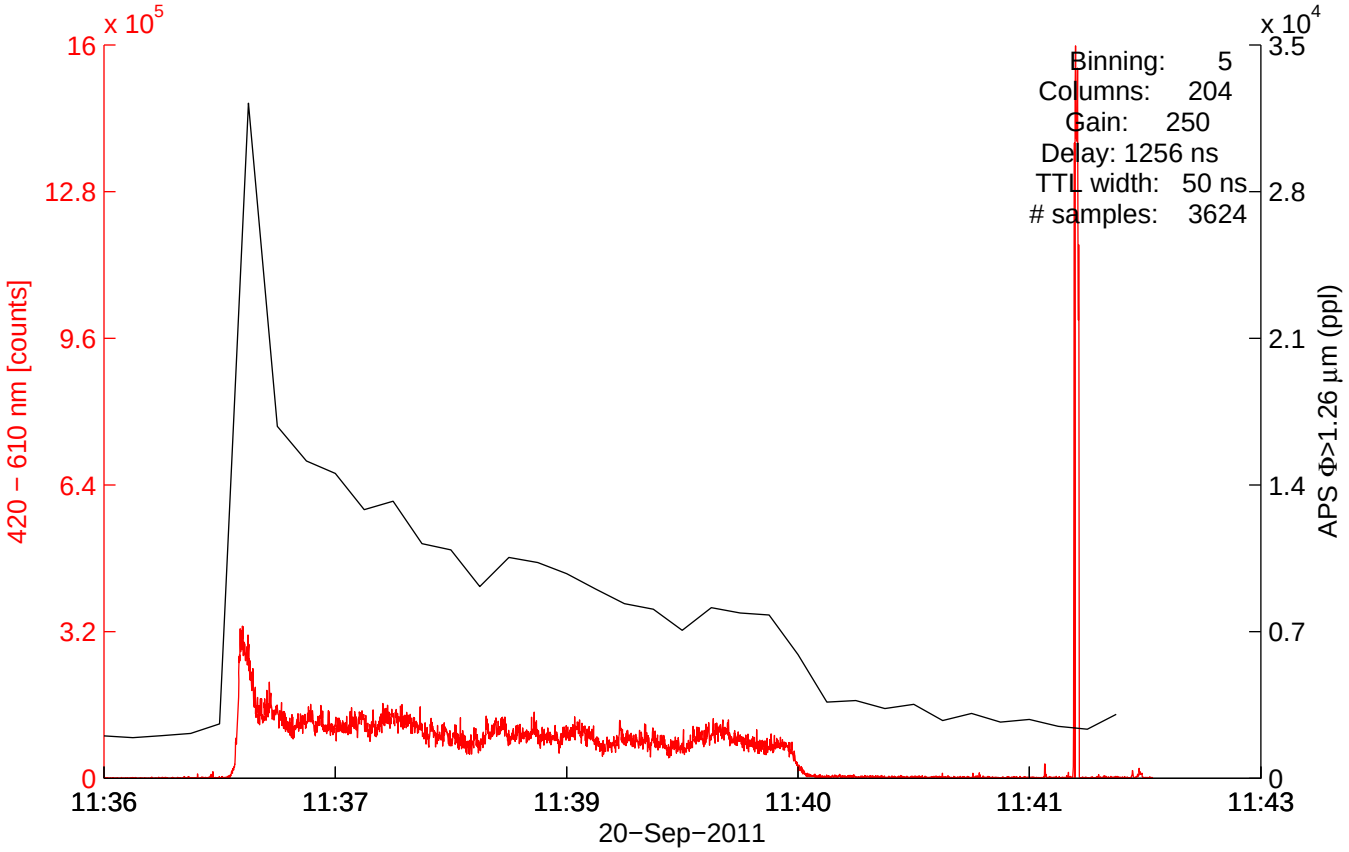
x 10^5
16
12.8
9.6
6.4
3.2
0
420 – 610 nm [counts]
x 10^4
3.5
2.8
2.1
1.4
0.7
0
APS Φ>1.26 µm (ppl)
Binning: 5
Columns: 204
Gain: 250
Delay: 1256 ns
TTL width: 50 ns
samples: 3624
11:36
11:37
11:39
11:40
11:41
11:43
20−Sep−2011

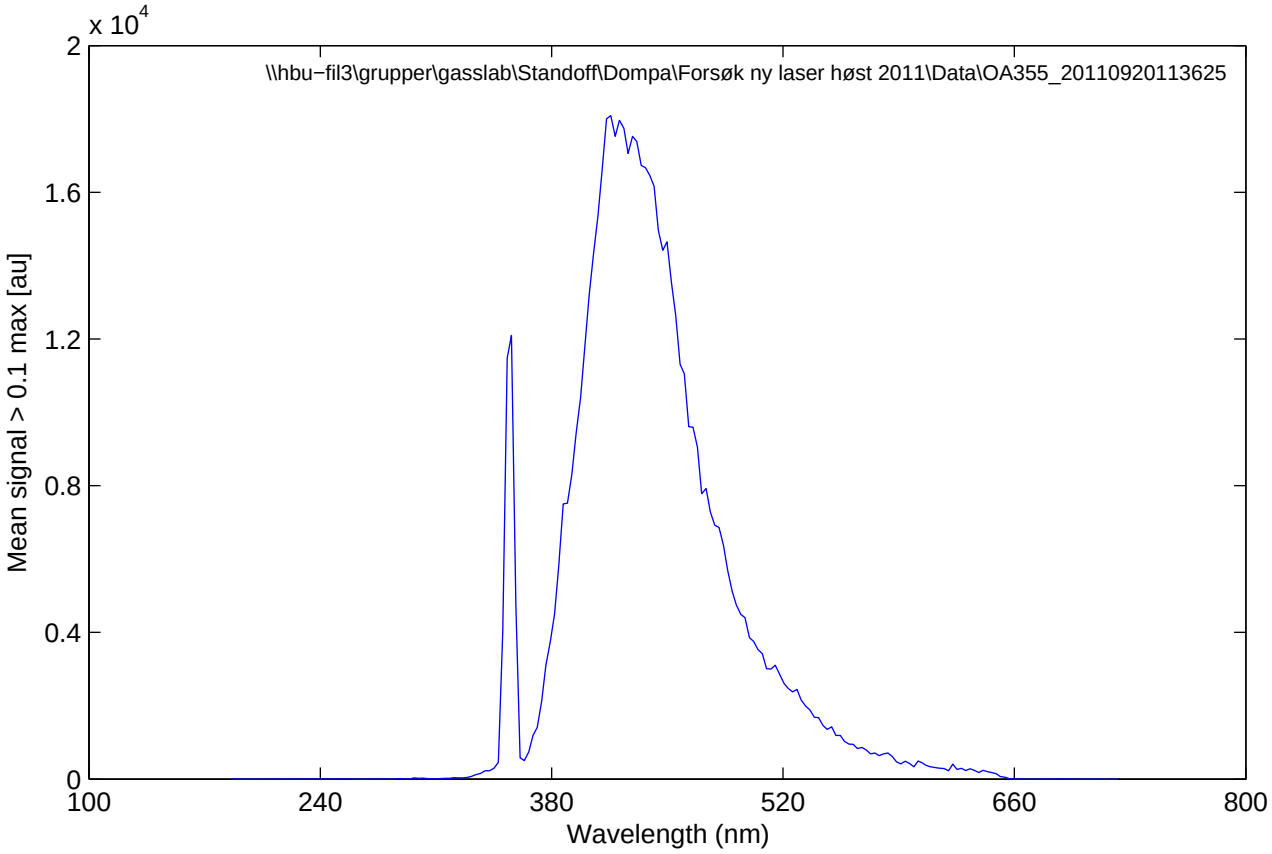
x 10^4
2
1.6
1.2
0.8
0.4
0
Mean signal > 0.1 max [au]
\\hbu−fil3\grupper\gasslab\Standoff\Dompa\Forsøk ny laser høst 2011\Data\OA355_20110920113625
100
240
380
520
660
800
Wavelength (nm)

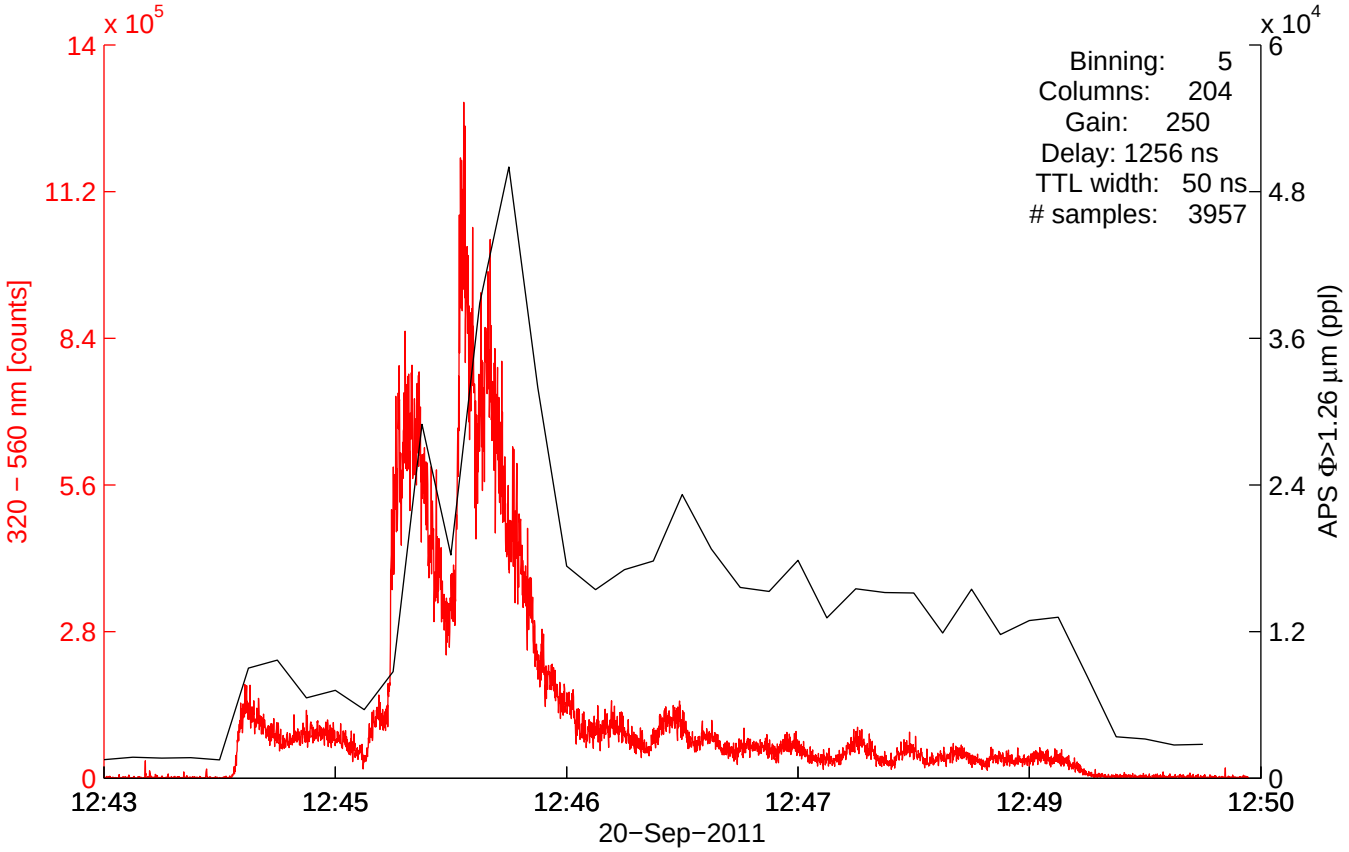
x 10^5
14
11.2
8.4
5.6
2.8
0
320 – 560 nm [counts]
x 10^4
6
4.8
3.6
2.4
1.2
0
APS Φ>1.26 µm (ppl)
Binning: 5
Columns: 204
Gain: 250
Delay: 1256 ns
TTL width: 50 ns
samples: 3957
12:43
12:45
12:46
12:47
12:49
12:50
20−Sep−2011

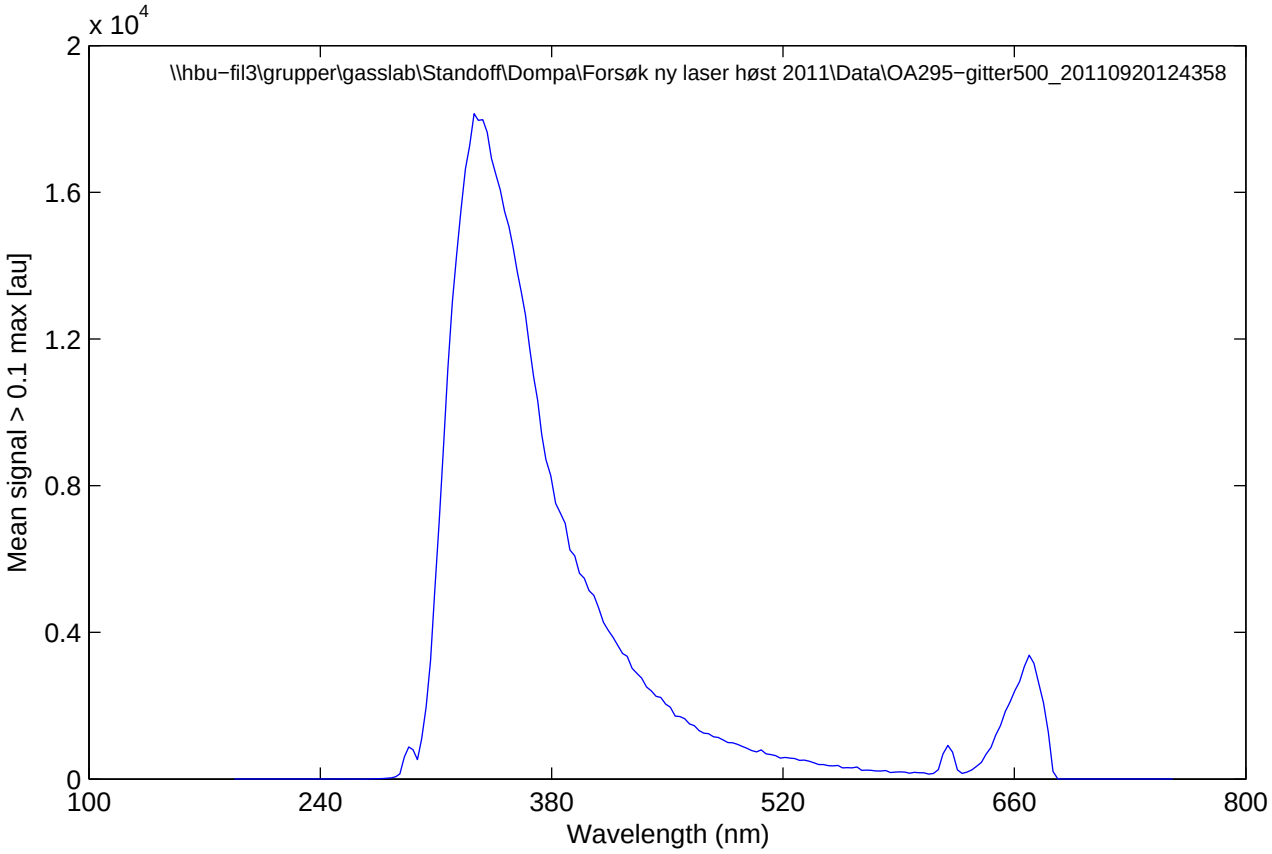
x 10^4
2
1.6
1.2
0.8
0.4
0
Mean signal > 0.1 max [au]
\\hbu−fil3\grupper\gasslab\Standoff\Dompa\Forsøk ny laser høst 2011\Data\OA295−gitter500_20110920124358
100
240
380
520
660
800
Wavelength (nm)

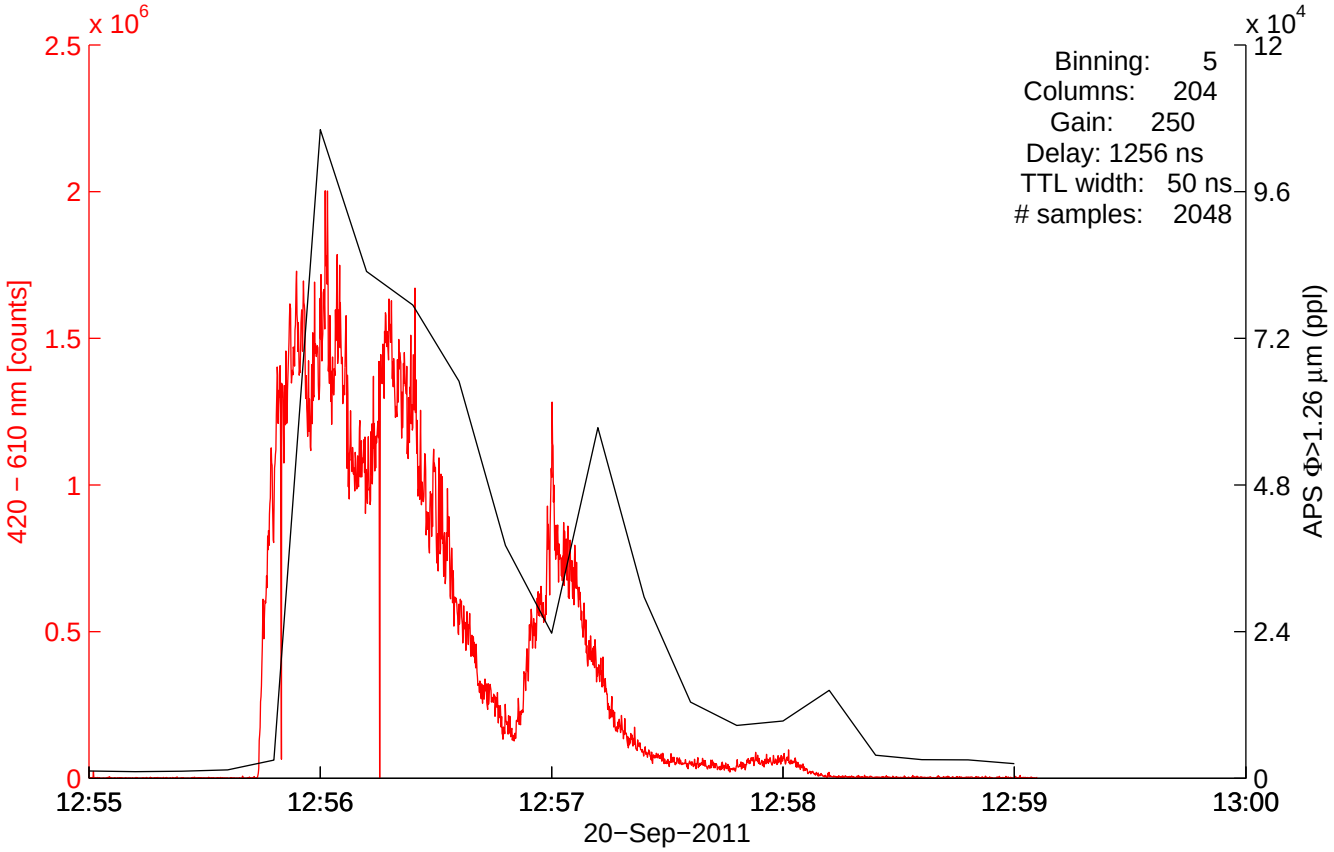
x 10^6
2.5
2
1.5
1
0.5
0
420 – 610 nm [counts]
x 10^4
12
9.6
7.2
4.8
2.4
0
APS Φ>1.26 µm (ppl)
Binning: 5
Columns: 204
Gain: 250
Delay: 1256 ns
TTL width: 50 ns
samples: 2048
12:55
12:56
12:57
12:58
12:59
13:00
20−Sep−2011

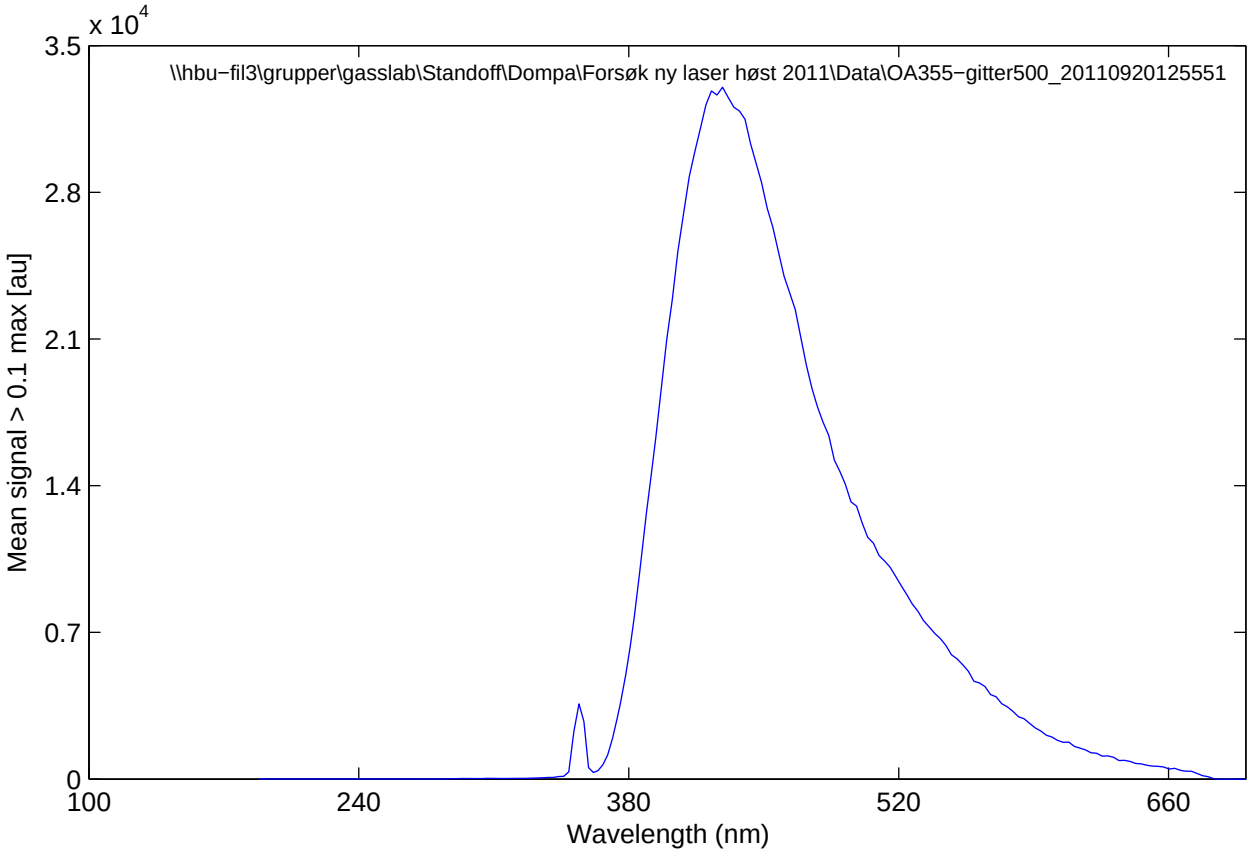
x 10^4
3.5
2.8
2.1
1.4
0.7
0
Mean signal > 0.1 max [au]
\\hbu−fil3\grupper\gasslab\Standoff\Dompa\Forsøk ny laser høst 2011\Data\OA355−gitter500_20110920125551
100
240
380
520
660
Wavelength (nm)

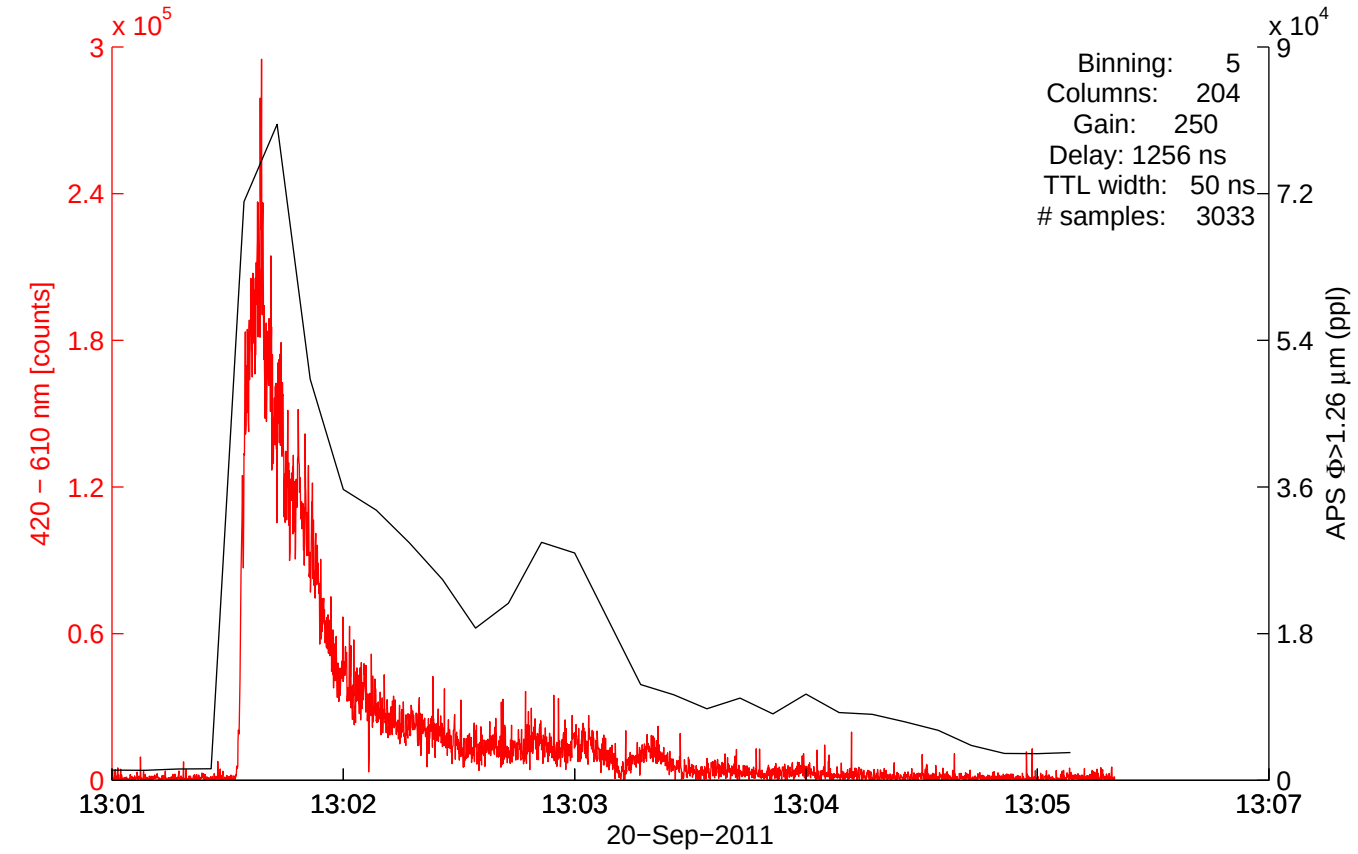
x 10^5
3
2.4
1.8
1.2
0.6
0
420 – 610 nm [counts]
x 10^4
9
7.2
5.4
3.6
1.8
0
APS Φ>1.26 µm (ppl)
Binning: 5
Columns: 204
Gain: 250
Delay: 1256 ns
TTL width: 50 ns
samples: 3033
13:01
13:02
13:03
13:04
13:05
13:07
20−Sep−2011

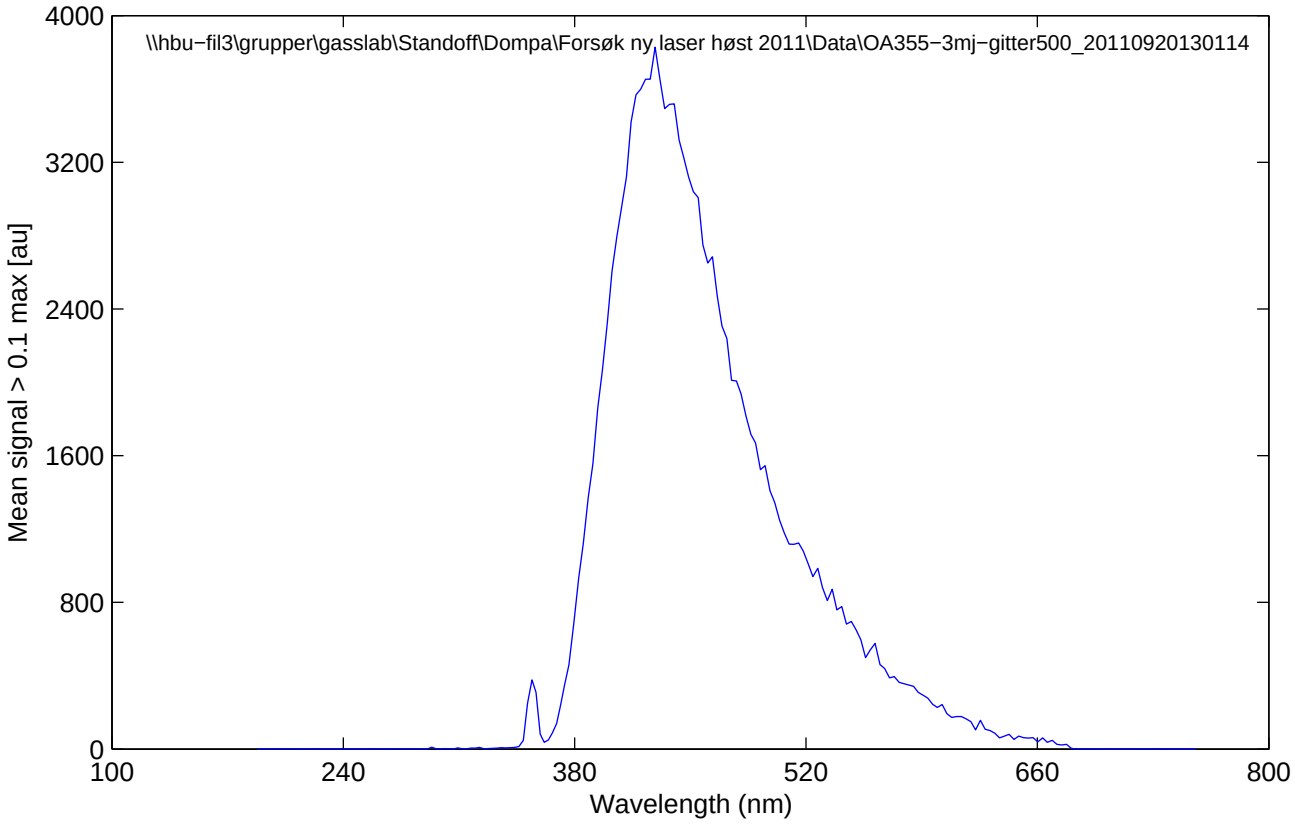
\\hbu−fil3\grupper\gasslab\Standoff\Dompa\Forsøk ny laser høst 2011\Data\OA355−3mj−gitter500_20110920130114
4000
3200
2400
1600
800
0
Mean signal > 0.1 max [au]
100
240
380
520
660
800
Wavelength (nm)

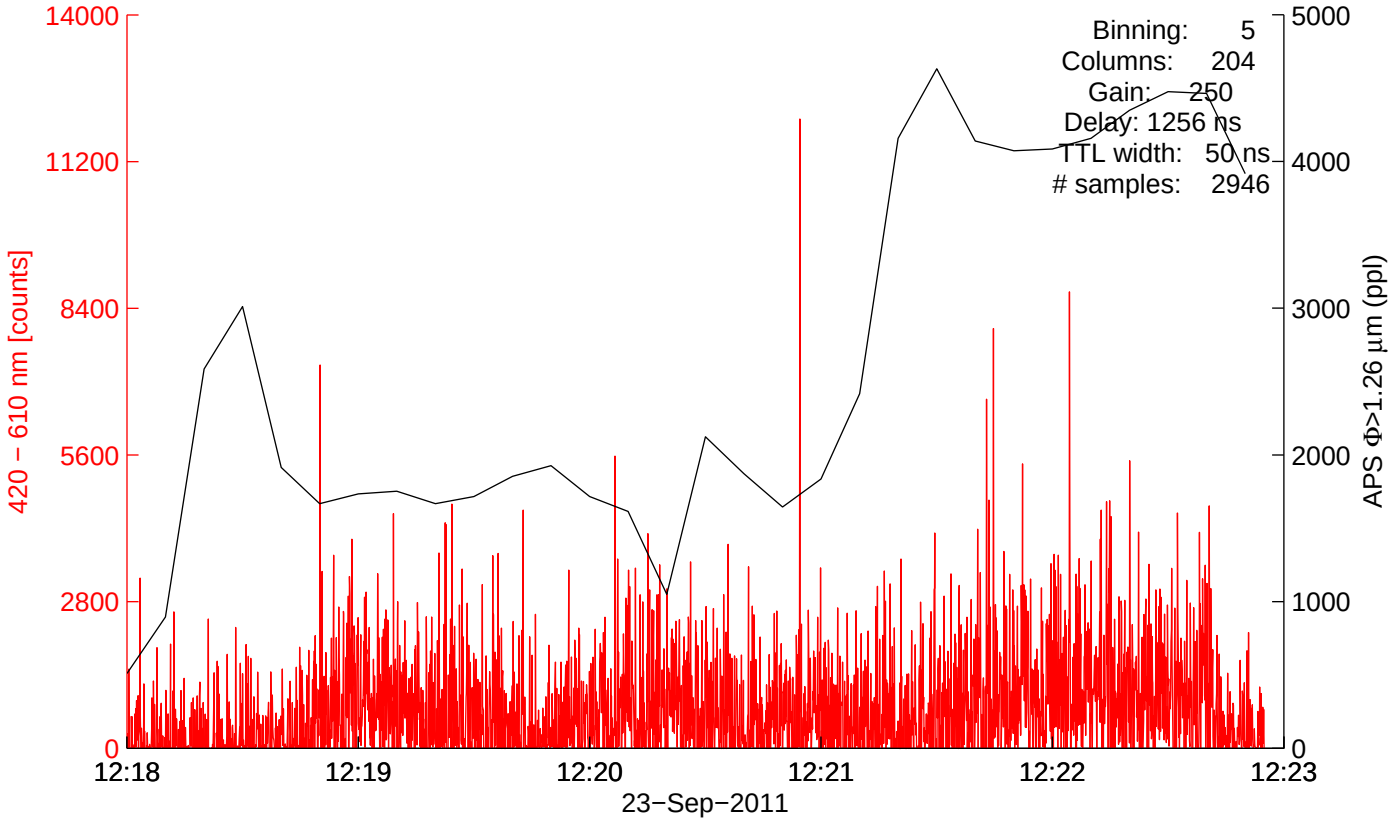
Binning: 5
Columns: 204
Gain: 250
Delay: 1256 ns
TTL width: 50 ns
samples: 2946
420 − 610 nm [counts]
APS Φ>1.26 µm (ppl)
14000
11200
8400
5600
2800
0
5000
4000
3000
2000
1000
0
12:18
12:19
12:20
12:21
12:22
12:23
23−Sep−2011

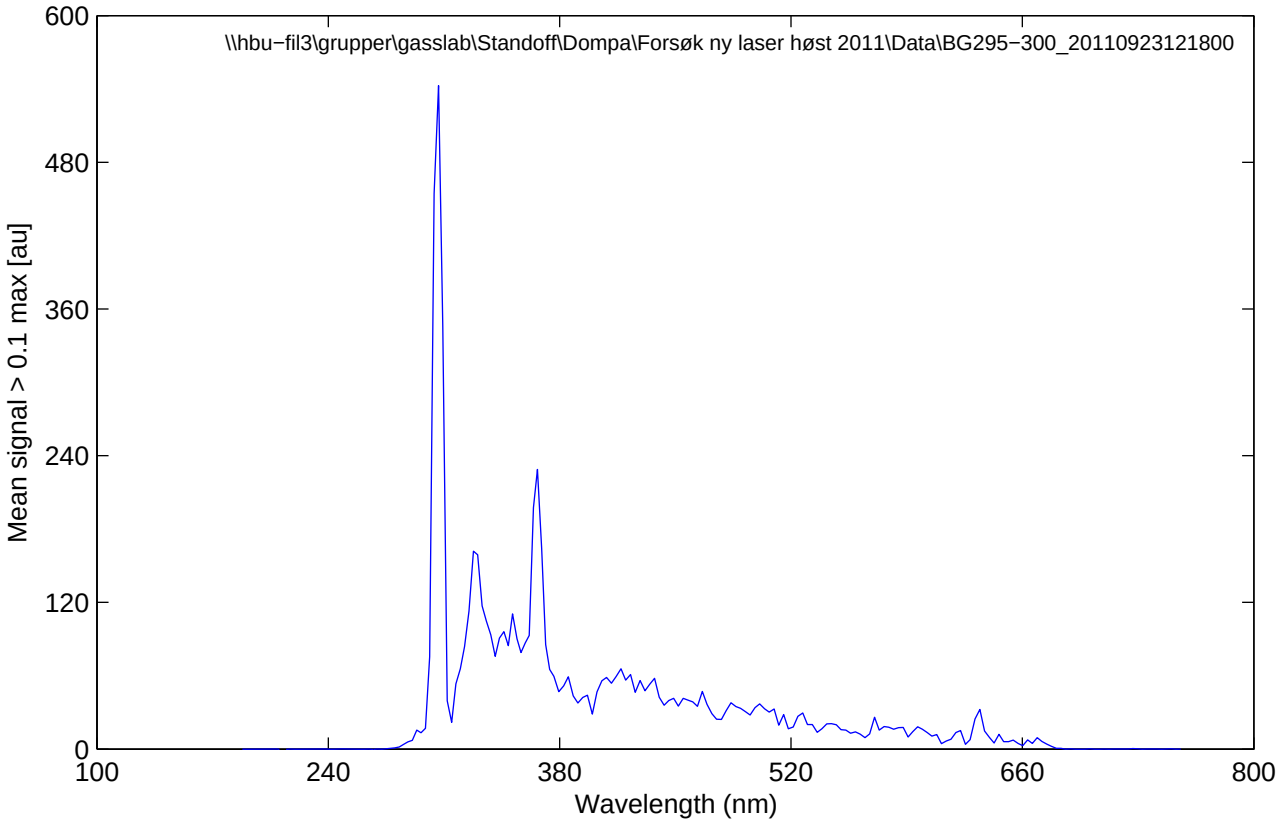
\\hbu−fil3\grupper\gasslab\Standoff\Dompa\Forsøk ny laser høst 2011\Data\BG295−300_20110923121800
Mean signal > 0.1 max [au]
600
480
360
240
120
0
100
240
380
520
660
800
Wavelength (nm)

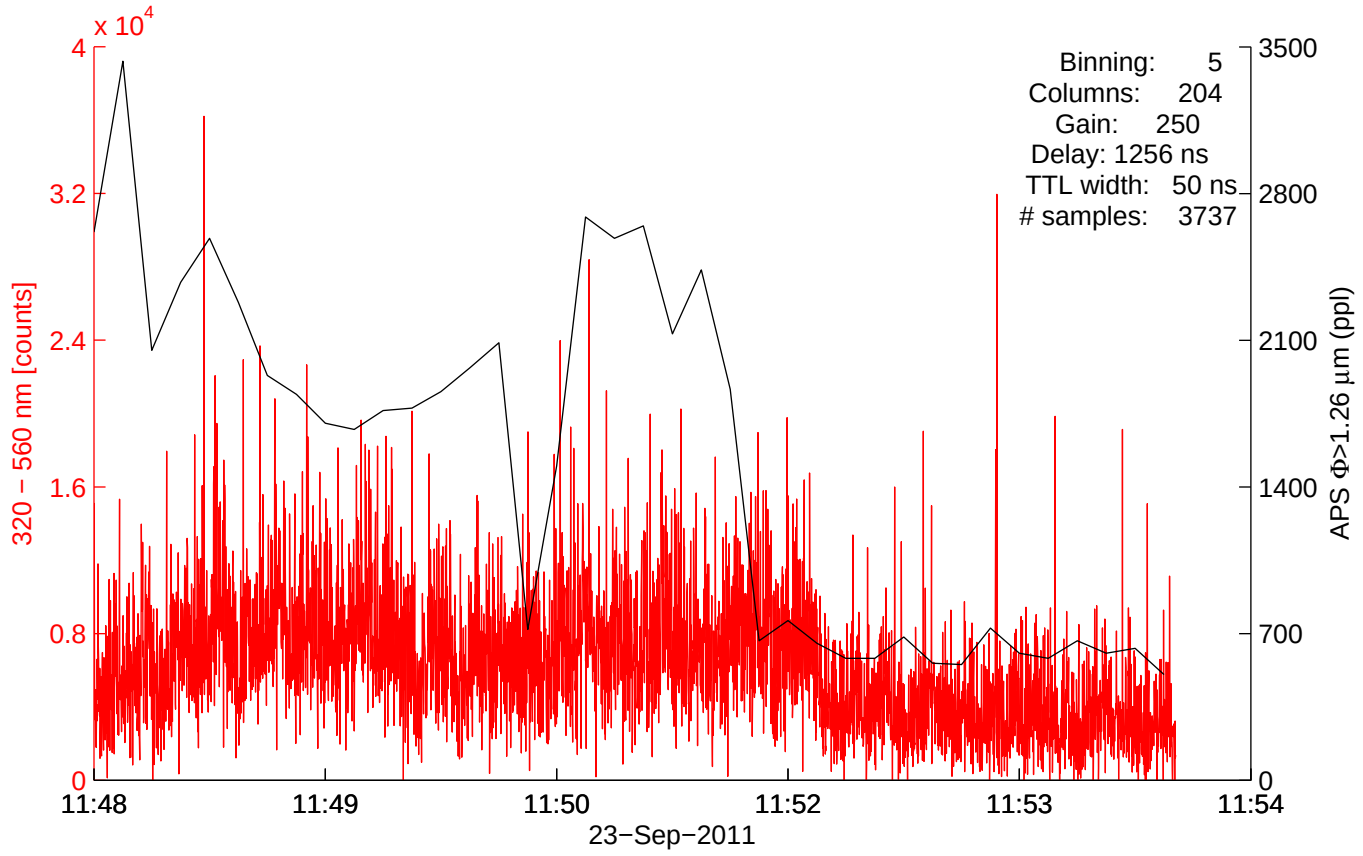
x 10^4
4
3.2
2.4
1.6
0.8
0
320 – 560 nm [counts]
3500
2800
2100
1400
700
0
APS Φ>1.26 µm (ppl)
Binning: 5
Columns: 204
Gain: 250
Delay: 1256 ns
TTL width: 50 ns
samples: 3737
11:48
11:49
11:50
11:52
11:53
11:54
23−Sep−2011

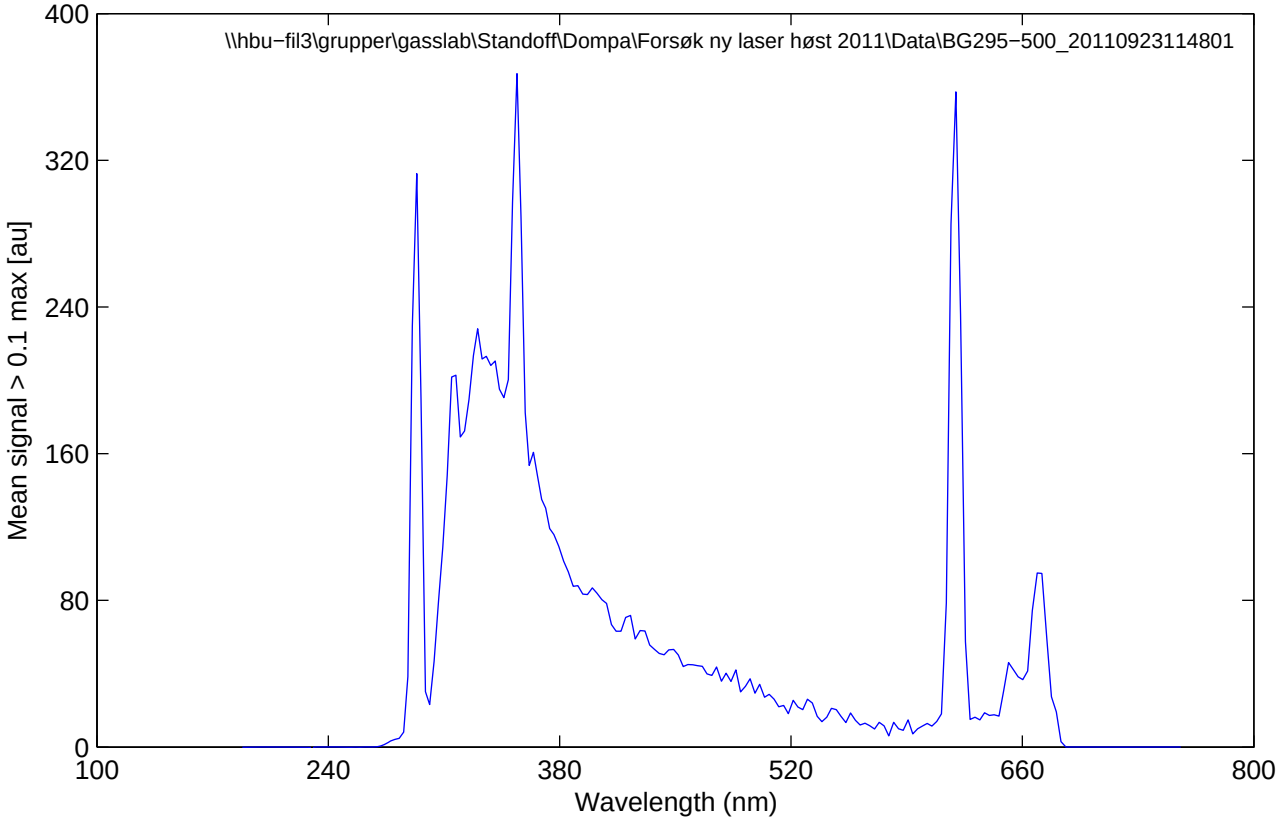
\\hbu−fil3\grupper\gasslab\Standoff\Dompa\Forsøk ny laser høst 2011\Data\BG295−500_20110923114801
400
320
240
160
80
0
Mean signal > 0.1 max [au]
100
240
380
520
660
800
Wavelength (nm)

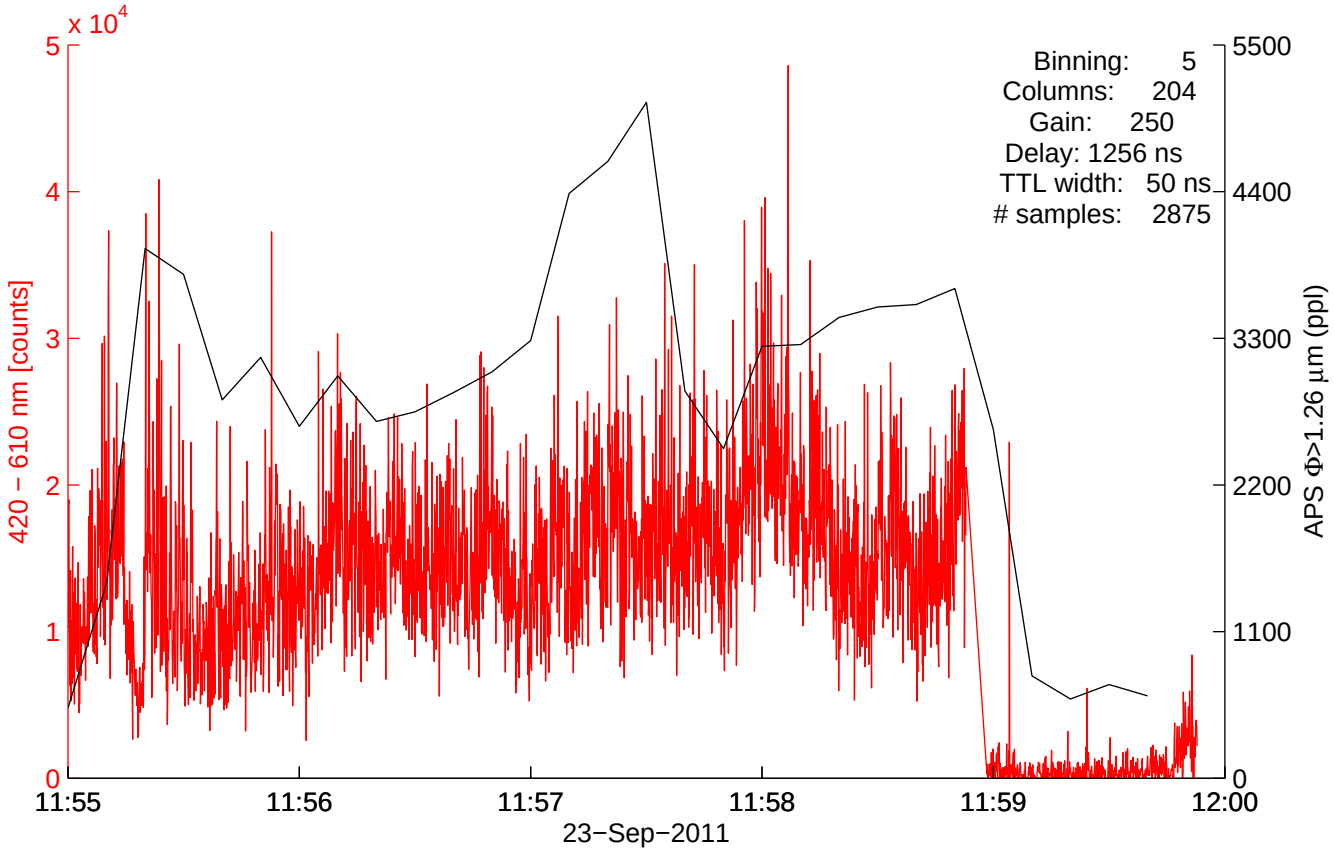
x 10^4
Binning: 5
Columns: 204
Gain: 250
Delay: 1256 ns
TTL width: 50 ns
samples: 2875
420 – 610 nm [counts]
APS Φ>1.26 µm (ppl)
11:55
11:56
11:57
11:58
11:59
12:00
23−Sep−2011

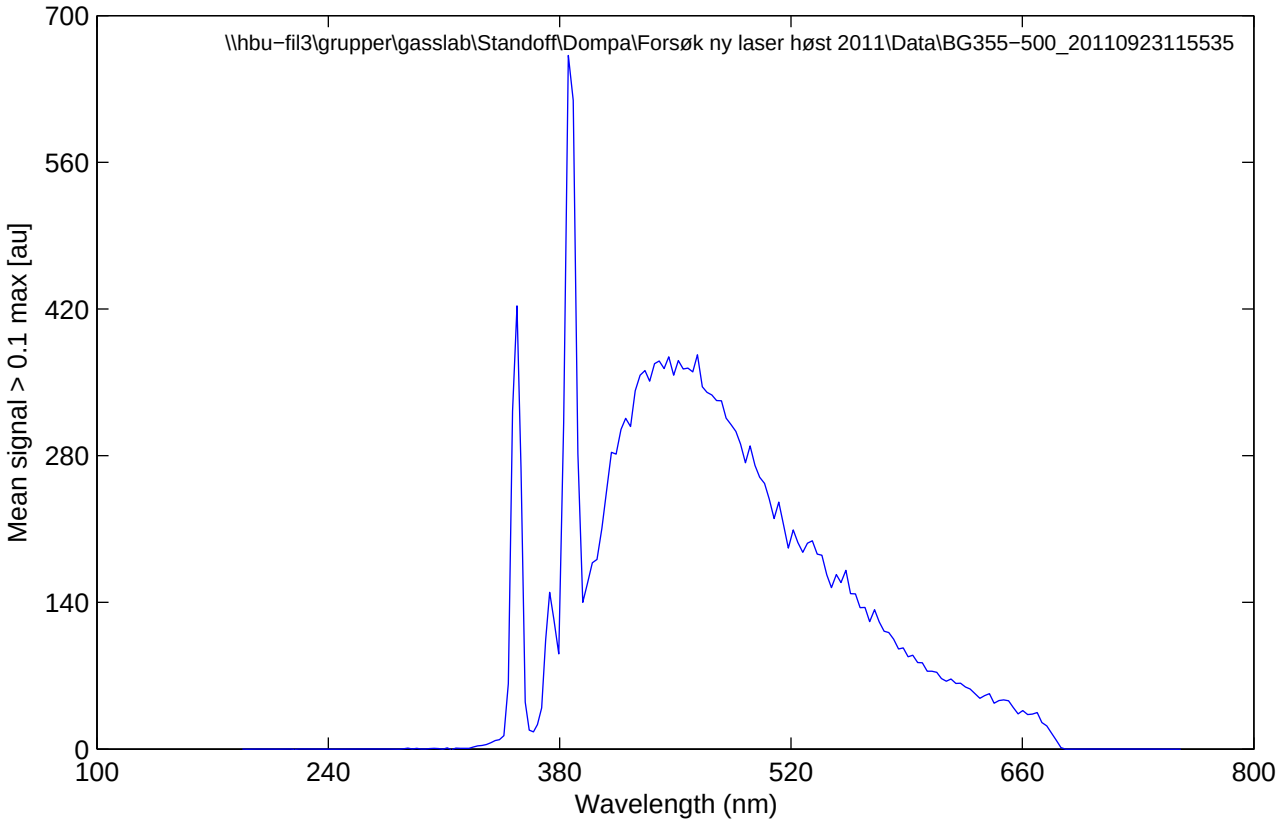
\\hbu−fil3\grupper\gasslab\Standoff\Dompa\Forsøk ny laser høst 2011\Data\BG355−500_20110923115535
Mean signal > 0.1 max [au]
Wavelength (nm)

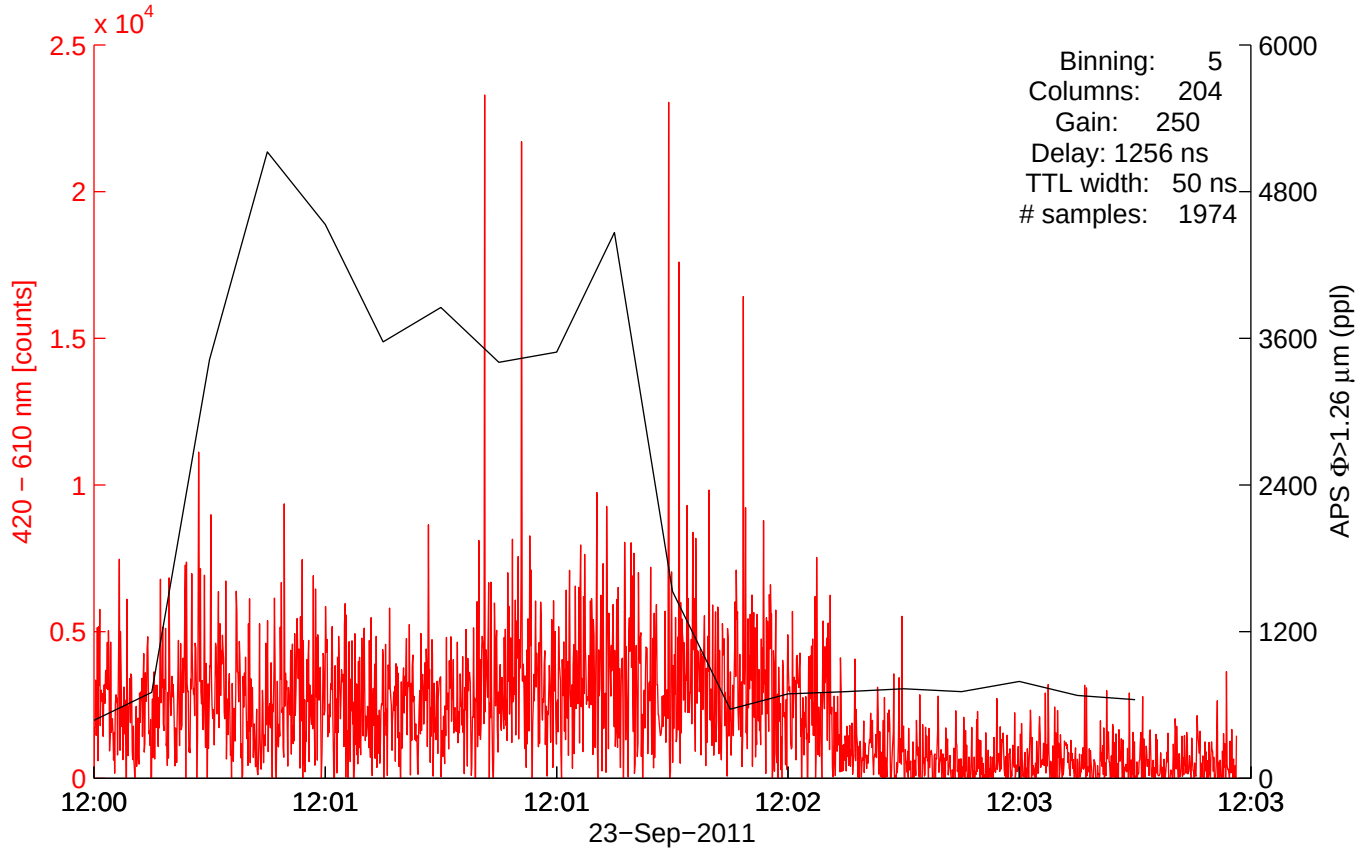
x 10^4
2.5
2
1.5
1
0.5
0
420 – 610 nm [counts]
6000
4800
3600
2400
1200
0
APS Φ>1.26 µm (ppl)
Binning: 5
Columns: 204
Gain: 250
Delay: 1256 ns
TTL width: 50 ns
samples: 1974
12:00
12:01
12:01
12:02
12:03
12:03
23−Sep−2011

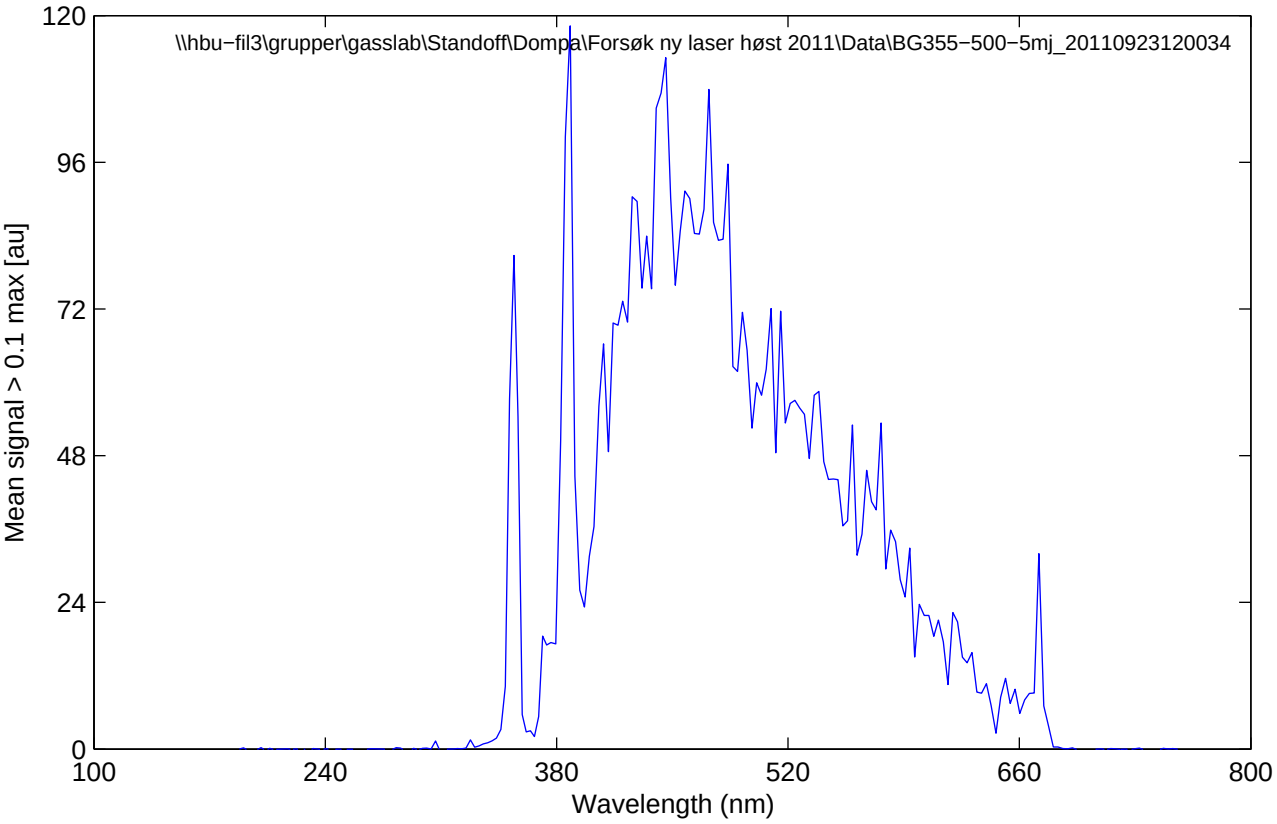
\\hbu−fil3\grupper\gasslab\Standoff\Dompa\Forsøk ny laser høst 2011\Data\BG355−500−5mj_20110923120034
120
96
72
48
24
0
Mean signal > 0.1 max [au]
100
240
380
520
660
800
Wavelength (nm)

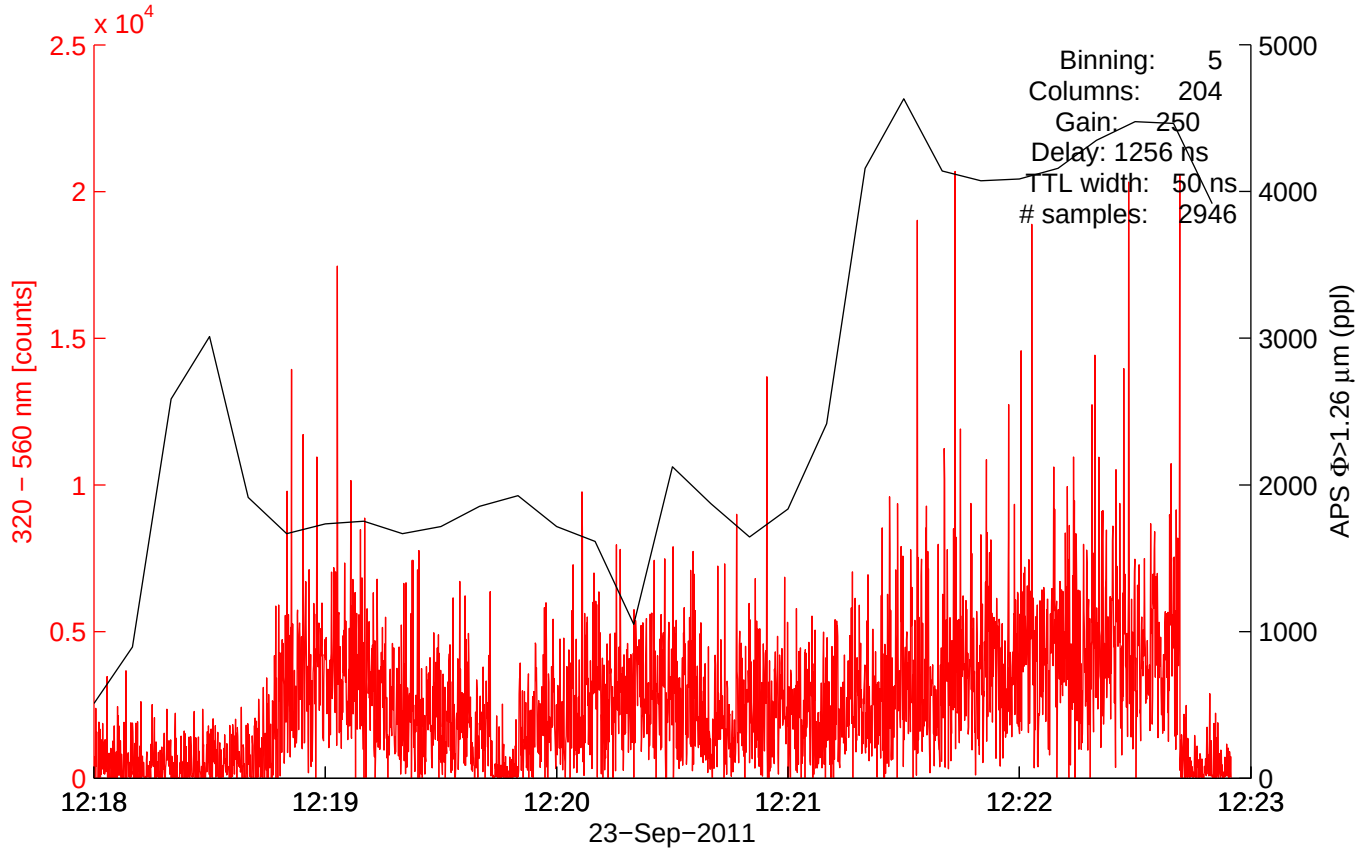
x 10^4
2.5
2
1.5
1
0.5
0
320 – 560 nm [counts]
5000
4000
3000
2000
1000
0
APS Φ>1.26 µm (ppl)
Binning: 5
Columns: 204
Gain: 250
Delay: 1256 ns
TTL width: 50 ns
samples: 2946
12:18
12:19
12:20
12:21
12:22
12:23
23−Sep−2011

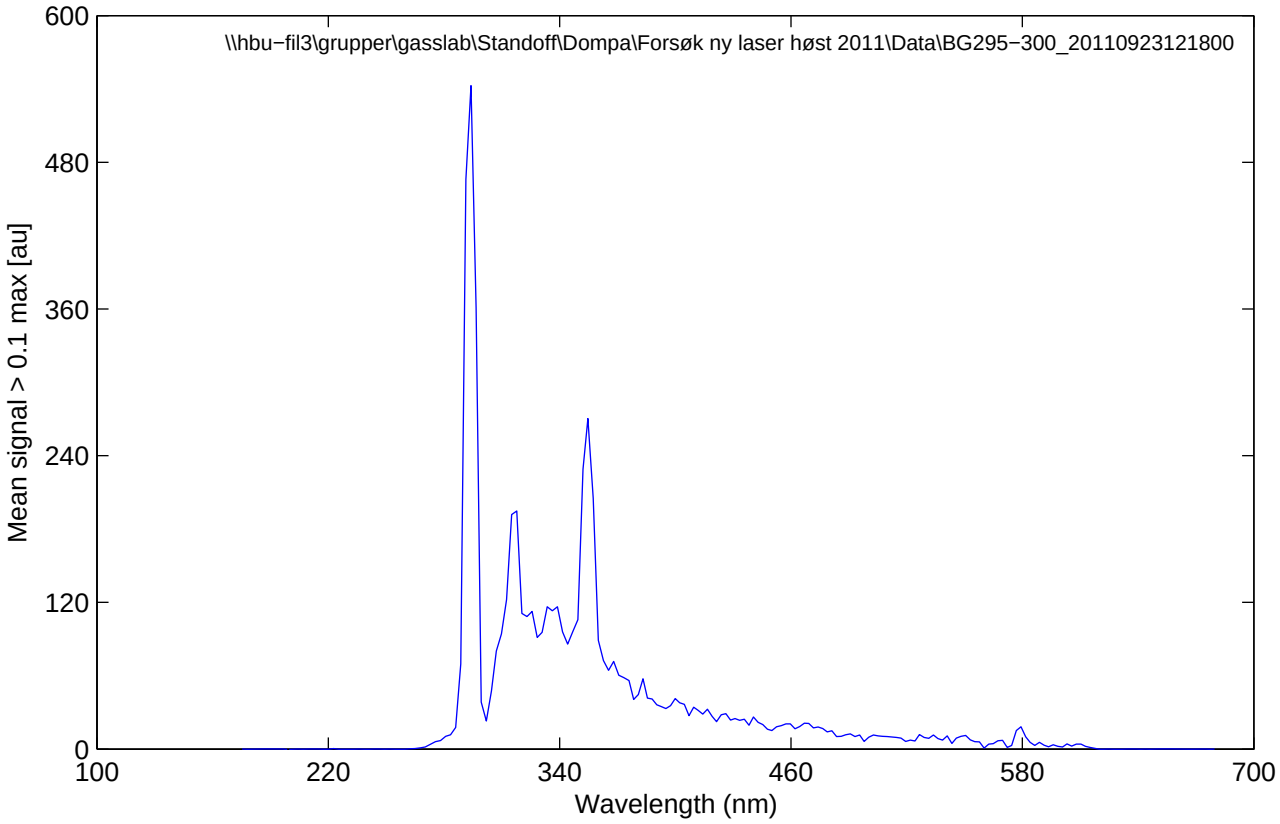
\\hbu−fil3\grupper\gasslab\Standoff\Dompa\Forsøk ny laser høst 2011\Data\BG295−300_20110923121800
600
480
360
240
120
0
Mean signal > 0.1 max [au]
100
220
340
460
580
700
Wavelength (nm)

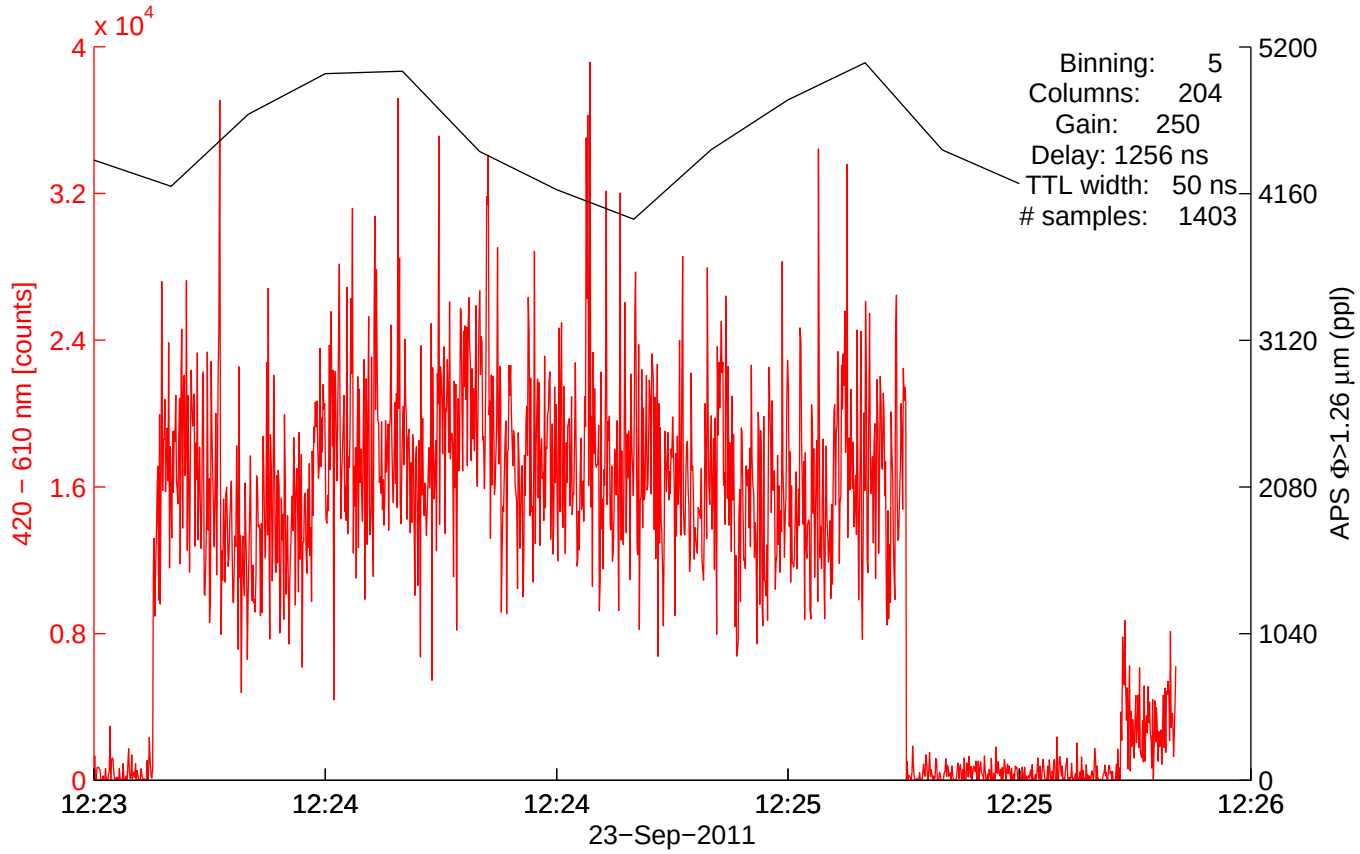
x 10^4
4
3.2
2.4
1.6
0.8
0
420 – 610 nm [counts]
5200
4160
3120
2080
1040
0
APS Φ>1.26 µm (ppl)
Binning: 5
Columns: 204
Gain: 250
Delay: 1256 ns
TTL width: 50 ns
samples: 1403
12:23
12:24
12:24
12:25
12:25
12:26
23−Sep−2011

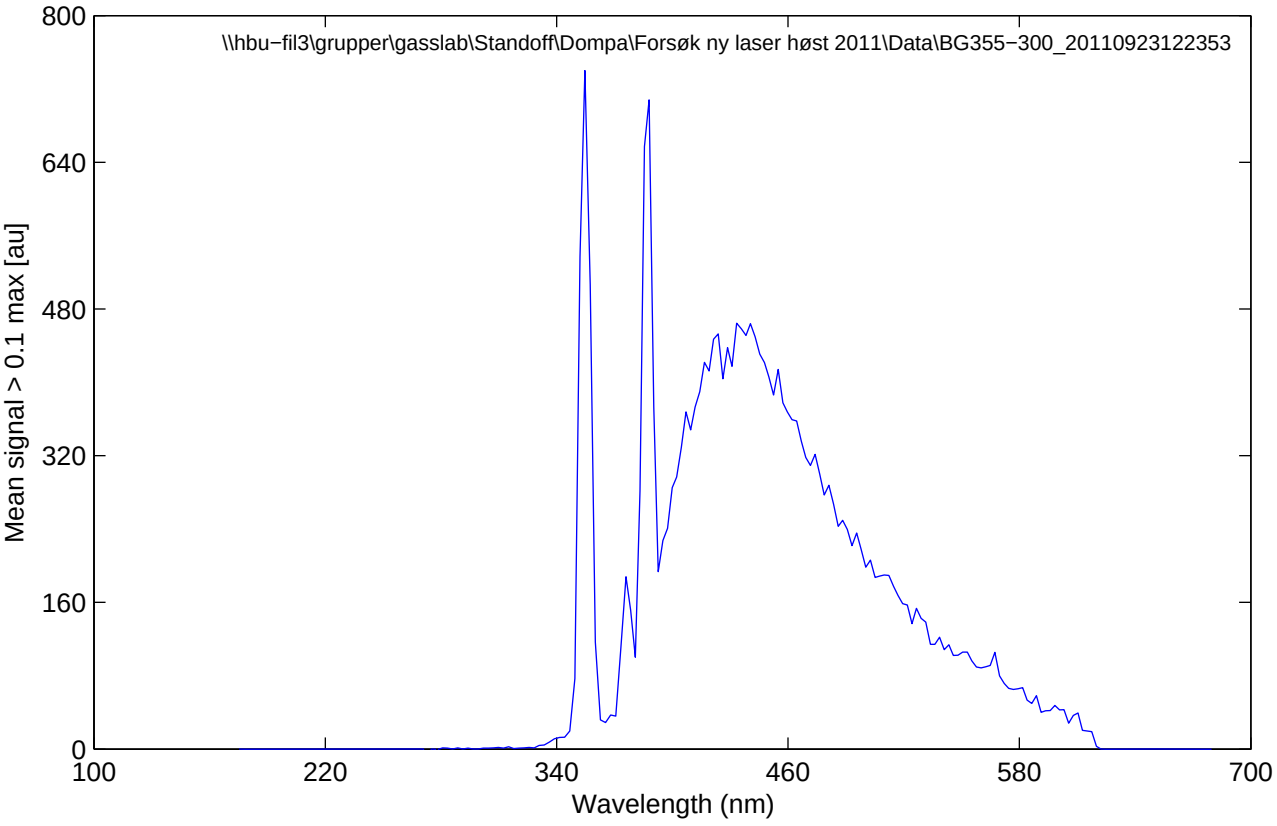
\\hbu−fil3\grupper\gasslab\Standoff\Dompa\Forsøk ny laser høst 2011\Data\BG355−300_20110923122353
800
640
480
320
160
0
Mean signal > 0.1 max [au]
100
220
340
460
580
700
Wavelength (nm)

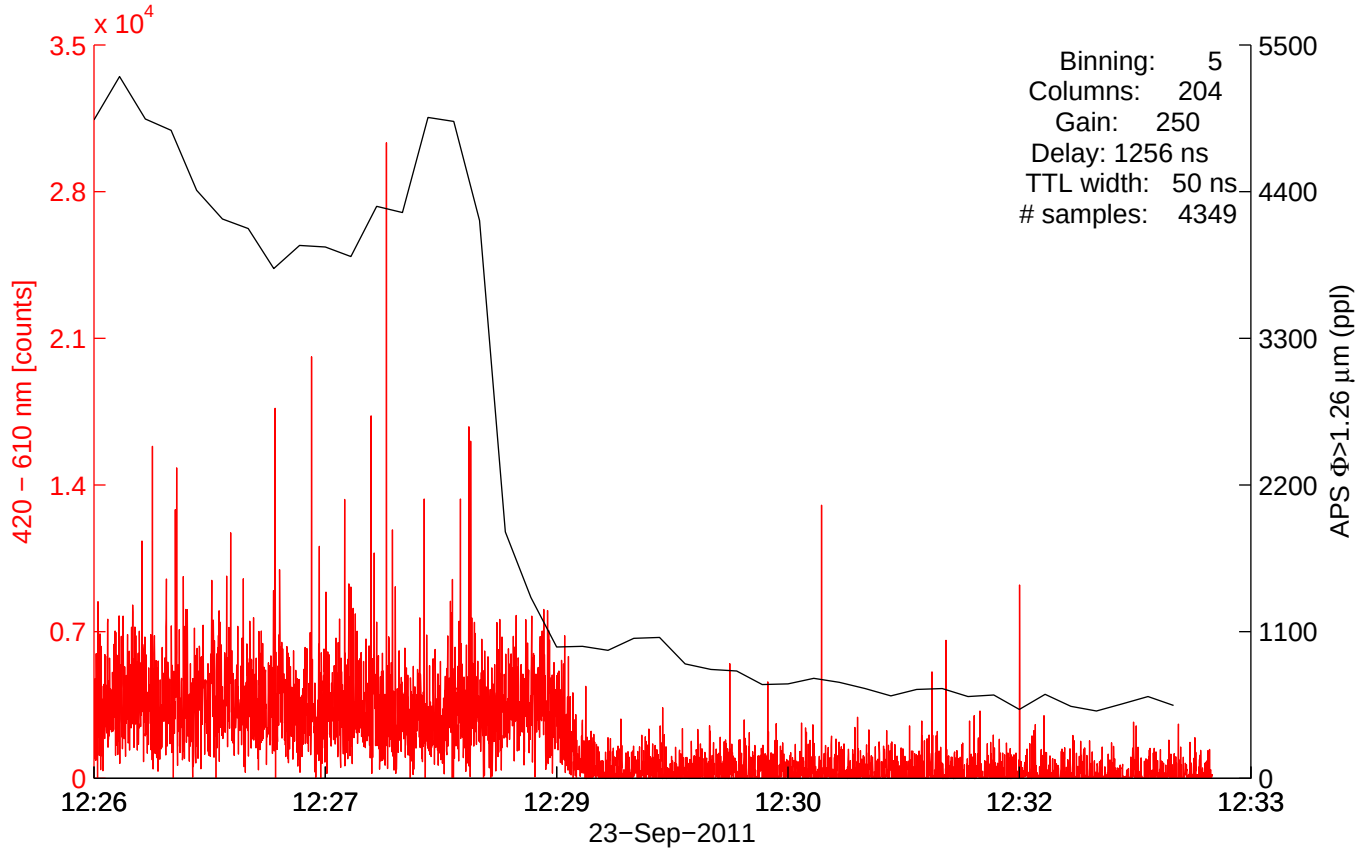
x 10^4
3.5
2.8
2.1
1.4
0.7
0
420 – 610 nm [counts]
5500
4400
3300
2200
1100
0
APS Φ>1.26 µm (ppl)
Binning: 5
Columns: 204
Gain: 250
Delay: 1256 ns
TTL width: 50 ns
samples: 4349
12:26
12:27
12:29
12:30
12:32
12:33
23−Sep−2011

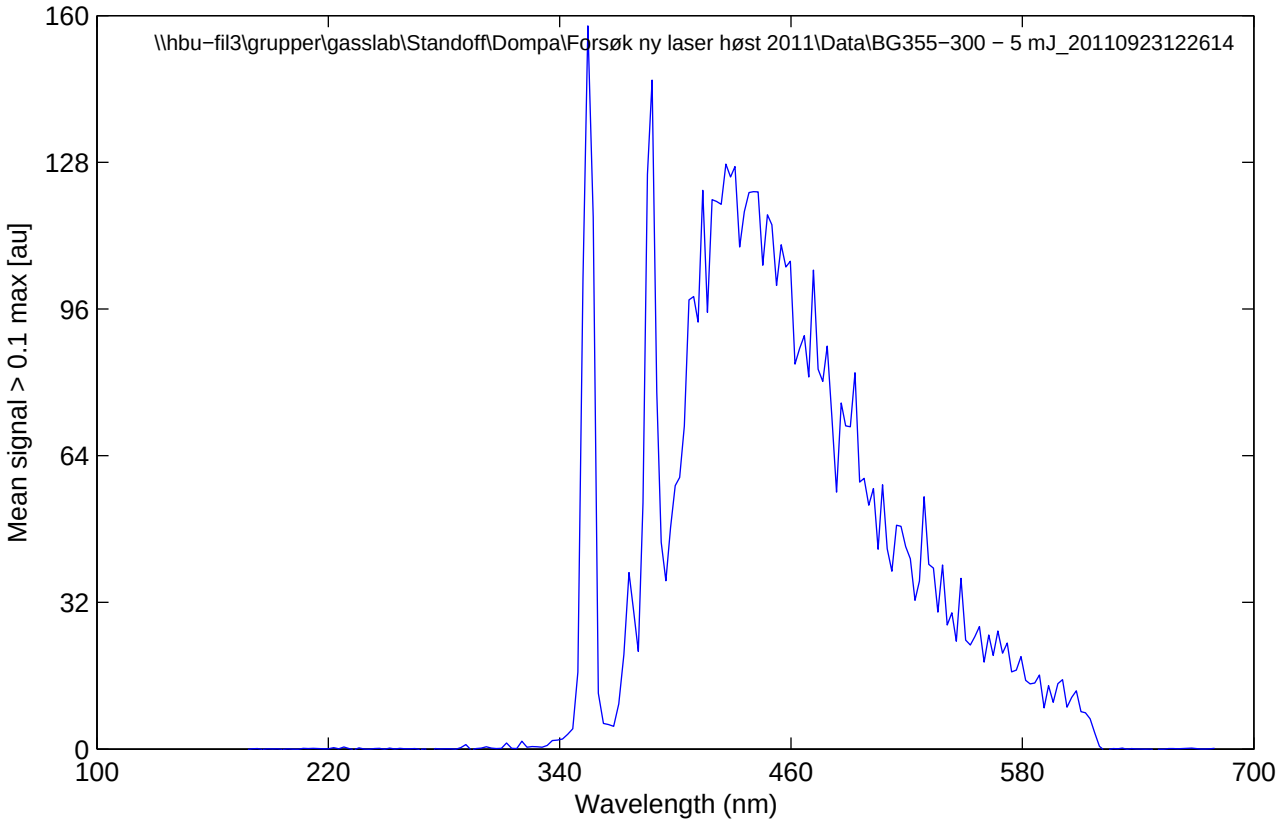
\\hbu−fil3\grupper\gasslab\Standoff\Dompa\Forsøk ny laser høst 2011\Data\BG355−300 − 5 mJ_20110923122614
160
128
96
64
32
0
Mean signal > 0.1 max [au]
100
220
340
460
580
700
Wavelength (nm)

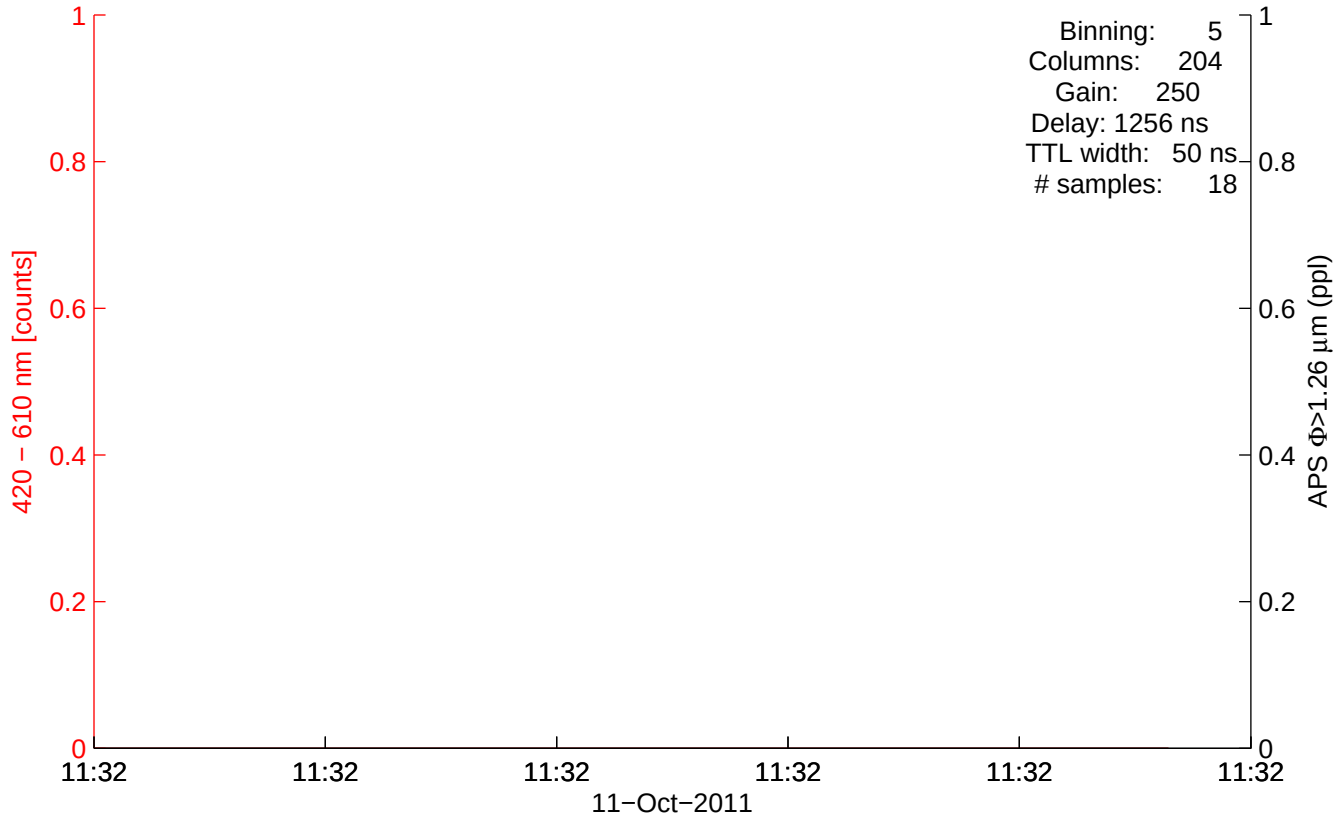
Binning: 5
Columns: 204
Gain: 250
Delay: 1256 ns
TTL width: 50 ns
samples: 18
420 – 610 nm [counts]
APS Φ>1.26 µm (ppl)
0
0.2
0.4
0.6
0.8
1
11:32
11:32
11:32
11:32
11:32
11:32
11−Oct−2011

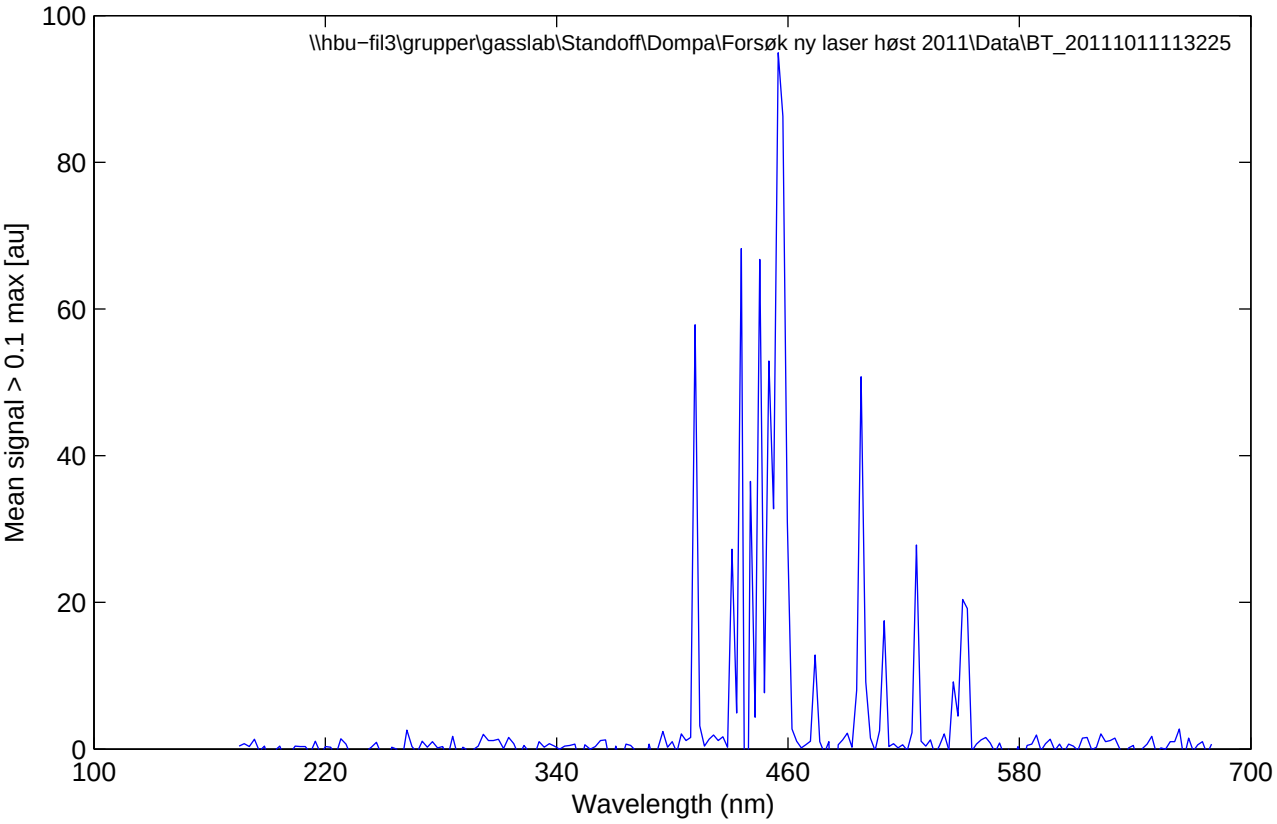
\\hbu−fil3\grupper\gasslab\Standoff\Dompa\Forsøk ny laser høst 2011\Data\BT_20111011113225
Mean signal > 0.1 max [au]
0
20
40
60
80
100
100
220
340
460
580
700
Wavelength (nm)

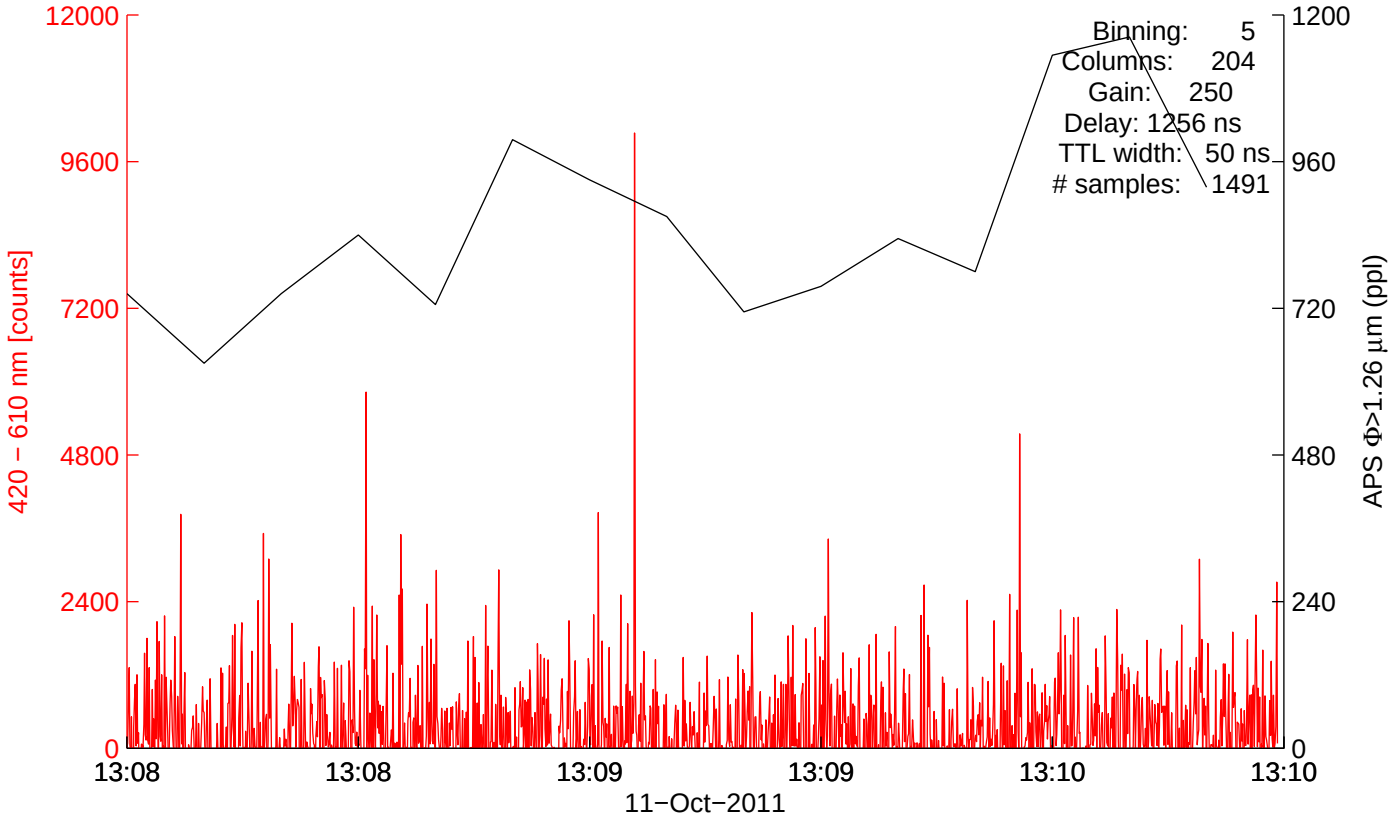
Binning: 5
Columns: 204
Gain: 250
Delay: 1256 ns
TTL width: 50 ns
samples: 1491
420 − 610 nm [counts]
APS Φ>1.26 µm (ppl)
12000
9600
7200
4800
2400
0
1200
960
720
480
240
0
13:08
13:08
13:09
13:09
13:10
13:10
11−Oct−2011

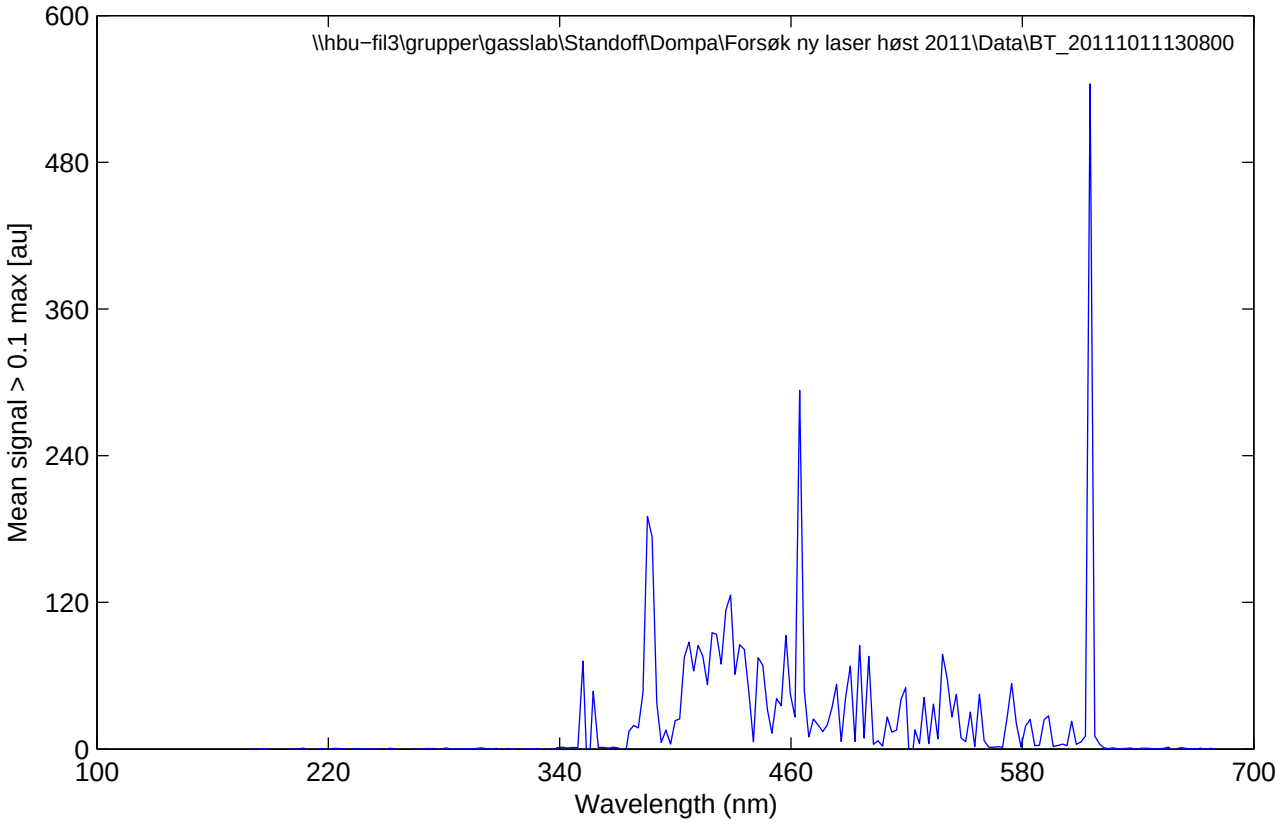
\\hbu−fil3\grupper\gasslab\Standoff\Dompa\Forsøk ny laser høst 2011\Data\BT_20111011130800
Mean signal > 0.1 max [au]
600
480
360
240
120
0
100
220
340
460
580
700
Wavelength (nm)

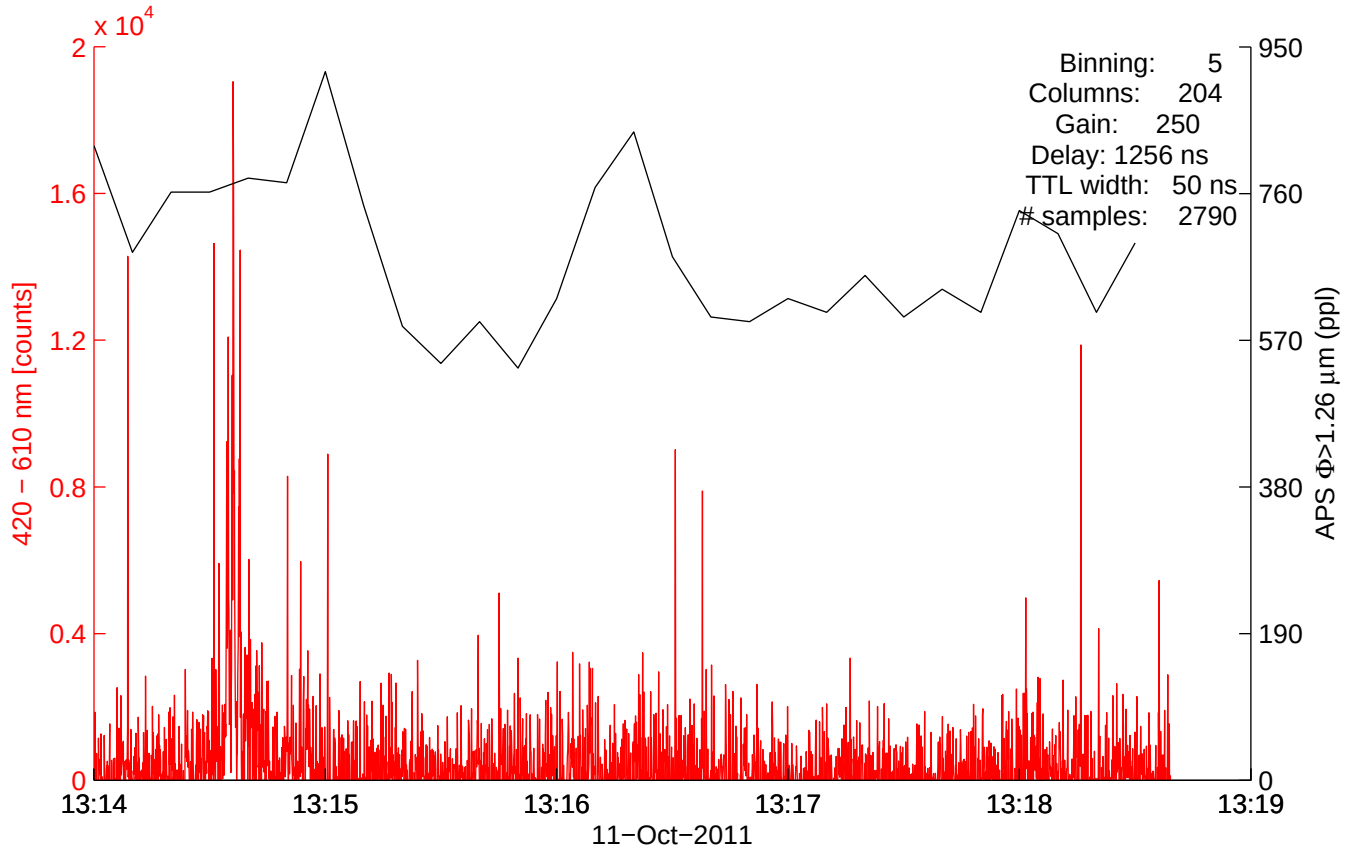
x 10^4
2
1.6
1.2
0.8
0.4
0
420 – 610 nm [counts]
950
760
570
380
190
0
APS Φ>1.26 µm (ppl)
Binning: 5
Columns: 204
Gain: 250
Delay: 1256 ns
TTL width: 50 ns
samples: 2790
13:14
13:15
13:16
13:17
13:18
13:19
11−Oct−2011

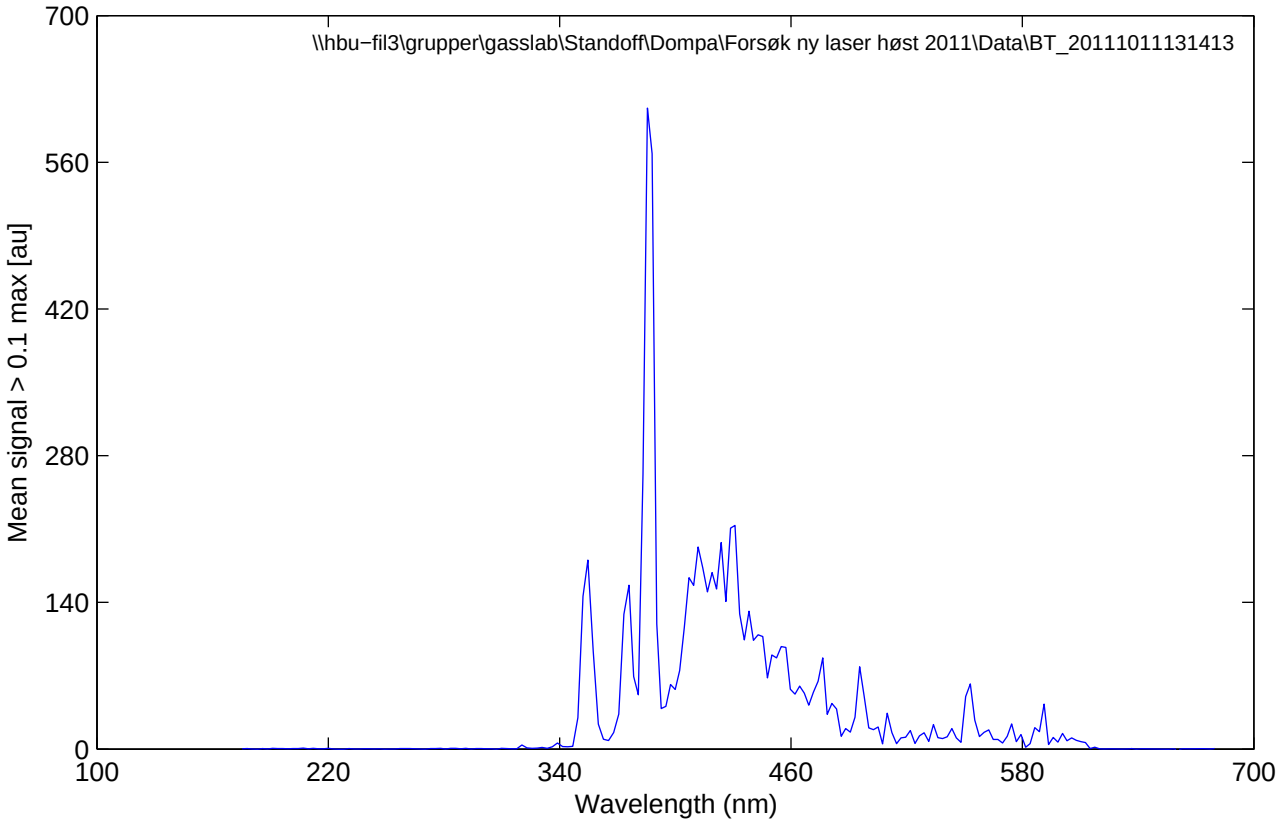
\\hbu−fil3\grupper\gasslab\Standoff\Dompa\Forsøk ny laser høst 2011\Data\BT_20111011131413
700
560
420
280
140
0
Mean signal > 0.1 max [au]
100
220
340
460
580
700
Wavelength (nm)

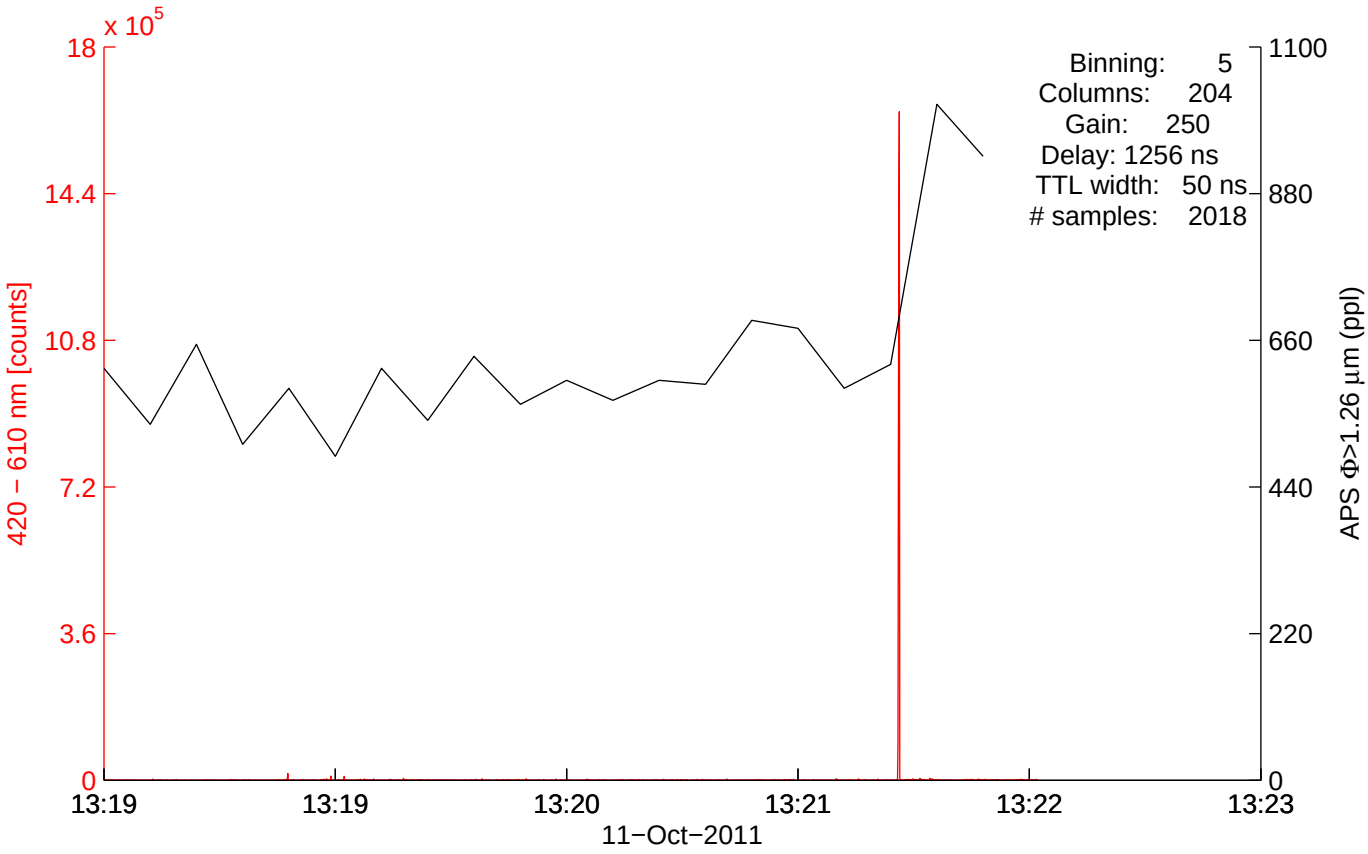
x 10^5
18
14.4
10.8
7.2
3.6
0
420 – 610 nm [counts]
1100
880
660
440
220
0
APS Φ>1.26 µm (ppl)
Binning: 5
Columns: 204
Gain: 250
Delay: 1256 ns
TTL width: 50 ns
samples: 2018
13:19
13:19
13:20
13:21
13:22
13:23
11−Oct−2011

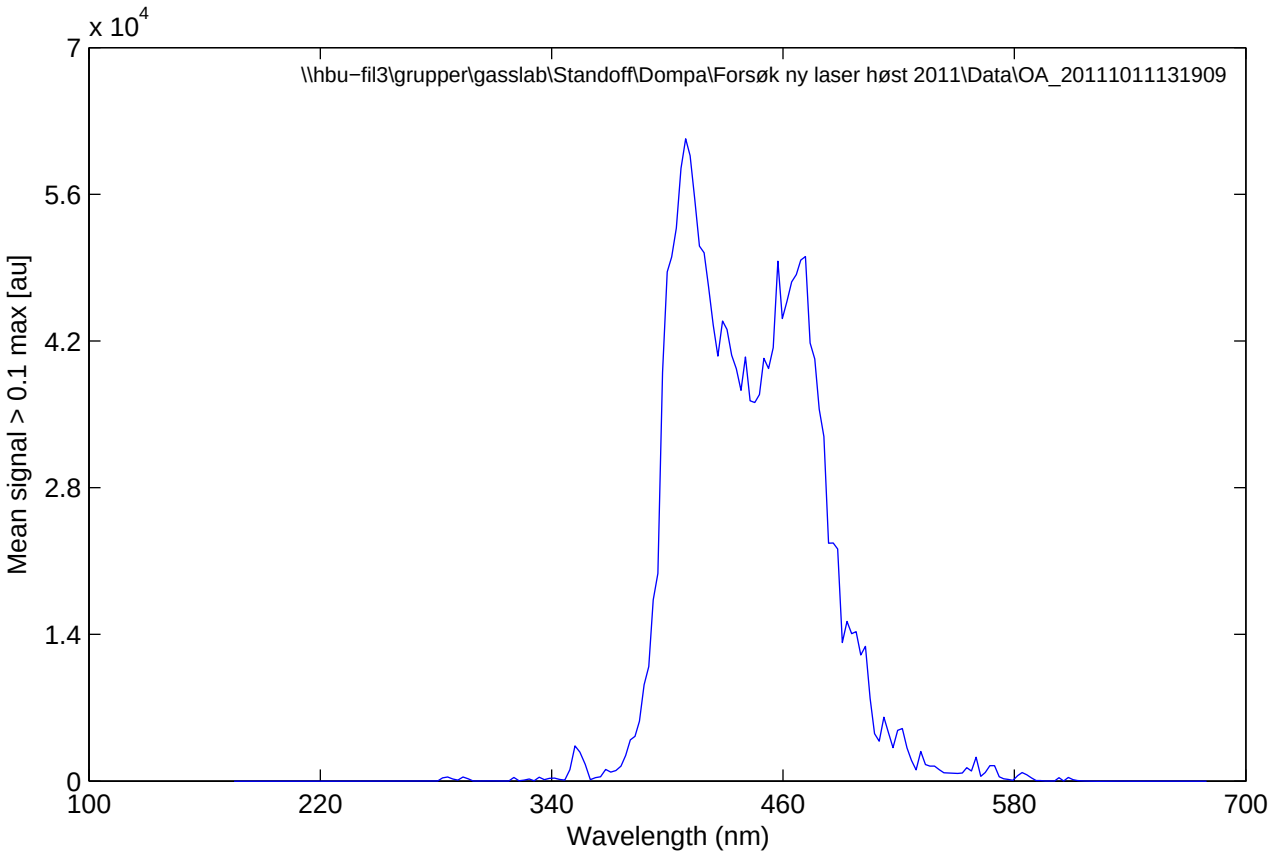
x 10^4
7
5.6
4.2
2.8
1.4
0
Mean signal > 0.1 max [au]
\\hbu−fil3\grupper\gasslab\Standoff\Dompa\Forsøk ny laser høst 2011\Data\OA_20111011131909
100
220
340
460
580
700
Wavelength (nm)

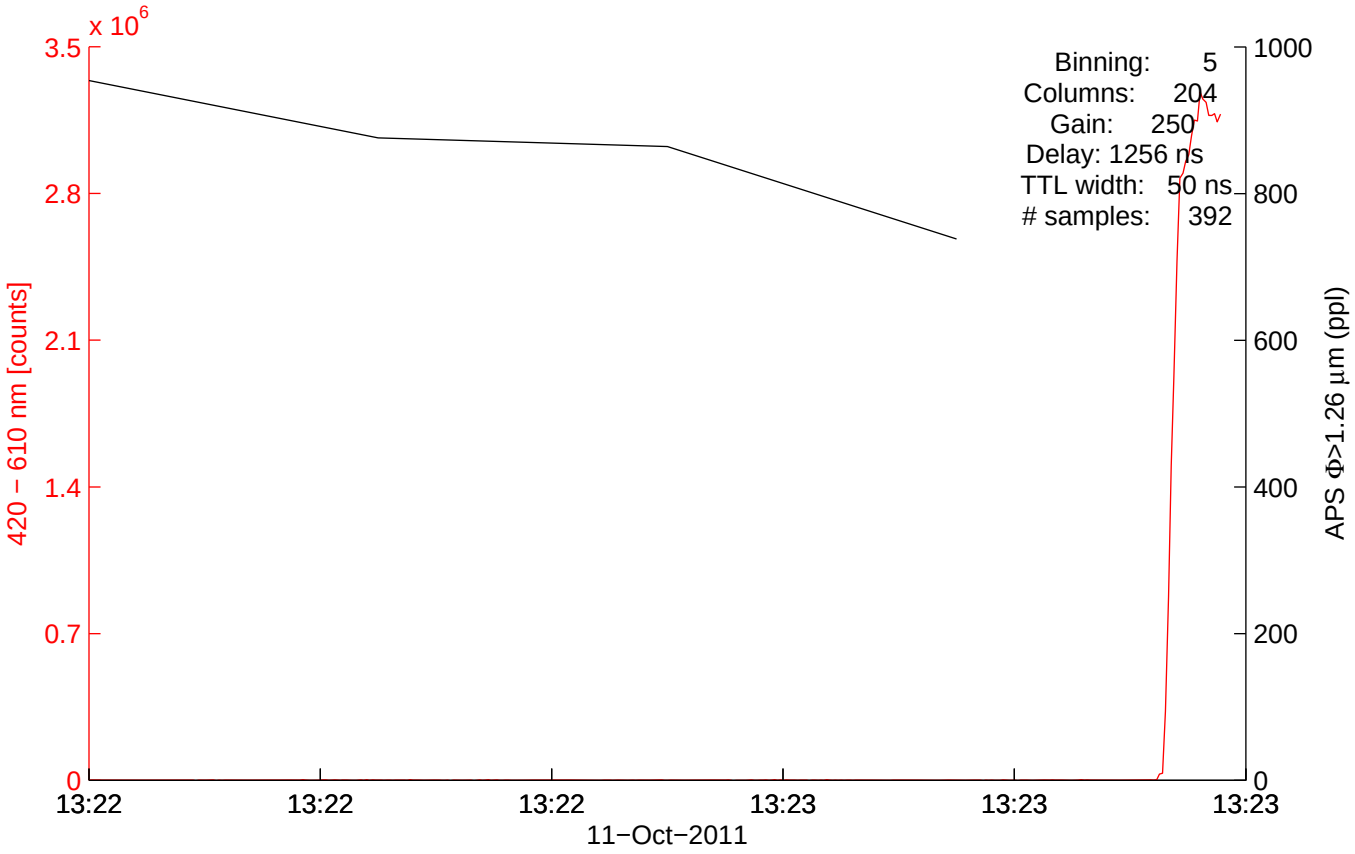
x 10^6
3.5
2.8
2.1
1.4
0.7
0
420 – 610 nm [counts]
1000
800
600
400
200
0
APS Φ>1.26 µm (ppl)
Binning: 5
Columns: 204
Gain: 250
Delay: 1256 ns
TTL width: 50 ns
samples: 392
13:22
13:22
13:22
13:23
13:23
13:23
11−Oct−2011

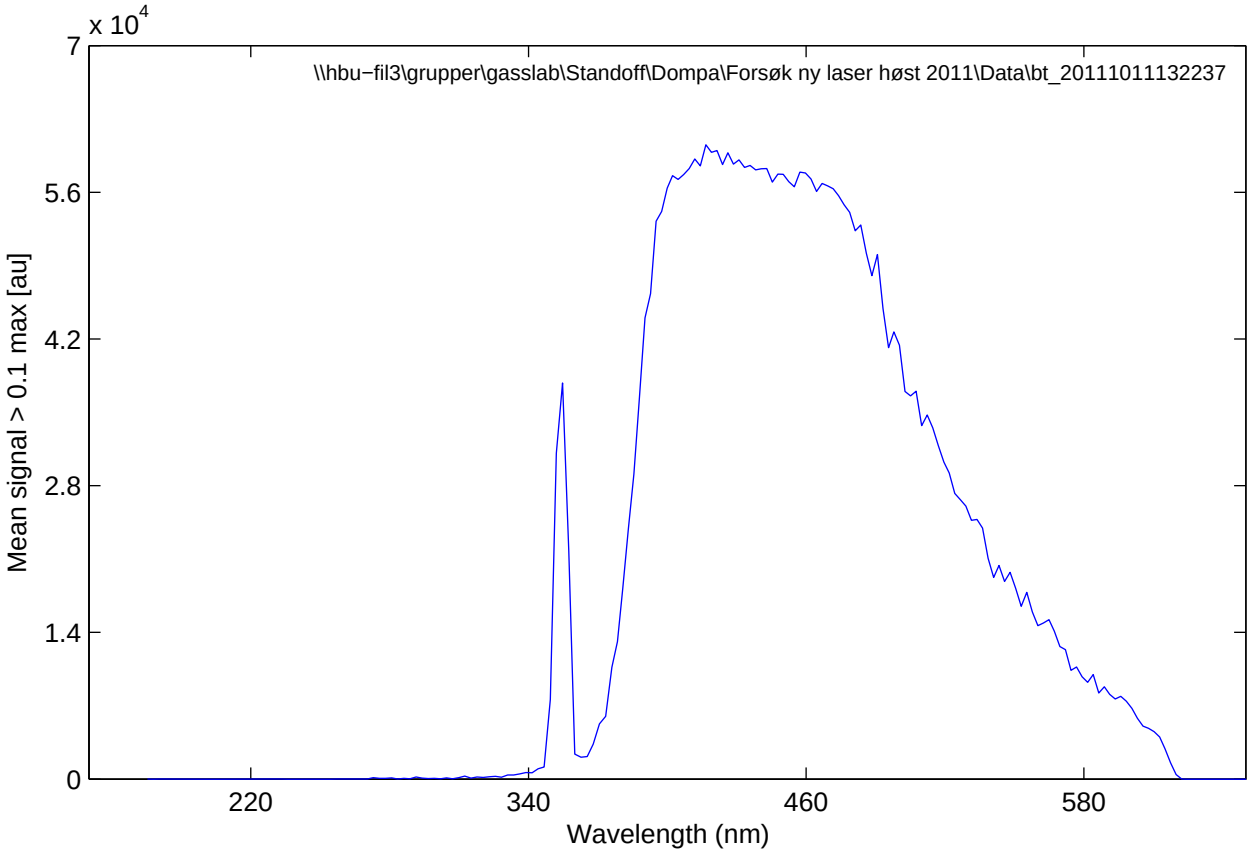
x 10^4
7
5.6
4.2
2.8
1.4
0
Mean signal > 0.1 max [au]
\\hbu−fil3\grupper\gasslab\Standoff\Dompa\Forsøk ny laser høst 2011\Data\bt_20111011132237
220
340
460
580
Wavelength (nm)

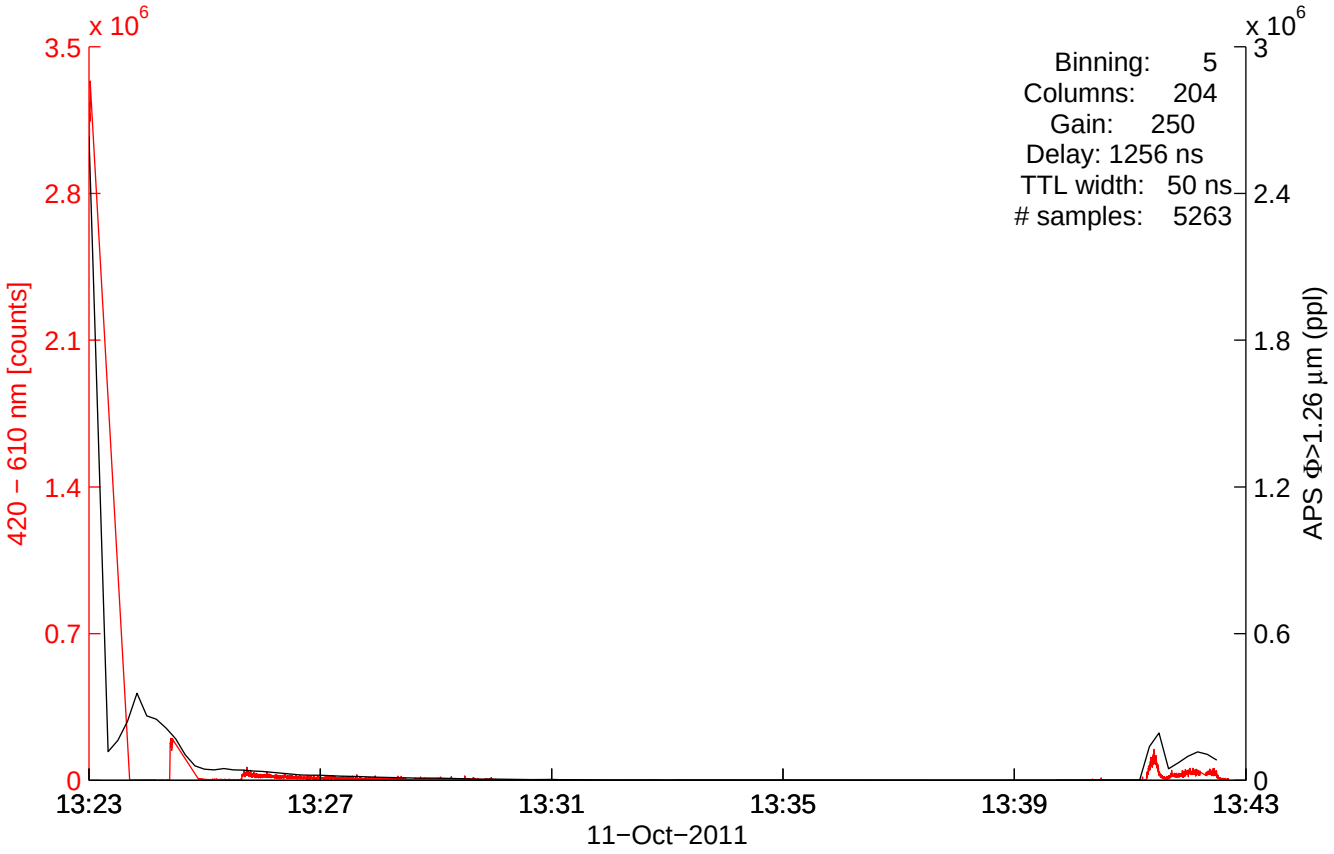
x 10^6
3.5
2.8
2.1
1.4
0.7
0
420 – 610 nm [counts]
x 10^6
3
2.4
1.8
1.2
0.6
0
APS Φ>1.26 µm (ppl)
Binning: 5
Columns: 204
Gain: 250
Delay: 1256 ns
TTL width: 50 ns
samples: 5263
13:23
13:27
13:31
13:35
13:39
13:43
11−Oct−2011

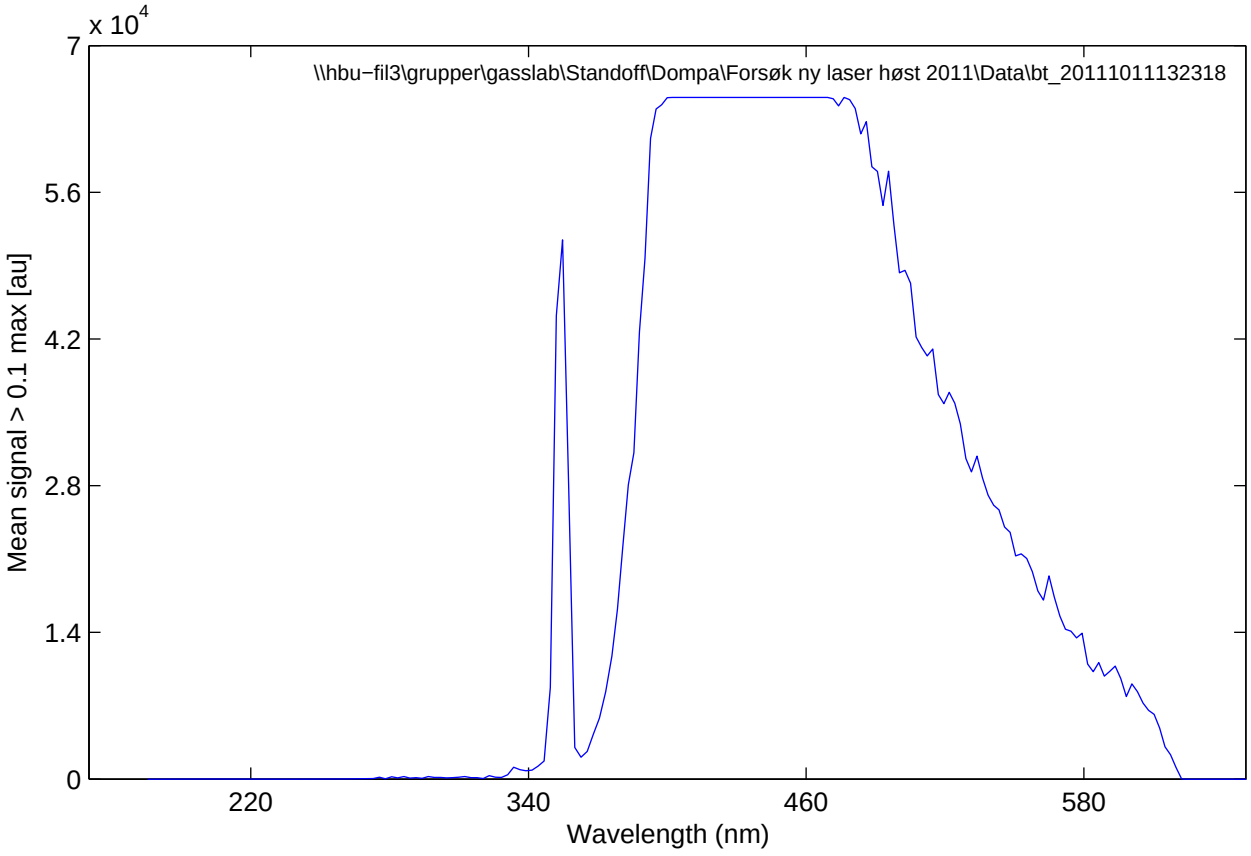
x 10^4
7
5.6
4.2
2.8
1.4
0
Mean signal > 0.1 max [au]
\\hbu−fil3\grupper\gasslab\Standoff\Dompa\Forsøk ny laser høst 2011\Data\bt_20111011132318
220
340
460
580
Wavelength (nm)

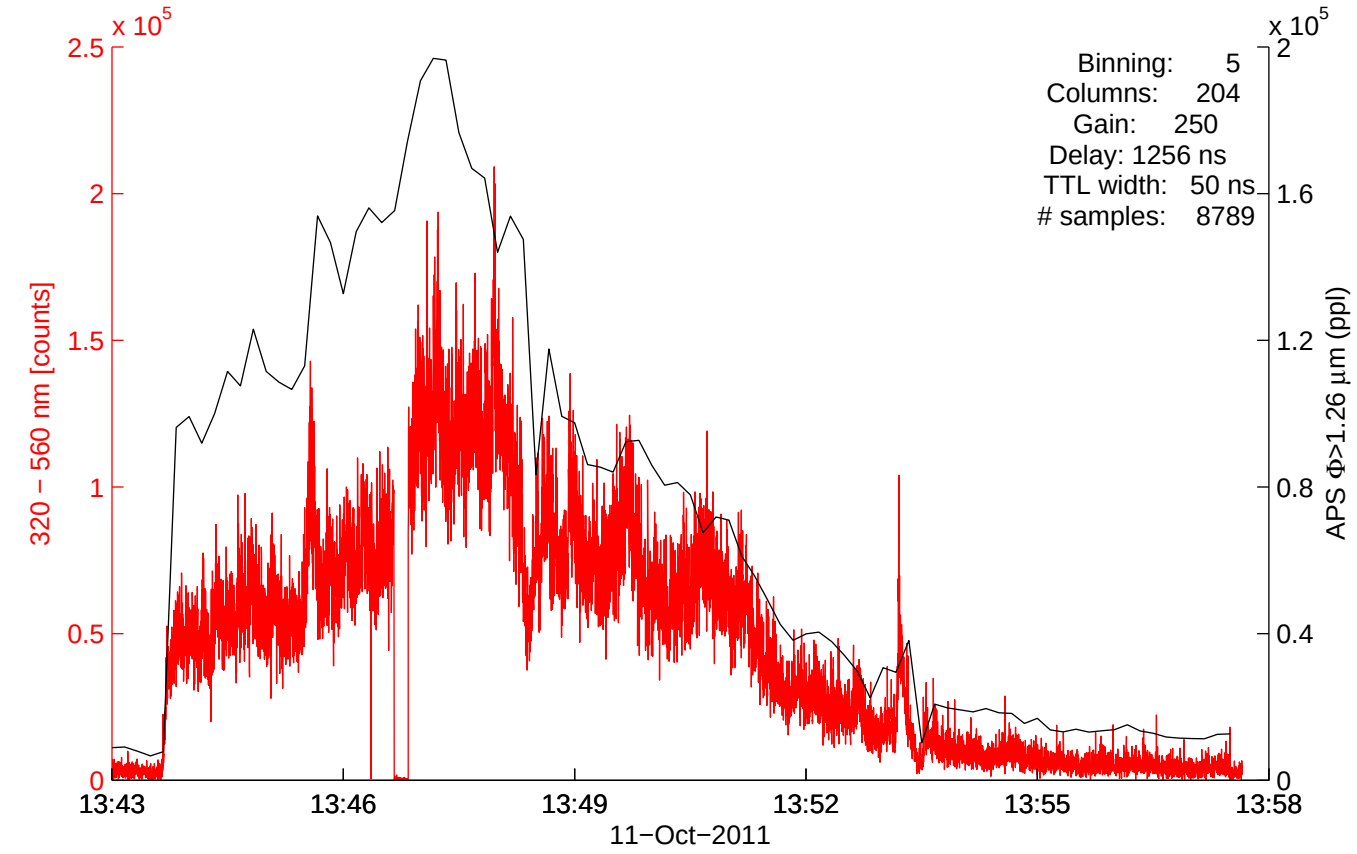
x 10^5
2.5
2
1.5
1
0.5
0
320 – 560 nm [counts]
x 10^5
2
1.6
1.2
0.8
0.4
0
APS Φ>1.26 µm (ppl)
Binning: 5
Columns: 204
Gain: 250
Delay: 1256 ns
TTL width: 50 ns
samples: 8789
13:43
13:46
13:49
13:52
13:55
13:58
11−Oct−2011

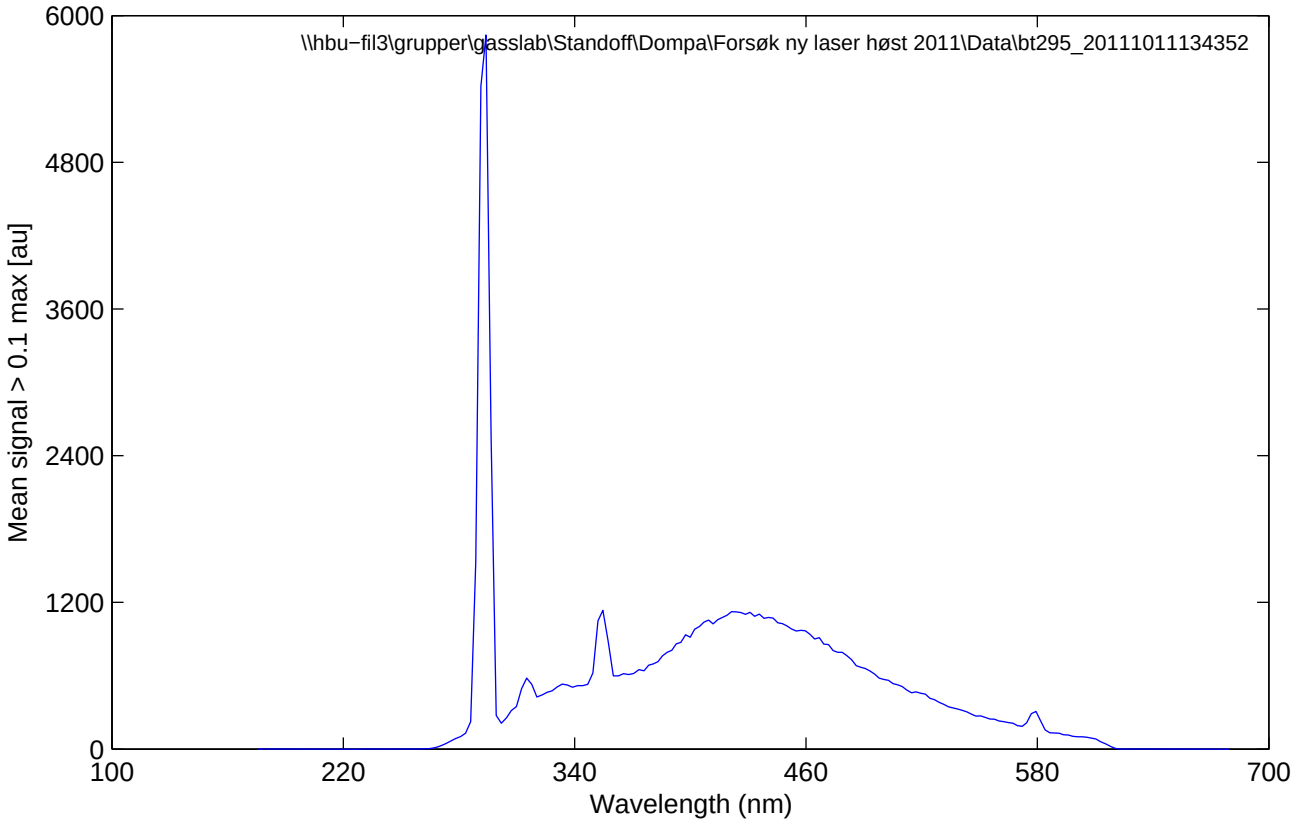
\\hbu−fil3\grupper\glasslab\Standoff\Dompa\Forsøk ny laser høst 2011\Data\bt295_20111011134352
6000
4800
3600
2400
1200
0
Mean signal > 0.1 max [au]
100
220
340
460
580
700
Wavelength (nm)

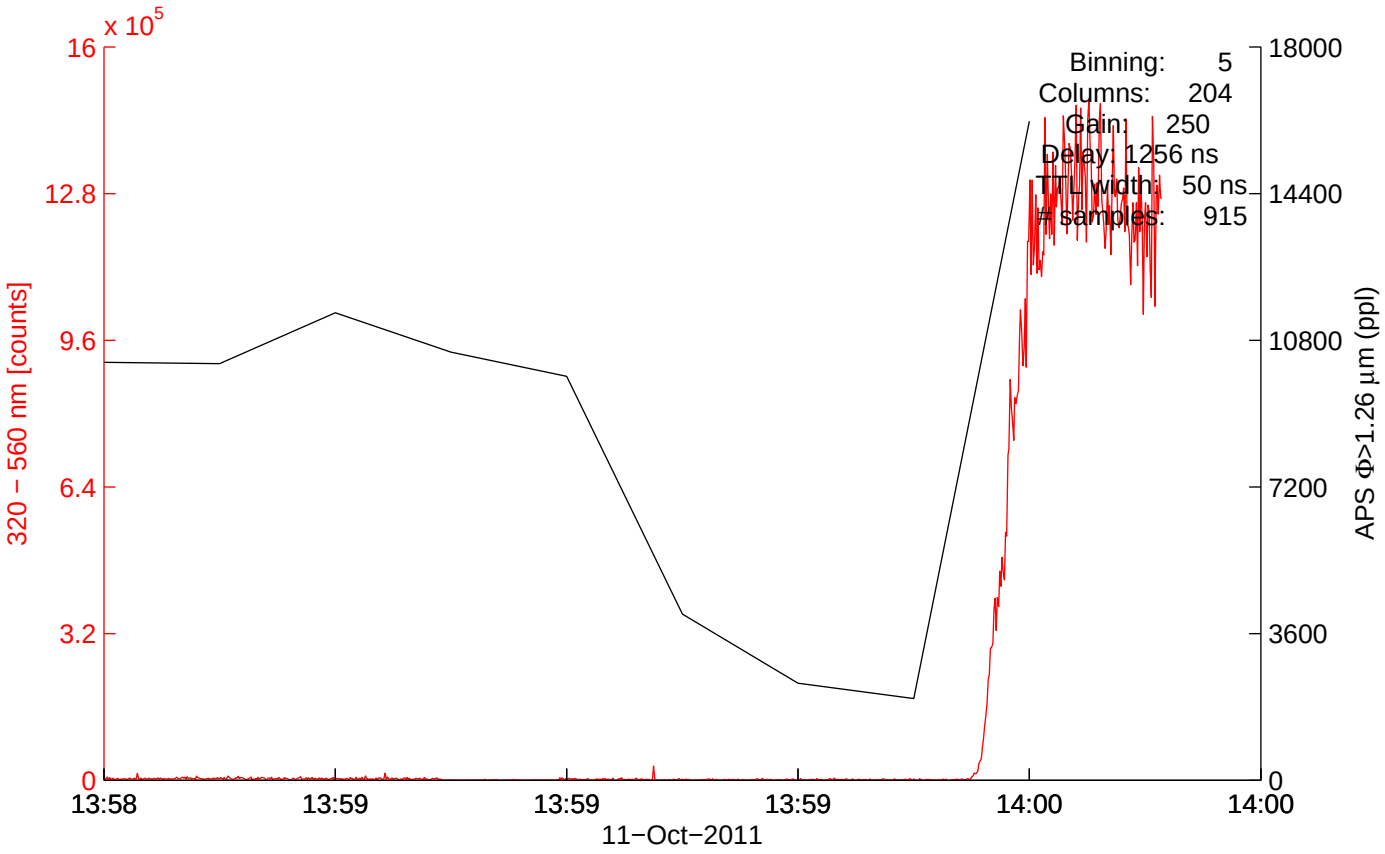
x 10^5
16
12.8
9.6
6.4
3.2
0
320 – 560 nm [counts]
18000
14400
10800
7200
3600
0
APS Φ>1.26 µm (ppl)
Binning: 5
Columns: 204
Gain: 250
Delay: 1256 ns
TTL width: 50 ns
samples: 915
13:58
13:59
13:59
13:59
14:00
14:00
11−Oct−2011

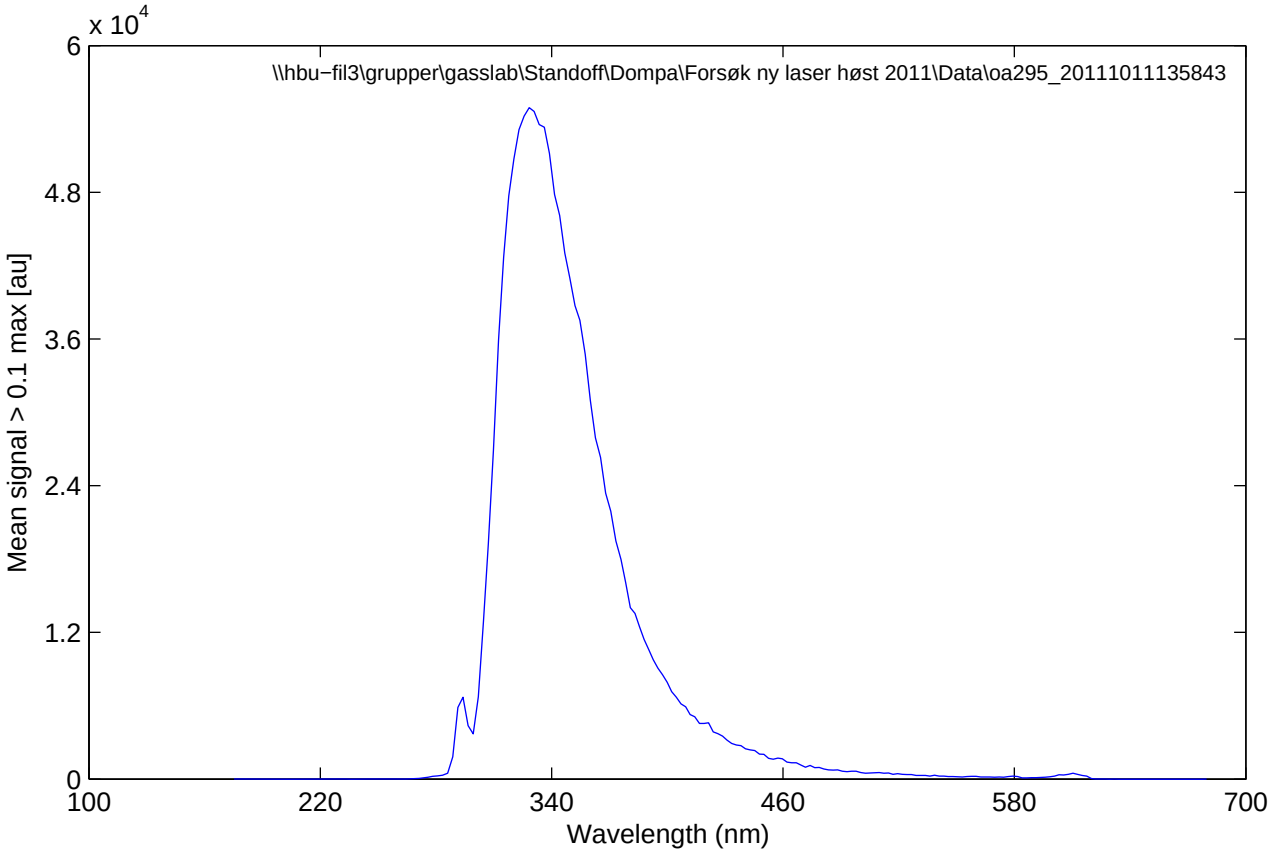
x 10^4
6
4.8
3.6
2.4
1.2
0
Mean signal > 0.1 max [au]
\\hbu−fil3\grupper\gasslab\Standoff\Dompa\Forsøk ny laser høst 2011\Data\oa295_20111011135843
100
220
340
460
580
700
Wavelength (nm)

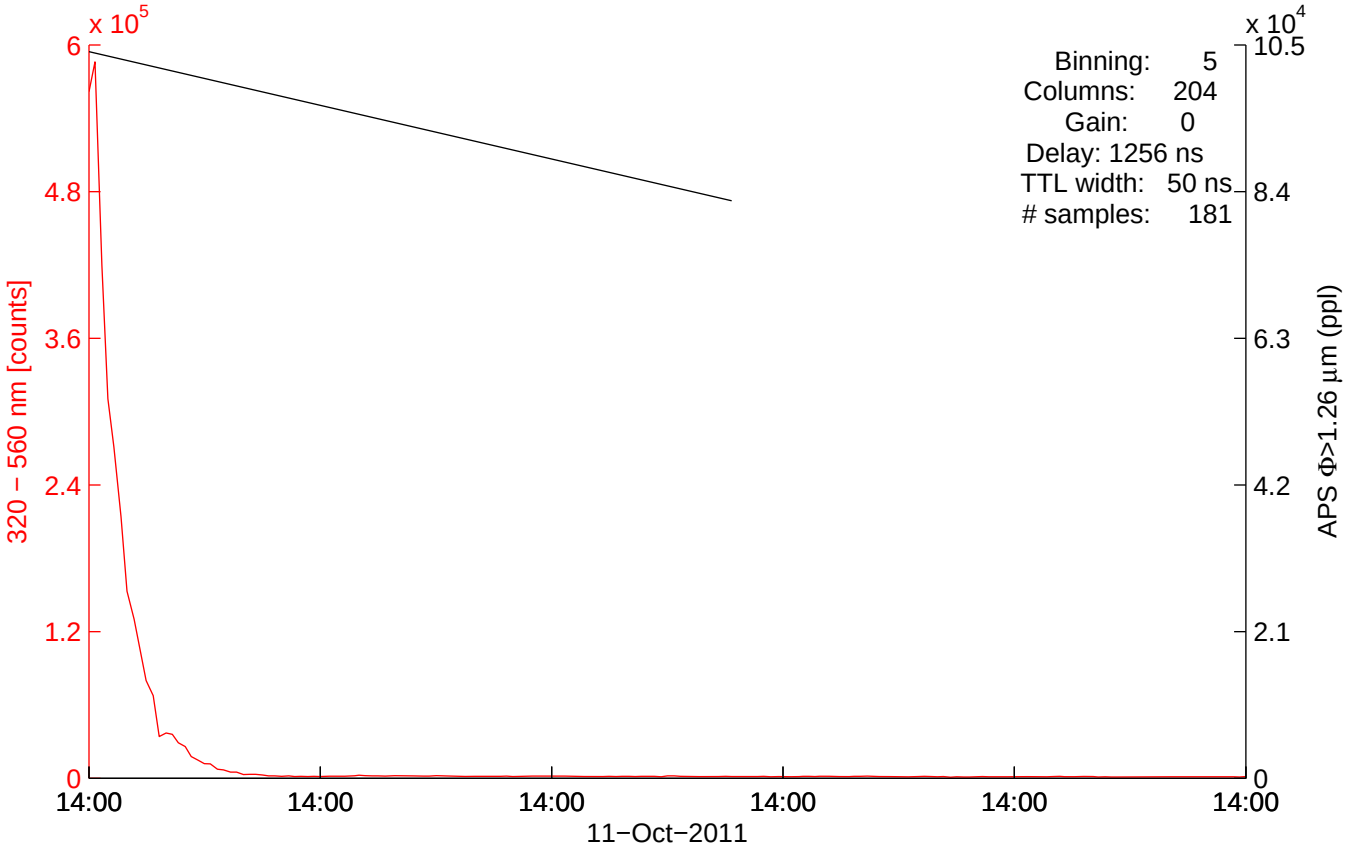
x 10^5
6
4.8
3.6
2.4
1.2
0
320 – 560 nm [counts]
x 10^4
10.5
8.4
6.3
4.2
2.1
0
APS Φ>1.26 µm (ppl)
Binning: 5
Columns: 204
Gain: 0
Delay: 1256 ns
TTL width: 50 ns
samples: 181
14:00
14:00
14:00
14:00
14:00
14:00
11−Oct−2011

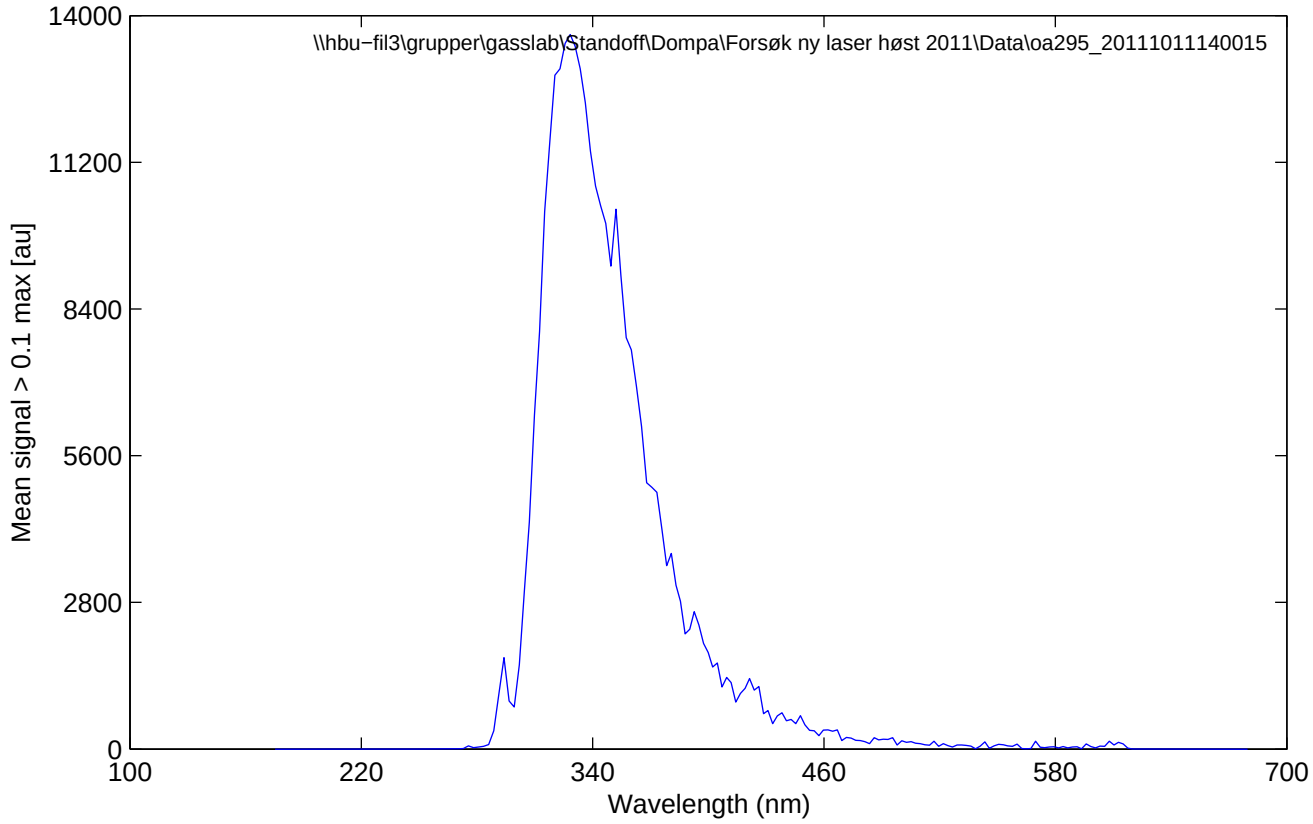
\\hbu−fil3\grupper\gasslab\Standoff\Dompa\Forsøk ny laser høst 2011\Data\oa295_20111011140015
14000
11200
8400
5600
2800
0
Mean signal > 0.1 max [au]
100
220
340
460
580
700
Wavelength (nm)

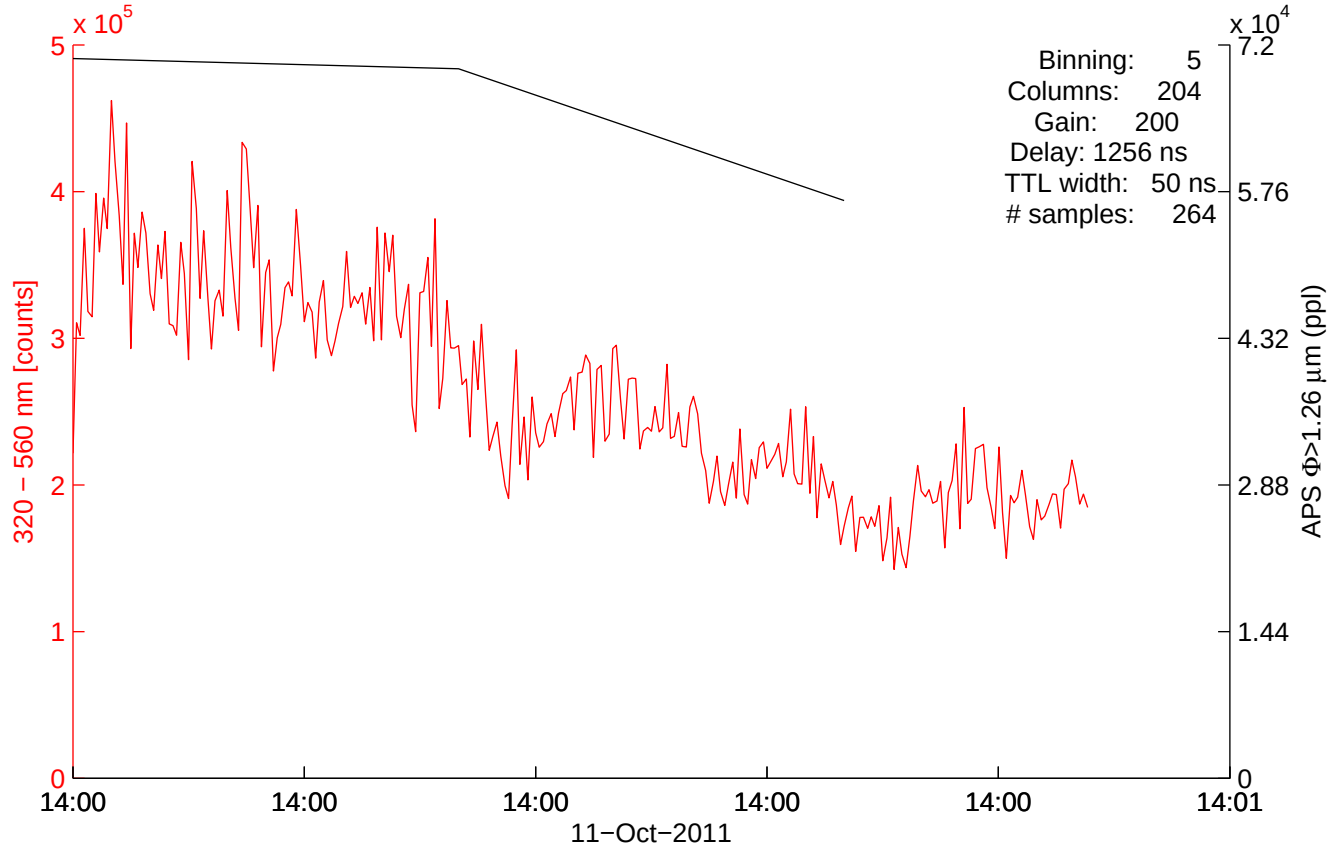
x 10^5
x 10^4
Binning: 5
Columns: 204
Gain: 200
Delay: 1256 ns
TTL width: 50 ns
samples: 264
320 – 560 nm [counts]
APS Φ>1.26 µm (ppl)
0
1
2
3
4
5
1.44
2.88
4.32
5.76
7.2
14:00
14:00
14:00
14:00
14:00
14:01
11−Oct−2011

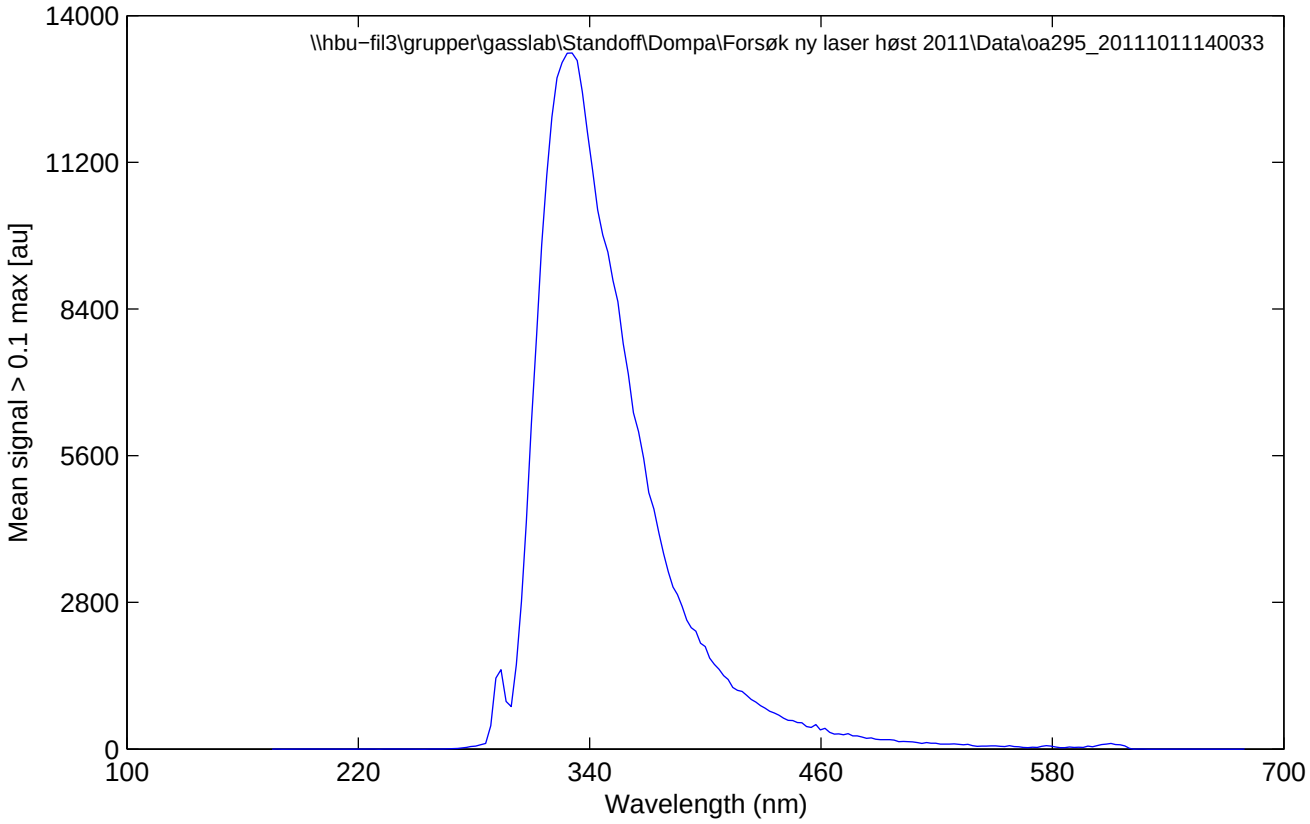
\\hbu−fil3\grupper\gasslab\Standoff\Dompa\Forsøk ny laser høst 2011\Data\oa295_20111011140033
Mean signal > 0.1 max [au]
0
2800
5600
8400
11200
14000
100
220
340
460
580
700
Wavelength (nm)

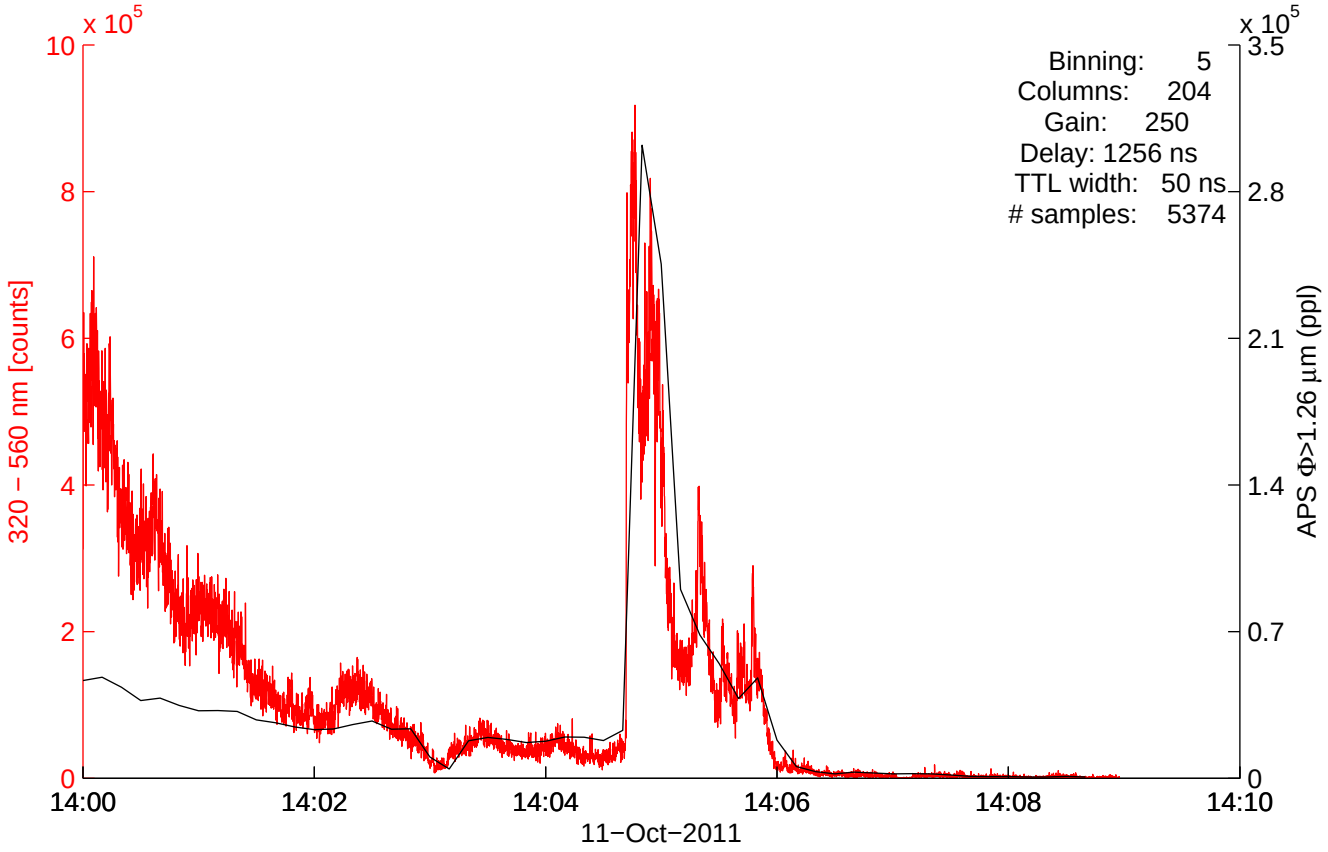
x 10^5
10
8
6
4
2
0
320 – 560 nm [counts]
x 10^5
3.5
2.8
2.1
1.4
0.7
0
APS Φ>1.26 µm (ppl)
Binning: 5
Columns: 204
Gain: 250
Delay: 1256 ns
TTL width: 50 ns
samples: 5374
14:00
14:02
14:04
14:06
14:08
14:10
11−Oct−2011

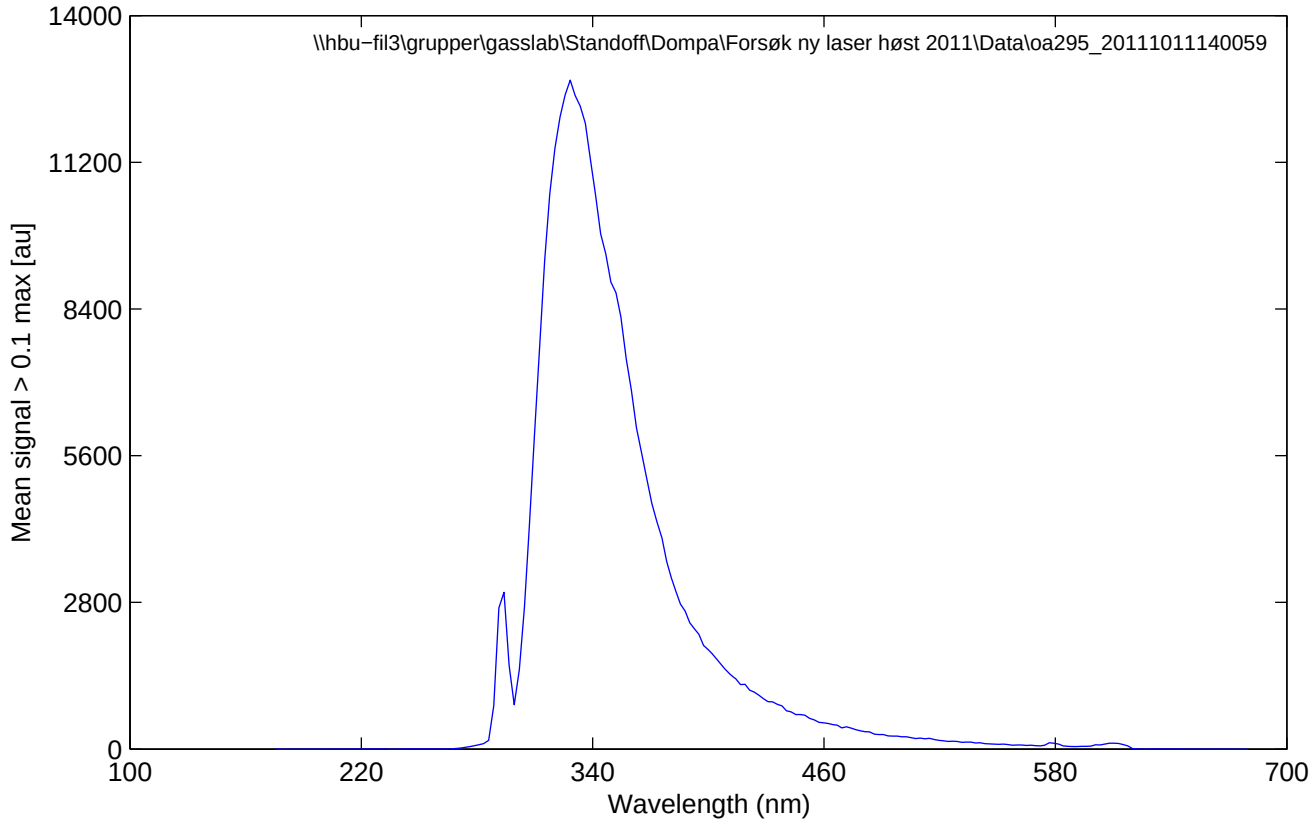
\\hbu−fil3\grupper\gasslab\Standoff\Dompa\Forsøk ny laser høst 2011\Data\oa295_20111011140059
14000
11200
8400
5600
2800
0
Mean signal > 0.1 max [au]
100
220
340
460
580
700
Wavelength (nm)